PHASE EQUILIBRIUM INVESTIGATION OF THE WATER AND ACETONITRILE SOLVENT WITH HEAVY HYDROCARBONS

by

CALEB NARASIGADU

[BSc. (Eng)]

University of KwaZulu Natal

Submitted in fulfillment of the academic requirements for
the degree of Master of Science in Engineering at the School
of Chemical Engineering, University of KwaZulu Natal

Durban

2006

ABSTRACT

Thermodynamics plays an important role for separation processes in chemical industries. Phase equilibrium is of special interest in chemical engineering as separation processes such as distillation and extraction involve phase contacting. The main focus of this research was the measurement of new phase equilibrium data for acetonitrile and water with heavy hydrocarbons that included: heptanoic acid, 1-nonanol, dodecane and 1-dodecene. Hence, binary vapour-liquid equilibrium (VLE), liquid-liquid equilibrium (LLE) and vapour-liquid-liquid equilibrium (VLLE) data were investigated.

The VLE and VLLE data were measured with the modified apparatus of Raal (Raal and Mühlbauer, 1998). The modification, undertaken by Ndlovu (2005), enabled measurement for VLLE systems. Isothermal binary VLE data for the (nonanol + 1-dodecene) system at 403.15 K was measured and VLLE data for the systems (acetonitrile + 1-dodecene) at 343.15 K, and (nonanol + water) at 353.15 K were investigated.

The LLE data were measured with the modified apparatus of Raal and Brouckaert (1992). The modification, introduced by Ndlovu (2005), improved thermal insulation and the sampling procedures. Binary LLE data for the systems (acetonitrile + 1-dodecene) at 1 atm and (water + 1-nonanol) at 1 atm were measured. Furthermore, ternary data at 323.15 K and 1 atm were also measured for the systems containing water + acetonitrile with the each of the following components: heptanoic acid, 1-nonanol, dodecane and 1-dodecene.
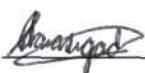
The experimental VLE data were regressed using two different methods: the combined method and the direct method. For the combined method, the second virial coefficients were calculated from the methods of Pitzer and Curl (1957) and Tsonopoulos (1974). The activity coefficients were calculated using three local-composition based activity coefficients models: the model of Wilson (1964), the NRTL model of Renon and Prausnitz (1968) and the modified UNIQUAC model of Anderson and Prausnitz (1978). For the direct method, the equation of state of Stryjek and Vera (1986) and the alpha function of Twu et al. (1991) in the equation of state of Peng and Robinson (1976) were employed. In addition, the mixing rules of Wong and Sandler (1992) and Twu and Coon (1996) were utilised. Furthermore, the *point test* of Van Ness et al. (1973) and the *direct test* of Van Ness (1995) were employed to test the thermodynamic consistency of the experimental VLE data measured in this work.

The experimental binary LLE data were regressed using the three-suffix Margules model, Van Laar (1910) model and the NRTL model of Renon and Prausnitz (1968) to obtain the temperature dependence of the model parameters. The experimental ternary LLE data were subjected to a two part correlation: the tie-line correlation and the binodal curve correlation. The tie-lines were correlated with the NRTL model of Renon and Prausnitz (1968) and the modified UNIQUAC model of Anderson and Prausnitz (1978). The binodal curves were correlated with the Hlavatý (1972) equation, ß-density function equation of Letcher et al. (1989) and the log γ equation of Letcher et al. (1986).
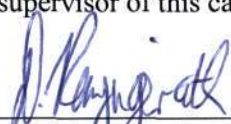
PREFACE

The work presented in this dissertation was performed at the University of KwaZulu-Natal from January 2004 to December 2006. The work was supervised by Professor D. Ramjugernath, Professor J. D. Raal and Doctor P. Naidoo.
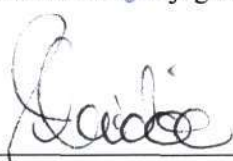
This dissertation is submitted as the full requirement for the degree M.Sc. in Chemical Engineering. All the work presented in this dissertation is original, unless otherwise stated. It has not (in whole or in part) been previously submitted to any tertiary institute as part of a degree.

_____

C. Narasigadu

As supervisor of this candidate, I approve this dissertation for submission:

_____   _____

Professor D. Ramjugernath   Professor J. D. Raal

_____

Doctor P. Naidoo

ACKNOWLEDGEMENTS

I would like to take this opportunity to acknowledge and thank the following people who have made a tremendous contribution to this work:

- Firstly, my Lord and Saviour, Jesus Christ, Who has made my tertiary education a reality.

- My supervisors, Professor D. Ramjugernath, Professor J. D. Raal and Doctor P. Naidoo for their expert knowledge, guidance and support.

- SASOL Ltd. for their financial assistance.

- The technical staff, Kelly Robertson, Les Henwood, Collen Mandri and Ayanda Khanyile for their work done on the equipment used in this project.

- My mum, Linda, my sister, Lisa, and my uncle, Jeeva, for their many years of wholehearted support, encouragement, love and motivation.

- My family, fellow postgraduate colleagues, friends and the congregation of C.R.C Tongaat church for their invaluable advice, support and friendship.

DEDICATION

To

my Lord and Saviour, Jesus Christ

Call to Me and I will answer you

and show you great and mighty things,

fenced in and hidden,

which you do not have knowledge of or understand

JEREMIAH 33:3

(AMPLIFIED BIBLE)

TABLE OF CONTENTS

LIST OF FIGURES

Chapter 2

Chapter 3

Chapter 4

Chapter 5

Chapter 6

Chapter 7

Appendix D

LIST OF PHOTOGRAPHS

Chapter 4

LIST OF TABLES

Chapter 7

Appendix B

Appendix C

Appendix E

NOMENCLATURE

English Letters

$A^{'}$	Constant in the Antoine vapour pressure equation
A^{*}	Constant in the Wagner vapour pressure equation
A^{*}	Term in the Peng-Robinson (1976) equation of state
A_{i}^{*}	Peak area obtained from the gas chromatograph
A_1, A_2, A_3	Parameters in the correlation of Hlavatý (1972)
A_{12}	Parameter in the three-suffix Margules and Van Laar (1910) models
A_{21}	Parameter in the three-suffix Margules and Van Laar (1910) models
A_{∞}^{E}	Excess Helmholtz free energy at infinite pressure
a	Intermolecular attraction force parameter in the Peng-Robinson (1976) equation of state
a_m	Intermolecular attraction force mixture parameter in the Peng-Robinson (1976) equation of state
a_t	Parameter in the correlation of Tsonopoulos (1974)
a_{vdw}	Intermolecular attraction force parameter in the van der Waals (1873) equation of state
$B^{'}$	Constant in the Antoine vapour pressure equation
B^{*}	Constant in the Wagner vapour pressure equation
B^{*}	Term in the Peng-Robinson (1976) equation of state
B^{**}	Term used in the pressure-temperature sensitivity equation of Raal et al. (2006), defined by Equation (7-7)
B_{ii}	Second Virial coefficient of pure component i [cm^3/mol]
B_{ij}	Second Virial coefficient for species i - species j interaction [cm^3/mol]
B_{virial}	Second Virial coefficient [cm^3/mol]
B^{0}	Parameter in the correlation of Pitzer and Curl (1957)
B^{1}	Parameter in the correlation of Pitzer and Curl (1957)
B_1, B_2, B_3	Parameters in the ß-density correlation of Letcher et al. (1989)
b	Molecular size parameter in the Peng-Robinson (1976) equation of state

b_m	Molecular size mixture parameter in the Peng-Robinson (1976) equation of state
b_t	Parameter in the correlation of Tsonopoulos (1974)
b_{vdw}	Molecular size parameter in the van der Waals (1873) equation of state
C'	Constant in the Antoine vapour pressure equation
C^*	Constant in the Wagner vapour pressure equation
C_1, C_2, C_3	Parameters in the log γ correlation of Letcher et al. (1986)
c	Numerical constant defined in Equation (3-74)
D	Summation term in the mixing rule of Wong and Sandler (1992)
$D^\bullet$	Constant in the Wagner vapour pressure equation
D^*	Parameter used for the LLE charts of Renon and Prausnitz (1968)
F_i	Response factor
f	Fugacity [kPa]
$\hat{f}$	Fugacity in solution [kPa]
$f^{(0)}$	Term in the correlation of Tsonopoulos (1974)
$f^{(1)}$	Term in the correlation of Tsonopoulos (1974)
$f^{(2)}$	Term in the correlation of Tsonopoulos (1974)
G	Molar or specific Gibbs energy [J/mol]
$\bar{G}$	Partial molar Gibbs energy [J/mol]
G_{ij}	Parameter in the NRTL model of Renon and Prausnitz (1968)
$g_{ij} - g_{ii}$	Parameter representing energy interactions between species in the NRTL model of Renon and Prausnitz (1968)
H	Enthalpy [J/mol]
$\bar{H}$	Partial molar enthalpy [J/mol]
$\Delta H_{VAP,i}$	Enthalpy of vaporisation [J/mol]
K	Equilibrium constant
k_{ij}	Binary interaction parameter
L'	Parameter in the Twu et al. (1991) alpha correlation
l_i	Parameter in the UNIQUAC model of Abrams and Prausnitz (1975)
l_{ij}	Binary interaction parameter for the mixing rule of Twu and Coon (1996)
M	Represents a general thermodynamic property

M'	Parameter in the Twu et al. (1991) alpha correlation
N'	Parameter in the Twu et al. (1991) alpha correlation
n	Number of moles
P	System pressure [kPa]
P'	Parachor
P^*	Three phase equilibrium pressure [kPa]
Q	Quadratic sum of second virial coefficients
q_i	Pure component area parameter in the UNIQUAC model of Abrams and Prausnitz (1975)
q_i'	Pure component area parameter in the modified UNIQUAC model (Anderson and Prausnitz, 1978)
R	Universal gas constant [J/mol.K]
R_d	Mean radius of gyration [Å]
r_i	Pure component volume parameter in the UNIQUAC model of Abrams and Prausnitz (1975)
S	Molar or specific entropy [cm^3/mol]
S^*	Parameter used for the LLE charts of Renon and Prausnitz (1968)
T	System temperature [°C or K]
T^*	Three phase equilibrium temperature [°C or K]
$u_{ij} - u_{ii}$	Parameter representing energy interactions between species in the UNIQUAC model of Abrams and Prausnitz (1975)
V	Molar or specific volume [cm^3/mol]
$\bar{V}$	Partial molar enthalpy [cm^3/mol]
x	Liquid phase mole fraction or composition
x'	Term used in the Wagner vapour pressure equation, defined by Equation (7-3)
x_A	Term used in the correlations of Hlavatý (1972), Letcher et al. (1989) and Letcher et al. (1986), defined by Equation (3-153)
x_B	Term used in the correlations of Hlavatý (1972), Letcher et al. (1989) and Letcher et al. (1986), defined by Equation (3-154)
x_i^0	Term used in the correlations of Hlavatý (1972), Letcher et al. (1989) and Letcher et al. (1986) in Equations (3-153) and (3-154)
x_{11}^0	Term used in the correlations of Hlavatý (1972), Letcher et al. (1989) and Letcher et al. (1986) in Equations (3-153) and (3-154)

y	Vapour phase mole fraction or composition
Z	Compressibility factor
z	Coordination number in the UNIQUAC model of Abrams and Prausnitz (1975)

Greek Letters

α	Scaling factor in the Peng-Robinson (1976) equation of state
α_{ij}	Parameter in the NRTL model of Renon and Prausnitz (1968) representing solution non-randomness
δ	Denotes a residual (e.g. dP)
δ_{ij}	Term relating the second Virial coefficients defined by Equation (3-29)
$\varepsilon, \varepsilon_A, \varepsilon_B$	Tolerances used for object functions
ε_P^*	Constant temperature term in the *direct test* of Van Ness (1995), defined by Equation (160)
ε_T^*	Constant pressure term in the *direct test* of Van Ness (1995), defined by Equation (161)
Φ	Ratio of fugacity coefficients and Poynting correction factor (Equation 3-24)
Φ_i^*	Segment fraction in the UNIQUAC model of Abrams and Prausnitz (1975)
ϕ	Fugacity coefficient
$\hat{\phi}$	Fugacity coefficient in solution
Γ_i	Temperature dependent constant of integration
γ	Activity coefficient
γ_i^∞	Infinite dilution activity coefficient
η	Solvation (unlike species) and association (pure species) parameters
κ	Characteristic constant in the Peng-Robinson (1976) equation of state
κ_0	Characteristic constant in the Peng-Robinson-Stryjek-Vera (1986) equation of state
κ_1	Pure component parameter in the Peng-Robinson-Stryjek-Vera (1986) equation of state
Λ_{ij}	Parameter in the Wilson (1964) model
$\lambda_{ij} - \lambda_{ii}$	Parameter representing molar interactions between species in the Wilson (1964) model

μ_d	Dipole moment
μ_i	Chemical potential of component i
θ_i	Area fraction in the UNIQUAC model of Abrams and Prausnitz (1975)
$\theta_i^{'}$	Area fraction in the modified UNIQUAC model (Anderson and Prausnitz, 1978)
σ	Standard deviation of Sen and Srivastava (1990), defined by Equation (3-155)
τ_{ij}	Parameter in the NRTL model of Renon and Prausnitz (1968)
ω	Acentric factor
ω_{ij}	Acentric factor for species i - species j interaction

Subscript

1	Denotes component 1
2	Denotes component 2
ad	Denotes an absolute deviation
c	Denotes a critical property
$calc$	Denotes a calculated value
exp	Denotes an experimental value
r	Denotes a reduced property

Superscript

C	Denotes a combinatorial property for the UNIQUAC model of Abrams and Prausnitz (1975)
E	Denotes an excess property
exp	Denotes an experimental value in the *direct test* of Van Ness (1995)
ig	Denotes an ideal gas
l	Denotes the liquid phase
R	Denotes a residual property
sat	Denotes a saturated value
v	Denotes the vapour phase
α	Denotes a thermodynamic phase
β	Denotes a thermodynamic phase
π	Denotes a thermodynamic phase

1

CHAPTER ONE

INTRODUCTION

Thermodynamic data on chemical compounds and their mixtures play an important role for separation processes in chemical industries as they are needed for efficient design and operation of chemical processing plants. Distillation is one of the most commonly employed separation process and relies on accurate vapour-liquid equilibrium (VLE) data. On the other hand, liquid-liquid equilibrium (LLE) data are needed for solvent extraction which provides prospects for substantial energy saving when compared to distillation, when a minor but high density constituent of the feed mixture is to be recovered (Humphrey et al., 1984). Hence, over the years there has been a considerable demand for experimentally measured phase equilibrium data.

Mixtures of acetonitrile and water are produced by several processes in chemical industries. A binary mixture of acetonitrile and water is primarily used as an extraction solvent for unsaturated hydrocarbons, and as a general purpose solvent for many compounds due to its selective miscibility. Numerous phase equilibrium data containing acetonitrile have been published in literature. However, there is little or no data published on systems of acetonitrile and water with a heavy hydrocarbon. This research therefore focussed on the measurement of

new phase equilibrium data for acetonitrile and water with heavy hydrocarbons that included: heptanoic acid, 1-nonanol, dodecane and 1-dodecene.

The study included VLE, LLE and vapour-liquid-liquid equilibrium (VLLE) measurements:

- Binary VLE for the (1-dodecene + 1-nonanol) system at 403.15 K.
- Binary LLE for the (acetonitrile + 1-dodecene) system at 1 atm.
- Binary LLE for the (water + 1-nonanol) system at 1 atm.
- Ternary LLE for the (water + acetonitile + heptanoic acid) system at 1atm and 323.15 K.
- Ternary LLE for the (water + acetonitile + 1-nonanol) system at 1 atm and 323.15 K.
- Ternary LLE for the (water + acetonitile + dodecane) system at 1 atm and 323.15 K.
- Ternary LLE for the (water + acetonitile + 1-dodecene) system at 1 atm and 323.15 K.
- Binary VLLE for the (acetonitrile + 1-dodecene) system at 343.15 K.
- Binary VLLE for the (water + 1-nonanol) system at 353.15 K.

The VLE and VLLE data were measured with the modified apparatus of Raal (Raal and Mühlbauer, 1998). The modification, undertaken by Ndlovu (2005), enabled measurements for VLLE systems. The LLE data were measured with the modified apparatus of Raal and Brouckaert (1992). The modification, introduced by Ndlovu (2005), improved thermal insulation and the sampling procedures. All the measured phase equilibrium data were then subjected to rigorous thermodynamic analyses. This involved regression of the data using various thermodynamic models in order to determine the models' parameters. In addition, the measured VLE data was subjected to thermodynamic consistency testing.

2

CHAPTER TWO

A REVIEW OF SOME EXPERIMENTAL TECHNIQUES

In principle, the measurement of phase equilibria involves the measurements of temperature, pressure and phase composition. However, in practice it is difficult to obtain experimental data of high accuracy. According to Walas (1985), care must be taken to ensure that the temperature and pressure are measured at the point where equilibrium really exists and that the withdrawal of samples for analysis does not disturb the equilibrium appreciably.

The purpose of this chapter is not to present an exhaustive review of all experimental techniques for phase equilibria. It will rather focus on the dynamic method (circulation method) for low pressure vapour-liquid equilibrium (VLE), which centres on recirculating stills. Experimental techniques for liquid-liquid equilibrium (LLE) will be discussed and finally some of the modified recirculating stills adapted for partially miscible systems that allow measurement of low pressure vapour-liquid-liquid equilibrium (VLLE) will be examined.

2.1 The Dynamic Method

The dynamic method, also known as the circulation method, has an advantage over other methods as it allows measurement of high accuracy to be obtained in a simple manner. In this method, a liquid mixture is charged into a distilling flask and brought to a boil where a continuous separation of the vapour phase from the liquid phase occurs. The vapour phase is then condensed into a receiver (except for methods with direct circulation of the vapour phase) and returned as condensate to mix with the boiling liquid. The dynamic method can be operated under isobaric or isothermal and steady-state conditions. Measurement of the thermodynamic properties such as temperature, pressure, liquid and vapour compositions are recorded when steady state conditions have been achieved.

The dynamic method can be classified into two categories (Hála et al., 1967):
- circulation of the vapour phase only
- circulation of both vapour and liquid phases

2.2 VLE Recirculating Stills

These stills allow for rapid and accurate measurement of VLE. There are several criteria that a recirculating still should satisfy, as outlined by Malanowski (1982):
- The design should be simple yet ensure accurate pressure and temperature measurements.
- Small samples should be required to analyse composition of vapour and liquid phases.
- Steady-state operation should be rapidly achieved if an equilibrium property (such as pressure) is changed.
- No vapour should be allowed to partially condense on the temperature sensor and overheating near the temperature sensor should be avoided.
- No liquid droplets should be entrained in the vapour phase.
- The circulated vapour must be well mixed with the boiling liquid to maintain uniform composition.
- A steady flow and composition of the circulated stream should be maintained.
- The apparatus should not contain any dead-volume that could hinder the attainment of equilibrium.
- The sampling procedure and introduction of material to the still should be accomplished without disturbing the equilibrium condition of the mixture.

4

The recirculating still overcame some of the major difficulties experienced in the area of phase equilibria in chemical engineering research. One such experimental challenge was the accurate measurement of VLE. However there are still many experimental challenges, like the perplexing diversity of phase equilibria in real systems (Raal and Mühlbauer, 1998).

2.2.1 Recirculation of Vapour Phase only

Othmer (1928) designed a recirculating still based on the work of Sameshima (1918), in which the vapour generated from the boiling liquid was sent to a condenser and the condensate was then returned to the boiling flask (refer to Figure 2-1). The design also incorporated sampling points for both vapour and liquid phases. However, this design had numerous shortcomings:

- The temperature measurement was unreliable as the measuring device was not in contact with both equilibrium phases.

- The condensate receiver was large and furthermore the condensate was not well stirred.

- The design displayed the possibility of partial condensation of saturated vapour on the wall of the boiling flask. This posed a serious problem as partial condensation of the equilibrium vapour would change its composition.

- Flashing of the vapour that is rich in the more volatile component, also posed a problem.

- Furthermore, there was no thorough stirring of the contents in the boiling chamber.
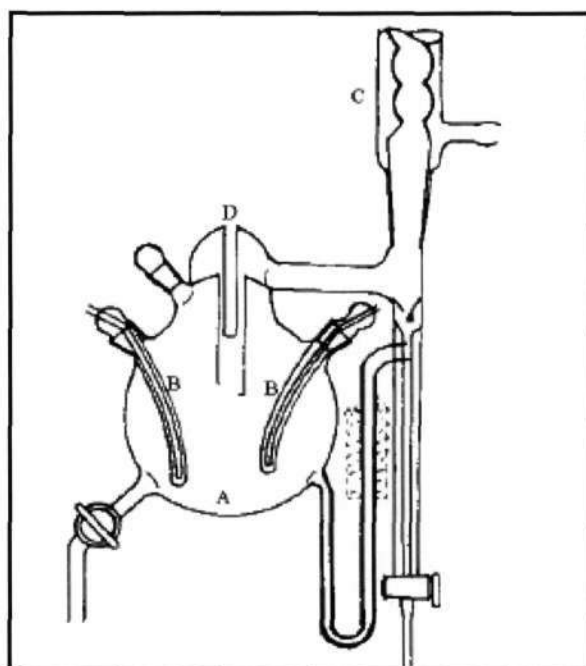
Figure 2-1: A schematic diagram of the Othmer still (Malanowski, 1982).
A – boiling chamber; **B** – immersion heaters; **C** – condenser; **D** – thermowell.

Many modifications were proposed for this still but due to the many disadvantages of this type of design, its use for accurate work is not advisable (Raal and Mühlbauer, 1998).

2.2.2 Recirculation of both Liquid and Vapour Phases

Gillespie (1946) designed a still that catered for the circulation of liquid and vapour phases based on earlier work done by Lee (1931), as shown in Figure 2-2. A Cottrell pump was used to aid circulation, which allowed more accurate temperature measurements (Cottrell, 1919). According to Coulson et al. (1948), this still was found to be superior to the designs of Othmer (1943) and Scatchard et al. (1938). However, this still was also found to contain some major drawbacks:

- The liquid sample, taken from the boiling chamber, is not in true equilibrium with the recirculated vapour sampled as condensate.

- The disengagement chamber is not insulated and therefore there is no prevention of partial condensation of the equilibrium vapour.

- The sampling procedure interrupts the still operation and hence disturbs the equilibrium compositions.

- The use of the Cottrell tube alone is not sufficient for the rapid attainment of equilibrium as mass transfer is limited due to small contact times and interfacial areas.

To overcome some of these drawbacks, Yerazunis et al. (1964) designed a still by modifying the separation chamber. The modification was based on the work done by Heertjies (1960) and Rose and Williams (1955). Heertjies (1960) suggested passing a vapour-liquid mixture through a packed column after exiting the Cottrell tube to improve the efficiency of the mass transfer in the packed section of the equilibrium chamber. Rose and Williams (1955) advocated the use of the vapour phase as a thermal barrier by allowing the vapour to flow upward over the equilibrium chamber. Yerazunis et al. (1964) showed their data to be highly consistent with thermodynamic requirements.

Raal and Mühlbauer (1998) designed a still based on the work of Heertjies (1960) and Yerazunis et al. (1964) to eliminate the sources of error in previous designs. In this design, the liquid and vapour are forced downward co-currently to achieve rapid and dynamic equilibrium. Furthermore, the packing in this design is readily accessible. Some of the special features of this still are:

6
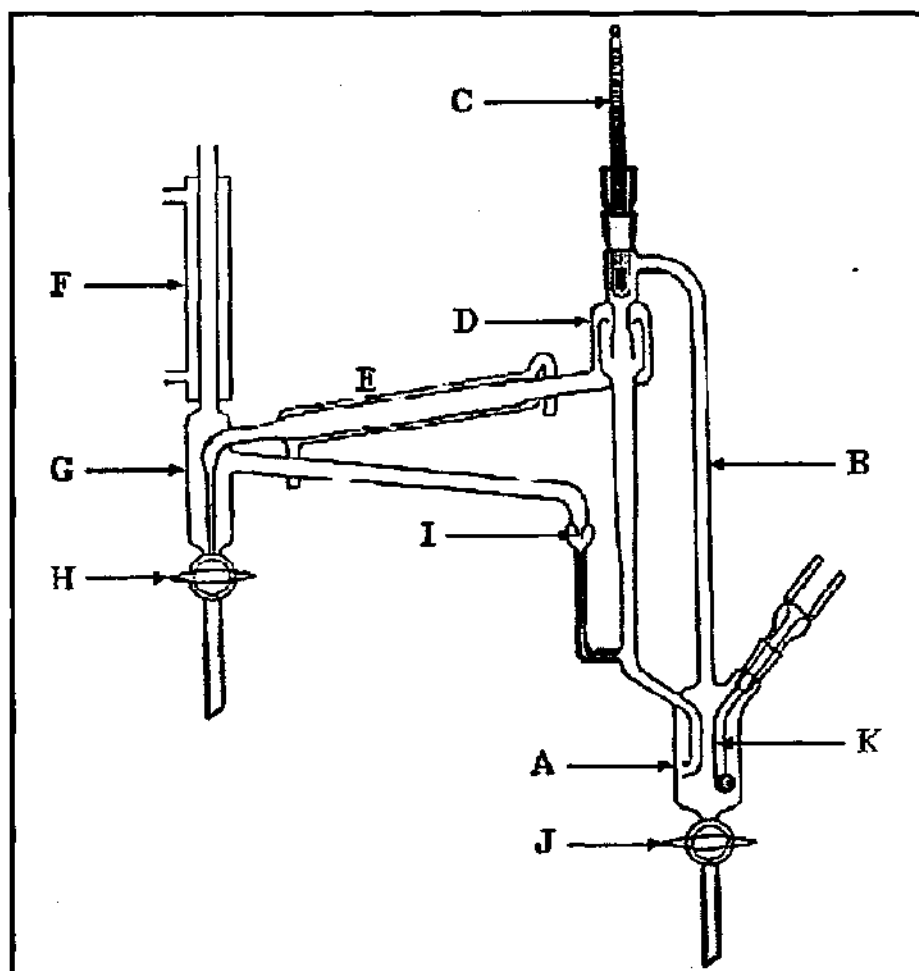
Figure 2-2: The original apparatus of Gillespie (1946).

A – boiling chamber; **B** – Cottrell tube; **C** – thermometer; **D** – vapour-liquid separating chamber; **E,F** – condensers; **G** – condensate receiver; **H** – condensate sample cock; **I** – droplet counter; **J** – liquid sample cock; **K** – internal heater.

- The establishment of equilibrium is not dependant on the Cottrell tube only, since the packing in the equilibrium chamber increases the mass transfer between the vapour and liquid phases, allowing rapid attainment of equilibrium.

- The Cottrell tube and equilibrium chamber are vacuum jacketed to prevent partial condensation of the vapour. The vacuum jacket also reduces heat losses and insulates the equilibrium region.

- Stirring is incorporated in both the boiling chamber and the condensate receiver by means of magnetic stirrers.

- The boiling chamber consists of internal and external heaters, where the internal heater provides rapid and smooth boiling while the external heater compensates for heat losses to the environment.

- The operation of the still is not disturbed by sampling.

This apparatus was used in this project but contained a modification, introduced by Ndlovu (2005), to incorporate partially miscible systems thus enabling low-pressure VLLE measurements. This modified still is discussed in detail in Chapter 4.

2.3 LLE Techniques

LLE data are generally much easier to measure than VLE data. In this section some useful methods and equipment for LLE measurements will be discussed, viz., the titration method, the laser-light scattering technique and the direct analytical method.

2.3.1 The Titration Method

The titration method is one of the most well-known methods for LLE measurements. In this method, one component is continuously added to a known amount of the other component or mixtures of components with unlimited miscibility in a stirred vessel until turbidity appears or disappears. The binodal curve is constructed based on the knowledge of the amounts of substances required for phase separation. The tie-lines are determined by analysis using refractive index or density. Alternatively, the tie-lines can also be obtained using the Karl-Fischer titration method, provided one of the components is water (Skoog et al., 1991). For a more detailed discussion on the titration method, the reader is suggested to consult work done by Briggs and Comings (1943), Rifai and Durandet (1962) and Letcher et al. (1989).

2.3.2 Laser-light Scattering Technique

The onset or disappearance of turbidity, as described in the titration method above, is a somewhat subjective judgement. Therefore, suitable instrumentations were developed to improve the judgement of the onset or disappearance of turbidity. One such apparatus that received recognition was developed by Benjamin et al. (1993), as shown in Figure 2-3. This technique uses a photocell to detect the intensity of scattered light. The experimental cloud point is then determined from a plot of intensity of scattered light versus temperature for a sample under investigation and hence the solubility curve is obtained.
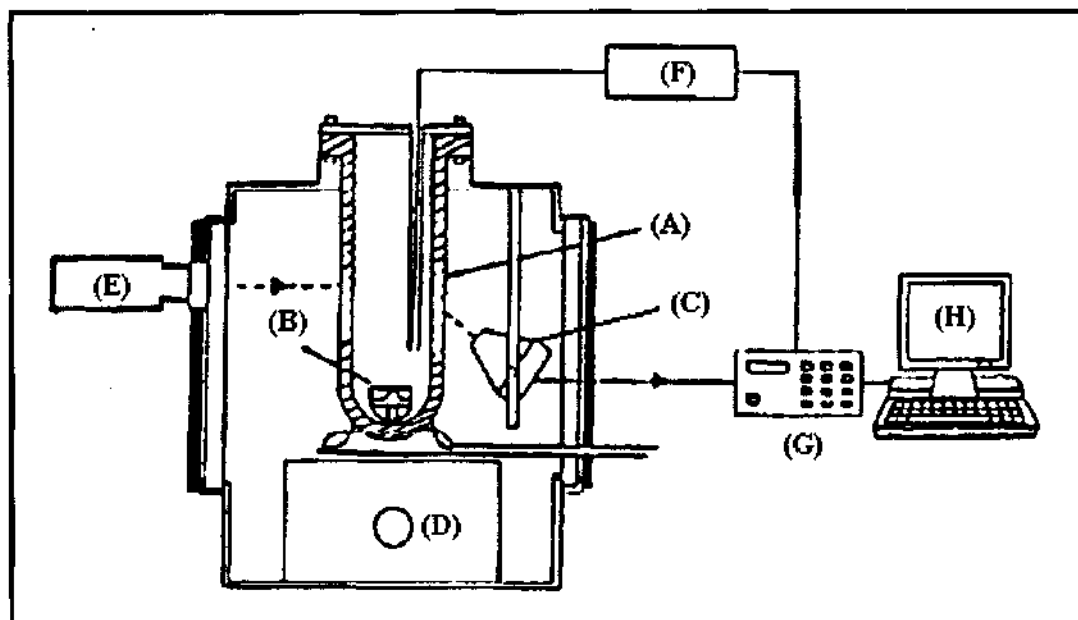
Figure 2-3: A schematic diagram of the apparatus used for mutual solubility measurements with laser-light scattering (Benjamin et al., 1993).

A – equilibrium vessel; B – stirrer chip; C – light sensor; D – magnetic stirrer; E – optical system; F – thermometer; G – digital multimeter; H – computer.

2.3.3 Direct Analytical Method

In the direct analytical method, a heterogeneous mixture is placed in an isothermal equilibrium cell. The mixture is then stirred for a sufficient time interval for equilibrium to be established and the phases are then allowed to separate. Samples are then withdrawn from each phase and analysed, where the analytical determination of the tie-lines is carried out using a combination of various physical and chemical methods. However, Moriyoshi et al. (1989) suggest that gas chromatography can be successfully used to determine the composition of each phase in equilibrium. The direct analytical method has the advantage of obtaining the binodal curve and the tie-line data simultaneously, since joining all tie-line data forms the binodal curve (a distinct advantage over the titration method). It is also applicable to systems containing more than three components (Novak et al., 1987).

The direct analytical method was used to obtain the LLE data required for this project using a double-walled glass cell, and the equilibrium phase compositions were determined by gas chromatography. The cell was a modification of the one used by Raal and Brouckaert (1992). The modifications were undertaken by Ndlovu (2005) and are discussed in greater detail in Chapter 4.

9

2.4 VLLE Recirculating Stills

In Section 2.2, the recirculating stills described were capable of measuring VLE data for homogenous systems only and thus, were incapable of determining equilibrium properties of partially miscible systems, primarily because the condensate for a given concentration range forms two liquid phases. However, systems that exhibit VLLE are of great importance in chemical industries, especially in the field of azeotropic distillation. In this section, some of the recirculating stills that enable the equilibrium properties of partially miscible systems to be measured will be examined.

2.4.1 Recirculation of Vapour Phase Only

Stockhardt and Hull (1931) proposed one of the first equilibrium stills that enabled measurement of VLE for systems with limited miscibility. Their apparatus had a unique feature; a flexible connection between the boiling flask and the condenser. This enabled the condensate to be totally refluxed or collected into a receiver. According to Smith and Bonner (1949), this apparatus was simple to set up, operate and also capable of producing good results. However, Smith and Bonner (1949) found that the apparatus produced vapours that were too rich in the more volatile component.

To try and eliminate some of the shortcomings of the apparatus of Stockhardt and Hull (1931), Baker et al. (1939) designed a still that prevented the condensed vapours going back to the boiling flask, based on the work done by Trimble and Potts (1935). However, the apparatus of Baker et al. (1939) does not reflect the true equilibrium temperature since the thermometer is not in contact with the two phases in equilibrium. Furthermore, Hála et al. (1967) mention that the apparatus cannot handle systems that are heterogeneous at the boiling point as mixing cannot achieve complete emulsification due to the large volume of the heterogeneous mixture in the still.

Smith and Bonner (1949) modified the apparatus of Baker et al. (1939) to eliminate production of vapours that are too rich in the more volatile component. However, the apparatus requires a large chemical volume and thus makes magnetic stirring inadequate. Therefore, Kollar (1952) suggested the use of mechanical mixing. However, the measurement of the equilibrium temperature is still inaccurate as the thermometer is not in contact with the two phases in equilibrium. Furthermore, partial condensation of the vapours may occur on the cooler parts of the boiling flask, consequently changing the true vapour composition. Nevertheless, according

to Gupta and Rawat (1991), the apparatus of Smith and Bonner (1949) is capable of producing good data.
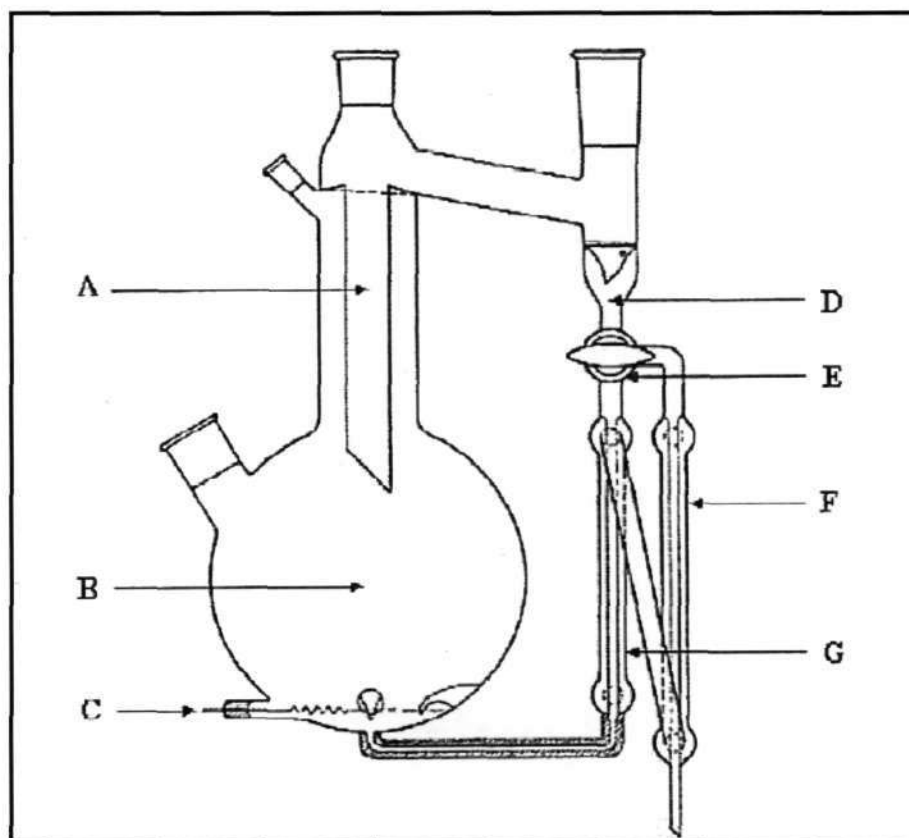
Figure 2-4: The apparatus of Smith and Bonner (1943).

A – vapour tube; **B** – boiling vessel; **C** – internal heater; **D** – condensate receiver; **E** – three way cock; **F, G** – condensers.

2.4.2 Recirculation of both Liquid and Vapour Phases

Following the work of Gillespie (1946), Thornton (1951) designed a recirculating still, using the principle of the Cottrell tube, that enabled circulation of both liquid and vapour phases for partially miscible systems. The main feature of this apparatus is the vapour insulated receiver that collects the condensate, located directly in the vapour space. The apparatus of Thornton (1951) relies exclusively on the principle of the Cottrell tube for the attainment of equilibrium. As mentioned earlier, the Cottrell tube allows short contact times and small interfacial areas, thus limiting the mass transfer between the liquid and vapour phases in the Cottrell tube (Raal and Mühlbauer, 1998).

Ellis and Garbett (1960) designed a recirculating still that enabled mixing of the liquid phase and vapour condensate by employing vibratory stirrers, thus allowing the measurement of

heterogeneous systems. The vibratory stirrers replace the Cottrell tube as the vibratory action stimulates emulsification of the two liquids. This arrangement thus enabled accurate measurement of the equilibrium temperature. However, the complexity of this apparatus and the long time taken to reach equilibrium discourages its use.

Van Zandijcke and Verhoeye (1974) proposed a design of a recirculating still based on the principle of the ebulliometer of Swietoslawski (1945), thus enabling VLE measurements for heterogeneous systems. This apparatus also employs the principle of the Cottrell tube, but allows the three phases to reach equilibrium before being sent together to the thermometer. One important advantage of this apparatus is that the vapour is not condensed, thus avoiding the difficulties associated with the separation of the two liquid phases. Van Zandijcke and Verhoeye (1974) found that mechanical mixing was unnecessary as the vapour and two liquid phases are able to rise together in the Cottrell tube. The liquid phase is not sampled with this apparatus. Rather, Van Zandijcke and Verhoeye (1974) measure LLE data at the boiling point employing another apparatus. However, like previous stills, the apparatus of Van Zandijcke and Verhoeye (1974) relies completely on the Cottrell tube for attainment of equilibrium.

Iwakabe and Kosuge (2001) found that the apparatus of Van Zandijcke and Verhoeye (1974) displayed a relatively large fluctuation of the temperature within the equilibrium chamber and also found the thermodynamic consistency of measured data to be poor. According to Gomis et al. (2000), the temperature fluctuations are due to inadequate mixing in the liquid phase and the discontinuity in the flow of the phases. Gomis et al. (2000) therefore designed a modified Gillespie (1946) type apparatus with an ultrasonic homogeniser that stirs the suspended liquid in the flask.

Iwakabe and Kosuge (2001) modified the apparatus of Van Zandijcke and Verhoeye (1974) that requires simple operation and a smaller chemical volume compared to previous stills. The apparatus also has a "built in" LLE cell, as shown in Figure 2-5. The apparatus has a shortcoming similar to previous stills as it depends solely on the Cottrell tube for the attainment of equilibrium.

Only a brief review for some of the experimental equipment and techniques on VLE, LLE and VLLE were presented in this chapter. A more detailed review of the experimental equipment and techniques for VLE, LLE and VLLE can be found in Raal and Mühlbauer (1998). An excellent review on the various experimental techniques for LLE can also be found in Novak et al. (1987).
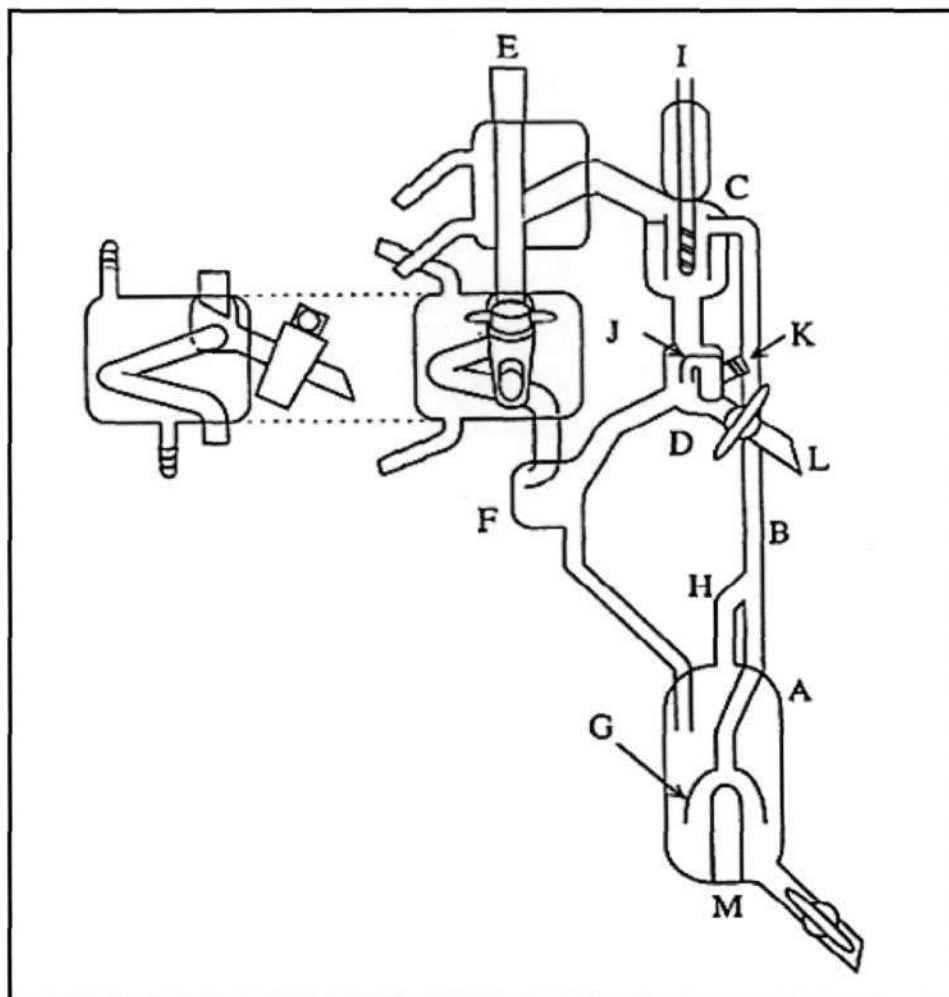
Figure 2-5: The apparatus of Iwakabe and Kosuge (2001).

A – boiling flask; **B** – Cottrell pump; **C** – equilibrium chamber; **D** – liquid collector; **E** – condenser; **F** – vapour-liquid mixing chamber; **G** – conical shaped cup; **H** – conduit for the upper liquid phase; **I** – thermometer well; **J** – LLE cell; **K** – sample port for the cell (J); **L** – sample tap for the liquid phase; **M** – electric heater.

3

CHAPTER THREE

THERMODYNAMIC FUNDAMENTALS AND PRINCIPLES

Thermodynamic properties and equations play an important role for separation processes in chemical industries. Phase equilibrium is of special interest in chemical engineering as separation processes such as distillation, extraction, leaching, adsorption and absorption, involve phase contacting. The equilibrium compositions of two phases are usually very different from one another and this difference enables one to separate mixtures by phase contacting operations (Prausnitz et al., 1999).

Many of the separation processes require multi-component phase equilibrium properties. However, phase equilibrium measurements for multi-component systems are difficult and frequently impractical. According to Raal and Mühlbauer (1998), the multi-component phase equilibrium properties can be predicted from the measurement of binary vapour-liquid equilibrium (VLE) data. Reliable ternary liquid-liquid equilibrium data (LLE) are also required to predict multi-component phase equilibrium properties for the design and evaluation of industrial units for separation processes (Vakili-Nezhaad et al., 2004). Phase equilibrium over the entire composition range depends on several variables such as temperature, pressure and the Gibbs excess energy. The theoretical treatment of binary VLE and binary/ternary LLE data

allows calculation of such variables and also enables extrapolation and interpolation to experimentally difficult conditions. Chemical thermodynamics provides the means for performing such tasks.

This chapter provides a review of the theoretical aspects and techniques of low-pressure VLE, atmospheric LLE, and low-pressure vapour-liquid-liquid equilibrium (VLLE) data correlation and analysis. The methods proposed for the evaluation of the fugacity and activity coefficients are examined. The analysis, regression and correlation of experimental data are also discussed. The review also includes the γ-Φ formulation (combined method) of VLE, the associated activity coefficient models and the modelling of VLE data using the equations of state by the Φ-Φ (direct) method. This chapter concludes with a discussion on the various thermodynamic consistency tests for VLE data. For a more detailed discussion on thermodynamic principles in the area of VLE and LLE, the following texts are recommended: Walas (1985), Prausnitz et al. (1999), Raal and Mühlbauer (1998) and Smith et al. (2001).

3.1 Fugacity and Fugacity Coefficient

According to Smith et al. (2001), equilibrium is a static condition in which no changes occur in the macroscopic properties of a system with time, and that in engineering practice, the assumption of equilibrium is justified when it leads to results of satisfactory accuracy. The criterion for phase equilibrium is given in Appendix A, where it is shown that the chemical potential (μ_i) serves as the fundamental criterion for phase equilibria. Unfortunately, the chemical potential is defined in relation to quantities that are immeasurable and for which absolute values are unknown (internal energy and entropy). Therefore, there are no absolute values for the chemical potential. However, G. N. Lewis introduced a meaningful quantity called fugacity, f_i, with units of pressure (Smith et al., 2001). Fugacity can be related to the chemical potential at constant temperature by the following equation:

$$\bar{G}_i = \Gamma_i(T) + RT \ln f_i \qquad (3\text{-}1)$$

where G_i (T) is an integration constant at temperature T and is a function of temperature only.

The partial molar Gibbs energy is given by:

$$\bar{G}_i = \left[\frac{\partial(nG)}{\partial n_i} \right]_{T,P,n_j} \qquad (3\text{-}2)$$

From the definition of chemical potential by Equation (A-6):

$$\mu_i = \bar{G}_i \tag{3-3}$$

Comparison of Equations (3-1) and (3-3) leads to the following relation of chemical potential and fugacity:

$$\mu_i = \Gamma_i(T) + RT \ln f_i \tag{3-4}$$

As the system is closed at equilibrium and all phases are at the same temperature, substitution of Equation (3-4) into Equation (A-14) results in:

$$f_i^\alpha = f_i^\beta = \ldots = f_i^\pi \tag{3-5}$$

for $i = 1, 2, \ldots, N$

For an ideal gas:

$$G_i^{ig} = \Gamma_i(T) + RT \ln P \tag{3-6}$$

where G_i (T) is the same integration constant as Equation (3-1) at temperature T and is still a function of temperature only. Introducing the theory of fugacity for a real fluid:

$$G_i = \Gamma_i(T) + RT \ln f_i \tag{3-7}$$

Subtracting Equations (3-6) and (3-7) at constant temperature and pressure yields:

$$G_i - G_i^{ig} = RT \ln \frac{f_i}{P} \tag{3-8}$$

The left-hand side of Equation (3-8) is defined as the residual Gibbs energy (G^R). The dimensionless ratio f_i/P is termed the fugacity coefficient of component i and symbolised as ϕ_i. Equations (3-6) through (3-8) are applicable to pure species. An expression equivalent to Equation (3-4) may be written for a species in solution:

$$\mu_i = \Gamma_i(T) + RT \ln \hat{f}_i \tag{3-9}$$

where $\hat{f}_i$ is the fugacity of species i in solution. Following Equation (3-5):

$$\hat{f}_i^\alpha = \hat{f}_i^\beta = \ldots = \hat{f}_i^\pi \qquad (3\text{-}10)$$

In terms of vapour-liquid equilibria, Equation (3-10) becomes:

$$\hat{f}_i^v = \hat{f}_i^l \qquad (3\text{-}11)$$

where for both equations, $i = 1, 2, \ldots, N$. The vapour and liquid phase fugacities must be related to experimental quantities such as temperature, pressure and composition to offer any significant contribution. This relation is made possible by extending the definition of the fugacity coefficient to include the fugacity coefficient of species i in solution, symbolised by $\hat{\phi}_i$, and another dimensionless function, γ_i, which is the activity coefficient of species i in solution (the activity coefficient is covered in more detail in Section 3.2). These relations are shown in Equations (3-12) and (3-13):

$$\hat{f}_i^v = y_i \hat{\phi}_i P \qquad (3\text{-}12)$$

$$\hat{f}_i^l = x_i \gamma_i f_i \qquad (3\text{-}13)$$

If a phase change from a saturated liquid to a saturated vapour at saturated pressure and constant temperature is now considered, the following relation can be concluded as a result of Equation (3-5):

$$f_i^v = f_i^l = f_i^{sat} \qquad (3\text{-}14)$$

where f_i^{sat} refers to the saturated fugacity of species i. The saturated fugacity coefficient, ϕ_i^{sat}, at saturated pressure is:

$$\phi_i^{sat} = \frac{f_i^{sat}}{P_i^{sat}} \qquad (3\text{-}15)$$

which leads to the following relation:

$$\phi_i^v = \phi_i^l = \phi_i^{sat} \qquad (3\text{-}16)$$

Differentiation of Equation (3-7) leads to:

$$dG_i = RTd \ln f_i \tag{3-17}$$

Considering the fundamental property relation for Gibbs energy, $dG = VdP - SdT$, and writing this for a particular species i in solution at constant composition and temperature results in:

$$dG_i = V_i dP \tag{3-18}$$

Eliminating dG_i by combination of Equations (3-17) and (3-18) yields:

$$d \ln f_i = \frac{V_i}{RT} dP \tag{3-19}$$

When Equation (3-19) is integrated, at constant temperature, from the initial state of a saturated liquid to the final state of a compressed liquid at pressure P the following result is obtained:

$$\ln \frac{f_i}{f_i^{sat}} = \frac{1}{RT} \int_{P_i^{sat}}^{P} V_i dP \tag{3-20}$$

where V_i represents the liquid molar volume. V_i is considered a weak function of pressure at temperatures much lower than the critical temperature, T_c. Hence V_i can be assumed approximately constant at the saturated liquid molar volume, V_i^l, when evaluating the integral in Equation (3-20), which then becomes:

$$\ln \frac{f_i}{f_i^{sat}} = \frac{V_i^l \left(P - P_i^{sat} \right)}{RT} \tag{3-21}$$

When f_i is made the subject of Equation (3-21) and combined with Equation (3-15) to eliminate f_i^{sat}, the following equation is obtained:

$$f_i = \phi_i^{sat} P_i^{sat} \exp \left[\frac{V_i^l \left(P - P_i^{sat} \right)}{RT} \right] \tag{3-22}$$

The exponential in Equation (3-22) is known as the Poynting factor, which provides the correction of the liquid phase fugacity from the vapour pressure to the system pressure. When Equations (3-12), (3-13) and (3-22) are combined, the following expression is obtained:

$$y_i \Phi_i P = x_i \gamma_i P_i^{sat} \tag{3-23}$$

where

$$\Phi_i = \frac{\hat{\phi}_i}{\phi_i^{sat}} \exp\left[\frac{-V_i^l \left(P - P_i^{sat} \right)}{RT} \right] \tag{3-24}$$

and the saturated liquid molar volume V_i^l, can be calculated from the equation proposed by Rackett (1970):

$$V_i = \left(V_c \right)_i \left(Z_c \right)_i^{\left[1 - \left(T_r \right)_i \right]^{0.2857}} \tag{3-25}$$

where Z is the compressibility factor, subscript c indicates the critical point and $\left(T_r \right)_i$ is the reduced temperature defined as $T / \left(T_c \right)_i$.

Equation (3-23) is a very useful general equation that relates liquid and vapour phases at equilibrium. In an ideal system, the vapour phase is represented by an ideal gas and the liquid phase by an ideal solution. Such a system displays the simplest possible VLE relation and is known as Raoult's Law (Smith et al., 2001). In Equation (3-24), Raoult's Law is obtained by setting Φ_i and γ_i to a value of one. According to Smith et al. (2001), the Poynting factor differs from unity by only a few parts per thousand at low to moderate pressures and thus its omission introduces negligible error. This assumption is reasonable for non-polar molecules at low pressure but becomes unacceptable for mixtures containing polar or associating molecules especially carboxylic acids (Prausnitz et al., 1980).

3.1.1 Fugacity Coefficients from the Virial Equation of State

Numerous methods are available to determine the fugacity coefficient of species in gaseous mixtures. The use of the Virial equation of state, which has its theoretical basis in statistical mechanics and represented by the Taylor series expansion, is one such method. At low to

moderate pressures, the Virial equation of state can be assumed to adequately describe the vapour phase and may be used to evaluate the fugacity coefficients. However, the application of an infinite series to practical calculations is impossible; therefore truncations of the Virial equation of state are employed where the degree of truncation is controlled by the temperature and pressure. The truncated (after the second term), generalised, pressure explicit form of the Virial equation of state, is suitable for describing the vapour phase at sub-critical temperatures and pressures up to 15 bar (Perry and Green, 1998). This equation is represented as:

$$Z = 1 + \frac{B_{virial}P}{RT} \qquad (3\text{-}26)$$

The dimensionless quantity Z is known as the compressibility factor and is defined as PV/RT. The compressibility factor is unity for an ideal gas. The symbol B_{virial}, represents the second Virial coefficient and is a function of temperature and composition (for mixtures). The composition dependence is based on statistical mechanics and is given by the following equation:

$$B_{mixture} = \sum_i \sum_j y_i y_j B_{ij} \qquad (3\text{-}27)$$

where y represents the mole fraction in a gas mixture and the indices i and j identify the species. The cross Virial coefficient B_{ij}, represents both pure components and mixture coefficients. It typifies a bimolecular interaction between species i and j and therefore $B_{ij} = B_{ji}$. When the truncated Virial equation of state is used to describe the vapour phase, the fugacity coefficient Φ_i of Equation (3-24), is modified to:

$$\Phi_i = \exp\left[\frac{\left(B_{ii} - V_i^l\right)\left(P - P_i^{sat}\right) + Py_j^2\delta_{ij}}{RT}\right] \qquad (3\text{-}28)$$

where

$$\delta_{ij} = 2B_{ij} - B_{ii} - B_{jj} \qquad (3\text{-}29)$$

The second Virial coefficient for pure components B_{ii}, and mixtures B_{ij}, can be determined by various experimental techniques. One such technique, discussed by Ramjugernath (2000), involves the calculation of volume in a high pressure VLE cell. The second Virial coefficients are made available in various compilations such as those by Dymond and Smith (1980) and

Cholinski et al. (1986). On the other hand, experimental data at desired temperatures or for species of interest are difficult if not impossible to obtain. Therefore, it became imperative that an acceptable correlation was found to enable calculation of the second Virial coefficients. Hayden and O'Connell (1975) state that values of the second Virial coefficients can be related to the equilibrium constant in a simple way, therefore if a correlation yields accurate values for such substances, it can be used for all substances. Some of the most widely used correlations are discussed below.

3.1.1.1 The Pitzer-Curl Correlation

Pitzer and Curl (1957) developed a correlation of the form:

$$\frac{B_{virial}P_c}{RT_c} = B^0 + \omega B^1 \tag{3-30}$$

where ω is a pure component constant called the acentric factor, which gives an indication of the nonsphericity of a molecule and is fully described by Pitzer et al (1955). The parameters B^0 and B^1 were found to be functions of the reduced temperature only, $T_r = T/T_c$, expressed as:

$$B^0 = 0.083 - \frac{0.422}{T_r^{1.6}} \tag{3-31}$$

and

$$B^1 = 0.139 - \frac{0.172}{T_r^{4.2}} \tag{3-32}$$

The pure component Virial coefficients are found from Equation (3-30). Prausnitz et al. (1999) later suggested a generalised equation to include the cross coefficients:

$$B_{ij} = \frac{R(T_c)_{ij}}{(P_c)_{ij}}\left(B^0 + \omega_{ij}B^1\right) \tag{3-33}$$

The cross coefficient parameters $(T_c)_{ij}$, $(P_c)_{ij}$ and ω_{ij} can be calculated from the empirical mixing rules suggested by Prausnitz et al. (1999):

$$(T_c)_{ij} = \sqrt{\left((T_c)_i - (T_c)_j\right)}(1-k_{ij}) \tag{3-34}$$

$$\left(P_c\right)_{ij} = \frac{\left(Z_c\right)_{ij} R\left(T_c\right)_{ij}}{\left(V_c\right)_{ij}}$$

(3-35)

and

$$\omega_{ij} = \frac{\omega_i + \omega_j}{2}$$

(3-36)

where

$$\left(Z_c\right)_{ij} = \frac{\left(Z_c\right)_i + \left(Z_c\right)_j}{2}$$

(3-37)

and

$$\left(V_c\right)_{ij} = \left(\frac{\left(V_c\right)_i^{1/3} + \left(V_c\right)_j^{1/3}}{2}\right)^3$$

(3-38)

The parameter k_{ij} in Equation (3-34) is an empirical binary interaction parameter. When species i and j are very similar in size and chemical nature, k_{ij} is set to a value of zero. Tarakad and Danner (1977) have provided guidelines for the estimation of k_{ij} when species i and j are not similar in size or chemical nature.

3.1.1.2 The Tsonopoulos Correlation

Tsonopoulos (1974) proposed a correlation which uses a modified form of the Pitzer-Curl (1957) correlation and is capable of calculating the second Virial coefficient for both non-polar and polar systems. For species that exhibit hydrogen bonding (like alcohols and water), two parameters are required. For non-polar gases:

$$\frac{B_{virial}P_c}{RT_c} = f^{(0)}\left(T_r\right) + \omega f^{(1)}\left(T_r\right)$$

(3-39)

where

$$f^{(0)}(T_r) = 0.1445 - \frac{0.330}{T_r} - \frac{0.1385}{T_r^2} - \frac{0.0121}{T_r^3} - \frac{0.000607}{T_r^8} \qquad (3\text{-}40)$$

and

$$f^{(1)}(T_r) = 0.0637 + \frac{0.331}{T_r^2} - \frac{0.423}{T_r^3} - \frac{0.008}{T_r^8} \qquad (3\text{-}41)$$

Polar compounds have a non-zero dipole moment. The dipole moment expresses the effect of electrostatic forces between molecules. To account for polar effects, an additional parameter is included in Equation (3-39):

$$\frac{BP_c}{RT_c} = f^{(0)}(T_r) + \omega f^{(1)}(T_r) + f^{(2)}(T_r) \qquad (3\text{-}42)$$

where

$$f^{(2)}(T_r) = \frac{a_i}{T_r^6} \qquad (3\text{-}43)$$

The effect of dimerization in hydrogen bonding compounds makes the temperature dependence of the polar effect more complex for the second Virial coefficient:

$$f^{(2)}(T_r) = \frac{a_i}{T_r^6} - \frac{b_i}{T_r^8} \qquad (3\text{-}44)$$

The parameters a_i and b_i are functions of the dipole moment and both assume positive values. They are determined by regression of experimental B_{virial} data for similar compounds.

The calculation of the second Virial cross coefficients use the same mixing rules for $\left(T_c\right)_{ij}$ and ω_{ij} as given in the Pitzer-Curl (1957) correlation. However, Tsonopoulos (1974) suggested a different mixing rule for $\left(P_c\right)_{ij}$:

$$\left(P_c\right)_{ij} = \frac{4\left(T_c\right)_{ij}\left(\left[\dfrac{\left(P_c\right)_i\left(V_c\right)_i}{\left(T_c\right)_i}\right] + \left[\dfrac{\left(P_c\right)_j\left(V_c\right)_j}{\left(T_c\right)_j}\right]\right)}{\left(\left(V_c\right)_i^{1/3} + \left(V_c\right)_j^{1/3}\right)^3} \qquad (3\text{-}59)$$

For polar/non-polar systems, it is assumed that B_{ij} has no polar term and therefore $\left(a_t\right)_{ij}$ and

$\left(b_t\right)_{ij}$ are set equal to zero. For polar/polar systems, B_{ij} is calculated by assuming that $\left(a_t\right)_{ij} = 0.5[\left(a_t\right)_i + \left(a_t\right)_j]$ and $\left(b_t\right)_{ij} = 0.5[\left(b_t\right)_i + \left(b_t\right)_j]$.

3.1.1.3 The Hayden and O'Connell Correlation

Hayden and O'Connell (1975) proposed a generalised correlation for determining the second Virial coefficients for simple and complex systems containing polar, non-polar and associating molecules. The total second Virial coefficient is considered a sum of several contributions:

$$B_{total} = B_{free} + B_{metastable} + B_{bound} + B_{chem}$$ (3-46)

where B_{free} refers to the contribution due to the interaction of molecules in which the physical forces are weak or unbound pairs of molecules, $B_{metastable}$ accounts for the *metastable* bound pairs of molecules, B_{bound} results from those compounds that have physically bound pairs of molecules and B_{chem} represents chemically bound pairs of molecules. The calculation procedure for this correlation is quite complex and will not be shown in detail here. The reader is referred to Appendix A of Prausnitz et al. (1980) for a detailed procedure.

The correlation of Hayden and O'Connell (1975) requires several basic parameters such as critical pressure P_c, critical temperature T_c, mean radius of gyration R_d, dipole moment μ_d and the association and solvation parameters η, for each compound. These parameters are made available in literature sources such as Fredunslund et al. (1977), Prausnitz et al. (1980), Reid et al. (1988) and the Dortmund Data Bank (DDB). Dipole moments are made available in McClellan (1963-1974) and can also be determined using the method proposed by Smyth (1955). The mean radius of gyration is determined using a property known as the parachor, P', calculated by the group contribution method (Reid et al., 1988). Harlacher and Braun (1970) describe the relationship between the mean radius of gyration and the parachor as:

$$P' = 50 + 7.6R_d + 13.75R_d^2$$ (3-47)

The parachor is first calculated from the group contribution method and then substituted into Equation (3-47), where the positive root indicates the value of R_d. The association and solvation parameters can be obtained from tables given by Prausnitz et al. (1980). For parameters not found in the tables, Fredunslund et al. (1977) suggested that the association and solvation

parameters for pure hydrocarbons, halogenated alkanes, ethers and sulphides should be set equal to zero and Prausnitz et al. (1980) suggested that values for a chemically similar system should be used. For interaction between components in a mixture, Hayden and O'Connell (1975) suggest that the association and solvation parameters η_{ij}, should be set equal to zero except for chemically similar components. Numerous other correlations exist for the determination of the second Virial coefficients but were not implemented in this project. These include the correlations of Black (1958), O'Connell and Prausnitz (1967), Nothnagel et al. (1973) and Tarakad and Danner (1977).

3.1.2 Fugacity Coefficients from a Cubic Equation of State

A cubic equation of state (EOS) can also be used to evaluate fugacity coefficients. The first attempt to develop a simple and generalized semi-empirical EOS that accounted for the behaviour of fluids both above and below the critical point was made by van der Waals (1873). His proposal was based on intermolecular forces and accounted for deviations from the ideal gas. However, the parameters in the van der Waals (1873) equation were not temperature dependent and this limited its application to describe highly non-ideal systems (Anderko, 1990).

3.1.2.1 The Peng-Robinson Equation of State

Many modifications were proposed to the semi-empirical relationship developed by van der Waals (1873) but the modifications developed by Redlich and Kwong (1949) and Soave (1972) were the most successful. However, according to Peng and Robinson (1976), there are still some shortcomings which the modifications of Redlich and Kwong (1949) and Soave (1972) have in common, where the most evident is the failure to generate satisfactory liquid density values. The Peng-Robinson EOS was employed for this project as it is capable of representing systems that display considerable deviations from ideality.

The Peng-Robinson EOS is given as:

$$P = \frac{RT}{V-b} - \frac{a(T)}{V(V+b)+b(V-b)} \tag{3-48}$$

The constant a is related to the intermolecular attraction force of molecules and is temperature dependent, while the constant b accounts for the molecular size of the molecule and is

considered to be temperature independent. These constants are determined from the following equations:

$$a_i(T) = a_i\{(T_c)_i\}\alpha_i\{(T_r)_i, \omega_i\}$$

(3-49)

$$b_i(T) = b_i(T_c)_i$$

(3-50)

where

$$a_i(T_c)_i = 0.45724\frac{R^2(T_c)_i^2}{(P_c)_i}$$

(3-51)

$$b_i(T_c)_i = 0.07780\frac{R(T_c)_i}{(P_c)_i}$$

(3-52)

$$\alpha_i\{(T_c)_i, \omega_i\} = \left[1 + \kappa_i\left(1 - (T_r)_i^{1/2}\right)\right]^2$$

(3-53)

The parameter κ_i, in Equation (3-53), is a constant characteristic of each substance. Peng and Robinson (1976) found a correlation of this constant with respect to the acentric factor:

$$\kappa_i = 0.37464 + 1.54226\omega_i - 0.26992\omega_i^2$$

(3-54)

To reduce the computational complexity when determining the fugacity coefficients, Equation (3-48) can be expressed in terms of the compressibility factor:

$$Z^3 - (1 - B^*)Z + \left(A^* - 3\{B^*\}^2 - 2B^*\right)Z - \left(A^*B^* - \{B^*\}^2 - \{B^*\}^3\right) = 0$$

(3-55)

where

$$A^* = \frac{a_m(T)P}{R^2T^2}$$

(3-56)

$$B^* = \frac{b_m P}{RT}$$

(3-57)

26

For a binary system, the largest root of Equation (3-55) corresponds to the vapour phase compressibility factor, whereas the smallest positive root corresponds to the liquid phase compressibility factor. The fugacity coefficient of species i for each phase is then calculated from:

$$\ln \hat{\phi}_i = \frac{b_i}{b_m}(Z-1) - \ln(Z - B^*) - \frac{A^*}{2\sqrt{2}B^*}\left(\frac{2\sum_k y_k a_{ki}}{a_m} - \frac{b_i}{b_m}\right)\ln\left[\frac{Z+\left(1+\sqrt{2}\right)B^*}{Z+\left(1-\sqrt{2}\right)B^*}\right] \qquad (3\text{-}58)$$

where a_m and b_m of Equations (3-56), (3-57) and (3-58) are obtained from mixing rules, discussed in Section 3.1.3. Peng and Robinson (1976) however, employed the following mixing rules:

$$a_m = \sum_i \sum_j x_i x_j a_{ij} \qquad (3\text{-}59)$$

$$b_m = \sum_i x_i b_i \qquad (3\text{-}60)$$

where

$$a_{ij} = \left(1 - \delta_{ij}\right)\left(a_i a_j\right)^{1/2} \qquad (3\text{-}61)$$

The parameter d_{ij} is known as the binary interaction parameter and is unique to each binary system. It should be mentioned that $d_{ij} = d_{ji}$. As mentioned previously, this parameter is found from the regression of experimental VLE data. Often, more theoretically based mixing rules are employed such as the Wong and Sandler (1992) mixing rule or the Twu-Coon (1996) mixing rule. These mixing rules provide substantial benefit in terms of both flexibility and accuracy and were thus employed for this project. They are further discussed in Section 3.1.3.

3.1.2.2 The Stryjek and Vera modified Peng-Robinson Equation of State

Stryjek and Vera (1986) modified the attractive term, $a(T)$, in the Peng-Robinson EOS by proposing a new temperature and acentric factor dependence of the attractive term. Furthermore, their modification made the Peng-Robinson EOS applicable to polar, non-polar, associating and non-associating molecules. All the equations already discussed for Peng-

Robinson EOS are applicable to the Stryjek and Vera modified Peng-Robinson EOS except Equation (3-54), which was modified as:

$$\kappa_i = \left(\kappa_0\right)_i + \left(\kappa_1\right)_i \left(1 + \left(T_r\right)_i^{0.5}\right)\left(0.7 - \left(T_r\right)_i\right)$$

(3-62)

where

$$\left(\kappa_0\right)_i = 0.378893 + 1.4897153\omega_i - 0.171131848\omega_i^2 + 0.0196554\omega_i^3$$

(3-63)

The parameter, κ_1, is an adjustable parameter that is unique to each species and is found from the regression of vapour pressure data. The same mixing rules used in the Peng-Robinson EOS were employed by Stryjek and Vera (1986). This EOS was employed for this project as the modification allows excellent prediction of vapour pressures at very low pressures for polar, non-polar, associating and non-associating compounds (Stryjek and Vera, 1986).

3.1.2.3 The Modified Alpha Correlation of Twu et al. (1991)

Twu et al. (1991) mentioned that the ability of a cubic EOS to correlate phase equilibria of mixtures depends upon the accurate prediction of pure component vapour pressures (achieved by use of a proper alpha function) and mixture properties (achieved by use of an appropriate mixing rule). Therefore, they modified the alpha function to improve the accuracy of vapour pressures for both low and extremely high boiling components:

$$\alpha_i\left(T_r\right)_i = \left(T_r\right)_i^{N'\left(M'-1\right)} e^{L'\left(1 - \left(T_r\right)_i^{N'M'}\right)}$$

(3-64)

where L', M' and N' are parameters that are unique to each component and are determined from the regression of experimental vapour pressure data. This modified alpha function has the advantage of being applicable to any cubic EOS. The modified alpha correlation of Twu et al. (1991) was chosen for this project as it represents both low and high boiling point components. It was employed in the Peng-Robinson EOS and therefore the same expressions developed for Peng-Robinson EOS were used for phase equilibrium calculations.

3.1.3 Mixing Rules for Cubic Equations of State

The representation of phase equilibria of mixtures when using equations of state is carried out with mixing rules. The mixing rules in an EOS characterises the interaction of molecules in a mixture. The simplest mixing rules, employed by Peng and Robinson (1976) and Stryjek and Vera (1986), are known as the van der Waals one-fluid-theory classical mixing rules and were shown in Equations (3-59) to (3-61). Over the years, many mixing rules have been developed with most of them being empirical in nature. A detailed review of the mixing rules available is presented by Raal and Mühlbauer (1998). It should be noted that the extrapolation of many mixing rules to multi-component mixtures is incoherent due to the invariance problem and the dilution effect (Hernández-Gaduza et al., 2001). These shortcomings were observed by Michelsen and Kistenmacher (1990) and are commonly known as the Michelsen-Kistenmacher-Syndrome. Therefore, two mixing rules that do not suffer the Michelsen-Kistenmacher-Syndrome were selected and used for this project: the mixing rules of Wong and Sandler (1992) and Twu and Coon (1996).

3.1.3.1 The Wong-Sandler Mixing Rule

Wong and Sandler (1992) developed a theoretically correct density-independent mixing rule for cubic equations of state that could accurately correlate VLE data. According to Wong and Sandler (1992), the mixing rule is applicable to both simple and complex systems comprised of polar and associating species. This mixing rule requires an activity coefficient model (discussed in Section 3.2.1) to calculate the excess Helmholtz free energy (a useful thermodynamic property like the excess Gibbs free energy). The correct use of the Helmholtz free energy at infinite pressure in this mixing rule provides the correct low and high densities without being density dependent. The mixing rule also provides quadratic composition dependence for the second Virial coefficients which is consistent with statistical mechanics (Wong and Sandler, 1992).

The mixing rule of Wong and Sandler (1992) states the mixture parameters a_m and b_m as:

$$\frac{a_m}{RT} = \frac{QD}{(1-D)} \tag{3-65}$$

$$b_m = \frac{Q}{(1-D)} \tag{3-66}$$

where Q and D are defined as:

$$Q = \sum_i \sum_j x_i x_j \left(b - \frac{a}{RT} \right)_{ij}$$

(3-67)

$$D = \sum_i x_i \frac{a_i}{b_i RT} + \frac{A_\infty^E}{cRT}$$

(3-68)

and A_∞^E is the excess Helmholtz free energy calculated at infinite pressure. The partial derivatives of a_m and b_m with respect to the number of moles are needed to evaluate the fugacity coefficients obtained from an EOS:

$$\frac{1}{RT} \left(\frac{1}{n} \frac{\partial n^2 a_m}{\partial n_i} \right) = D \frac{\partial n b_m}{\partial n_i} + b_m \frac{\partial n D}{\partial n_i}$$

(3-69)

$$\frac{\partial n b_m}{\partial n_i} = \frac{1}{(1-D)} \left(\frac{1}{n} \frac{\partial n^2 Q}{\partial n_i} \right) - \frac{Q}{(1-D)^2} \left(1 - \frac{\partial n D}{\partial n_i} \right)$$

(3-70)

with the corresponding partial derivatives of Q and D given by:

$$\left(\frac{1}{n} \frac{\partial n^2 Q}{\partial n_i} \right) = 2 \sum_j x_j \left(b - \frac{a}{RT} \right)_{ij}$$

(3-71)

$$\frac{\partial n D}{\partial n_i} = \frac{a_i}{b_i RT} + \frac{\ln \gamma_i^\infty}{c}$$

(3-72)

and

$$\ln \gamma_i^\infty = \frac{1}{RT} \frac{\partial n A_\infty^E}{\partial n_i}$$

(3-73)

$$c = \frac{1}{\sqrt{2}} \ln \left(\sqrt{2} - 1 \right)$$

(3-74)

According to Wong and Sandler (1992), the excess Helmholtz free energy has the advantage of being much less pressure dependent than the excess Gibbs free energy, and hence, the correct behaviour is obtained at both low and infinite pressure. For this project, the NRTL activity

30

coefficient model (discussed in Section 3.2.1.2) was used to describe the excess Helmholtz free energy at infinite pressure and the infinite dilution activity coefficients, $\ln \gamma_i^\infty$:

$$\frac{A_\infty^E}{RT} = \sum_i x_i \left(\frac{\sum_j x_j \tau_{ji} g_{ji}}{\sum_k x_k g_{ki}} \right) \qquad (3\text{-}75)$$

$$\ln \gamma_i^\infty = \frac{\sum_j x_j \tau_{ji} g_{ji}}{\sum_k x_k g_{ki}} + \sum_j \frac{x_j g_{ij}}{\sum_k x_k g_{kj}} \left(\tau_{ij} - \frac{\sum_l x_l \tau_{lj} g_{lj}}{\sum_k x_k g_{kj}} \right) \qquad (3\text{-}76)$$

The following equation is used to assist in the calculation of Equation (3-67):

$$\left(b - \frac{a}{RT} \right)_{ij} = \frac{\left(b_i - \dfrac{a_i}{RT} \right) + \left(b_j - \dfrac{a_j}{RT} \right)}{2} \left(1 - k_{ij} \right) \qquad (3\text{-}77)$$

The binary interaction parameter, k_{ij}, is obtained from the regression of binary experimental VLE data.

3.1.3.2 The Twu-Coon Mixing Rule

Twu and Coon (1996) developed new mixing rules that depended only on composition and temperature. According to Twu and Coon (1996), the new mixing rules were developed for cubic equations of state and were successfully applied to complex mixtures. Twu and Coon (1996) also state that the new mixing rules are more flexible than the Wong-Sandler mixing rules, and reduce to the classical van der Waals mixing rules, when the parameters in the non-random excess Helmholtz free energy are set to value of zero.

The mixture parameters a_m and b_m according to the mixing rule of Twu and Coon (1996) are:

$$a_m = b_m \left(\frac{a_{vdw}}{b_{vdw}} + \frac{1}{c} \frac{A_\infty^E}{RT} \right) \qquad (3\text{-}78)$$

$$b_m = \frac{b_{vdw} - a_{vdw}}{1 - \left(\dfrac{a_{vdw}}{b_{vdw}} + \dfrac{1}{c} \dfrac{A_\infty^E}{RT} \right)} \tag{3-79}$$

where a_{vdw} and b_{vdw} are the a and b parameters from an EOS evaluated using the classical van der Waals mixing rules:

$$a_{vdw} = \sum_i \sum_j x_i x_j \sqrt{a_i a_j} \left(1 - k_{ij}\right) \tag{3-80}$$

$$b_{vdw} = \sum_i \sum_j x_i x_j \left[\frac{1}{2}(b_i + b_j)\right]\left(1 - l_{ij}\right) \tag{3-81}$$

Since Q and D are defined differently for the Twu-Coon mixing rules, the partial derivatives of a and b also differ:

$$\frac{1}{na}\left(\frac{\partial n^2 a}{\partial n_i}\right) = \frac{1}{b}\left(\frac{\partial nb}{\partial n_i}\right) + \frac{1}{D}\left(\frac{\partial nD}{\partial n_i}\right) \tag{3-82}$$

$$\frac{1}{b}\left(\frac{\partial nb}{\partial n_i}\right) = \frac{1}{Q}\left[\frac{1}{n}\left(\frac{\partial n^2 Q}{\partial n_i}\right)\right] - \frac{1}{1-D}\left[1 - \left(\frac{\partial nD}{\partial n_i}\right)\right] \tag{3-83}$$

with Q and D defined as:

$$Q = b_{vdw} - \frac{a_{vdw}}{RT} \tag{3-84}$$

$$D = \frac{a_{vdw}}{b_{vdw}} + \frac{1}{c}\frac{A_\infty^E}{RT} \tag{3-85}$$

and the partial derivatives of Q and D are:

$$\left(\frac{\partial nD}{\partial n_i}\right) = \frac{a_{vdw}}{b_{vdw}}\left(\left[\frac{1}{na_{vdw}}\left(\frac{\partial n^2 a_{vdw}}{\partial n_i}\right)\right] - \left[\frac{1}{b_{vdw}}\left(\frac{\partial nb_{vdw}}{\partial n_i}\right)\right]\right) + \frac{1}{c}\ln \gamma_i^\infty \tag{3-86}$$

$$\frac{1}{Q}\left[\frac{1}{n}\left(\frac{\partial n^2 Q}{\partial n_i}\right)\right] = \frac{2\sum_j x_j \left(b_{ij} - a_{ij}\right)}{\sum_i \sum_j x_i x_j \left(b_{ij} - a_{ij}\right)} \qquad (3\text{-}87)$$

The partial derivatives of a_{vdw} and b_{vdw} are given by:

$$\frac{1}{na_{vdw}}\left(\frac{\partial n^2 a_{vdw}}{\partial n_i}\right) = \frac{2}{a_{vdw}}\sum_j x_j a_{ij} \qquad (3\text{-}88)$$

$$\frac{1}{b_{vdw}}\left(\frac{\partial n b_{vdw}}{\partial n_i}\right) = \frac{2}{b_{vdw}}\sum_j x_j b_{ij} - 1 \qquad (3\text{-}89)$$

The constant c is the same constant used in the mixing rule of Wong and Sandler (1992), already given in Equation (3-74). The NRTL activity coefficient model was also used to describe the excess Helmholtz free energy, A_∞^E, and the infinite dilute activity coefficients, $\ln \gamma_i^\infty$. Therefore, Equations (3-75) and (3-76) are also applicable to the Twu-Coon mixing rules. The cross parameters a_{ij} and b_{ij} are calculated from:

$$a_{ij} = \sqrt{a_i a_j}\left(1 - k_{ij}\right) \qquad (3\text{-}90)$$

$$b_{ij} = \frac{1}{2}\left(b_i + b_j\right)\left(1 - l_{ij}\right) \qquad (3\text{-}91)$$

As seen from Equations (3-90) and (3-91), the mixing rule of Twu and Coon (1996) has two binary interaction parameters, k_{ij} and l_{ij}. These parameters are also found from the regression of binary experimental VLE data.

3.2 Activity and Activity Coefficient

In Section 3.1, the liquid phase activity coefficient was introduced as a factor to account for the liquid phase non-idealities. The activity coefficient is completely defined if the standard-state fugacity is specified (Prausnitz et al., 1980). The standard-state fugacity of species i is taken as the fugacity of species i at the same temperature as that of the mixture and at some specified condition of pressure and composition. To obtain some physical sense of the activity coefficient, Gess et al. (1991) mention that the concept of excess properties must be introduced. Excess properties are defined as the difference between the actual property value of a solution

and the value it would have as an ideal solution at the same pressure, temperature and composition. The activity coefficient for species i is given as:

$$\gamma_i = \frac{\hat{f}_i}{x_i f_i} \qquad (3\text{-}92)$$

and may also be expressed in terms of the Gibbs energy as:

$$\bar{G}_i = \Gamma_i(T) + RT \ln \hat{f}_i \qquad (3\text{-}93)$$

The Lewis/Randall rule can be used to represent ideal solution behaviour:

$$\hat{f}_i^{id} = x_i f_i \qquad (3\text{-}94)$$

For an ideal solution, Equation (3-93) becomes:

$$\bar{G}_i^{id} = \Gamma_i(T) + RT \ln x_i f_i \qquad (3\text{-}95)$$

When Equation (3-95) is subtracted from Equation (3-93), an equation expressing the partial molar Gibbs energy results:

$$\bar{G}_i^E = RT \ln \gamma_i \qquad (3\text{-}96)$$

The fundamental excess-property relation was derived by Van Ness (1959) to show the inter-relation and significance of various excess thermodynamic properties:

$$d\left(\frac{nG^E}{RT}\right) = \frac{nV^E}{RT} dP - \frac{nH^E}{RT^2} dT + \sum_i \frac{\bar{G}_i^E}{RT} dn_i \qquad (3\text{-}97)$$

When Equations (3-96) and (3-97) are combined, an alternative form of the fundamental excess-property relation, in terms of the activity coefficient, is obtained:

$$d\left(\frac{nG^E}{RT}\right) = \frac{nV^E}{RT} dP - \frac{nH^E}{RT^2} dT + \sum_i \ln \gamma_i dn_i \qquad (3\text{-}98)$$

By inspection, Equations (3-97) and (3-98) show that:

$$\ln \gamma_i = \left[\frac{\partial \left(nG^E / RT \right)}{\partial n_i} \right]_{P,T,n_j} \tag{3-99}$$

Using the properties of a partial molar quantity, the following equations hold for a binary mixture:

$$\ln \gamma_1 = \frac{G^E}{RT} + \frac{x_2 d \left(G^E / RT \right)}{dx_1} \tag{3-100}$$

$$\ln \gamma_2 = \frac{G^E}{RT} + \frac{x_1 d \left(G^E / RT \right)}{dx_2} \tag{3-101}$$

Since $\ln \gamma_i$ is a partial molar property with respect to G^E / RT :

$$\frac{G^E}{RT} = \sum_i x_i \ln \gamma_i \tag{3-102}$$

The excess property equations are quite useful as V^E, H^E and γ_i may all be accessed experimentally. It can be also be seen that the molar excess Gibbs energy is a function of measurable system properties; pressure, temperature and composition. The Gibbs-Duhem equation also relates excess properties to the activity coefficient and is expressed as:

$$\sum_i x_i d \ln \gamma_i = \frac{\bar{V}_i^E}{RT} dP - \frac{\bar{H}_i^E}{RT^2} dT \tag{3-103}$$

At constant temperature and pressure, Equation (3-103) becomes:

$$\sum_i x_i d \ln \gamma_i = 0 \tag{3-104}$$

The Gibbs-Duhem equation finds an important application in thermodynamic consistency testing of VLE data (refer to Section 3.6).

3.2.1 Liquid Phase Activity Coefficient Models

Activity coefficients can be evaluated using liquid phase activity coefficient models, which are independent of the vapour composition. According to Walas (1985), many equations have been developed for the correlation of activity coefficients with the liquid phase compositions and temperature. The liquid phase compositions are usually expressed in mole fractions, volume fractions or molecular surface fractions. The volume or molecular surface fractions are preferable when the molecules differ substantially in size or chemical nature. Some of the well-known models of activity coefficients include: the Wilson, NRTL (Non-Random Two Liquid) and the modified UNIQUAC (UNIversal QUAsi-Chemical) model. These models were employed in this project and are discussed below. In all of these mathematical models, the molar excess Gibbs energy is expressed as a function of the liquid mole fraction. The activity coefficients are then calculated for each component with the aid of Equation (3-99).

3.2.1.1 The Wilson Equation

Wilson (1964) developed a model based on the concept of local composition, which occur within a liquid solution. Local compositions are different from the overall mixture composition and according to Smith et al. (2001) are presumed to account for short-range order and non-random molecular orientations that result from differences in molecular size and intermolecular forces. According to Prausnitz et al. (1999), the Wilson equation appears to provide a good representation for a variety of miscible mixtures and is particularly useful for solutions of polar or associating components in non-polar solvents. Furthermore, the Wilson equation can be readily generalised to multi-component systems without introducing parameters other than for the constituent binaries. Raal and Mühlbauer (1998), on the other hand, note that the Wilson equation has two disadvantages. Firstly, the equation cannot predict liquid miscibility. Secondly, the equation is inappropriate for systems in which the natural logarithms of the activity coefficient, when plotted against the liquid mole fraction, show a maximum or minimum. Due to these shortcomings, many modifications were proposed to improve the Wilson equation. One such modification, proposed by Tsuboka and Katayama (1975) and well-known as the T-K-Wilson equation, allows satisfactory prediction of systems that exhibit partial miscibility. The Wilson expression for the excess Gibbs energy for a system consisting of m components is:

$$\frac{G^E}{RT} = -\sum_{i=1}^{m} x_i \ln\left(\sum_{j=1}^{m} x_j \Lambda_{ij}\right)$$

(3-105)

where Λ_{ij} and Λ_{ji} are the adjustable Wilson parameters which are related to the pure component liquid volumes by:

$$\Lambda_{ij} = \frac{V_j}{V_i}\exp\left[-\frac{\lambda_{ij}-\lambda_{ii}}{RT}\right]$$
(3-106)

$$\Lambda_{ji} = \frac{V_i}{V_j}\exp\left[-\frac{\lambda_{ji}-\lambda_{jj}}{RT}\right]$$
(3-107)

The activity coefficient for any component k is given by:

$$\ln\gamma_k = -\ln\left(\sum_{j=1}^{m}x_j\Lambda_{kj}\right)+1-\sum_{i=1}^{m}\frac{x_i\Lambda_{ik}}{\sum_{j=1}^{m}x_j\Lambda_{ij}}$$
(3-108)

The parameters $(\lambda_{ij}-\lambda_{ii})$ and $(\lambda_{ji}-\lambda_{jj})$ characterise the molecular interactions between the species i and j. Equations (3-106) and (3-107) show the approximate temperature dependence of the adjustable parameters.

3.2.1.2 The NRTL (Non-Random Two Liquid) Equation

Renon and Prausnitz (1968) proposed an improved local composition model, known as the Non-Random Two Liquid (NRTL) equation, which was based on the two-liquid model of Scott (1956) and an assumption of non-randomness similar to that used by Wilson (1964). This equation has a major advantage over the Wilson (1964) equation as it is capable of predicting both partially miscible and completely miscible systems. According to Raal and Mühlbauer (1998), the NRTL equation is suitable for highly non-ideal systems and is readily generalised to multi-component systems. The NRTL equation for a system consisting of m components is expressed as:

$$\frac{G^E}{RT} = \sum_{i=1}^{m}x_i\frac{\sum_{j=1}^{m}\tau_{ji}G_{ji}x_j}{\sum_{l=1}^{m}G_{li}x_l}$$
(3-109)

where

$$G_{ij} = \exp\left(-\alpha_{ij}\tau_{ij}\right)$$

(3-110)

$$\tau_{ij} = \frac{g_{ij} - g_{jj}}{RT}$$

(3-111)

The activity coefficient for any component i is given by:

$$\ln\gamma_i = \frac{\sum\limits_{j=1}^{m}\tau_{ji}G_{ji}x_j}{\sum\limits_{l=1}^{m}G_{li}x_l} + \sum\limits_{j=1}^{m}\frac{x_jG_{ij}}{\sum\limits_{l=1}^{m}G_{lj}x_l}\left(\tau_{ij} - \frac{\sum\limits_{r=1}^{m}x_r\tau_{rj}G_{rj}}{\sum\limits_{l=1}^{m}G_{lj}x_l}\right)$$

(3-112)

As seen in the above equations, the NRTL equation consists of the following parameters: $(g_{ij}\text{-}g_{jj})$, $(g_{ji}\text{-}g_{ii})$ and a_{ij}. The $(g_{ij}\text{-}g_{jj})$ and $(g_{ji}\text{-}g_{ii})$ parameters represent the interaction between species i and j. The parameter a_{ij} is a constant that is characteristic of the randomness of the mixture, where a value of zero indicates that the mixture is completely random. In their publication, Renon and Prausnitz (1968) note that $a_{ij} = a_{ji}$ and they also provide guidelines for suitable values of a_{ij}. However, many authors have found that these values can be used out of the limitations suggested by Renon and Prausnitz (1968) to give better predictions. It has thus become accepted that suitable values for a_{ij} fall in the range of -1 to 0.5, since the activity coefficients are relatively insensitive to values of a_{ij} within this range. According to Walas (1985), the value of a_{ij} should be approximately 0.3 for non-aqueous mixtures and approximately 0.4 for aqueous organic systems. However, Raal and Muhlbauer (1998) have found these suggestions to be inconclusive and mention that a suitable value for a_{ij} should be found from the reduction of experimental data.

3.2.1.3 The Modified UNIQUAC (UNIversal QUasi-Chemical) Equation

The original UNIQUAC equation was developed by Abrams and Prausnitz (1975) who incorporated the two-liquid model and the theory of local composition. The UNIQUAC equation consists of two parts: a combinatorial part that takes into account the differences in sizes and shapes of the molecules and the residual part that is due to the intermolecular forces between the molecules. In the form of an equation, this is represented as:

$$\frac{G^E}{RT} = \left(\frac{G^E}{RT}\right)_{combinatorial} + \left(\frac{G^E}{RT}\right)_{residual}$$

(3-113)

Anderson and Prausnitz (1978) modified the UNIQUAC equation to obtain better agreement for systems containing water or lower alcohols. Similar to the NRTL equation, the modified UNIQUAC equation may also be readily extended to represent multi-component mixtures. For a system consisting of m components, the two parts of the Gibbs excess energy of the modified UNIQUAC equation, as given by Prausnitz et al. (1999), are:

$$\left(\frac{G^E}{RT}\right)_{combinatorial} = \sum_{i=1}^{m} x_i \ln \frac{\Phi_i^*}{x_i} + \frac{z}{2}\sum_{i=1}^{m} q_i x_i \ln \frac{\theta_i}{\Phi_i^*} \qquad (3\text{-}114)$$

$$\left(\frac{G^E}{RT}\right)_{residual} = -\sum_{i=1}^{m} q_i' x_i \ln \left(\sum_{j=1}^{m} \theta_j' \tau_{ji}\right) \qquad (3\text{-}115)$$

where z is the co-ordination number that is usually set equal to a value of ten. The segment fraction, Φ^*, and the area fractions, θ and θ', are given by:

$$\Phi_i^* = \frac{r_i x_i}{\sum_{j=1}^{m} r_j x_j} \qquad (3\text{-}116)$$

$$\theta_i = \frac{q_j x_j}{\sum_{j=1}^{m} q_j x_j} \qquad (3\text{-}117)$$

$$\theta_i' = \frac{q_i' x_i}{\sum_{j=1}^{m} q_j' x_j} \qquad (3\text{-}118)$$

The parameter r is a pure component molecular structure constant that accounts for the size of the molecules. The parameters q and q' are also pure component molecular structure constants and they account for the external surface area of the molecules, where q' was introduced by Anderson and Prausnitz [1978] to obtain better agreement for systems containing water or lower alcohols. It should be noted that in the original formulation of the UNIQUAC equation, $q = q'$. All these pure component molecular structure parameters are evaluated from molecular structure contributions for various groups and subgroups and are outlined in Raal and Mühlbauer (1998).

The adjustable parameters, t_{ij}, are related to the characteristic energies (u_{ij}-u_{jj}) by:

$$\tau_{ij} = \exp\left(-\left[\frac{u_{ij} - u_{jj}}{RT}\right]\right)$$

(3-119)

The activity coefficient for any component i is given by:

$$\ln \gamma_i = \ln \gamma_i^C + \ln \gamma_i^R$$

(3-120)

$$\ln \gamma_i^C = \ln \frac{\Phi_i}{x_i} + \frac{z}{2} q_i \ln \frac{\theta_i}{\Phi_i} + l_i - \frac{\Phi_i}{x_i} \sum_{j=1}^{m} x_j l_j$$

(3-121)

$$\ln \gamma_i^R = -q_i' \ln \left(\sum_{j=1}^{m} \theta_j' \tau_{ji} \right) + q_i' - q_i' \sum_{j=1}^{m} \frac{\theta_j' \tau_{ij}}{\sum_{k=1}^{m} \theta_k' \tau_{kj}}$$

(3-122)

where

$$l_i = \frac{z}{2}(r_i - q_i) - (r_i - 1)$$

(3-123)

The UNIQUAC equation is applicable to a wide variety of non-electrolyte liquid mixtures containing polar or non-polar fluids that also includes partially miscible mixtures. The main shortcomings of this equation are its algebraic complexity and the need for pure component structural parameters. For this project, only the modified UNIQUAC equation was considered.

3.3 Vapour-Liquid Equilibrium (VLE)

Phase diagrams are frequently used to summarise VLE data. The most well-known phase diagrams include T-x-y, P-x-y and x-y plots. The VLE behaviour of binary systems can be loosely classified as belonging to one of five types (Raal and Mühlbauer, 1998). Type I classifies systems for which all compositions have boiling points between those of the pure substances or more commonly known as the intermediate-boiling systems. Types II and III classify systems which contain homogeneous azeotropes; type II describes minimum boiling homogenous azeotropes and type III describes maximum boiling homogenous azeotropes. An azeotrope is a term used to describe a state in which the vapour composition is exactly the same as the liquid composition. Separation at the azeotrope is not possible by conventional distillation. Gmehling and Onken (1977-1982) provide a compilation of data for such states. Type IV contains systems with partially miscible liquid phases and a single heterogeneous

azeotrope. The azeotropic temperature provides a sub-classification to type *IV*; (a) the azeotropic temperature is below the pure component boiling temperatures or (b) the azeotropic temperature is intermediate between the pure component boiling temperatures. Type *V* classifies systems with partial liquid miscibility and both a homogeneous and heterogeneous azeotrope. The first three types are most commonly encountered and are displayed in Figure 3-1.
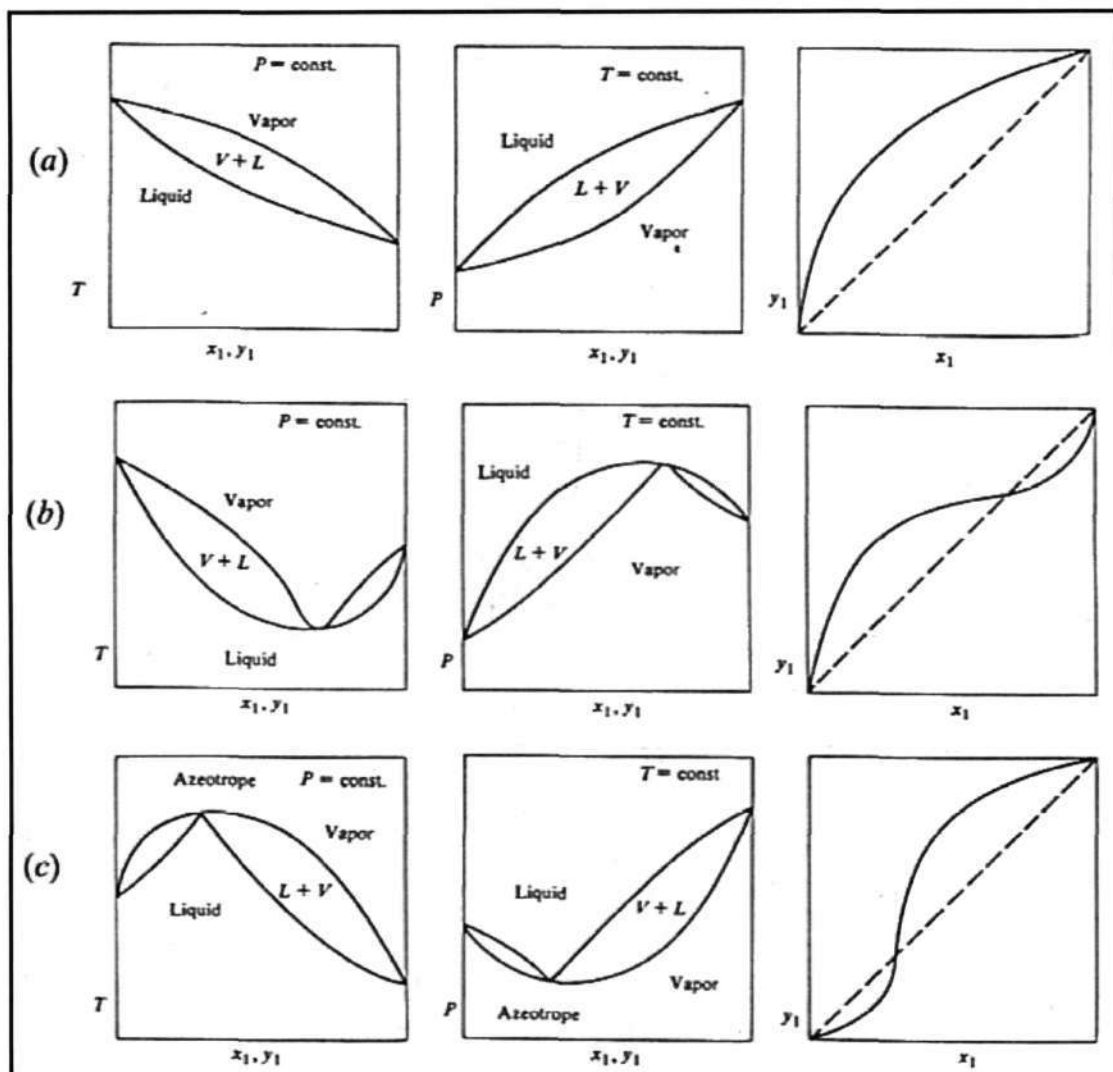
Figure 3-1: Common types of binary *T-x-y*, *P-x-y* and *x-y* phase equilibrium diagrams: *(a)* intermediate-boiling systems; *(b)* systems displaying a minimum boiling azeotrope; *(c)* systems displaying a maximum boiling azeotrope (Raal and Muhlbauer, 1998).

41

3.3.1 Low Pressure VLE Data Regression

Design methods for separation processes require quantitative estimates of fluid phase equilibria. Sometimes, phase equilibrium data are available and these estimates can be found without much effort. Unfortunately, in many cases the required equilibrium data are not available and it becomes quite difficult to make rough estimates on a rational basis. Therefore, predictive models (such as cubic equations of state with mixing rules or liquid phase activity coefficient models) have been developed to help alleviate this common problem in the design of chemical processes. The equilibrium data are often correlated to these models to yield a set of parameters that are specific to each system studied and the model employed. These model parameters are quite important as they also allow prediction of equilibrium data at experimentally difficult conditions.

There are different methods available for the regression of isothermal and isobaric VLE data. However, only the two well-known methods were used to study the VLE data measured for this project. The first method is known as the γ-Φ formulation of VLE or more commonly known as the combined method, while the second method is known as the Φ-Φ method or the direct method. The combined method uses an equation of state (like the Virial equation of state used for this project) to calculate the fugacity coefficients that describe the vapour phase non-idealities, while an activity coefficient model is used to calculate the activity coefficients that describe the liquid phase non-idealities. In the direct method, the fugacity coefficients are used to describe the non-idealities in both the vapour and liquid phases and are calculated using an equation of state (such as a cubic equation of state employed in this project).

There are different calculation procedures for each method which depend on the nature of the VLE data. For isothermal VLE data, the pressure and vapour composition are calculated (bubble point pressure computation), whereas for isobaric VLE data, the temperature and vapour composition are calculated (bubble point temperature computation) for each experimental point. Therefore, a set of data points comprising of P-x values at a specified temperature or T-x values at a specified pressure are sufficient to allow determination of the activity coefficient model parameters. However, Smith et al. (2001) encourages the measurement of the vapour phase mole fractions to allow thermodynamic consistency testing, which is discussed in Section 3.6. It should be noted that the activity coefficient model parameters are temperature dependent (Walas, 1985). The data reduction for isothermal VLE data is simple as the temperature dependence of the model parameters can be considered insignificant and thus the model parameters can be treated as constants. However, the temperature dependence of the model parameters is significant for the reduction of isobaric

VLE data and must therefore be taken into account. The combined method and the direct method are discussed in greater detail below.

3.3.1.1 The Combined (γ-Φ) Method

As mentioned earlier, this method relies upon liquid phase activity coefficient models to represent VLE data. These models have been proposed to correlate the activity coefficients from a relationship of the molar excess Gibbs energy, the liquid composition and temperature, with the liquid composition expressed as a mole fraction (x_i). Usually, more than one model is used for VLE data regression, as one can determine which model provides a better fit of the experimental data for a particular system. In this project, the three most well-known models were used: the Wilson, NRTL and modified UNIQUAC models.

In order to obtain the model parameters, a suitable algorithm must be used for VLE regression. The following steps are used for the regression of an isothermal set of experimental binary VLE data using the combined method:

1. The temperature, liquid phase compositions and the pure component properties are used as inputs for the regression. A suitable expression for the excess Gibbs energy, as a function of composition, is then selected.

2. The parameters corresponding to the G^E expression from step 1 are assigned with reasonable estimates. The activity coefficients that correspond to the G^E expression from step 1 are then determined from Equations (3-100) and (3-101). The vapour phase is initially assumed ideal and therefore the fugacity coefficients (Φ_i) are initially set to unity to allow an initial calculation of the overall system pressure. The saturated pressures (P_i^{sat}) are then evaluated from a suitable vapour pressure correlation (such as the Antoine equation).

3. According to the law of mass conservation, $Sx_i = Sy_i = 1$. The overall system pressure is therefore obtained from the manipulation of Equation (3-23) as:

$$P = \frac{x_1\gamma_1 P_1^{sat}}{\Phi_1} + \frac{x_2\gamma_2 P_2^{sat}}{\Phi_2} \tag{3-124}$$

4. The vapour mole fractions are then found from:

$$y_i = \frac{x_i \gamma_i P_i^{sat}}{\Phi_i P} \qquad\qquad (3\text{-}125)$$

5. Once the vapour mole fractions have been calculated, the fugacity coefficients are then evaluated from Equation (3-28) using a suitable correlation for the second Virial coefficients (as discussed in Section 3.1.1). The system pressure is then recalculated using Equation (3-124). The model parameters are then optimised by employing a regression technique with a suitable objective function that yields the best fit to the experimental P-x data for the entire composition range.

The regression procedure outlined above is the same for isobaric data with the exception that the temperature is not constant and its variations must be taken into account. The regression technique employed in the fifth step above requires an objective function. For this work, the minimisation of the sum of the squares of the differences between the calculated and measured pressures was employed in the determination of the model parameters:

$$S = \sum(\delta P)^2 \qquad\qquad (3\text{-}126)$$

where the difference between the model and experimental values is commonly termed a residual and symbolised as d. Other objective functions may also be used such as dy_1, $\delta\gamma_1$, $\delta\gamma_2$ and $d(G^E/RT)$. However, according to Van Ness et al. (1978), Equation (3-126) is at least as good as any other and is the most simplest and direct objective function. Furthermore, Van Ness and Abbott (1982) state that the objective function of Equation (3-126) is successful in reducing isothermal VLE data and may even be superior to any other maximum likelihood method. Van Ness and Abbott (1982) also mention that replacing the pressure with temperature in Equation (3-126), provides the best objective function for regressing isobaric VLE data. Therefore Equation (3-126) was chosen as the objective function for regressing isothermal VLE data measured in this project. Marquardt (1963) and Gess et al. (1991) have developed methods that use the objective function of Equation (3-126) in the above mentioned algorithm. However, computer software programmes such as MATLAB (employed in this project) have built in functions that allow such calculations to be performed with much ease. The regression procedure for isobaric and isothermal data are summarised in Figures 3.2 and 3.3 respectively.

Read T, x_1 and pure component properties. Set a tolerance, e, for the objective function.

Set all $\Phi_i = 1$ for initial iteration. Evaluate P_i^{sat} and y_i

Calculate the overall pressure, P, from Equation (3-124).

Display the system pressure, P, and the set of y_i values

Yes

Is $dP < e$?

No

Calculate the set of y_i values from Equation (3-125) and evaluate the set of Φ_i values from Equation (3-28)

Recalculate the overall pressure, P

Figure 3-2: Flow diagram for the bubble point pressure iteration for the combined method (Smith et al., 2001).

Read P, x_1 and pure component properties. Set a tolerance, e, for the objective function.

Display the system temperature, T, and the set of y_i values

Set all $\Phi_i = 1$ for initial iteration. Evaluate T_i^{sat}

Calculate T from
$$T = \sum_i x_i T_i^{sat}$$

Yes

No   Is $dT < e$?

Evaluate P_i^{sat} and γ_i.
Evaluate P_j^{sat} from
$$P_j^{sat} = \frac{P}{\sum_i (x_i \gamma_i / \Phi_i)(P_i^{sat} / P_j^{sat})}$$
Find T using P_j^{sat}

Recalculate the overall temperature, T

Evaluate P_i^{sat} and the set of y_i values

Re-evaluate Φ_i and γ_i and evaluate P_j^{sat} again to find T

Figure 3-3: Flow diagram for the bubble point temperature iteration for the combined method (Smith et al., 2001).

46

3.3.1.2 The Direct (Φ-Φ) Method

The direct method is an alternative to the combined method for the modelling of low pressure VLE (Perry and Green, 1998). This method uses an equation of state (EOS) to represent both the vapour and liquid non-idealities by use of the fugacity coefficients. From Equation (3-11), one obtains:

$$\hat{f}_i^l = x_i\hat{\phi}_i^l = \hat{f}_i^v = y_i\hat{\phi}_i^v \tag{3-127}$$

The fugacity coefficients are obtained from:

$$\ln\hat{\phi}_i^l = \left(\frac{1}{RT}\right)\int_{V^l}^{\infty}\left[\left(\frac{\partial P}{\partial n_i}\right)_{T,V,n_j} - \frac{RT}{V^l}\right]dV - \ln\left[\frac{PV^l}{n_T RT}\right] \tag{3-128}$$

$$\ln\hat{\phi}_i^v = \left(\frac{1}{RT}\right)\int_{V^v}^{\infty}\left[\left(\frac{\partial P}{\partial n_i}\right)_{T,V,n_j} - \frac{RT}{V^v}\right]dV - \ln\left[\frac{PV^v}{n_T RT}\right] \tag{3-129}$$

where n_T refers to the total number of moles in the system and the terms within the integral and the natural logarithm are evaluated using a suitable EOS. The equilibrium ratio, K_i, is defined as the ratio of the vapour composition to the liquid composition and often used to simplify calculations when using the direct method. From Equation (3-127), the following result is achieved:

$$K_i = \frac{y_i}{x_i} = \frac{\hat{\Phi}_i^v}{\hat{\Phi}_i^l} \tag{3-130}$$

There are many challenges associated with the direct method. Raal and Mühlbauer (1998) summarise these challenges as:

1. Selection of the most appropriate EOS that describes both the liquid phase and the vapour phase non-idealities. As a main criterion, the EOS must be flexible enough to fully describe the pressure, volume and temperature behaviour of a pure substance for both phases in the temperature and pressure range under study.

2. Selection of appropriate mixing rules that are required to extend the pure component form of the EOS to mixtures. Mixing rules are somewhat empirical in nature and tend to be system specific.

47

3. Location of the appropriate roots for liquid and vapour molar densities when higher than cubic equations of state are used.

Furthermore, Valderrama (2003) notes some of the major advantages and disadvantages of the cubic equations of state;

Advantages:

1. They can be equally applicable to both low pressure and high pressure systems.

2. They are third degree in volume and hence calculations are relatively simple to perform.

3. They can be tuned to give accurate values for any volumetric or thermodynamic property for most applications.

4. The extension to mixtures is relatively easy using mixing and combining rules of any complexity.

Disadvantages:

1. Actual pressure, volume and temperature data tend to follow a fourth degree equation instead of a cubic equation.

2. Cubic equations cannot represent all properties of a fluid in all different ranges of pressure and temperature.

3. Mixing and combining rules are empirical since the interactions between unlike molecules are unknown. Hence, interaction parameters are usually required. Furthermore, applications to complex mixtures might require several interaction parameters, even with the use of modern mixing rules.

The interaction parameters of the mixing rules (refer to Section 3.1.3) are obtained from the reduction of experimental VLE data. This regression technique is similar to that of the combined method, already discussed in Section 3.3.1.1. Figures 3.4 and 3.5 summarise these procedures in a flow diagram for isobaric VLE data reduction and isothermal VLE data reduction respectively.

48

Read T, x_i and pure component properties.
Set tolerances, e_A and e_B for the objective functions.

Display the system pressure, P, and the set of y_i values

Input initial pressure guess:
$$P = \sum x_i P_i^{sat} \quad \text{or}$$
$$P_{k+1} = P_k + 0.1.$$

Evaluate $\hat{\phi}_i^l$ and $\hat{\phi}_i^v$ to obtain
$$K_i = \hat{\phi}_i^l / \hat{\phi}_i^v$$

Obtain new estimate for overall pressure, P, using the Secant iteration procedure

Calculate: $Kx = \sum K_i x_i$ and
$$y_i = \frac{K_i x_i}{\sum K_i x_i}$$

Recalculate $\hat{\phi}_i^v$, K_i, $K_i x_i$ and Kx

No

Yes

$Kx_{k+1} - 1 < \varepsilon_B$

No

$Kx_{k+1} - Kx_k < \varepsilon_A$

Yes

Figure 3-4: Flow diagram for the bubble point pressure iteration for the direct method (Smith et al., 2001).

49
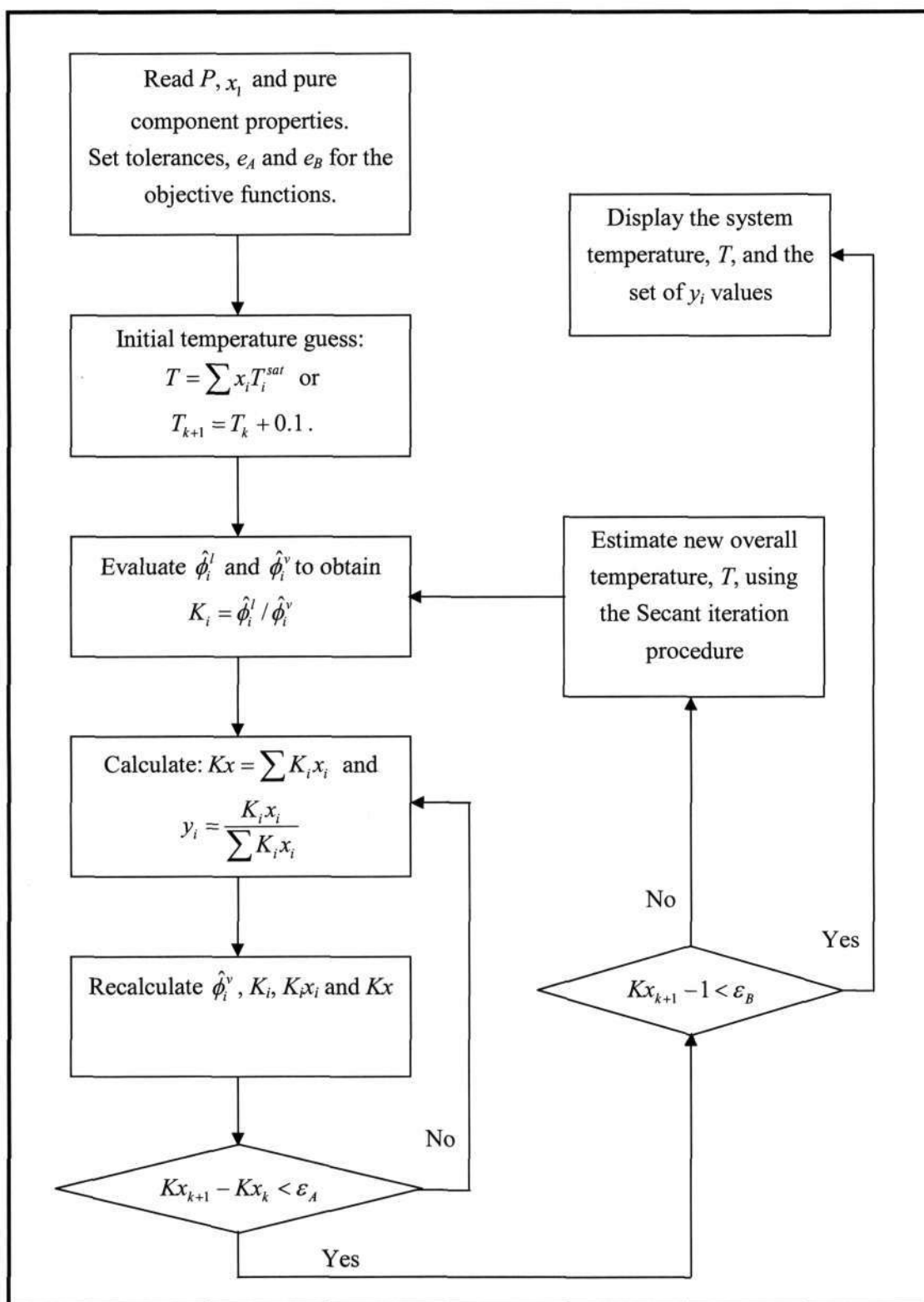
Figure 3-5: Flow diagram for the bubble point temperature iteration for the direct method (Smith et al., 2001).

3.4 Liquid-Liquid Equilibrium (LLE)

Pairs of chemical species that do not form a single homogeneous phase when they are mixed in a certain composition range and allowed to reach thermodynamic equilibrium, give rise to a phenomenon known as liquid-liquid equilibrium (LLE). Such a system splits into two liquid phases of different compositions. According to Smith et al. (2001), this phenomenon occurs because of another criterion that exists for phase equilibrium in a closed system. This criterion is obtained when the Gibbs energy is a minimum with respect to all possible changes at a given temperature and pressure (discussed further in Section 3.4.3). Therefore LLE occurs when such a system achieves a lower Gibbs energy by forming two liquid phases rather than one phase.

LLE is strongly influenced by temperature and the effect of pressure is significant only at high pressures or near the critical point (Walas, 1985). There are generally two types of LLE in literature. One type concerns the LLE of binary mixtures as a function of temperature at a constant pressure. This type is encountered in an azeotropic distillation column where the condensed distillate forms two liquid phases. The other type focuses on the LLE of ternary mixtures at a fixed temperature and pressure and finds its use in liquid-liquid extraction.

3.4.1 Binary Systems

The phase diagrams of binary systems that are restricted to liquid phases are quite simple in form. Some examples of T-x diagrams that are commonly encountered are shown in Figure 3-6. The diagram in Figure 3-6 (a) is known as an "island curve", which consists of an upper critical solution temperature (UCST), symbolised as T_U, and a lower critical solution temperature (LCST), symbolised as T_L, and is seldom encountered. LLE is possible at temperatures between T_U and T_L. In Figure 3-6 (b), the UCST may not exist if the mixture bubble point is lower than the UCST, while in Figure 3-6 (c), the LCST may not exist if freezing occurs at a temperature higher than the LCST. The curves in Figure 3-6 are known as solubility curves or binodal curves. At any specific temperature within the binodal curve, points A and B denote the equilibrium points with compositions x_1^α and x_1^β respectively. When the binodal curves intersect both the bubble and freezing point curves, a fourth type of behaviour is observed (Sorensen et al., 1979 and 1980).
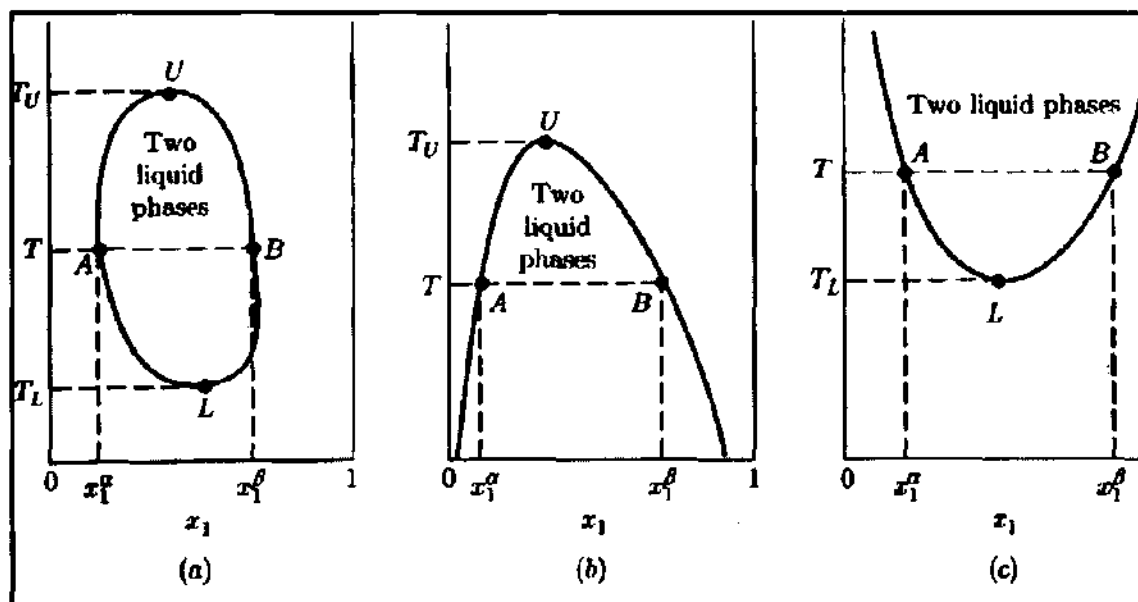
Figure 3-6: Three common types of constant pressure binary LLE diagrams: (a) "an island curve", (b) "a convex curve" and (c) "a concave curve", where α and β refer to the two liquid phases (Smith et al., 2001).

3.4.2 Ternary Systems

Data for ternary LLE are measured at a fixed temperature and pressure and are best represented by a triangular phase diagram. This geometrical representation was introduced by Roozeboom in 1894 as an equilateral "Gibbs triangle" with lines ruled parallel to each side. From the conservation of mass, the mole fractions of the three components of a ternary system must satisfy:

$$x_1 + x_2 + x_3 = 1 \tag{3-131}$$

The sum of the distances to a point inside an equilateral triangle measured parallel to the edges is equal to the length of the side of the triangle. Hence, a phase diagram drawn as an equilateral triangle with unit length ensures that Equation (3-131) is satisfied. The ternary LLE data measured in this project are represented on triangular diagrams as shown in Figure 3-7.

Each vertex of the triangular phase diagram represents a pure component and the binodal curve separates the single phase region (above the binodal curve) from the two-phase region (below the binodal curve). The tie-lines in the two-phase region are constructed experimentally by determining the composition of the two phases in equilibrium, as shown in Figure 3-7. The plait point, also known as the critical point, represents the point on the binodal curve where the compositions of the two phases in equilibrium are identical.
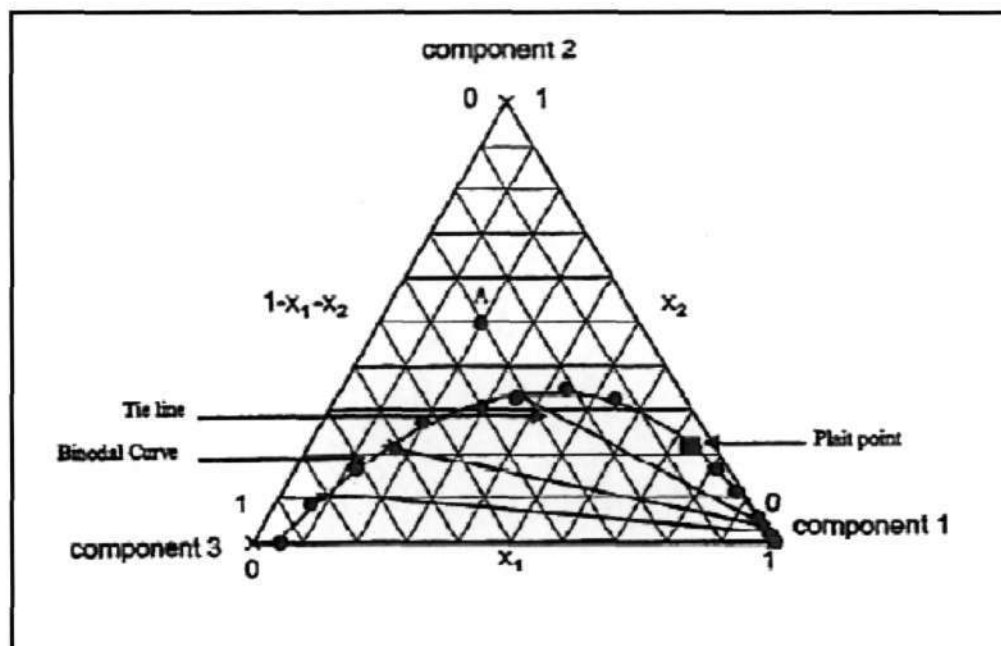
Figure 3-7: Graphical representation of ternary liquid-liquid equilibrium data using a triangular phase diagram (Novak et al., 1987).

The binodal curves for a ternary system exhibit a greater variety than for a binary system (Novak et al., 1987). Treybal (1963) classified the two major types of triangular diagrams: Types I and II. In type I, only one binary pair exhibits immiscibility while the other two binary pairs are miscible, as shown in Figure 3-8 (a). According to Sørensen et al. (1979) this type is most frequently encountered and represents approximately 75 % of the measured ternary systems. The type II systems have two binary pairs that display partial miscibility and the third binary pair is completely miscible, as portrayed in Figure 3-8 (b). However, if the two binary pairs are sufficiently immiscible, then Figure 3-8 (d) is obtained instead of Figure 3-8 (b). According to Novak et al. (1987), the diagrams in Figure 3-8 (b), (c), (d) and (e) are less encountered as they require a certain combination of binary system non-ideality. Variations of the triangular diagrams, including other types, are discussed in more detail by Sørensen et al. (1979), Null (1980) and Novak et al. (1987). The ternary systems studied in this project are of Types I and II.
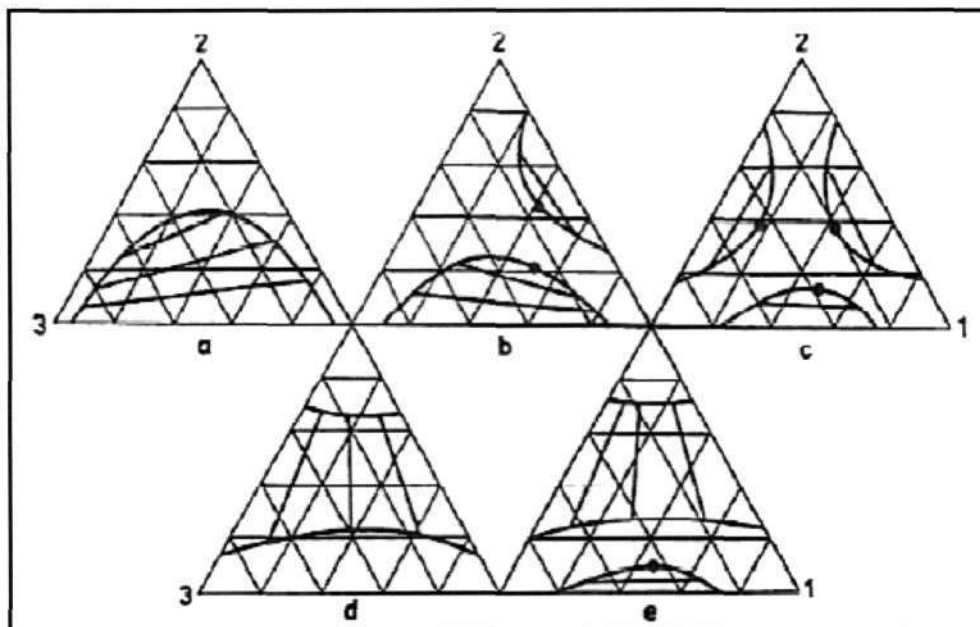
Figure 3-8: Basic types of ternary systems with a two phase region (Novak et al., 1987).

3.4.3 Theoretical Treatment of LLE

A stable system is one that has a minimum Gibbs energy at a fixed temperature and pressure and according to Smith et al. (2001), the stability criterion indicates that a liquid mixture will split into separate liquid phases if it can lower its Gibbs energy by doing so. To illustrate this, a typical curve for the Gibbs energy of mixing (defined as $\Delta G = G - Sx_i G_i$, where G refers to the mixture Gibbs energy and G_i to the pure component Gibbs energy) for a binary partially miscible liquid at a constant temperature and pressure is shown in Figure 3-9.
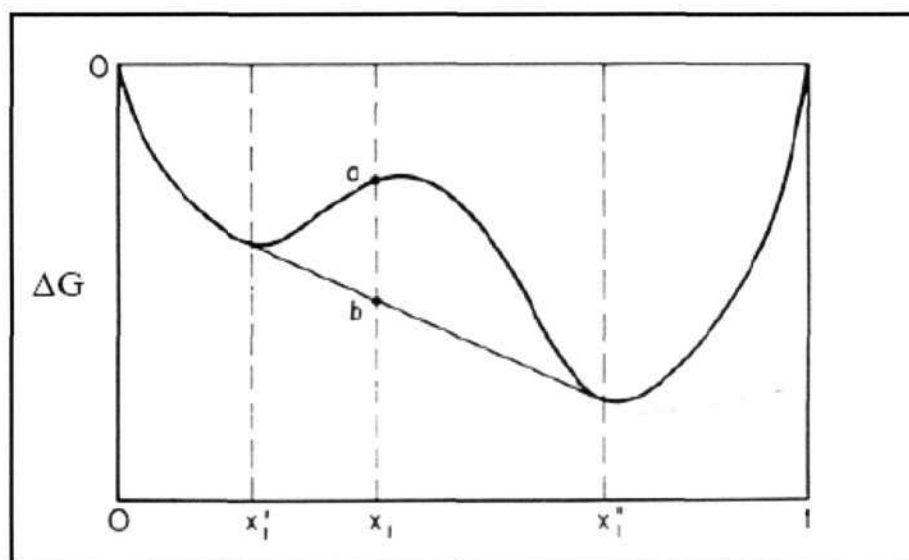
Figure 3-9: Molar Gibbs energy of mixing for a partially miscible binary system

(Prausnitz et al., 1999).

According to the stability criterion, a mixture with composition corresponding to point a in Figure 3-9 will split into separate phases with compositions x_1' and x_1''. The molar Gibbs energy change upon mixing is given by point b, where b represents the lowest possible Gibbs energy that the mixture may attain subject to the conditions of constant temperature, pressure and the overall composition x_1.

The mathematical interpretation of Figure 3-9 requires that at constant temperature and pressure, ΔG and its first and second derivatives must be continuous functions of x_1, and the second derivative must everywhere be positive. For a binary system this implies:

$$\frac{d^2 \Delta G}{dx_1^2} > 0$$

(3-132)

In terms of the Gibbs excess energy for a binary system, stability requires:

$$\frac{d^2 \left(G^E / RT \right)}{dx_1^2} > -\frac{1}{x_1 x_2}$$

(3-133)

Now, from the criterion of phase equilibrium, application of Equation (3-10) to two liquid phases, denoted by a and β, results in:

$$\hat{f}_i^\alpha = \hat{f}_i^\beta$$

(3-134)

Introduction of the activity coefficient and considering each pure species as a liquid at the temperature of the system, leads to:

$$x_i^\alpha \gamma_i^\alpha = x_i^\beta \gamma_i^\beta$$

(3-135)

where $i = 1, 2, \ldots, N$ for both Equations (3-134) and (3-135). Equation (3-135) is considered the fundamental relation for LLE. As mentioned earlier, the effect of pressure is only effective at high pressures or near the critical point. In addition, the effect of pressure on the activity coefficients may be ignored for moderate pressures. It should also be noted that, unlike low pressure VLE, the role of the activity coefficients in LLE are the only thermodynamic contribution to an LLE calculation.

3.4.4 Atmospheric LLE Data Regression

Some liquid phase activity coefficient models are unable to predict LLE as they fail the stability criterion (discussed in Section 3.4.3) to predict separate liquid phases. The Wilson (1964) equation is one such model that fails to meet the stability criterion, as outlined by Smith et al. (2001), and is therefore not able to predict LLE. Therefore, LLE data can only be regressed by models that pass the stability criterion.

The regression of LLE data is different from VLE data as LLE contains two liquid phases in equilibrium and no vapour phase is present. Hence, a liquid phase activity coefficient model (such as those discussed in Section 3.2.1) is used to represent both liquid phases. The application of a liquid phase activity coefficient model to the equilibrium criterion, allows the parameters of the model to be found by regression of experimental data.

It should be noted that the direct method, employing an EOS, can also be used to regress LLE data. However, this method is only prominent for the modelling of high-pressure LLE data where the effect of pressure on phase equilibria cannot be neglected (Walas, 1985 and Raal and Mühlbauer, 1998). Since the LLE data measured for this project were done at atmospheric pressure, the direct method was not used for this work and will not be further discussed. For a detailed discussion of this method, the reader is referred to Liu et al. (2002) and Ohta et al. (2004).

In the following sub-sections, a discussion on the modelling of mutual solubility data for binary systems, the regression of tie-line data for ternary systems and the correlation of binodal curves for ternary systems will be presented.

3.4.4.1 Mutual Solubility Data (Binary Systems)

According to Raal and Mühlbauer (1998), at least two data points for each phase at different temperatures are needed to obtain the temperature dependent parameters of the liquid phase activity coefficient model used. The three-suffix Margules (originally proposed in 1895), Van Laar (1910) and the NRTL equations were used to model the mutual solubility data measured for this project. The three-suffix Margules and Van Laar (1910) equations were chosen to model the mutual solubility data for this project as they are simple equations that have been used in the past for binary LLE representation and offer comparative algebraic simplicity. The

NRTL equation was chosen as this equation is suitable for modelling both LLE and VLE data and also offers the added advantage of being applicable to multi-component systems.

The molar excess Gibbs energy for the three-suffix Margules is:

$$\frac{G^E}{RT} = x_1 x_2 \left[A_{12} x_2 + A_{21} x_1 \right]$$

(3-136)

The corresponding activity coefficients are given by:

$$\ln \gamma_1 = \left[A_{12} + 2 \left(A_{21} - A_{12} \right) x_1 \right] x_2^2$$

(3-137)

$$\ln \gamma_2 = \left[A_{21} + 2 \left(A_{12} - A_{21} \right) x_2 \right] x_1^2$$

(3-138)

Applying the equilibrium criterion, Equation (3-135), and using the above expression for the activity coefficients, allows the parameters A_{12} and A_{21} to be found:

$$\frac{A_{12}}{A_{21}} = \frac{2\psi_2 \ln\left(x_2^\beta \middle/ x_2^\alpha \right) + \zeta_1 \ln\left(x_1^\beta \middle/ x_1^\alpha \right)}{2\psi_1 \ln\left(x_1^\beta \middle/ x_1^\alpha \right) + \zeta_2 \ln\left(x_2^\beta \middle/ x_2^\alpha \right)}$$

(3-139)

$$A_{21} = \frac{\ln\left(\dfrac{1 - x_1^\beta}{1 - x_1^\alpha} \right)}{\left(x_1^\alpha \right)^2 \left[1 + 2 x_2^\alpha \left\{ \dfrac{A_{12}}{A_{21}} - 1 \right\} \right] - \left(x_1^\beta \right)^2 \left[1 + 2 x_2^\beta \left\{ \dfrac{A_{12}}{A_{21}} - 1 \right\} \right]}$$

(3-140)

where, $\psi_i = \left(x_i^\alpha \right)^2 - \left(x_i^\beta \right)^2 - \left(x_i^\alpha \right)^3 + \left(x_i^\beta \right)^3$ and $\zeta_i = \left(x_i^\alpha \right)^2 - \left(x_i^\beta \right)^2 - 2\left(x_i^\alpha \right)^3 + 2\left(x_i^\beta \right)^3$

The molar Gibbs excess energy for the Van Laar (1910) equation is:

$$\frac{G^E}{RT} = \frac{A_{12} A_{21} x_1 x_2}{x_1 A_{12} + x_2 A_{21}}$$

(3-141)

where the corresponding activity coefficients are:

$$\ln \gamma_1 = A_{12} \left[\frac{A_{21} x_2}{x_1 A_{12} + x_2 A_{21}} \right]^2$$ (3-142)

$$\ln \gamma_2 = A_{21} \left[\frac{A_{12} x_1}{x_1 A_{12} + x_2 A_{21}} \right]^2$$ (3-143)

Similar to the three-suffix Margules equation, the parameters A_{12} and A_{21} are obtained from:

$$\frac{A_{12}}{A_{21}} = \frac{\left(\frac{x_1^\alpha}{x_2^\alpha} + \frac{x_1^\beta}{x_2^\beta} \right) \left(\frac{\ln \left(\frac{x_1^\beta}{x_1^\alpha} \right)}{\ln \left(\frac{x_2^\alpha}{x_2^\beta} \right)} \right) - 2}{\frac{x_1^\alpha}{x_2^\alpha} + \frac{x_1^\beta}{x_2^\beta} - 2 \frac{x_1^\alpha x_1^\beta \ln \left(\frac{x_1^\beta}{x_1^\alpha} \right)}{x_2^\alpha x_2^\beta \ln \left(\frac{x_2^\alpha}{x_2^\beta} \right)}}$$ (3-144)

$$A_{12} = \frac{\ln \left(\frac{x_1^\beta}{x_1^\alpha} \right)}{\left[1 + \left(\frac{A_{12}}{A_{21}} \right) \left(\frac{x_1^\alpha}{x_2^\alpha} \right) \right]^{-2} - \left[1 + \left(\frac{A_{12}}{A_{21}} \right) \left(\frac{x_1^\beta}{x_2^\beta} \right) \right]^{-2}}$$ (3-145)

According to Raal and Mühlbauer (1998), equations with more than two parameters cannot be used to model solubility data unless all subsequent parameters are fixed at some trial value/s. Therefore for a binary system, the non-randomness parameter, a_{12}, in the NRTL equation is fixed to allow calculation of the other two parameters; t_{12} and t_{21}. Prausnitz et al. (1999) suggest that the value of a_{12} should be obtained from experimental results of the same class of compounds as those under study. Due to its algebraic complexity, the parameters in the NRTL equation cannot be solved for in as simple a manner as shown for the three-suffix Margules equation and the Van Laar (1910) equation. Therefore, Renon and Prausnitz (1969) have published useful graphs (Figures 3-10 to 3-12) to assist in the computation of the other two parameters; t_{12} and t_{21}. The graphs yield two parameters, S^* and D^*, which are related to the NRTL parameters by:

$$S^* = \frac{1}{2} (\tau_{21} + \tau_{12})$$ (3-146)

58

$$D^* = \frac{1}{2}\left(\tau_{21} - \tau_{12}\right) \tag{3-147}$$
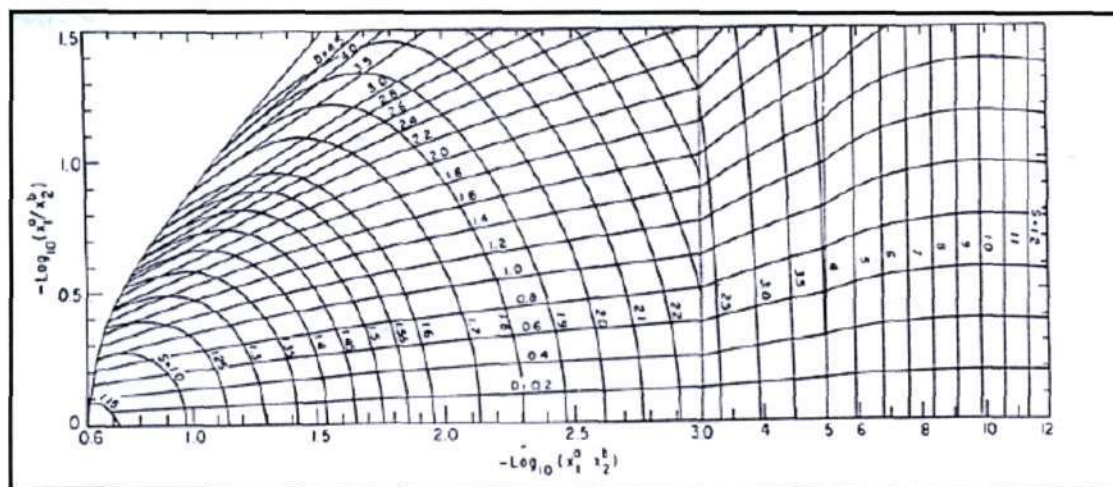
Figure 3-10: Method for finding NRTL equation parameters (with $a_{12} = 0.2$) from mutual liquid solubilities (Renon and Prausnitz, 1969).
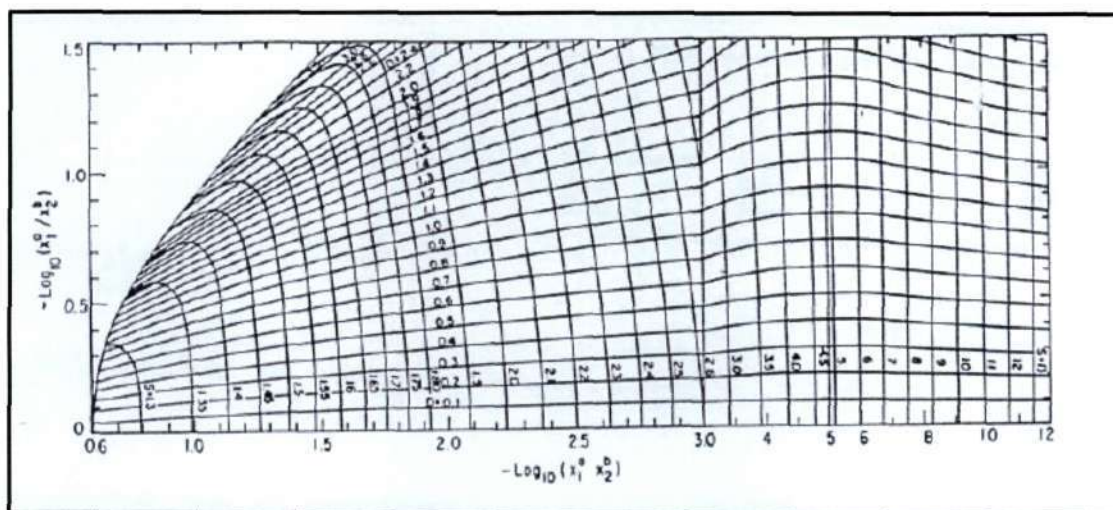
Figure 3-11: Method for finding NRTL equation parameters (with $a_{12} = 0.3$) from mutual liquid solubilities (Renon and Prausnitz, 1969).
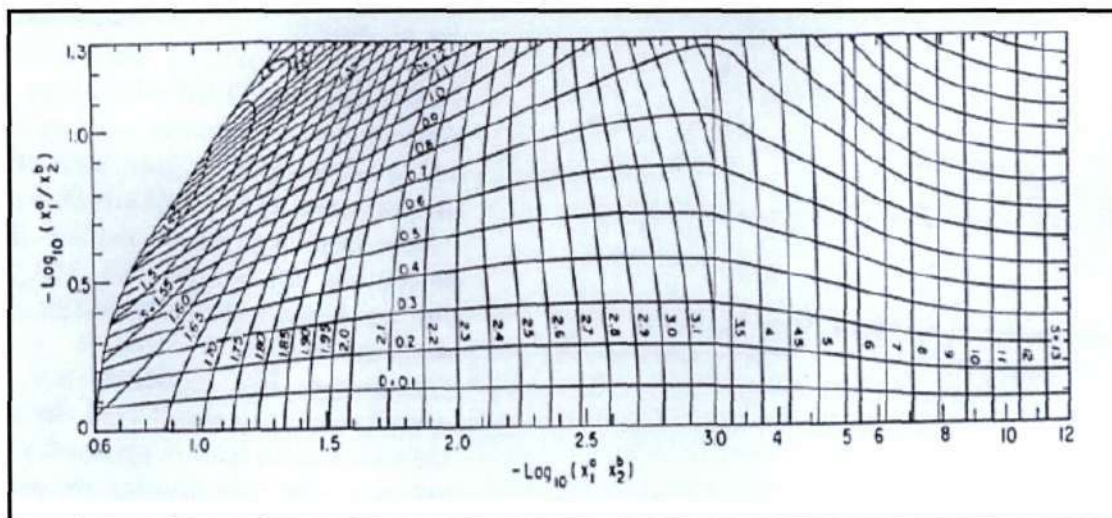
Figure 3-12: Method for finding NRTL equation parameters (with $a_{12} = 0.4$) from mutual liquid solubilities (Renon and Prausnitz, 1969).

3.4.4.2 Tie-line Correlation (Ternary Systems)

The NRTL and the modified UNIQUAC equations were used to correlate the experimental tie-line data for the ternary systems measured in this work. These models meet the stability criterion (discussed in Section 3.4.3) and are well-known to correlate both VLE and LLE data. Furthermore, these models are capable of handling complex systems. Both the NRTL and the modified UNIQUAC equations were introduced in Sections 3.2.1.2 and 3.2.1.3 respectively.

The parameters of these models are usually estimated by the optimisation of a suitable objective function. There are two techniques available for solving this optimisation problem: the least square objective function minimisation or the likelihood function maximisation. For both these cases the objective function is non-linear and non-convex in terms of the optimisation variables. Novak et al. (1987) suggested the use of the least square objective function optimisation minimisation technique as it is more attractive and commonly used. Therefore, this technique was employed for this work with the following objective function as suggested by Novak et al. (1987):

$$F(P) = \sum_{i=1}^{n} \left\{ x_{1i}^{\alpha}(expt) - x_{1i}^{\alpha}(calc)(P,T) \right\}_{i}^{2} +$$
$$\left\{ x_{2i}^{\alpha}(expt) - x_{2i}^{\alpha}(calc)(P,T) \right\}_{i}^{2} +$$
$$\left\{ x_{1i}^{\beta}(expt) - x_{1i}^{\beta}(calc)(P,T) \right\}_{i}^{2} +$$
$$\left\{ x_{2i}^{\beta}(expt) - x_{2i}^{\beta}(calc)(P,T) \right\}_{i}^{2}$$

(3-148)

where P is the parameters vector, n is the number of experimental points, a and β refer to the two liquid phases in equilibrium and (exp) and $(calc)$ refer to the experimental and calculated mole fractions respectively. The root mean square deviation (rmsd) can give an indication of the precision of a correlation:

$$rmsd = \left\{ \frac{\sum_a \sum_b \sum_c \{x_{abc}(expt) - x_{abc}(calc)\}^2}{6k} \right\}$$

(3-149)

where x is the mole fraction, k is the number of experimental points and the subscripts a, b and c designate the component, phase and tie-line respectively. The equations and algorithms used in the calculation of the composition of the liquid phases follow the method suggested by Walas (1985).

3.4.4.3 Binodal Curve Correlation (Ternary Systems)

The equation of Hlavatý (1972) has until recently been the only successful method in fitting an equation to the binodal curve for a ternary liquid mixture with only one pair of immiscible liquids. Three equations have been fitted to the ternary data for each system measured in this work that follow the work of Hlavatý (1972).

The Hlavatý (1972) equation with coefficients A_i is given by:

$$x_2 = A_1 x_A \ln x_A + A_2 x_B \ln x_B + A_3 x_A x_B$$

(3-150)

Unfortunately, there exists a major shortcoming of this equation; the independent variables of this equation are highly correlated and slight changes in the binodal curve data produce large changes in the magnitude of the coefficients A_1, A_2 and A_3.

Therefore, Letcher et al. (1989) proposed an equation that provides a better fit and did not suffer from the disadvantage of the Hlavatý (1972) equation. This equation is known as the ß-density function equation with coefficients B_i:

$$x_2 = B_1 (1 - x_A)^{B_2} x_A^{B_3}$$

(3-151)

Another equation proposed by (Letcher et al., 1986), known as the log γ equation, does not suffer the disadvantage of being highly correlative. This equation follows the work done by Schultz and Crouse (1973), who described the distribution of mass fractions of a body subjected to successive random divisions of its randomly divided parts as a log γ distribution. Letcher et al. (1986) found that the binodal curves are similar in shape to the densities of the log γ distribution obtained by Schultz and Crouse (1973). The log γ equation with coefficients C_i is given by:

$$x_2 = C_1 \left(-\ln x_A \right)^{C_2} x_A^{C_3}$$

(3-152)

where, for Equations (150), (151) and (152):

$$x_A = \frac{\left(x_1 + 0.5x_2 - x_1^0 \right)}{x_{11}^0 - x_1^0}$$

(3-153)

$$x_B = \frac{\left(x_{11}^0 - x_1 - 0.5x_2 \right)}{x_{11}^0 - x_1^0}$$

(3-154)

where x_1 denotes the mole fraction composition of component 1, x_2 denotes the mole fraction composition of component 2, and x_{11}^0 and x_1^0 are the values of x_1 on the binodal curve which cut the $x_2 = 0$ axis. Equations (3-150) to (3-152) are fitted to the binodal curves with the standard deviations s defined as:

$$\sigma = \left\{ \sum_{k=1}^{n} \left[x_2(calc) - x_2(expt) \right]_k^2 / (n-3) \right\}^{1/2}$$

(3-155)

where n is the number of data points and 3 is the number of estimated coefficients (Sen and Srivastava, 1990).

3.5 Vapour-Liquid-Liquid Equilibrium (VLLE)

The binodal curves that represent LLE can intersect the VLE bubble point curve. When this occurs, a phenomenon known as vapour-liquid-liquid equilibrium (VLLE) is obtained. In this section only consider the case of binary systems will be considered, since only binary systems displaying VLLE were considered for this project.
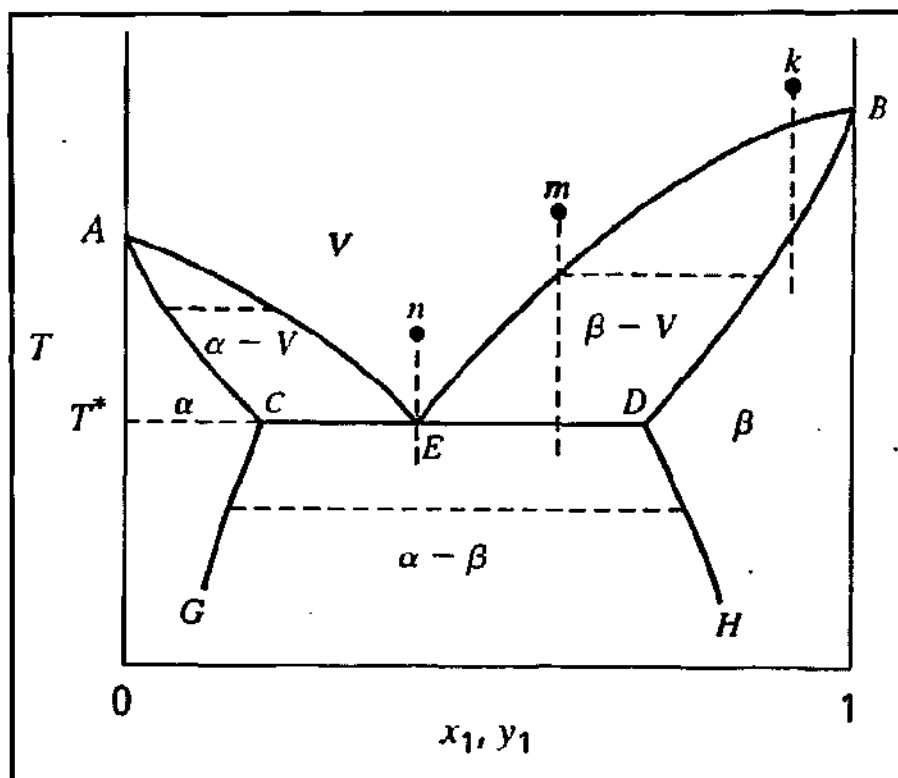
Figure 3-13: A typical *T-x-y* diagram at constant pressure for a binary system exhibiting VLLE (Smith et al., 2001).

According to the Gibbs phase rule, a binary VLLE system has only one degree of freedom. Hence, if the pressure is specified for a binary system, the temperature and the compositions for all three phases are fixed. The state of three phases in equilibrium fall on a horizontal line at T^* (the three phase equilibrium temperature) when represented on a $T-x-y$ diagram, as shown in Figure 3-13. The points C and D represent the two liquid phases in equilibrium with the vapour phase, represented by point E. According to Smith et al. (2001), if more of either species is added to a system whose overall composition lies between point C and D and the three phase equilibrium pressure is maintained, the Gibbs phase rule necessitates that the temperature and the compositions of the phases be unchanged. However, to comply with the law of mass conservation, the relative amounts of the phases adjust themselves to reflect the change in overall composition of the system. For temperatures above T^* and depending on the overall composition, the system may be a single liquid phase (represented by α or β), a vapour phase (represented by V) or a mixture of the two phases (represented by α-V or β-V). For temperatures below T^*, the system is represented by LLE.

VLLE can also be measured at a constant temperature and Figure 3-14 portrays a typical $P-x-y$ diagram, where the three phase equilibrium pressure is identified as P^*. Since pressure has only

a weak influence on liquid solubilities, the phase boundaries separating the three phase regions are almost vertical.
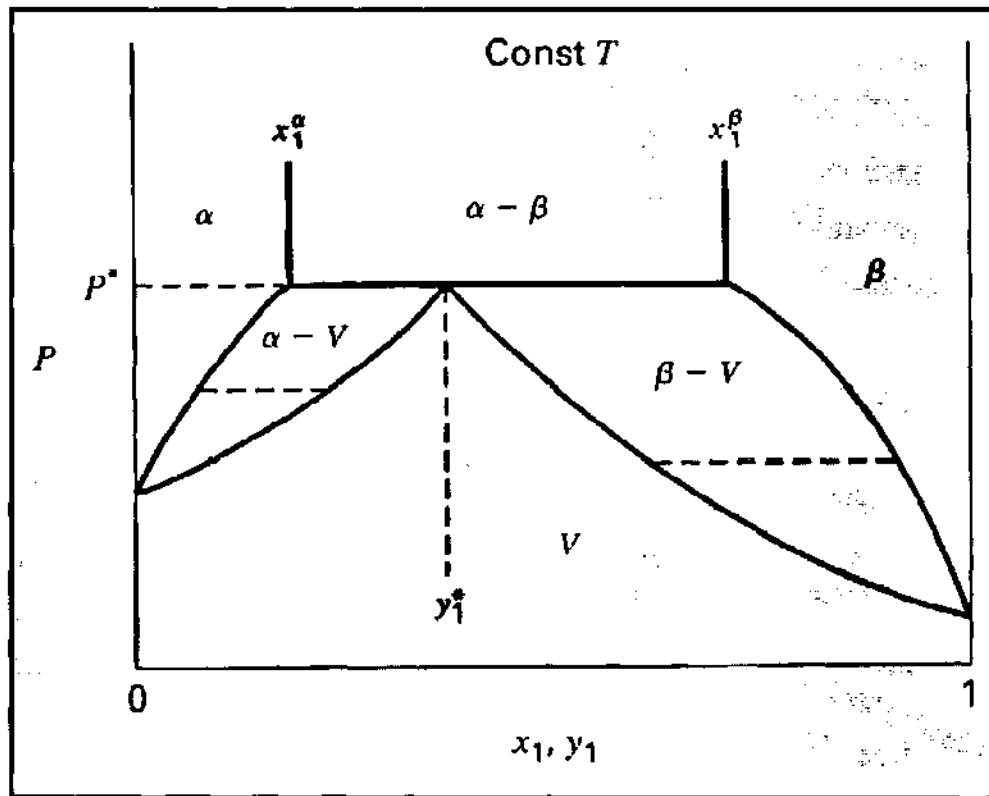
Figure 3-14: A typical P-x-y diagram at a constant temperature for two partially miscible liquids (Smith et al., 2001).

The calculation of low pressure VLLE is calculated in the same way as for low pressure VLE systems. Therefore, applying the criterion for phase equilibrium (Equation 3-10) for the regions where a single liquid is in equilibrium with its vapour results in:

$$\hat{f}_i^\alpha = \hat{f}_i^\beta = \hat{f}_i^v \qquad (3\text{-}156)$$

where a and β represent the two phases in equilibrium with the corresponding vapour phase represented as v. When the liquid fugacities and the vapour fugacity are eliminated in favour of the activity coefficient and the fugacity coefficient, the following result is obtained for a binary system:

$$y_1 \Phi_1 P = x_1^\alpha \gamma_1^\alpha P_1^{sat} = x_1^\beta \gamma_1^\beta P_1^{sat} \qquad (3\text{-}157)$$

$$y_2 \Phi_2 P = x_2^\alpha \gamma_2^\alpha P_2^{sat} = x_2^\beta \gamma_2^\beta P_2^{sat} \qquad (3\text{-}158)$$

It can be noted from Equations (3-157) and (3-158) that a total of five independent variables need to be solved (x_1^α, x_1^β, y_1, T and P). According to the Gibbs phase rule, when one of the variables is specified, the other four independent variables can be solved.

3.5.1 Low Pressure VLLE Data Regression

In Section 3.4.3, it was mentioned that models which do not pass the stability criterion cannot be used to regress LLE data. The models that are used to correlate VLLE data should pass the stability criterion as well since two separate liquid phases are present. The regression technique for low pressure VLLE data is the same as for low pressure VLE data. However, the direct method is not recommended for low pressure VLLE data regression since this method is only important for high pressure LLE regression. Therefore, only the combined method is considered for VLLE data regression in this work. The NRTL and the modified UNIQUAC equations were used for the liquid phase non-ideality and the Virial equation of state (with the correlations for the second Virial coefficients) was employed for the vapour phase non-ideality.

3.6 Thermodynamic Consistency Tests

The measurement of temperature, pressure and both liquid and vapour compositions for a binary VLE system, results in an "over-specification" of the system. Nevertheless, this allows one of the four measured variables to be used to test for thermodynamic consistency. According to Smith et al. (2001), the vapour compositions usually display the greatest error and thus the thermodynamic consistency tests usually focus on the vapour compositions (y-data) to determine the thermodynamic consistency of the VLE data.

The Gibbs-Duhem equation forms the basis of all thermodynamic consistency tests and was introduced in Section 3.2:

$$\sum_i x_i d\ln\gamma_i = \frac{\bar{V}_i^E}{RT}dP - \frac{\bar{H}_i^E}{RT^2}dT \qquad (3\text{-}103)$$

VLE data is said to be thermodynamically consistent if it conforms to the Gibbs-Duhem equation. Over the years, the evaluation of thermodynamic consistency of VLE data has received a great deal of attention in the literature with many adaptations of the Gibbs-Duhem equation being introduced. The *slope test*, which compared slopes of curves drawn to fit $\ln\gamma_1$ and $\ln\gamma_2$ vs x_1 graphs, was one of the earliest tests used but according to Van Ness (1995), this

test proved to be tedious and led to uncertainty. Therefore, the *area test* was introduced as an improvement over the *slope test* (Herington, 1947 and Redlich and Kister, 1948). However, Walas (1985) mentions that the *area test* is a necessary but insufficient condition as individual data may be off in ways that compensate each other. For instance, the pressure is cancelled off and hence one of the most accurately measured system properties is lost. This means that the test would sometimes pass data sets that were inconsistent while failing data sets that actually were consistent. Therefore, the *area test* was not considered for this project but rather two well-known thermodynamic consistency tests were employed: the *point test* of Van Ness et al. (1973) and the *direct test* of Van Ness (1995).

It should be noted that LLE data cannot be tested for thermodynamic consistency (Raal and Mühlbauer, 1998). This is due to two reasons: firstly, the direct determination of individual activity coefficients is not possible as the experimental LLE data furnish only a ratio of activity coefficients and secondly, the LLE data do not extend over a continuous composition range (a requirement for thermodynamic consistency testing).

On the other hand, VLLE data can be tested for thermodynamic consistency with the *point test* only applicable to the homogenous region (VLE region). The *direct test* however, can be applied to the entire composition range.

3.6.1 The Point Test

Van Ness et al. (1973) introduced the *point test* as an improvement to the *area test*. As mentioned earlier, when all four variables are measured for a complete binary VLE data set, an "over-specification" of the system is obtained. Therefore, any three experimentally determined variables can be used to obtain the fourth variable by employing a suitable correlation. As mentioned above, the vapour compositions introduce the most error and are thus used to test for thermodynamic consistency. The *point test* compares the measured vapour compositions (y_{exp}) to the calculated values (y_{calc}), where the calculated values are found from data regression using the combined or the direct method. This comparison generates residuals, Δy, which provides a good indication of the consistency of the VLE data. Danner and Gess (1990) provide a quantitative criterion for the consistency of VLE data by proposing that the absolute average deviation, Δy_{ad}, should be less than 0.01 for the data to be thermodynamically consistent:

$$\Delta y_{ad} = \frac{1}{n}\left(\left|y_{exp} - y_{calc}\right|\right)$$
(3-159)

66

where n refers to the number of experimental data points. This criterion was also used for the data measured in this work.

3.6.2 The Direct Test

Van Ness (1995), who developed this test, describes it as being a long sought goal – a simple and direct test of thermodynamic consistency for each point of a VLE data set with respect to the Gibbs-Duhem equation itself. The formulation of this test requires the following definitions:

$$\varepsilon_P^* = \frac{V^E}{RT}\frac{dP}{dx_1} \tag{3-160}$$

$$\varepsilon_T^* = \frac{-H^E}{RT^2}\frac{dT}{dx_1} \tag{3-161}$$

where ε_P^* is zero for isobaric data and ε_T^* is zero for isothermal data and consequently only one e term (ε_P^* for isothermal data or ε_T^* for isobaric data) is required for the derivation of the direct test. Writing Equations (3-98) and (3-103) for one mole of liquid phase, with $g = G^E / RT$, the following expressions are obtained:

$$\frac{dg}{dx_1} = \ln\frac{\gamma_1}{\gamma_2} + \varepsilon^* \tag{3-162}$$

$$x_1\frac{d\ln\gamma_1}{dx_1} + x_2\frac{d\ln\gamma_2}{dx_1} - \varepsilon^* = 0 \tag{3-163}$$

where ε^* depends on the nature of the VLE data (either isobaric or isothermal). Writing Equation (3-102) for a binary system:

$$g = x_1\ln\gamma_1 + x_2\ln\gamma_2 \tag{3-164}$$

Representing the experimental value of g with g^{exp} and differentiating Equation (3-164) with respect to x_1:

$$\frac{dg^{exp}}{dx_1} = x_1 \frac{d\ln\gamma_1^{exp}}{dx_1} + \ln\gamma_1^{exp} + x_2 \frac{d\ln\gamma_2^{exp}}{dx_1} - \ln\gamma_2^{exp} \qquad (3\text{-}165)$$

which may also be written as:

$$\frac{dg^{exp}}{dx_1} = \ln\frac{\gamma_1^{exp}}{\gamma_2^{exp}} + \varepsilon + x_1 \frac{d\ln\gamma_1^{exp}}{dx_1} + x_2 \frac{d\ln\gamma_2^{exp}}{dx_1} - \varepsilon^* \qquad (3\text{-}166)$$

When Equation (3-166) is subtracted from Equation (3-162) and written in terms of residuals $(dg = g - g^{exp})$, one obtains:

$$\frac{d(\delta g)}{dx_1} = \delta\ln\frac{\gamma_1}{\gamma_2} - \left(x_1 \frac{d\ln\gamma_1^{exp}}{dx_1} + x_2 \frac{d\ln\gamma_2^{exp}}{dx_1} - \varepsilon^* \right) \qquad (3\text{-}167)$$

If an isothermal or isobaric data set is reduced with $S(dg)^2$ as the objective function then the term $d(dg) / dx_1$ is effectively zero. Therefore:

$$\delta\ln\frac{\gamma_1}{\gamma_2} = x_1 \frac{d\ln\gamma_1^{exp}}{dx_1} + x_2 \frac{d\ln\gamma_2^{exp}}{dx_1} - \varepsilon^* \qquad (3\text{-}168)$$

According to the Gibbs-Duhem equation, the right hand side of Equation (3-168) is required to be zero for thermodynamically consistent data, where the residual on the left provides a direct measure of deviations from the Gibbs-Duhem equation. According to Van Ness (1995), the extent to which values of this residual fail to scatter about zero provides a measure of the departure of the data from thermodynamic consistency.

Table 3-1: Consistency index for the direct test of Van Ness (1995) showing the root mean square values (RMS).

Index	RMS $\delta\ln(\gamma_1/\gamma_2)$	
1	>0	=0.025
2	>0.025	=0.050
3	>0.050	=0.075
4	>0.075	=0.100
5	>0.100	=0.125
6	>0.125	=0.150
7	>0.150	=0.175
8	>0.175	=0.200
9	>0.200	=0.225
10	>0.225	

Van Ness (1995) also developed a quantitative criterion for this test, as shown in Table 3-1. The table contains indices to quantify the degree to which the data departs from consistency, where an index of one signifies excellent data and an index of ten very poor data.

4

CHAPTER FOUR

EQUIPMENT DESCRIPTION

In Chapter 2, some of the recirculating stills for the measurement of vapour-liquid equilibrium (VLE) and vapour-liquid-liquid equilibrium (VLLE) data were introduced. Chapter 2 also introduced some of the experimental techniques and equipment for the measurement of liquid-liquid equilibrium (LLE) data. This chapter will focus on a more detailed description of the equipment used in this project: the VLE recirculating still of Raal and Mühlbauer (1998), as modified by Ndlovu (2005) for partially miscible systems and the LLE apparatus of Raal and Brouckaert (1992), also modified by Ndlovu (2005). This chapter will also discuss the measurement and control of temperature and pressure, as well as the sampling and analysis of the equilibrium phases.

4.1 The Vapour-Liquid Equilibrium Apparatus

The VLE apparatus of Raal and Mühlbauer (1998) has been successfully used by many researchers: Joseph et al. (2001), Sewnarain et al. (2002) and Clifford (2004) to name a few. Recently, this still was modified by Ndlovu (2005) to enable VLLE measurements of partially miscible systems. This modified still was used for this project and consisted of the following equipment:

- The VLE dynamic still (discussed in more detail in Section 4.1.1).
- A 50 L ballast tank.
- A Techne cooling coil unit.
- A WIKA model P10 pressure transmitter.
- A WIKA model 5001 6 ½ digit pressure display.
- Eight Pt-100 temperature sensors.
- A WIKA model 4003 4 ½ digit temperature display.
- A Labotech water bath complete with ethylene glycol solution as the cooling medium and a pump.
- Four AC Voltage regulators.
- Three DC power supplies.
- A BUCHI model B-721 pressure controller.
- An EDWARDS Model 3 vacuum pump.
- A CN-40 temperature controller.
- A FUTEK SSR 40 DA solid state relay.
- A six-port two-position GC valve.
- A solenoid valve (Clippard valve).
- The Hewlett Packard Model 5890 Series II gas chromatograph.

Photograph 4-1 shows the setup of the experimental equipment. The pressure controller actuates a two-way control valve and leads to a vacuum pump, allowing precise control of the pressure at desired values. One of the central features of this still is the special modification for partially miscible systems that allows the superheated take-off of the vapour samples directly to the gas chromatograph for composition analyses.
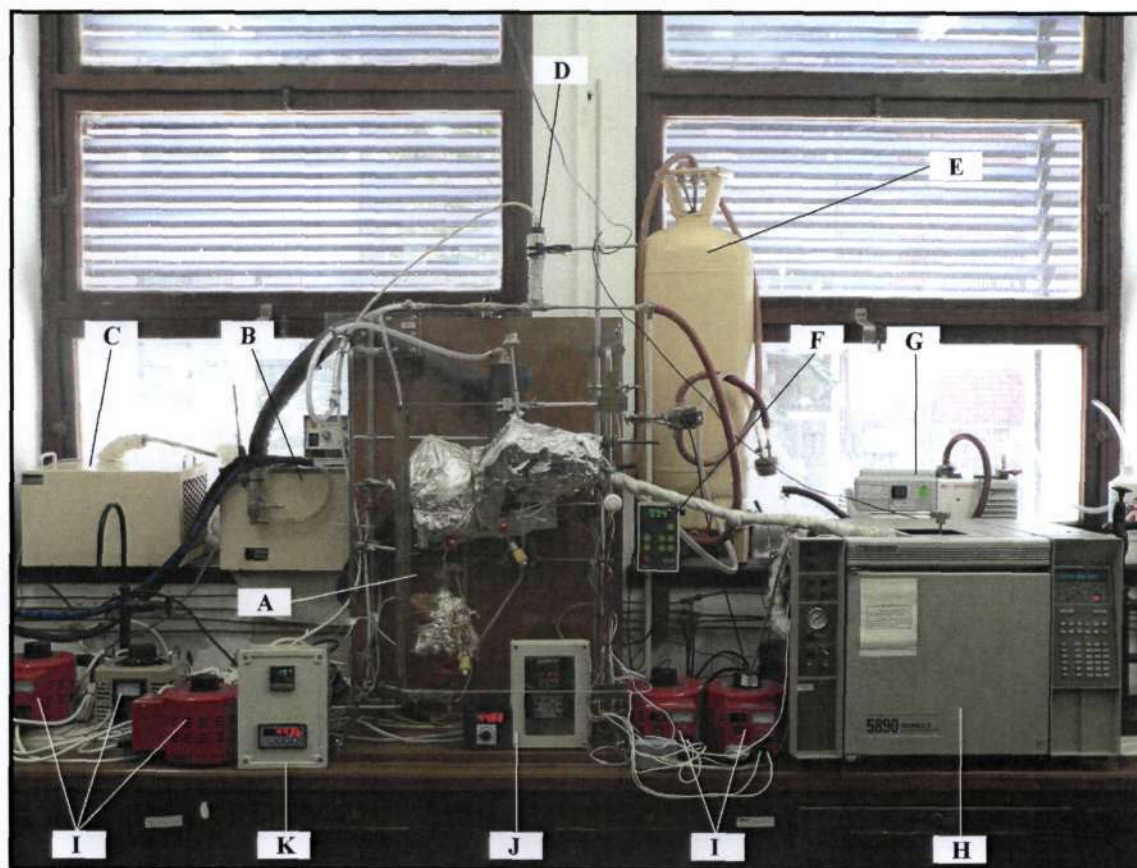
Photograph 4-1: Experimental setup of the VLE equipment.

A – VLE apparatus with insulation; **B** – Labotech water bath with temperature controller for cooling medium; **C** – Techne cooling coil unit; **D** – WIKA model P10 pressure transmitter; **E** – 50 L ballast tank; **F** – BUCHI model B-721 pressure controller; **G** – Edwards model 3 vacuum pump; **H** – Hewlett Packard 5890 Series II gas chromatograph; **I** – AC voltage regulators; **J** – CN-40 temperature controller with temperature selector switch; **K** – temperature and pressure display units.

4.1.1 The Vapour-Liquid Equilibrium Still

The glass VLE dynamic still was designed by Raal (Raal and Mühlbauer, 1998). As mentioned in Chapter 2, this still was based on the work of Heertjies (1960) and Yerazunis et al. (1964). Figure 4-1 provides a detailed view of the still and shows the modification introduced by Ndlovu (2005).

A main feature of this design is the packed equilibrium chamber (F) that is vacuum-insulated (E), thus ensuring adiabatic operation of the chamber. A liquid mixture is charged into the boiling chamber (A) and brought to a boil by internal and external heaters (B and Q

72

respectively). The internal heater, encased in a glass insert, consists of a heater cartridge that provides the actual drive for boiling. It also provides nucleation sites for smooth boiling and allows precise control of the circulation rate. The external heater consists of nichrome wire that is wrapped around the boiling chamber, which compensates for the heat losses to the environment.
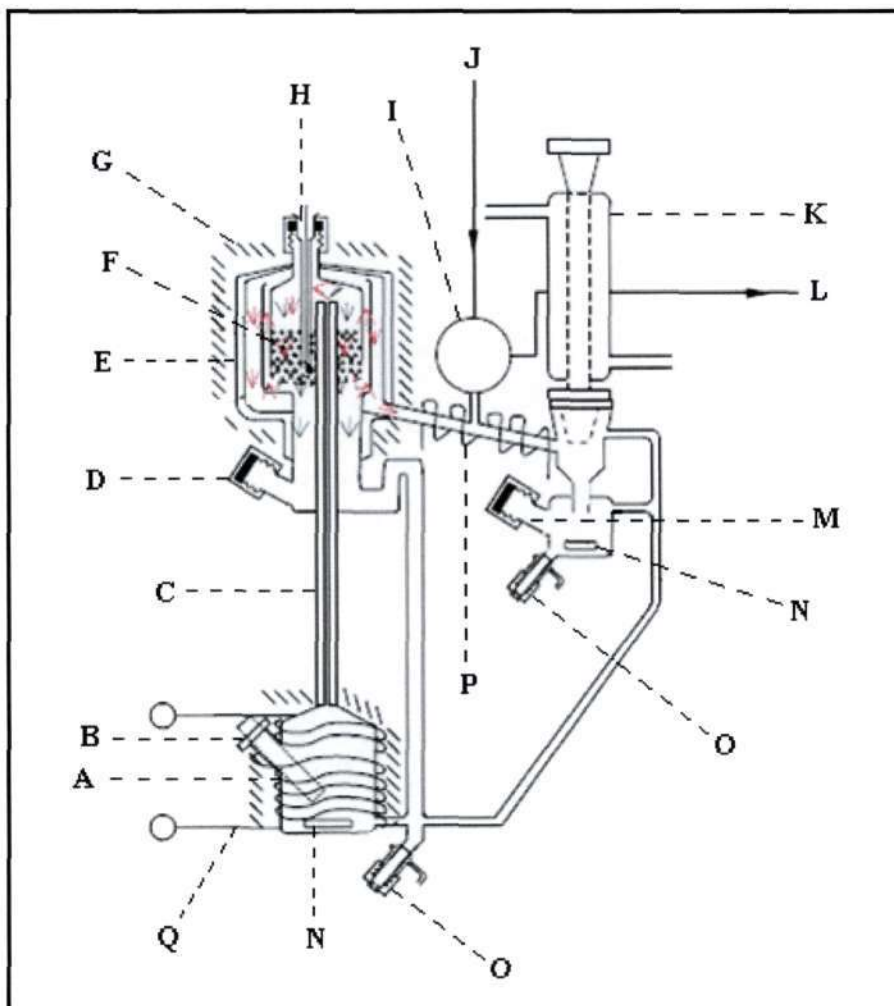
Figure 4-1: Schematic diagram of the VLE still (Ndlovu, 2005).

A – boiling chamber; B – glass insert housing the internal heater; C – insulated Cottrell tube; D – liquid sampling point; E – vacuum jacket; F – equilibrium chamber with stainless steel wire mesh packing; G – insulation; H – glass insert housing the Pt-100 temperature sensor; I – six-port GC valve; J – helium gas from cylinder; K – condenser; L – superheated sample to GC; M – vapour sampling point; N – magnetic stirrers; O – drain valves; P – nichrome resistance wire for superheated vapour; Q – nichrome resistance wire for external heating.

The boiling generates a vapour-liquid mixture that is forced upward through the vacuum-insulated Cottrell tube (C) and then downward into the vacuum-jacketed equilibrium chamber (F). The equilibrium chamber is packed with stainless-steel wire mesh cylinders measuring 3

mm in diameter to provide a large interfacial area that ensures significant contact between the vapour and liquid phases. This arrangement has an advantage of achieving equilibrium rapidly, even for species with a high relative volatility. A Pt-100 temperature sensing element is situated within the packing (H) to provide an accurate measurement of the system's equilibrium temperature. The bottom of the equilibrium chamber consists of holes to allow disengagement of the liquid and vapour phases. The liquid flows into a small liquid trap to allow sampling for composition analysis before overflowing to the boiling chamber, while the vapour flows upward around the equilibrium chamber providing an important thermal lag. The vapour then flows to a condenser (K) where the condensate collects in a condensate receiver before overflowing to the boiling chamber via a standpipe leg.

For systems that exhibit limited miscibility, partial condensation of vapour must be avoided as this would necessarily change the true equilibrium vapour composition. To avoid this, Ndlovu (2005) suggested keeping the temperature of the outside walls of the equilibrium chamber at 5 °C higher than the equilibrium chamber. This was achieved by using a CN-40 temperature controller connected to a FUTEK SSR 40 DA solid state relay which regulated the power supply to the nichrome wire wrapped around the equilibrium chamber.

Other innovative features include:

- The direct analysis of vapour composition by gas chromatography that avoids the difficulties of analysing a two-phase condensate.
- The packing in the equilibrium chamber increases the mass transfer between the liquid and vapour phases, thus allowing rapid attainment of phase equilibrium and eliminating the dependence on the Cottrell tube as the only means of establishing equilibrium.
- Magnetic stirrers were included in the boiling chamber and the condensate receiver to achieve efficient mixing. Stirring in the condensate receiver eliminates possible temperature and concentration gradients that might have existed in the vapour condensate, thus ensuring reproducibility for sample analysis. Stirring within the boiling chamber ensures that the returning condensate is thoroughly mixed with the contents of the boiling chamber, thus preventing flashing.
- The packing in the equilibrium chamber is easily accessible through the top of the still, thus enabling the packing height to be adjusted especially for highly volatile systems that display difficulty in establishing equilibrium.

4.1.2 Temperature Measurement and Control

A Pt-100 temperature sensor connected to a temperature display, was used to measure the equilibrium temperature. Other Pt-100 temperatures sensors were also used for the measurement of the temperature of the equilibrium chamber wall, the vapour sample loop and the vapour take-off stream and were all connected to a single temperature display via a selector switch. These temperatures were important for the composition analysis of a vapour sample to avoid partial condensation of the vapour phase. All the Pt-100 temperature sensors were calibrated before use to obtain accurate temperature readings (refer to Chapter 5 for the calibration procedure).

The temperature for each isothermal VLE/VLLE system was manually controlled by carefully adjusting the pressure, where increasing the pressure results in an increase of the system temperature and decreasing the pressure lowers the system temperature. The accuracy of the measured temperature was estimated to be within ±0.02 °C and the accuracy of the temperature control varied between 0.01 and 0.05 °C.

4.1.3 Pressure Measurement and Control

The system pressure was measured using a WIKA model P10 pressure transmitter and effectively controlled with a BUCHI model B-721 pressure controller that utilised a two-way solenoid valve connected to a vacuum pump and a vent to the atmosphere. The calibration procedure is discussed in Chapter 5. The pressure accuracy was estimated as ±0.03 kPa and controlled to within 0.01 kPa for isobaric operation.

4.1.4 Sampling

Liquid samples were withdrawn directly from the sample trap using a gas-tight syringe through a chemically resistant septum. The gas-tight syringe ensured that no sample was lost during the sampling process. The vapour phase was sampled by a special sampling mechanism that was designed especially for partially miscible systems, where the vapour sample was sent from the still to the gas chromatograph (GC) before condensation via a superheated gas line. This was achieved by using a six-port two-position GC valve in conjunction with a solenoid valve (Clippard valve) connected to a vacuum pump. Figure 4-2 shows the sampling procedure employed by Ndlovu (2005) that was also used for this project.

To avoid the partial condensation of vapours in the sampling lines, Ndlovu (2005) mounted the six-port two-position GC valve and Clippard valve onto an aluminium block that was heated using two 10 mm ID × 40 mm L heater cartridges, rated at 200 Watts each. The aluminium block and heater cartridges were also employed for this project.
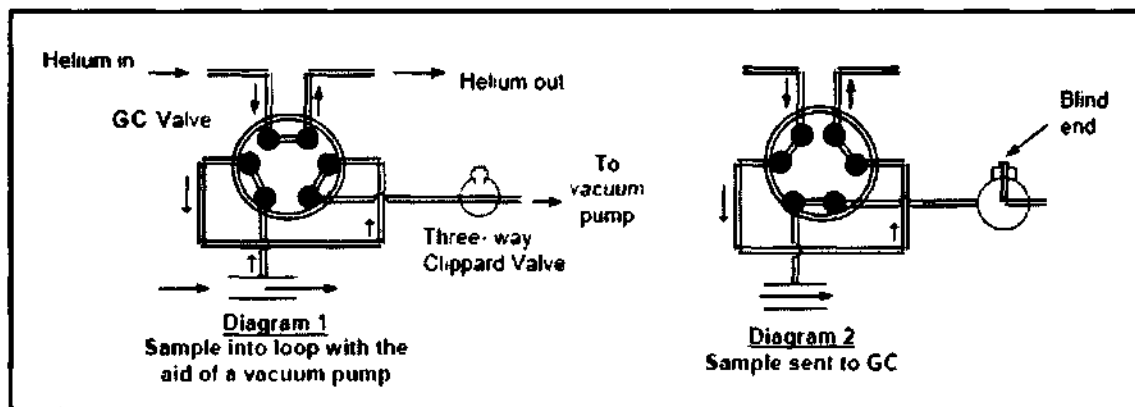
Figure 4-2: Stages involved in the vapour sampling process (Ndlovu, 2005).

4.1.5 Composition Analysis

The equilibrium liquid and vapour samples were accurately analysed by gas chromatography using the Hewlett Packard 5890 Series II GC with a thermal conductivity detector, which used helium as the carrier gas. A 3 m × 1/8 inch stainless steel CRS chromosorb W-HP 80/100 OV-17 silicone (10%) packed column was used for component separation in the GC. The operation, calibration and sampling procedures of the GC are discussed in Chapter 5.

4.2 The Liquid-Liquid Equilibrium Apparatus

As mentioned in Chapter 2, the analytical method using a double-walled glass cell was used to measure the LLE data in this project. In addition to the double-walled glass cell, the following equipment were also used:

- Two Pt-100 temperature sensors.
- Two 4 ½ digit temperature displays.
- A Labcon water bath complete with a temperature controller, pump and ethylene glycol solution.
- A motor with stirrer and DC power supply.

Photograph 4-2 shows the setup of the experimental equipment. All the LLE data were measured at constant temperatures. The constant temperatures were achieved by circulating

ethylene glycol solution from the water bath, using a pump, through the double-walled glass cell, thus providing a jacket to the cell. The contents of the cell were stirred using a miniature variable speed DC motor.

Photograph 4-2: Experimental setup of the LLE equipment.

A – DC power supply; **B** – temperature display units; **C** – Labotech water bath with temperature controller for heating medium; **D** – LLE apparatus with insulation; **E** – motor with stirrer.

4.2.1 The Liquid-Liquid Equilibrium Cell

The double-walled glass cell used for this project was a modification of a previous apparatus (Raal and Brouckaert, 1992). The modification was undertaken by Ndlovu (2005). A schematic diagram of the modified cell is shown in Figure 4-3. The modification improved the thermal insulation of the cell by circulating the ethylene glycol solution through the lid of the cell, unlike the previous apparatus that had a Teflon endcap press-fitted onto the equilibrium cell. The contact between the lid of the cell and the rest of the cell was via a ground glass joint, thus improving the sealing of the cell and preventing contamination from the surroundings. The modification also improved the sampling procedure from the cell. The previous apparatus had a single sampling point and thus could not prevent possible contamination of the samples. The

modified cell of Ndlovu (2005) allowed for higher accuracy for composition analysis by employing two sampling points (A and F). The lid of the cell housed a thermo-well into which a Pt-100 temperature sensor (B) was placed. To achieve mixing of the cell contents, a stirrer (G) driven by a miniature variable speed DC motor was used. A Teflon coated bar (E) held the stirrer in the upright position that prevented excessive vibration when the stirrer was in operation and also assisted with the sealing of the apparatus.
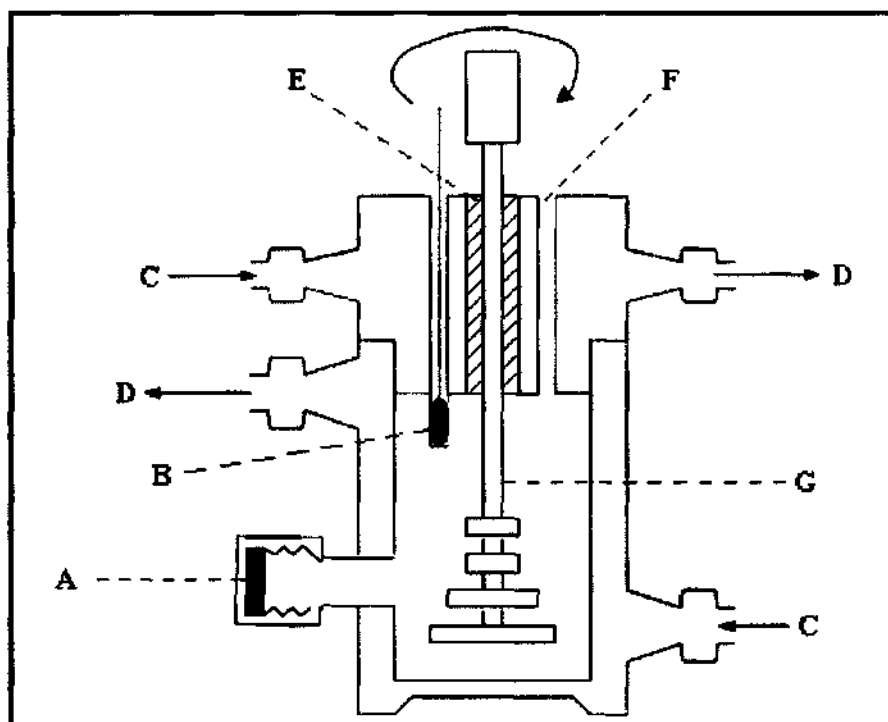
Figure 4-3: Schematic diagram of the LLE cell (Ndlovu, 2005).

A – sample point for denser liquid phase; B – Pt-100 temperature sensor in a thermo-well; C – ethylene glycol solution into the LLE cell jacket; D – ethylene glycol solution away from the LLE cell; E – Teflon coated bar; F – sample point for lighter liquid phase; G – stirrer driven by DC motor.

4.2.2 Temperature Measurement and Control

Two Pt-100 temperature sensors were used for temperature measurements: one for the water bath temperature and the second for the equilibrium temperature. The Pt-100 temperature sensor that was used to measure the water bath temperature was fitted into a thin walled stainless steel tube and fully immersed into the water bath. The Pt-100 temperature sensor for the equilibrium temperature was placed in the thermo-well of the cell, where a drop of oil was immersed in the thermo-well to increase the contact area between the sensor and the glass wall.

A temperature controller, fitted with a pump, was used to circulate the ethylene glycol solution through the jacketed cell walls and control its temperature within range of ± 0.02 °C.

4.2.3 Sampling and Composition Analysis

Once equilibrium was achieved, the liquid samples from each phase were withdrawn using a gas-tight liquid syringe. All the LLE data were analysed by gas chromatography using the Chrompack 9000 GC with a thermal conductivity detector and helium as the carrier gas. A 2 m × 1/8 inch stainless steel Tenax TA 80/100 packed column was used for component separation in the GC. The Chrompack 9000 GC had a "built in" temperature ramp function that was necessary to analyse samples for all ternary LLE systems and was therefore chosen over the Hewlett Packard Series II GC used for the VLE/VLLE systems. The operation, calibration and sampling procedures of the GC are discussed in Chapter 5.

5

CHAPTER FIVE

EXPERIMENTAL PROCEDURE

The accurate measurements of VLE, LLE and VLLE data are only possible if the equipment used for the thermodynamic measurement of such quantities as temperature, pressure and composition are correctly operated and calibrated. Furthermore, sample preparation and analysis also play an important role. Therefore, this chapter will focus on the preparation, calibration and the operation of both the VLE apparatus and the LLE apparatus.

5.1 The Vapour-Liquid Equilibrium Apparatus

5.1.1 Preparation

5.1.1.1 Leak Detection

Leaks have an adverse effect on the measurement and control of pressure. Therefore, it is important than the apparatus is operated without any leaks. The usual method of leak detection

involves the pressurising of the apparatus and application of a soapy solution to joints that are suspected for possible leaks, bubbles are observed when a leak is present. However, the apparatus used in this work was made of glass and thus could not withstand any pressure greater than atmospheric pressure. Furthermore, all measurements for this project were done at pressures lower than atmospheric pressure.

Hence, an alternative method was used to detect for any leaks. This method involved drawing a vacuum in the apparatus with the aid of the vacuum pump and then controlling the pressure in the system to a specified value. When the pressure reached a stable value, the pump and controller were then switched off and the apparatus was completely isolated for at least two hours. An increase in the pressure of the system indicated a leak in the apparatus. Joints on the apparatus that were suspected of containing a leak were sprayed with a volatile chemical (acetone was used for this project) and the confirmation of a leak was seen as a small increase in the system pressure. The increase in pressure is caused by the vaporisation of the volatile chemical. The identified leaks were then eliminated by applying high vacuum grease on ground glass joints and vacuum seals on steel pipe joints.

5.1.1.2 Cleaning of the VLE Apparatus

The VLE apparatus was thoroughly cleaned prior to the calibration of the pressure transmitter and temperature sensor. Cleaning the apparatus is imperative as any contaminants in the system have a considerable effect on the VLE data. The cleaning process involved circulating acetone in the VLE apparatus under isobaric conditions for approximately an hour. The acetone was then drained from the apparatus and the process repeated with clean acetone. For chemicals that were difficult to remove, the VLE apparatus was cleaned for a third time. After the final cleaning, the acetone was drained from the apparatus and any residual acetone was flashed off with the aid of a vacuum pump.

5.1.2 Calibration

5.1.2.1 Pressure Transmitter Calibration

The pressure calibration was undertaken first as the temperature sensor calibration requires an accurate pressure reading. The WIKA P10 pressure transmitter was calibrated using a standard pressure transmitter that was connected to the VLE apparatus. The standard pressure transmitter was calibrated by WIKA to provide an accurate pressure reading. The BUCHI pressure controller was used to set a specific pressure reading in the VLE apparatus. When the system

pressure reached a stable reading, the pressure from the WIKA P10 pressure transmitter (read from the pressure display unit that was connected to it) and the standard pressure transmitter were recorded. The procedure was repeated for various pressure readings within the anticipated pressure range. When the actual pressure (from the standard pressure transmitter) was plotted against the display pressure (from the WIKA P10 pressure transmitter), a linear response was observed, as shown in Figure 5-1. The pressure accuracy was estimated as ±0.03 kPa and controlled to within 0.01 kPa.

$$P_{actual} = 0.9998(P_{display}) + 0.1578$$
$$R^2 = 1$$
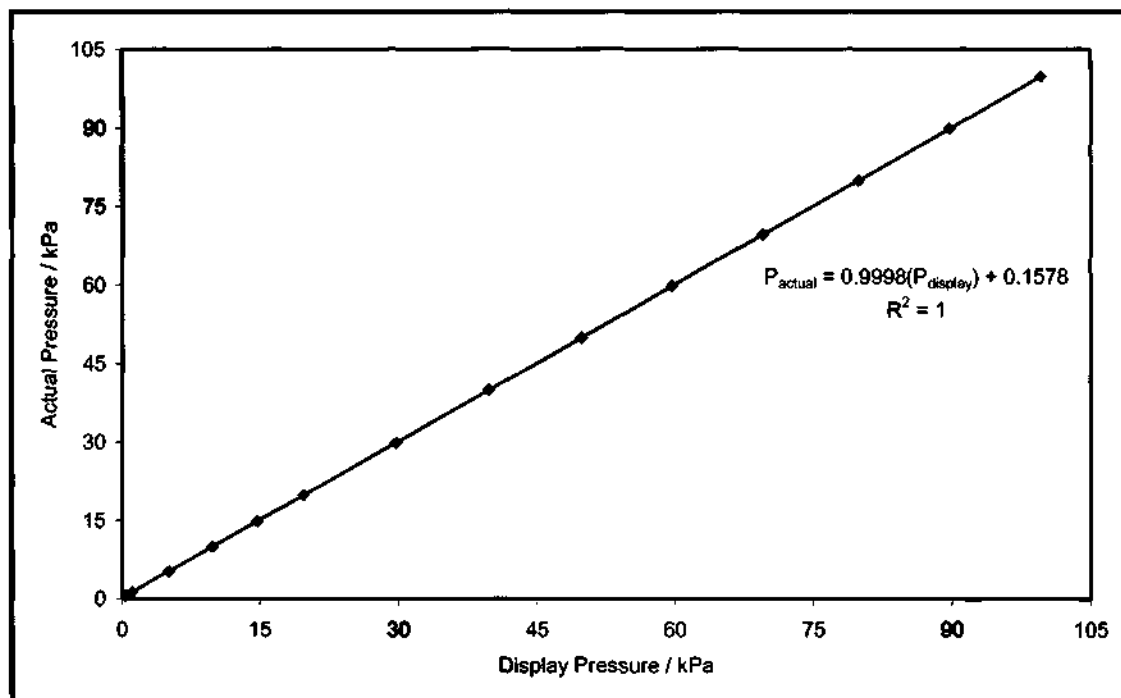
Figure 5-1: Pressure transmitter calibration for the VLE apparatus.

5.1.2.2 Temperature Sensor Calibration

A Class A Pt-100 temperature sensor was used to measure the equilibrium temperature within the VLE apparatus. Unlike the pressure calibration, the temperature calibration was carried out using very pure chemicals (>99.5 mass % pure). Two chemicals (ethyl acetate {low boiling} and decane {high boiling}) were used to ensure the temperature calibration covered the full experimental temperature range. The calibration process involved the isobaric operation of the VLE apparatus over a range of pressures. The temperature sensor reading (obtained from the digital temperature display connected to the temperature sensor) was recorded for each pressure reading. The actual temperature was obtained using Antoine's equation at these pressures, where the Antoine constants for each chemical were taken from Reid et al. (1988). The actual temperature was then plotted against the display temperature to yield the temperature

calibration. Figure 5-2 shows the temperature calibration with a least squares line fitted to the data. The accuracy of the measured temperature was estimated to be within ±0.02 °C and the precision of the temperature control varied between 0.01 and 0.05 °C.
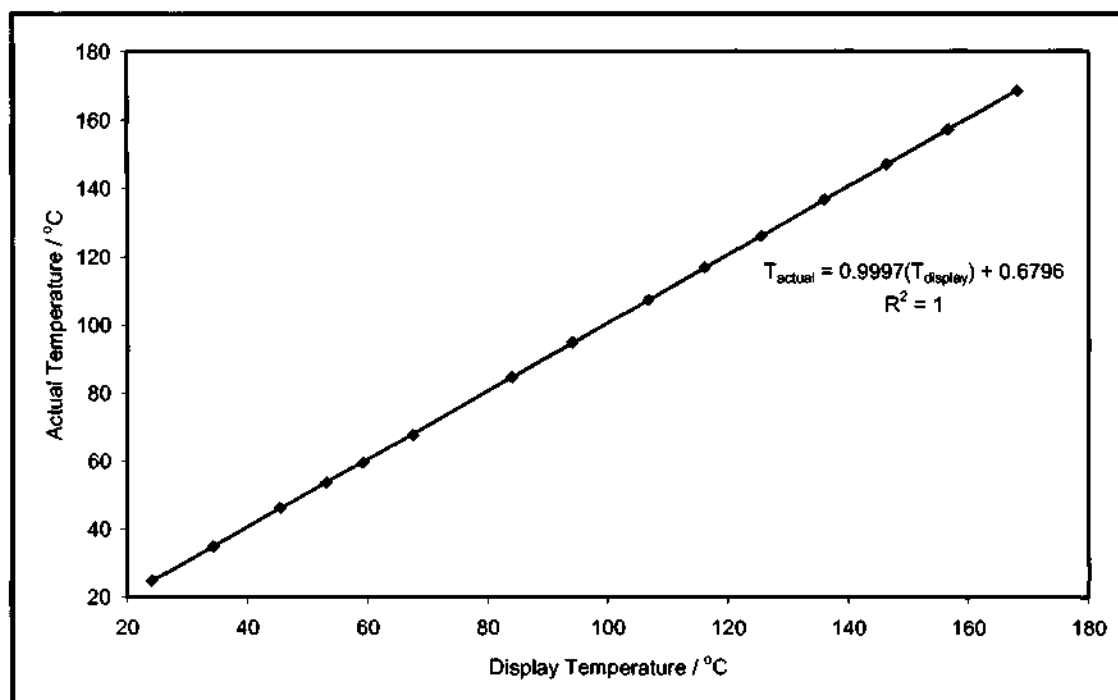
Figure 5-2: Temperature sensor calibration for the VLE apparatus.

5.1.2.3 Gas Chromatograph Calibration

As mentioned in Section 4.1.5, a Hewlett Packard 5890 series II gas chromatograph (GC) with a thermal conductivity detector, which used helium as the carrier gas was used to obtain accurate composition measurements for the VLE systems studied in this project. A 3 m × 1/8 inch stainless steel CRS chromosorb W-HP 80/100 OV-17 silicone (10%) packed column was employed for component separation in the GC. The operating condition for this GC is presented in Table 5-1.

The GC calibration followed the area ratio method suggested by Raal and Mühlbauer (1998). Standard mixtures were prepared gravimetrically over the entire composition spectrum and analysed. To prevent detector overloading, sample volumes of 0.5 μl were used. Generally, the number of moles (n) passing the detector in a GC is proportional to the peak area (A^*) that is obtained from an electronic integrator:

$$n_i = A_i^* F_i \qquad (5\text{-}1)$$

where, F_i is defined as the proportionality constant and is known as the response factor. However, the peak area (A^*) depends on the amount of sample injected and since this amount is not generally reproducible, Raal and Mühlbauer (1998) suggest the use of area ratios. For a binary system:

$$\frac{n_1}{n_2} = \left(\frac{F_1}{F_2}\right)\left(\frac{A_1^*}{A_2^*}\right) = \frac{x_1}{x_2} \qquad (5\text{-}2)$$

The response factor ratio, F_1/F_2, is obtained from the plot of A_1^* / A_2^* versus x_1 / x_2 over the full composition range and should extrapolate through the origin. Equation (5-2) indicates that the response factor ratio, F_1/F_2, is necessarily constant for a linear plot of A_1^* / A_2^* versus x_1 / x_2 and is obtained as the slope of this plot. Furthermore, the inverse of the slope for the linear plot of A_1^* / A_2^* versus x_2 / x_1 should equal to F_1/F_2 (i.e. F_1/F_2 should equal the inverse of F_2/F_1 and visa versa). The shape of the calibration plots depend on the detector type and the system under investigation. Therefore, non-linear plots are not uncommon, especially for thermal conductivity detectors. However, these plots should also pass through the origin. The accuracy of the GC analysis for the mole fraction composition was within 1×10^{-3}. The operating conditions for the Hewlett Packard 5890 Series II GC is presented in Table 5-1.

Table 5-1: Operating conditions for the Hewlett Packard 5890 series II gas chromatograph.

Operating Condition	System	
	Cyclohexane + Ethanol	1-Dodecene + 1-Nonanol
Gas flowrate [ml/min]	30	30
Oven Temperature Profile Temperature [°C]	140	160
TCD Detector Temperature [°C]	160	210
Injector Profile Temperature [°C]	160	210

5.1.3 Operating Procedures

5.1.3.1 Isobaric Operation

The Techne cooling coil unit and the pump of the Labotech water bath were first switched on to allow the ethylene glycol solution to reach a sufficiently low temperature (about 5 °C). Once this temperature was achieved, the power supply to the temperature and pressure displays, the pressure controller and the motors for the stirrers were then switched on. The clean still was then charged with only one of the pure components, until the liquid filled the boiling chamber to a level ± 4 cm above the top of this chamber and the condensate receiver was full. This ensured that the material would be forced up the Cottrell tube once boiling began. The vacuum pump was then switched on and the pressure controller was set to the desired operating pressure. At this point, the pressure in the still decreased towards the set-point pressure.

The internal and external heaters were then switched on to bring the liquid in the boiling chamber to a boil, where the internal heater provided the principle heating and the external heater compensated for heat losses to the environment. For VLLE systems only, the heater cartridges on the sampling valve block and the nichrome heating wire around the vapour sampling lines and the equilibrium chamber were also switched on. It is important that adequate heat be applied to achieve a vigorous pumping action in the Cottrell tube and a good circulation rate, where the circulation rate is determined by observing the drop rate from the condenser. The power supply from the internal heater to the still was then increased until the plateau region was found. According to Kneisl et al. (1989), this is the region where the boiling temperature does not change for a slight increase in the power input. Kneisl et al. (1989) also found the boiling temperature to be a function of the power input. Thus, operation in the plateau region is critical, as operation outside this region gives rise to incorrect boiling point temperatures. Once operation in the plateau region was achieved, the system was allowed to reach equilibrium, at which point the temperature and composition are constant. For most systems, equilibrium is attained within thirty minutes. However, for the systems measured in this work, an equilibration time of approximately fifty minutes was found to be sufficient.

Once equilibrium had been established, the temperature was then noted. For VLE systems, the liquid and vapour samples were then withdrawn through the sample septa using a gas-tight liquid syringe and analysed by gas chromatography. Sample injections for each phase were made into the GC to obtain the compositions, where an average deviation for the area ratios within a tolerance of 0.001 was used. For VLLE systems, the temperature controller that regulates the heat to the outside wall of the equilibrium chamber was set to a temperature that

was 5 °C above the equilibrium temperature. The temperatures of the sampling valves and the vapour sample line to the GC were manually adjusted to also reach a temperature that was 5 °C above the equilibrium temperature, by carefully varying the voltage to the heater cartridges within the aluminium heating block and the nichrome wire. Once these temperatures were established, the vapour samples were withdrawn using the sampling system specifically designed for partially miscible systems (already discussed in Section 4.1.4) and the liquid samples were withdrawn and analysed in the same manner as for the VLE systems.

A small volume of the liquid was then removed from the still, either from the liquid sampling chamber or the vapour condensate receiver, and a similar volume of the second component of the binary system was then added to the still. This allowed the system composition to be adjusted. The new mixture was allowed to reach equilibrium and the liquid and vapour samples were then withdrawn and analysed. This procedure was repeated until the entire composition range had been covered.

5.1.3.2 Isothermal Operation

Isothermal operation of the still was dependant on the successful operation of the still under isobaric mode, as the isothermal operation was manually controlled. Hence, the start-up procedure is the same as for isobaric operation. The pressure in the still was first set to a value such that when equilibrium was reached, the equilibrium temperature was close to the operating temperature. The isobaric operation was then stopped and the temperature was manually adjusted to its desired value, where increasing or decreasing the pressure had the effect of increasing or decreasing the temperature respectively. Once the desired temperature was found, the plateau was then found and the pressure corresponding to the desired temperature was noted. Liquid and vapour samples were then withdrawn and analysed in the same manner as for the isobaric operation.

5.2 The Liquid-Liquid Equilibrium Apparatus

5.2.1 Preparation

5.2.1.1 Cleaning of the LLE Apparatus

The LLE apparatus was quite simple to set up and disassemble. This therefore allowed the LLE apparatus to be easily cleaned. Once disassembled, the LLE cell, header and stirrer were

thoroughly cleaned with acetone in a fume-hood. The disassembled parts were then left in the fume-hood to allow the excess acetone to evaporate for approximately thirty minutes. The LLE apparatus was then easily re-assembled.

5.2.2 Calibration of Temperature Sensors

The equilibrium temperature for LLE measurements were obtained from a temperature sensor placed in the thermo-well of the cell (see Section 4.2.2). The cell temperature sensor was calibrated using a standard temperature probe TE - 4023 from WIKA. Once the LLE apparatus was set up, the cell was then filled with clean distilled water and the pump of the Labotech water bath was switched on to allow water to circulate through the jacket of the cell. The standard temperature probe was then placed into the distilled water that filled the cell. The temperature sensor of the cell was connected to a temperature display unit while the standard temperature probe was connected to multi-meter to allow the resistance of the probe to be read. A desired temperature was then set on the temperature controller of the Labotech water bath and the system was allowed to reach thermal equilibrium. Once thermal equilibrium was established, the corresponding readings from the temperature display unit and the multi-meter were recorded. The above process was then repeated for a set of temperatures within the anticipated temperature range by increasing the temperature of the circulating ethylene-glycol solution. A calibration chart for the standard temperature probe was provided by WIKA to enable the actual temperatures to be determined from the resistance values measured with the multi-meter. This therefore allowed the actual temperatures to be plotted against the cell temperatures, as shown in Figure 5-3. The accuracy of the measured temperature was estimated to be within ±0.02 °C and the precision of the temperature control was within ±0.02 °C.

The bath temperature sensor was calibrated following the same procedure outlined for the cell temperature sensor calibration using the same standard temperature probe. This time however, both the bath temperature sensor and the standard temperature probe were immersed in the Labotech water bath. The bath temperature sensor was connected to another temperature display unit but the standard temperature probe was connected to the same multi-meter used for the cell temperature sensor calibration. Figure 5-4 shows the calibration obtained. The accuracy of the measured temperature was estimated to be within ±0.03 °C and the precision of the temperature control was within ±0.02 °C.

$$T_{actual} = 1.013(T_{dislay}) - 1.3027$$
$$R^2 = 1$$
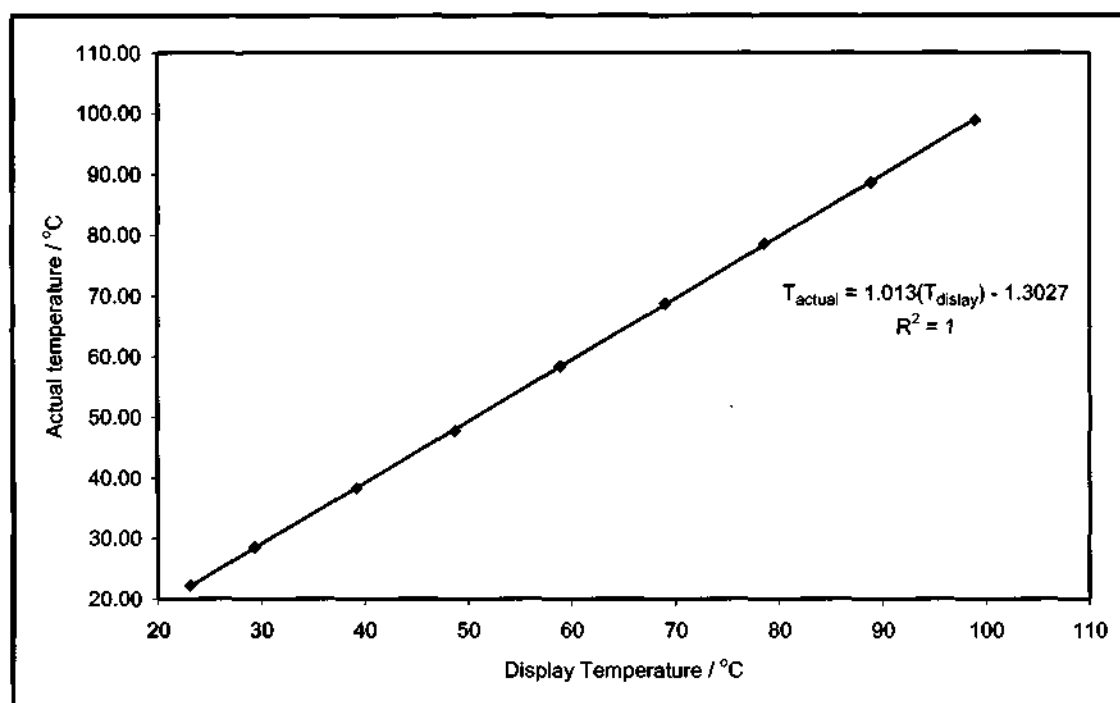
Figure 5-3: Cell temperature sensor calibration for the LLE apparatus.

$$T_{actual} = 0.9987(T_{display}) + 1.1002$$
$$R^2 = 0.9998$$
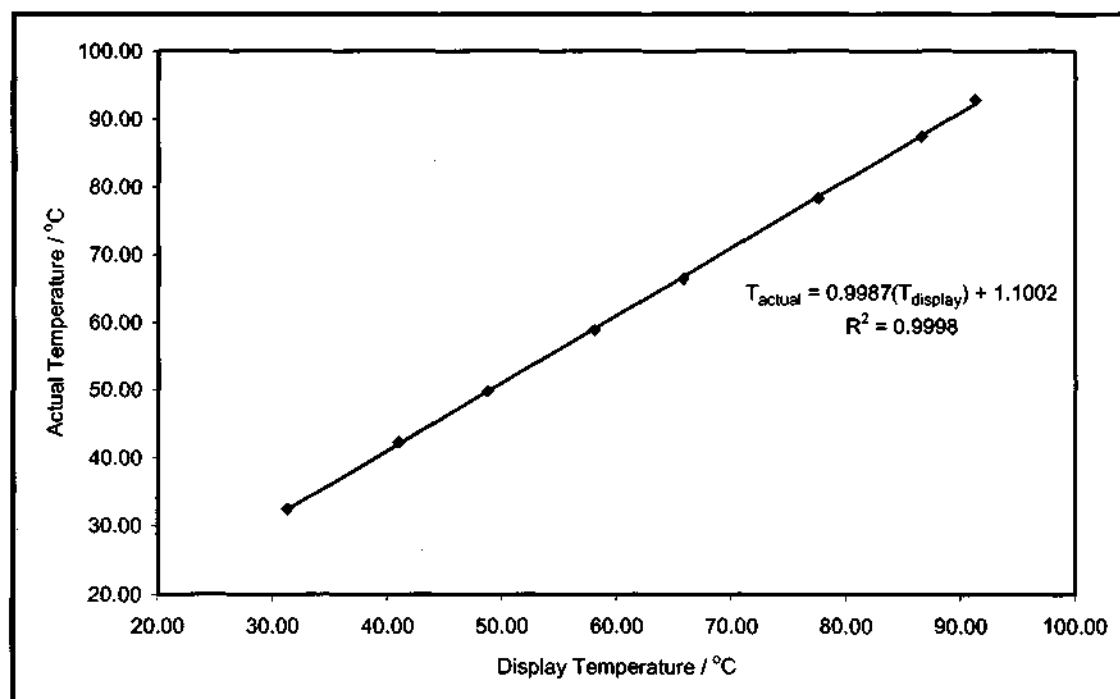
Figure 5-4: Bath temperature sensor calibration for the LLE apparatus.

5.2.3 Gas Chromatograph Calibration

Composition analysis for all LLE systems was done using the Chrompack 9000 GC with a thermal conductivity detector, which used helium as the carrier gas. A 2 m × 1/8 inch stainless steel Tenax TA 80/100 packed column was used to separate the components in the GC. The GC calibration for LLE work required a suitable solvent (ethanol was used for all systems studied in this work) to make all heterogeneous mixtures miscible. Therefore, a different packed column was used as the components of the LLE measurements could not be separated with the GC column that was used for the VLE measurements. Furthermore, the Chrompack 9000 GC was chosen over the Hewlett Packard Series II GC as the former contained a temperature ramp function that was necessary to separate the components for each LLE system studied. The calibration procedure followed the area ratio method of Raal and Mühlbauer (1998), already outlined in Section 5.1.2.3. For ternary systems however, two pairs of components were needed to determine all the component compositions. This was achieved by a simple and direct relation of the response factor ratios as outlined by Raal and Mühlbauer (1998). The accuracy of the GC analysis for the mole fraction composition was within 1×10^{-4}. The operating conditions for the Chrompack 9000 GC is presented in Table 5-2.

Table 5-2: Operating conditions for the Chrompack 9000 gas chromatograph.

Operating Condition	System	
	Test Systems	All New Systems
Gas flowrate [ml/min]	30	30
Oven Temperature Profile		
Initial temperature [°C]	210	120
Hold time [min]	-	4
Temperature ramp [°C/min]	-	45
Final temperature [°C]	-	220
Hold time [min]	-	3
TCD Detector		
Temperature [°C]	225	240
Attenuation	4	4
Injector Profile		
Temperature [°C]	225	240

5.2.4 Operating Procedure

5.2.4.1 Binary LLE Measurements

The two components were firstly added into the clean cell in such as manner that an immiscible mixture was formed, where it was also ensured that the interface between the two liquid phases was above the sampling point of the denser liquid phase. The temperature controller of the water bath was then set to a desired temperature. The pump and the motor for the stirrer were then switched on. The mixture was then stirred for approximately an hour. The two liquid phases were then allowed to reach thermodynamic equilibrium for approximately thirty minutes, depending on the system studied. Sample injections for each phase were then taken and injected into the GC for composition analysis, where an average deviation for the area ratios within a tolerance of 0.001 was used. The system was then confirmed to be at thermodynamic equilibrium once the composition of each sample for each phase remained constant and the temperature was then recorded.

The temperature was then raised by setting a higher temperature on the temperature controller of the water bath and the above procedure was then repeated. This was done for several temperatures over the interval of interest. All LLE measurements were done at atmospheric pressure. Once all the measurements were complete for a specific system, the temperature controller, pump and stirrer motor were then switched off and the mixture was then allowed to cool before the apparatus was cleaned.

5.2.4.2 Ternary LLE Measurements

The experimental procedure was carried out using the method described by Alders (1959). Initially, a binary mixture was added into the clean cell in the same manner as for the binary LLE measurements. The thermodynamic equilibrium compositions for this binary mixture were determined using the same procedure as described for the binary LLE measurements at the desired temperature for the ternary LLE measurement. Once these compositions were determined, a small volume of the third component was then added to the system and the new mixture was stirred at a low enough speed to prevent emulsification for approximately an hour. The mixture was then allowed approximately thirty minutes (depending on the system studied) to reached thermodynamic equilibrium and the compositions of each phase were then analysed following the same procedure as described for the binary LLE measurements. The above procedure was then repeated for increasing increments of the third component until the phase envelope was completed.

6

CHAPTER SIX

EXPERIMENTAL RESULTS

The precision and accuracy of pressure, temperature and composition measurement and the purity of the reagents used greatly influence the accuracy of the experimental results obtained. Therefore, to ensure correct operation of the vapour-liquid equilibrium (VLE) apparatus, a test system was measured: (cyclohexane + ethanol) at 40 kPa. Two test systems were also measured with the liquid-liquid equilibrium (LLE) apparatus: a binary system of (heptane + methanol) and a ternary system of (heptane + toluene + methanol). These test systems were chosen as they are difficult to measure, non-ideal and reliable literature data were available for verification. The purities of the chemicals used in this work were also determined to ensure the accuracy of the measured data.

New VLE data for the system 1-dodecene + 1-nonanol at 403.15 K, binary LLE data for the systems; (acetonitrile + 1-dodecene) and (water + 1-nonanol) and ternary LLE data for the systems; (water + acetonitrile + heptanoic acid), (water + acetonitrile + 1-nonanol), (water + acetonitrile + dodecane) and (water + acetonitrile + 1-dodecene) were then measured at 323.15 K.

This chapter thus presents the results of the chemical purity analysis for the reagents used in this work and the experimental vapour pressure data. Also included are the VLE and LLE results for the test systems and new systems, already mentioned above that were measured in this work. The analyses of the experimental measurements are presented in Chapter 7.

6.1 Chemical Purity

Cyclohexane, ethanol, toluene and ethyl acetate were purchased from Capital Laboratory Suppliers cc. Acetonitrile, methanol, heptane, heptanoic acid, decane and dodecane were purchased from Merck, while 1-nonanol and 1-dodecene were obtained from Fluka and distilled water was used. All reagents were used without further purification as gas chromatographic analysis, following the method of Raal and Mühlbauer (1998), revealed no significant impurities. The chemical purities were further analysed by refractive index measurement and compared with literature values. The gas chromatographic analysis and the refractive index measurements are presented in Table 6-1.

Table 6-1: Chemical purities and refractive indices.

Reagent	Refractive Index (293.15 K)		GC Analysis (Mass %)	Min. Purity (Mass %)[b]
	Experimental	Literature[a]		
Acetonitrile	1.3441	1.3442	99.9	99.9
Heptanoic Acid	1.4175	1.4170	99.3	99.0
1-Nonanol	1.4322	1.4340	99.1	98.0
Dodecane	1.4217	1.4216	99.5	99.0
1-Dodecene	1.4301	1.4300	99.5	99.0
Ethyl Acetate	1.3721	1.3720	99.8	99.7
n-Decane	1.4096	1.4102	99.5	99.5
Methanol	1.3286	1.3288	99.6	99.8
Heptane	1.3877	1.3878	99.8	99.8
Toluene	1.4964	1.4961	99.6	99.8
Water	1.3330	1.3328	99.8	-

[a]Weast et al. (1982-1983)

[b]Stated by supplier

6.2 Vapour Pressure Data

Vapour pressure data were measured using the VLE apparatus for all chemicals that were used for VLE or VLLE measurements. These chemicals included: ethanol, cyclohexane, acetonitrile, water, 1-nonanol and 1-dodecene. The experimental data are presented in Tables 6-2 to 6-6 and are shown graphically in Figures 6-1 to 6-5. All the experimentally measured vapour pressure data were compared to literature values found in Reid et al. (1988). The vapour pressure data were regressed to obtain parameters for the Antoine and Wagner equations, discussed further in Section 7.2.

Table 6-2: Vapour pressure data for ethanol.

Experimental	
P	T
[kPa]	[K]
15.25	309.96
20.23	315.51
30.19	323.59
40.25	329.77
50.11	334.58
60.07	338.79
70.03	342.32
79.99	345.44
89.95	348.40
100.01	351.06

Table 6-3: Vapour pressure data for cyclohexane.

Experimental	
P	T
[kPa]	[K]
20.23	308.05
30.19	318.02
40.15	325.84
50.11	331.88
60.07	337.30
70.03	341.83
79.99	346.09
89.95	349.87
98.91	352.78

Table 6-4: Vapour pressure data for acetonitrile.

Experimental	
P	T
[kPa]	[K]
15.02	303.92
25.17	316.12
34.75	324.21
45.05	331.01
54.49	336.31
69.14	343.21
84.93	349.41
100.50	354.71

Table 6-5: Vapour pressure data for water.

Experimental	
P	T
[kPa]	[K]
30.29	342.71
40.38	349.41
53.43	356.20
60.39	359.50
76.44	365.50
80.34	366.80
93.36	371.00

Table 6-6: Vapour pressure data for 1-nonanol.

Experimental	
P	T
[kPa]	[K]
1.26	374.20
3.38	392.49
5.27	401.59
7.06	408.19
9.15	414.19
13.64	423.18

Table 6-7: Vapour pressure data for 1-dodecene.

Experimental	
P	T
[kPa]	[K]
1.30	362.30
3.19	381.00
6.17	396.49
10.17	409.39
15.15	420.59
17.08	423.18
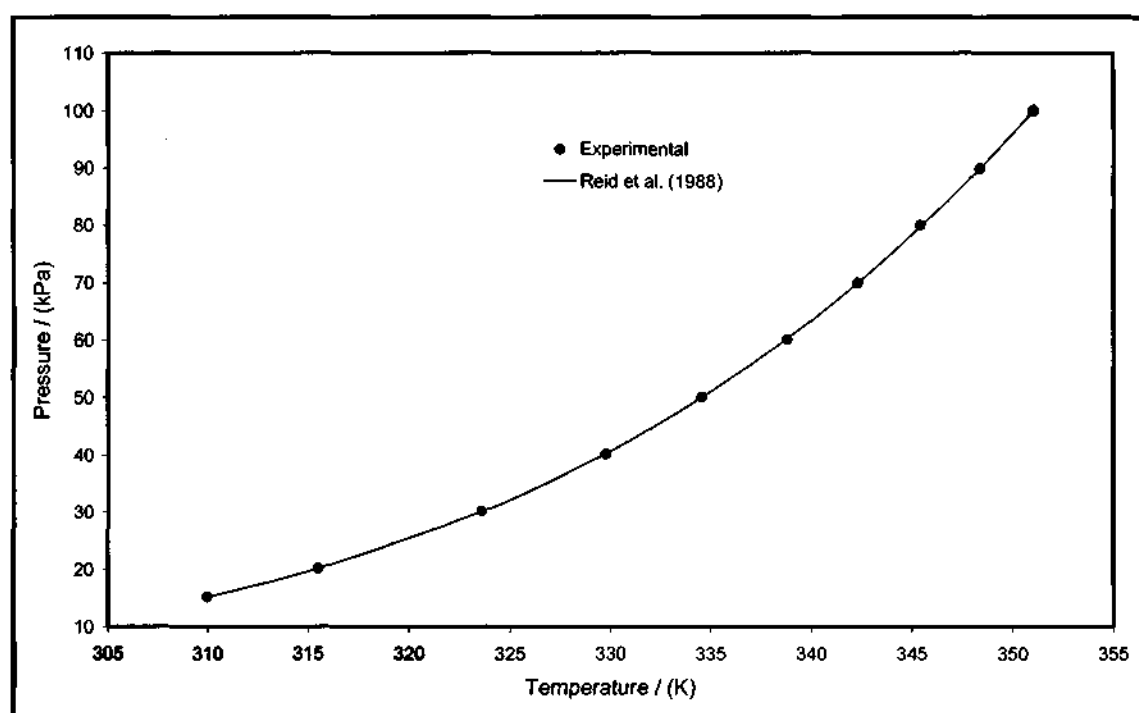
Figure 6-1: Vapour pressure curve for ethanol.
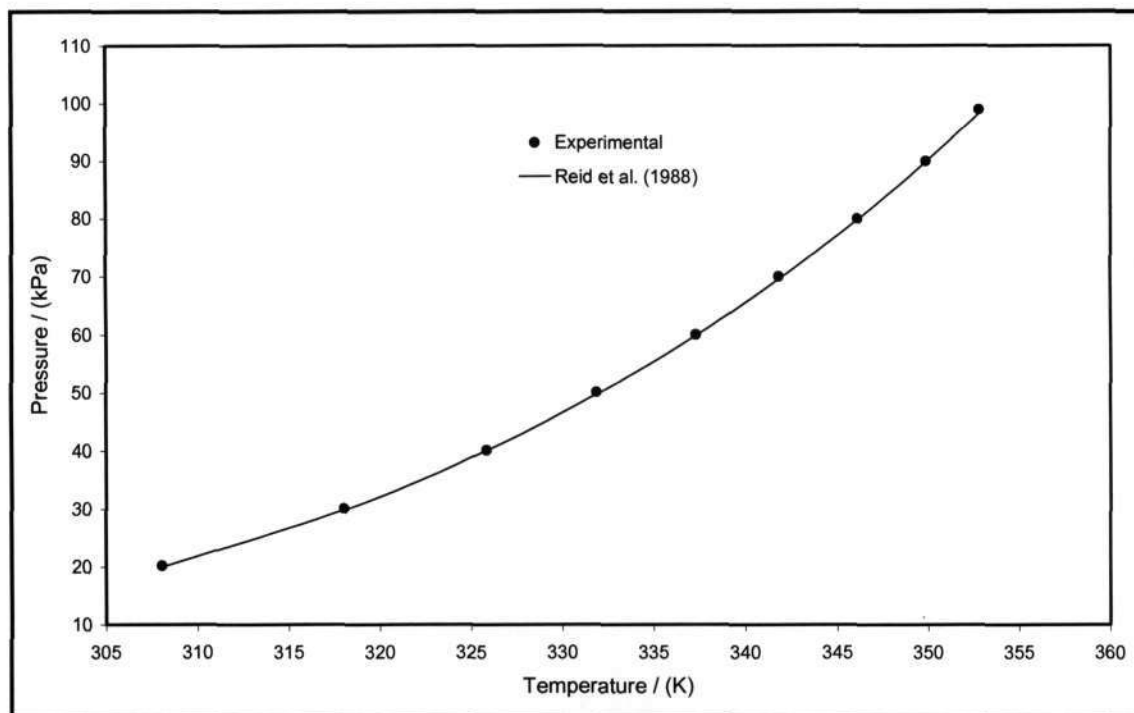
Figure 6-2: Vapour pressure curve for cyclohexane.
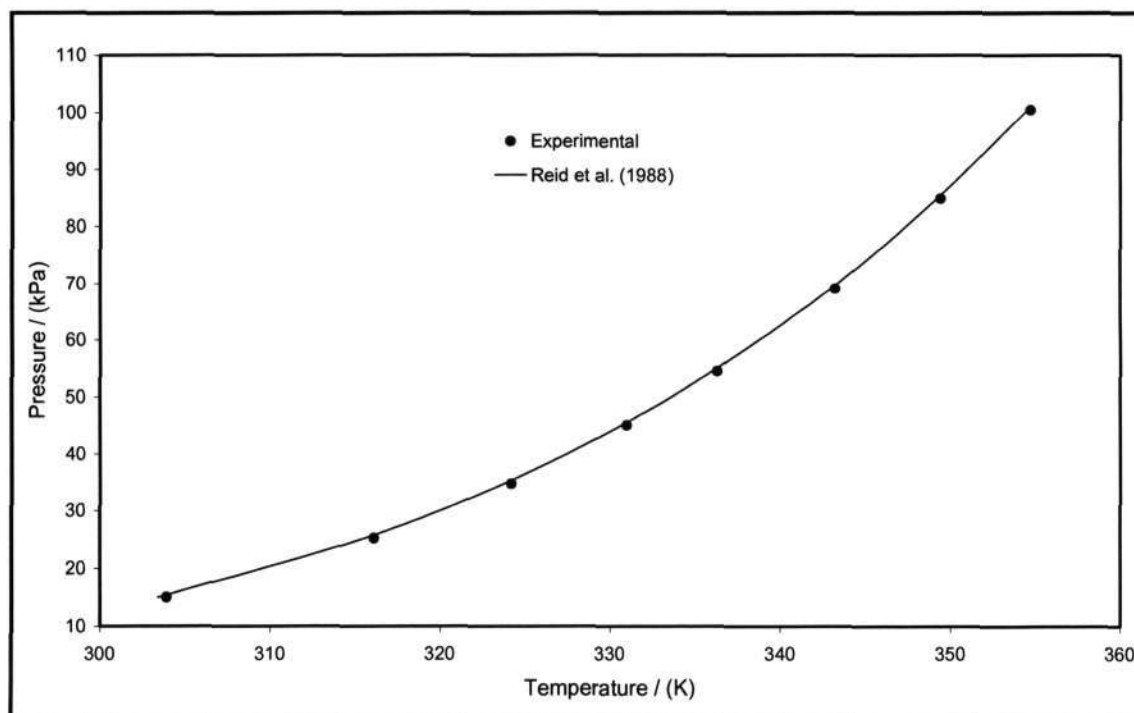
Figure 6-3: Vapour pressure curve for acetonitrile.
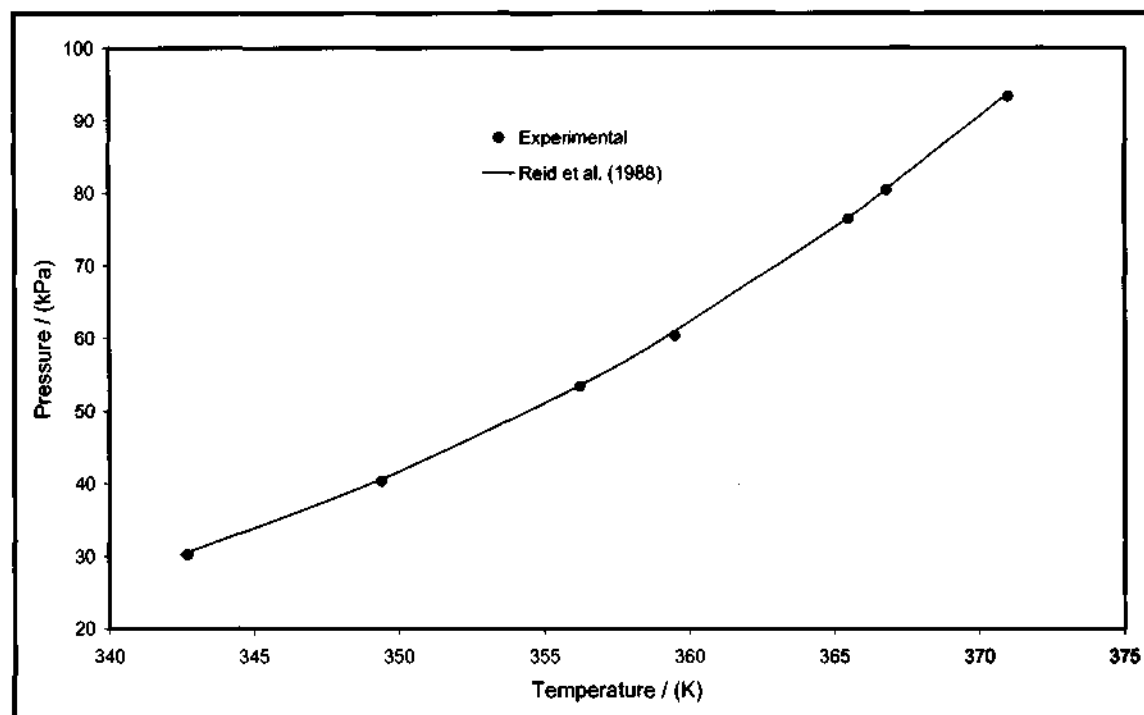
Figure 6-4: Vapour pressure curve for water.
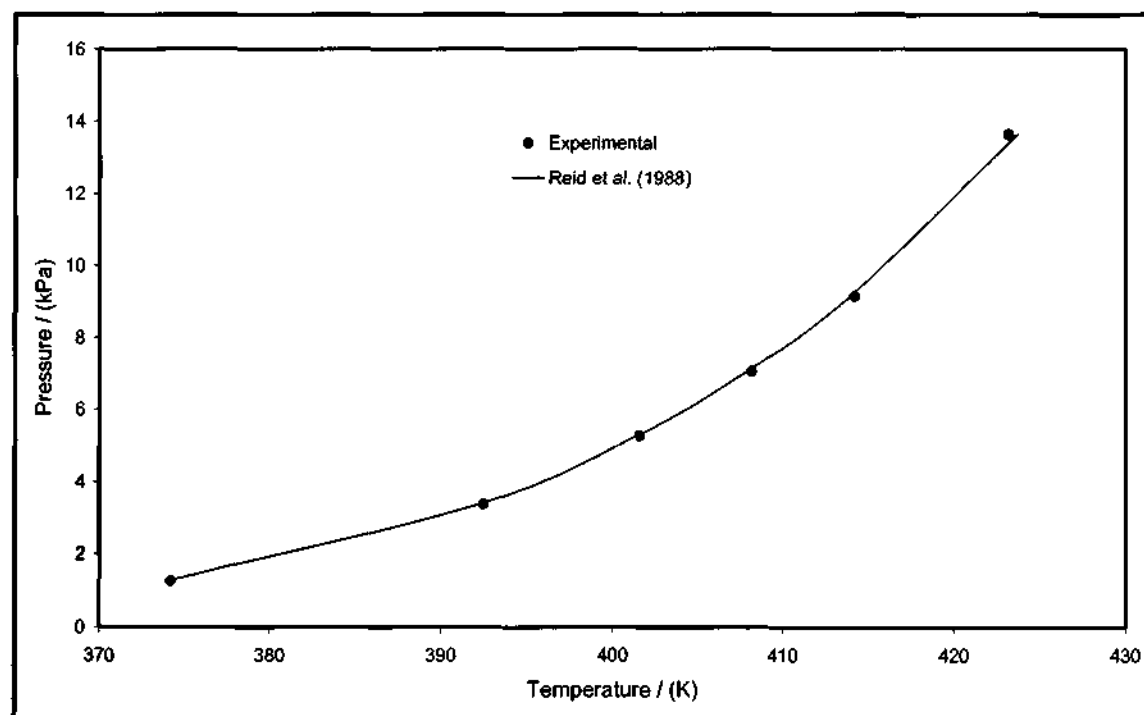
Figure 6-5: Vapour pressure curve for 1-nonanol.
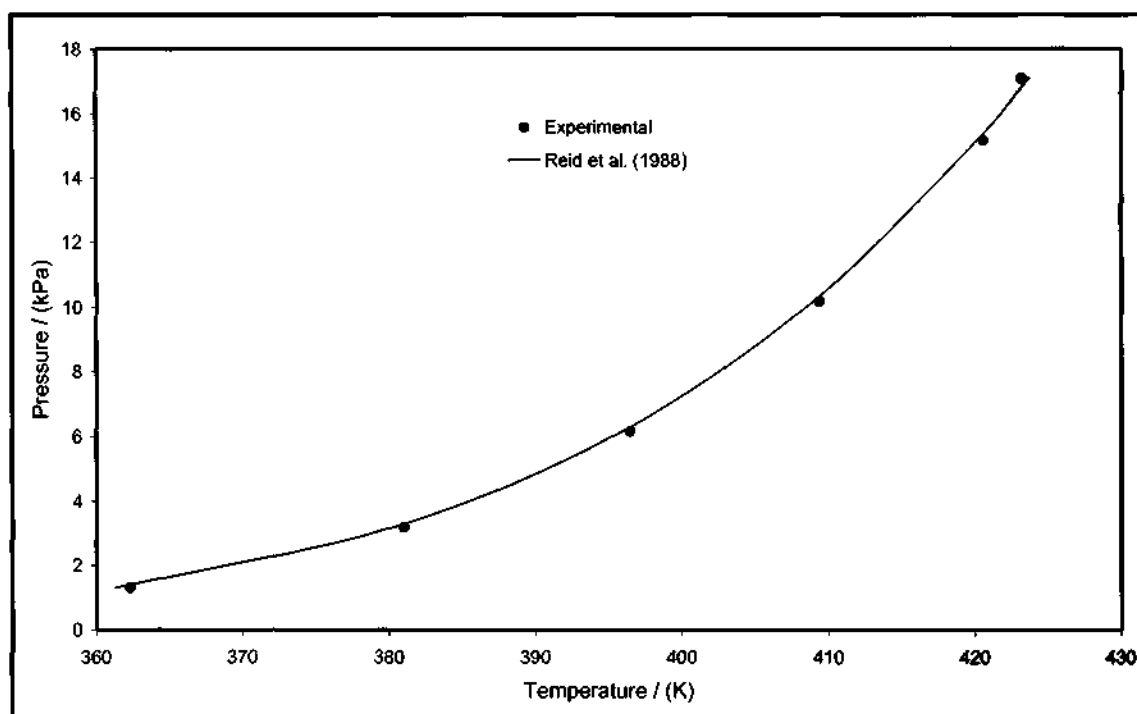
Figure 6-6: Vapour pressure curve for 1-dodecene.

6.3 Vapour-Liquid Equilibrium Results

The Hewlett Packard 5890 Series II gas chromatograph was used to obtain the compositions of both the vapour and liquid phases at equilibrium for the VLE systems, with the operating conditions given in Table 5-1. For both VLE systems, the estimated precision of the mole fraction composition was within 1×10^{-3}.

6.3.1 Cyclohexane (1) + Ethanol (2)

The cyclohexane (1) + ethanol (2) system at an isobar of 40 kPa was chosen as a test system for the VLE apparatus as this system was non-ideal and reliable literature data was available for comparison. The data measured by Joseph et al. (2001) at 40 kPa was used for comparison. The gas chromatographic calibration graphs, experimental data and the x-y and T-x-y plots are presented below.
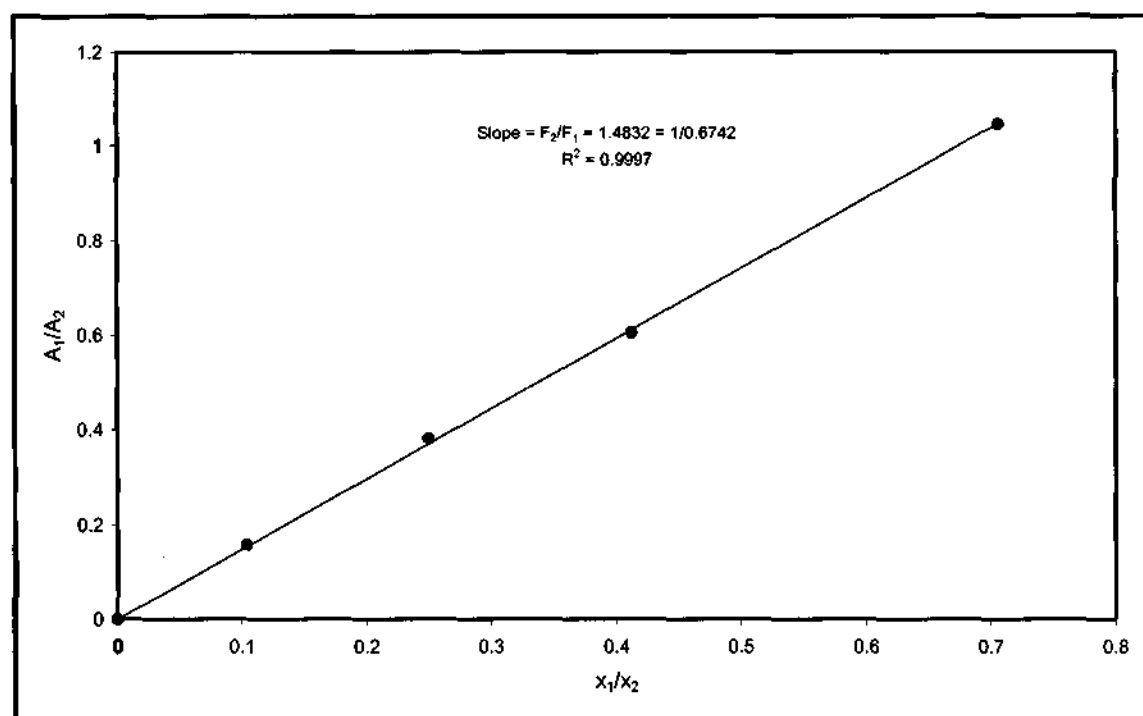
Figure 6-7: GC calibration graph the cyclohexane (1) + ethanol (2) system (cyclohexane dilute region).
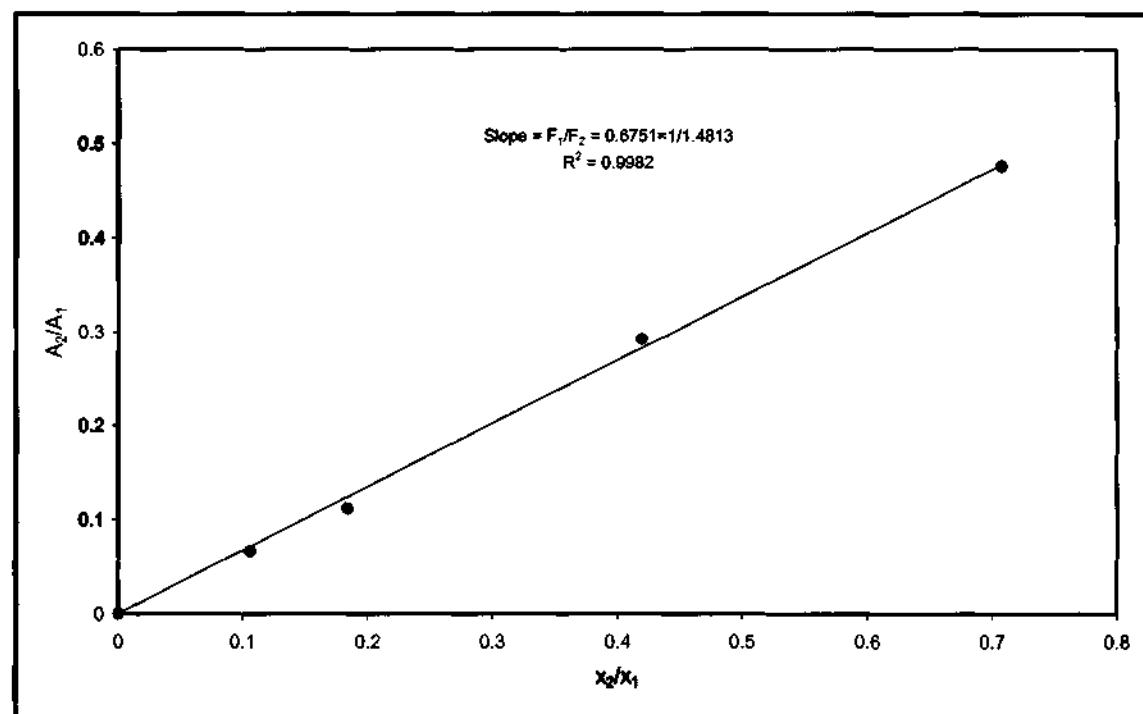
Figure 6-8: GC calibration graph for the cyclohexane (1) + ethanol (2) system (ethanol dilute region).

Table 6-8: Vapour-liquid equilibrium data for cyclohexane (1) + ethanol (2) at 40 kPa.

T [K]	x_1	y_1
329.77	0.000	0.000
325.14	0.026	0.196
322.17	0.052	0.321
321.01	0.073	0.367
318.87	0.117	0.446
318.12	0.131	0.465
317.67	0.148	0.48
315.04	0.362	0.589
314.54	0.485	0.619
314.52	0.563	0.628
315.85	0.937	0.677
317.72	0.968	0.736
320.86	0.982	0.839
325.84	1.000	1.000
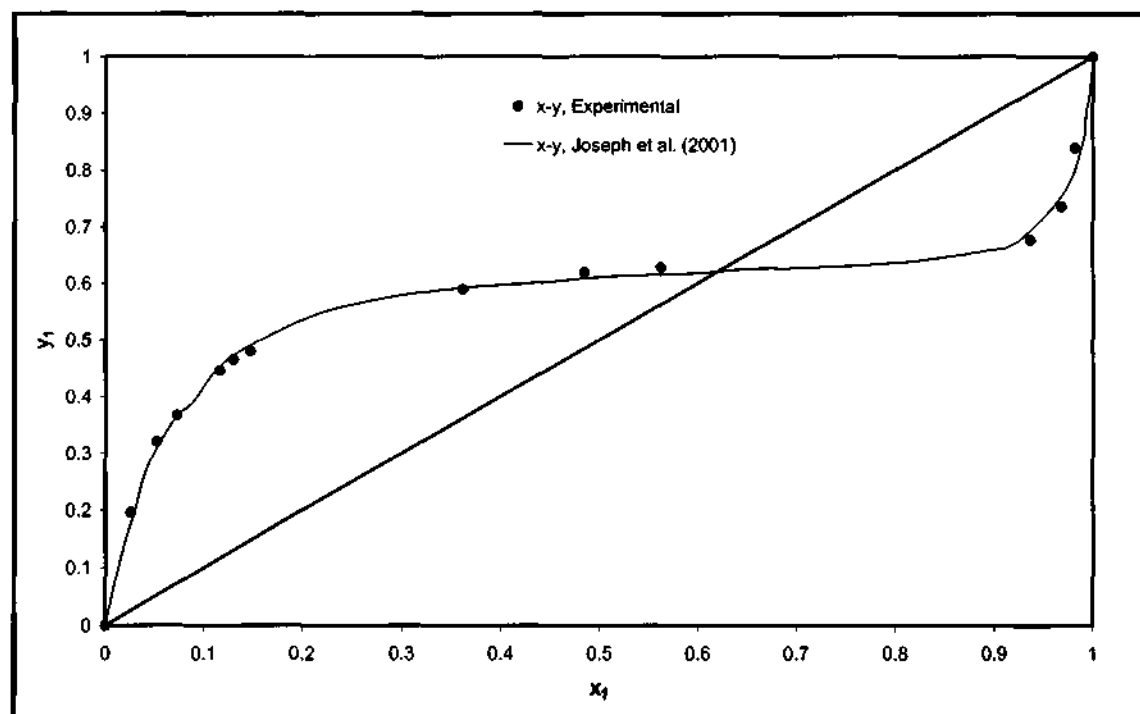
Figure 6-9: x-y curve for the cyclohexane (1) + ethanol (2) system at 40 kPa.
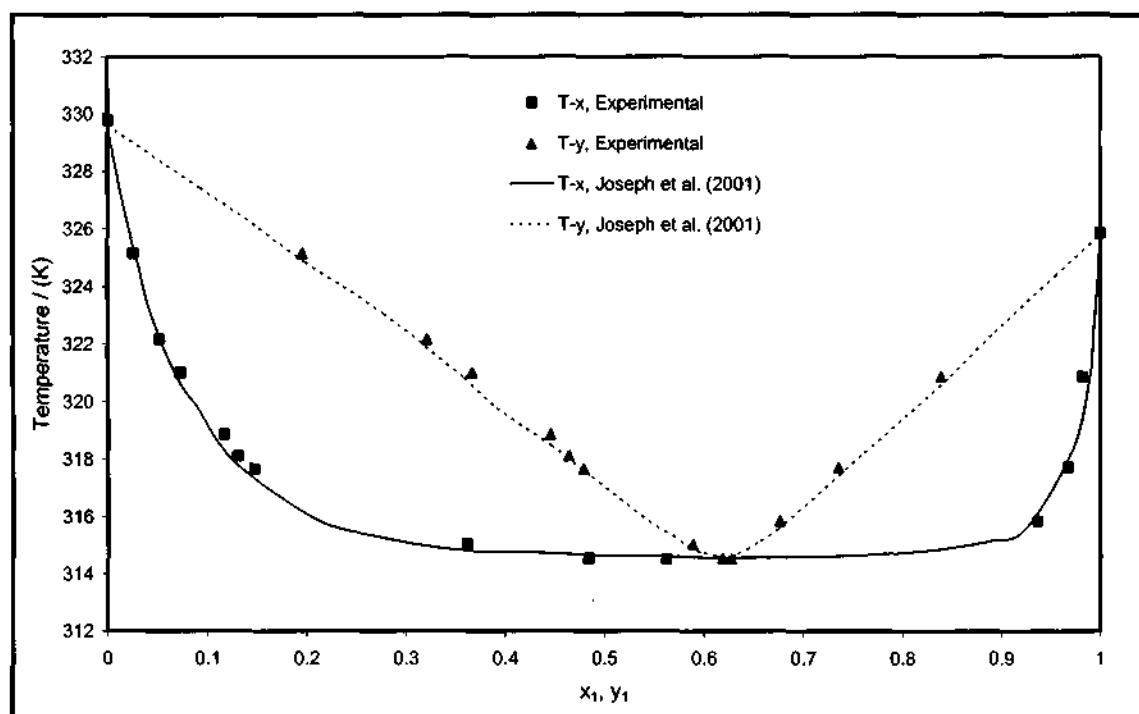
Figure 6-10: T-x-y curve for the cyclohexane (1) + ethanol (2) system at 40 kPa.

6.3.2 1-Dodecene (1) + 1-Nonanol (2)

Data for this system has not been previously measured at an isotherm of 403.15 K. Interestingly, it was found that this system displayed an azerotrope at approximately $x_1 = y_1 = 0.71$. The gas chromatographic calibration graphs, experimental data and the x-y and T-x-y plots are presented below.
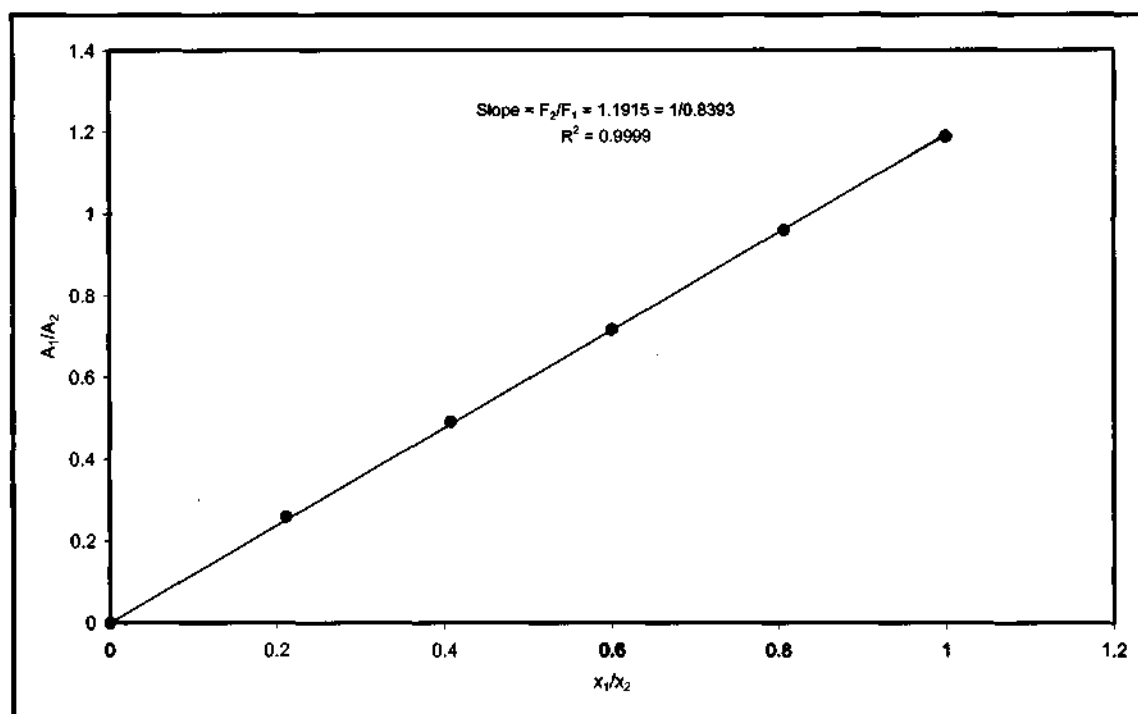
Figure 6-11: GC Calibration graph for the 1-dodecene (1) + 1-nonanol (2) system (1-dodecene dilute region).
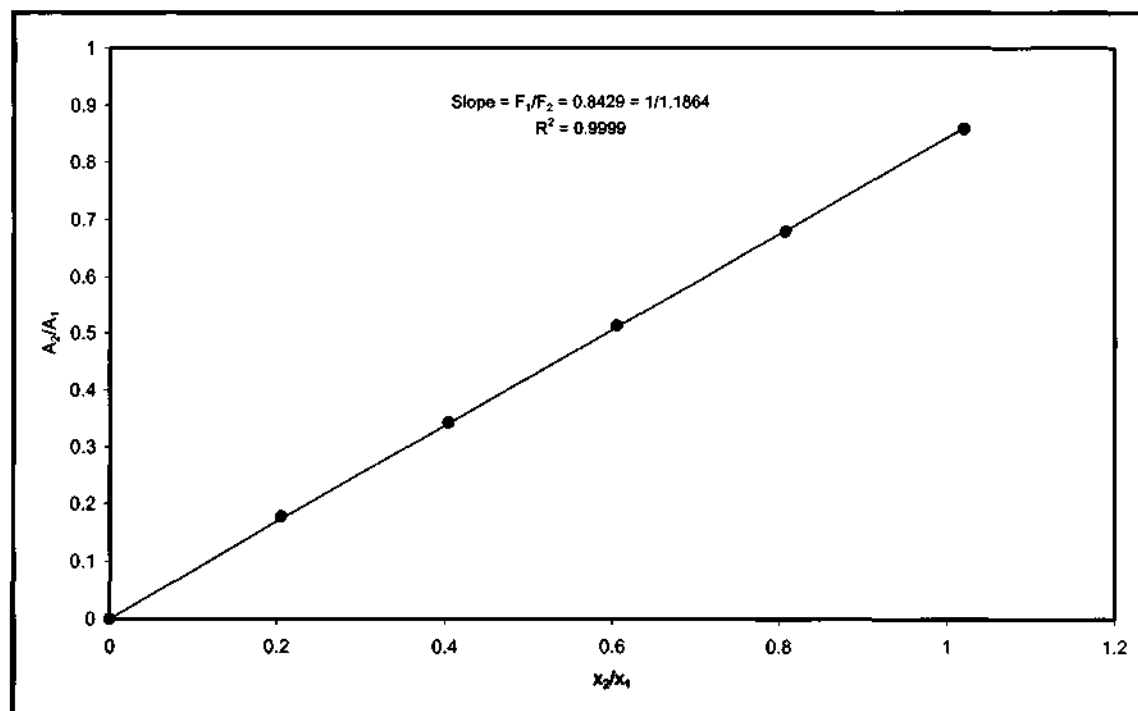
Figure 6-12: GC calibration graph for the 1-dodecene (1) + 1-nonanol (2) system (1-nonanol dilute region).

Table 6-9: Vapour-liquid equilibrium for 1-dodecene (1) + 1-nonanol (2) at 403.15 K.

P [kPa]	x_1	y_1
5.64	0.000	0.000
6.59	0.097	0.242
7.18	0.170	0.357
8.04	0.311	0.550
8.22	0.367	0.585
8.43	0.444	0.618
8.70	0.586	0.664
8.73	0.643	0.679
8.74	0.685	0.698
8.74	0.718	0.714
8.59	0.834	0.768
8.05	1.000	1.000
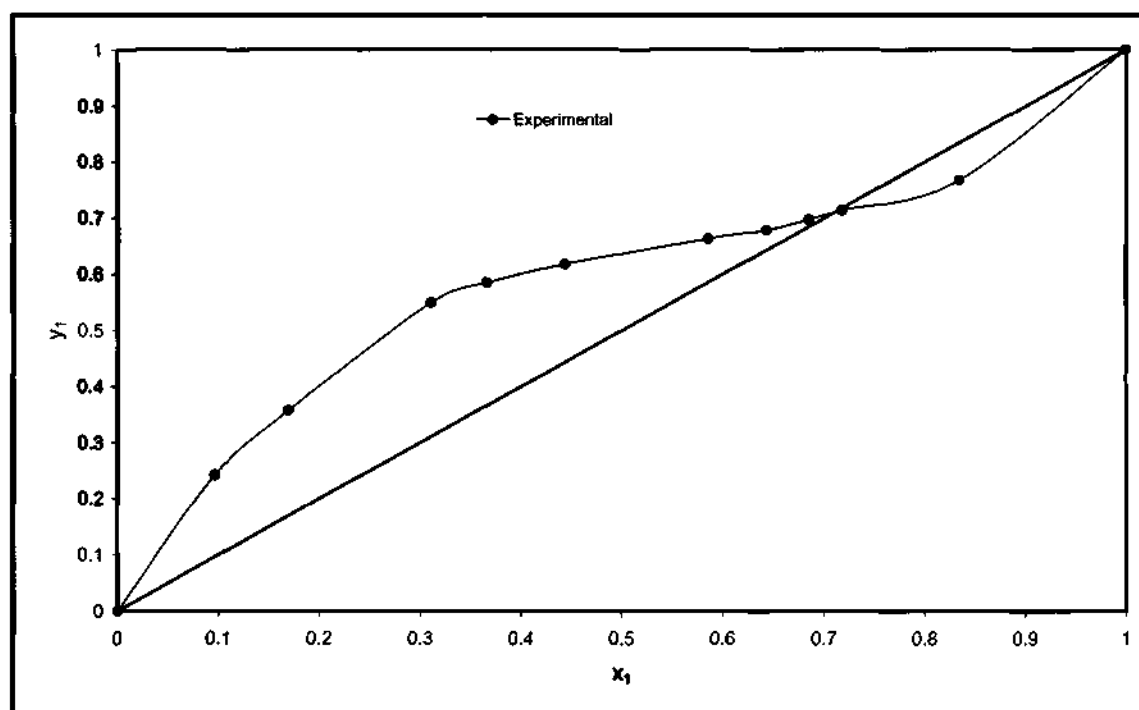
Figure 6-13: x-y curve for the 1-dodecene (1) + 1-nonanol (2) system at 403.15 K.
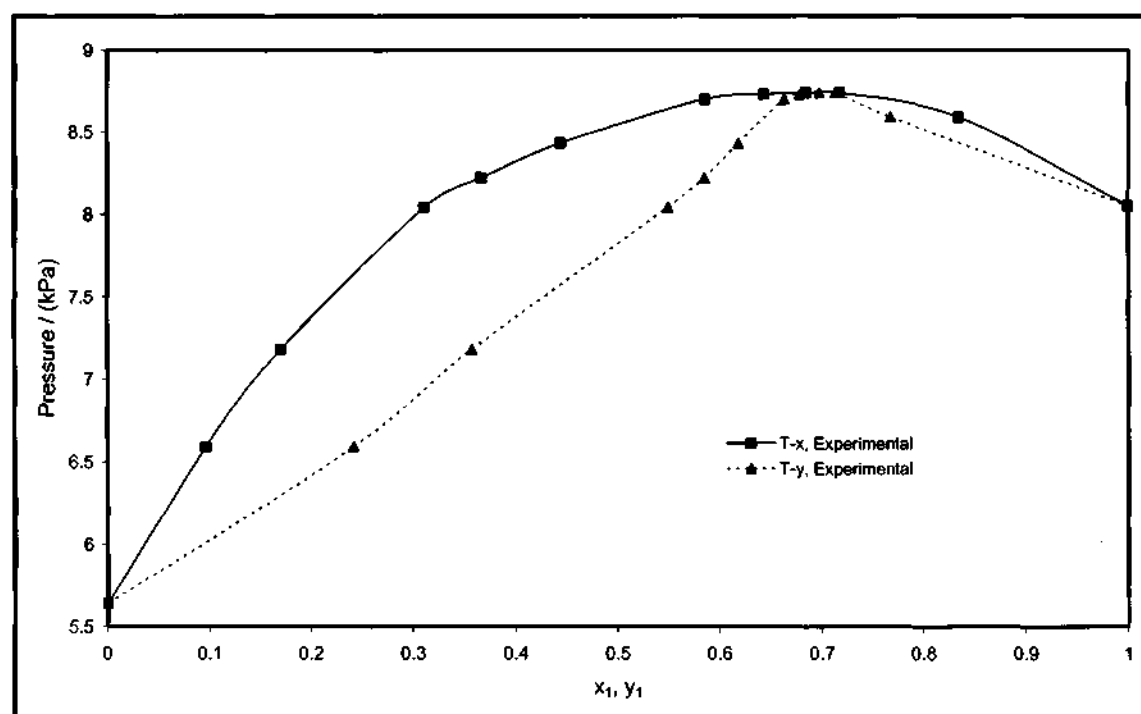
Figure 6-14: P-x-y curve for the 1-dodecene (1) + 1-nonanol (2) system at 403.15 K.

6.4 Liquid-Liquid Equilibrium Results

6.4.1 Binary Systems

The equilibrium liquid phase compositions were determined using the Chrompack 9000 gas chromatograph under the operating conditions of Table 5-2. The calibration procedure for the binary systems followed the method of Raal and Mühlbauer (1998). For all binary LLE systems measured, the estimated precision of the mole fraction composition was within 1×10^{-4}.

6.4.1.1 Heptane (1) + Methanol (2)

The data measured by Nagatani et al. (1987) was used for comparison as the authors used a similar LLE apparatus to one employed in this work. The gas chromatographic calibration graphs, the experimental data and the T-x plot are presented below.
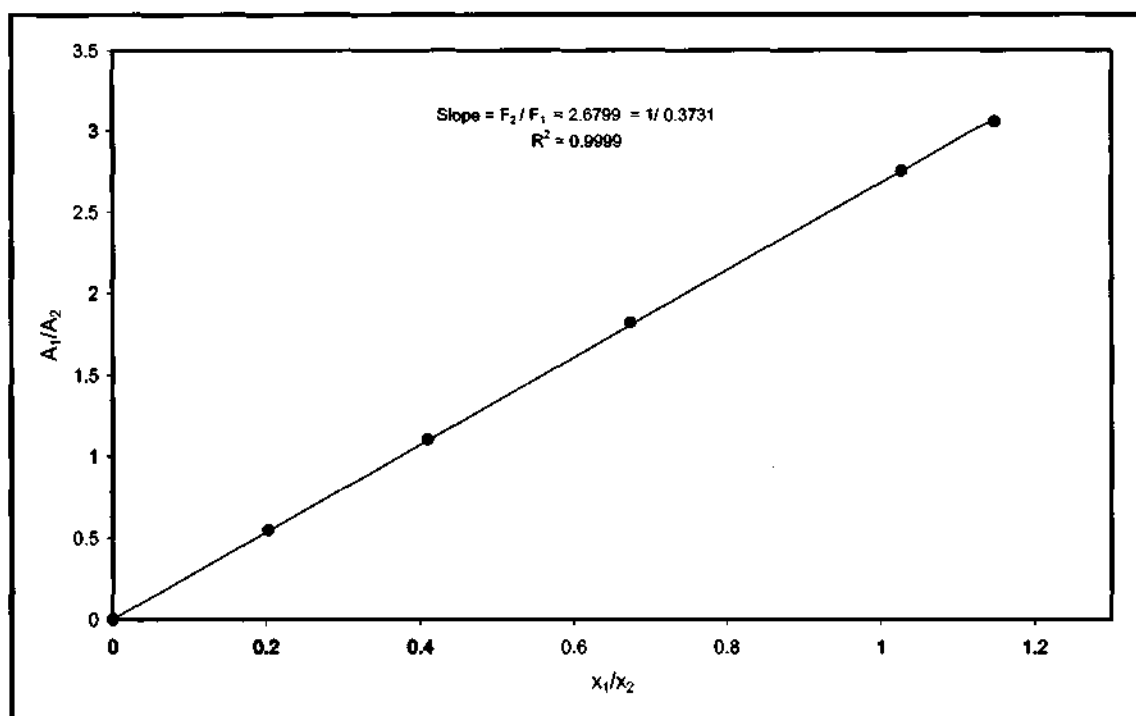
Figure 6-15: GC calibration graph for the heptane (1) + methanol (2) system (heptane dilute region).
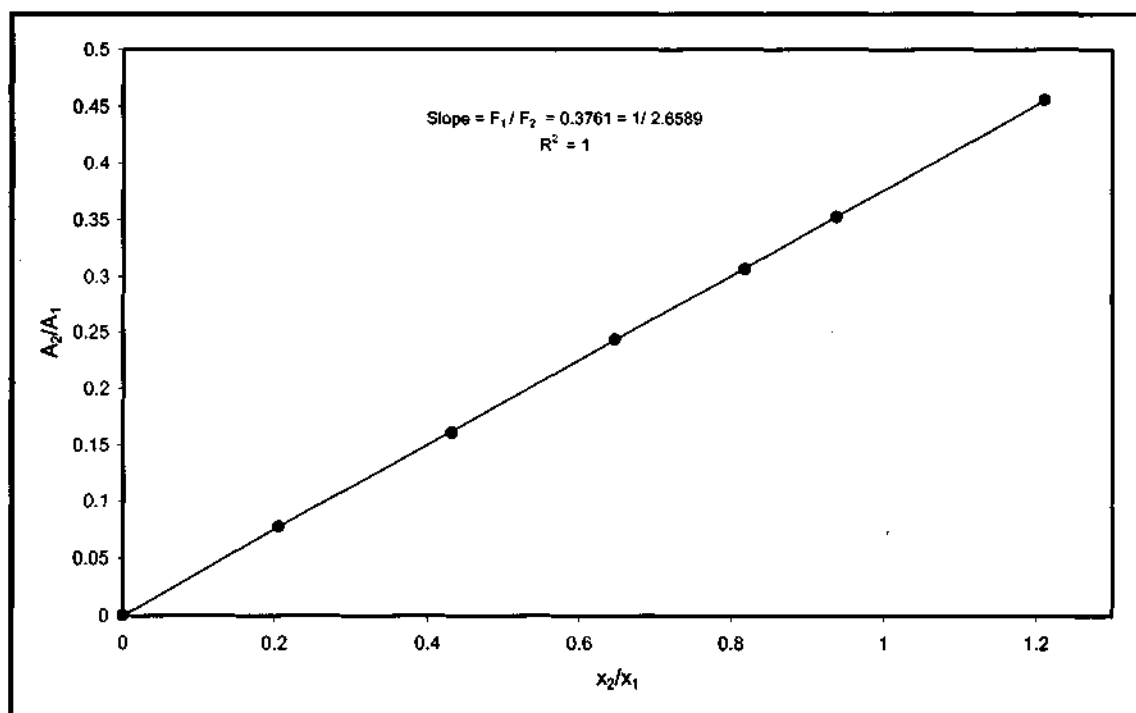
Figure 6-16: GC calibration graph for the heptane (1) + methanol (2) system (methanol dilute region).

Table 6-10: Liquid-liquid equilibrium data for heptane (1) + methanol (2) at 1 atm.

Temp [°C]	Phase I		Phase II	
	x_1	x_2	x_1	x_2
25.04	0.8456	0.1544	0.0998	0.9002
30.00	0.8018	0.1982	0.1128	0.8872
34.96	0.7645	0.2355	0.1256	0.8744
39.72	0.7193	0.2807	0.1505	0.8495
44.99	0.6454	0.3546	0.1707	0.8293
49.85	0.5463	0.4537	0.2082	0.7918
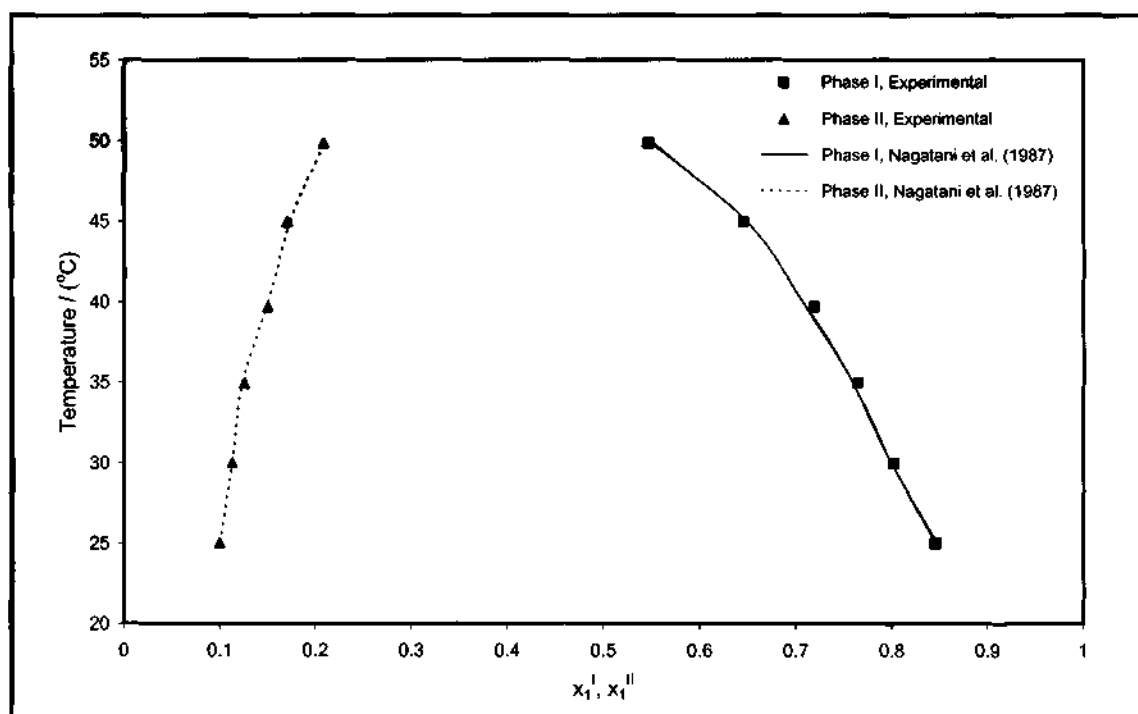
Figure 6-17: T-x plot for the heptane (1) + methanol (2) system at 1 atm.

6.4.1.2 1-Dodecene (1) + Acetonitrile (2)

This system was not previously measured and is presented as new LLE data. The gas chromatographic calibration graphs, the experimental data and the T-x plot are presented below.
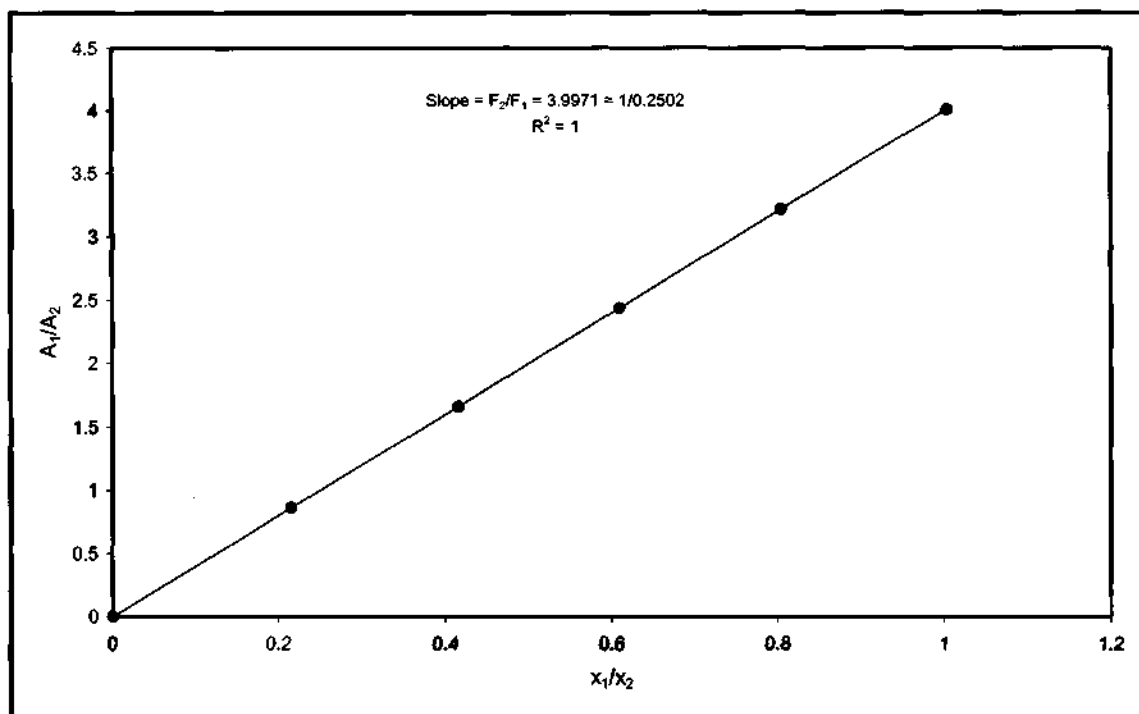
Figure 6-18: GC calibration graph the 1-dodecene (1) + acetonitrile (2) system (1-dodecene dilute region).
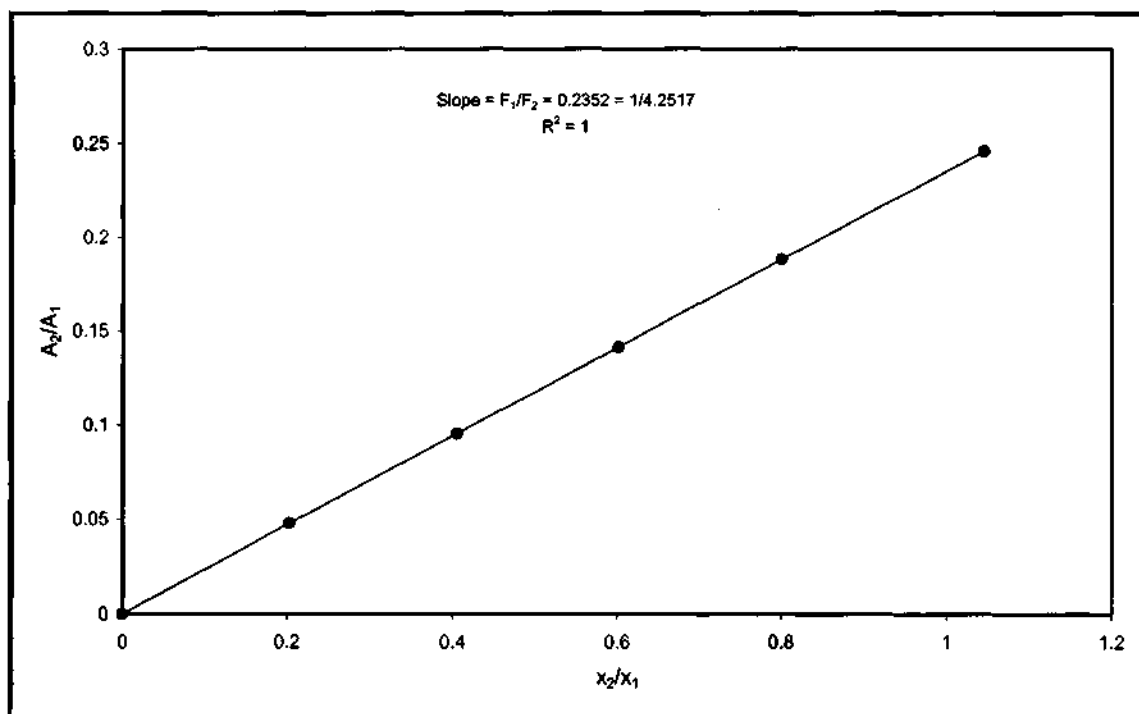
Figure 6-19: GC calibration graph for the 1-dodecene (1) + acetonitrile (2) system (acetonitrile dilute region).

Table 6-11: Liquid-liquid equilibrium data for 1-dodecene (1) + acetonitrile (2) at 1 atm.

Temp	Phase I		Phase II	
[°C]	x_1	x_2	x_1	x_2
50.16	0.7696	0.2304	0.0487	0.9513
55.02	0.7341	0.2659	0.0595	0.9405
60.09	0.7046	0.2954	0.0668	0.9332
65.05	0.6757	0.3243	0.0842	0.9158
70.08	0.6464	0.3536	0.1034	0.8966
75.08	0.5963	0.4037	0.1255	0.8745
80.04	0.4778	0.5222	0.2283	0.7717
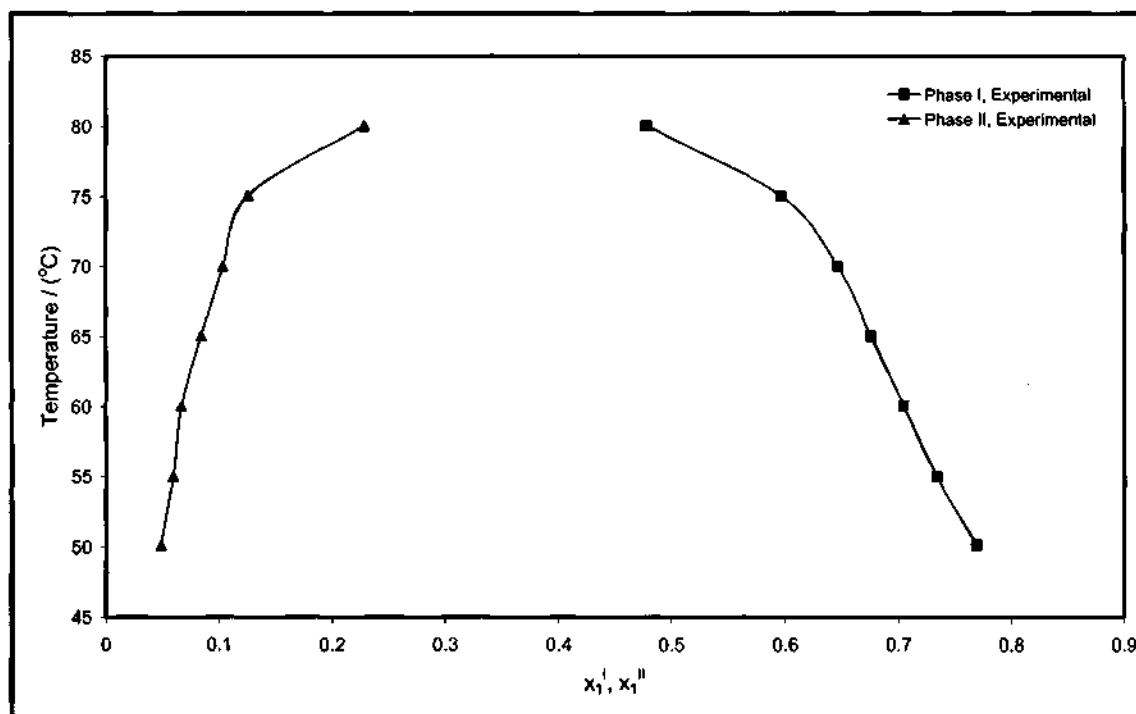
Figure 6-20: T-x plot for the 1-dodecene (1) + acetonitrile (2) system at 1 atm.

6.4.1.3 1-Nonanol (1) + Water (2)

This system is also presented as new LLE data as it has not been previously measured. The gas chromatographic calibration graphs, the experimental data and the T-x plot are presented below.

108
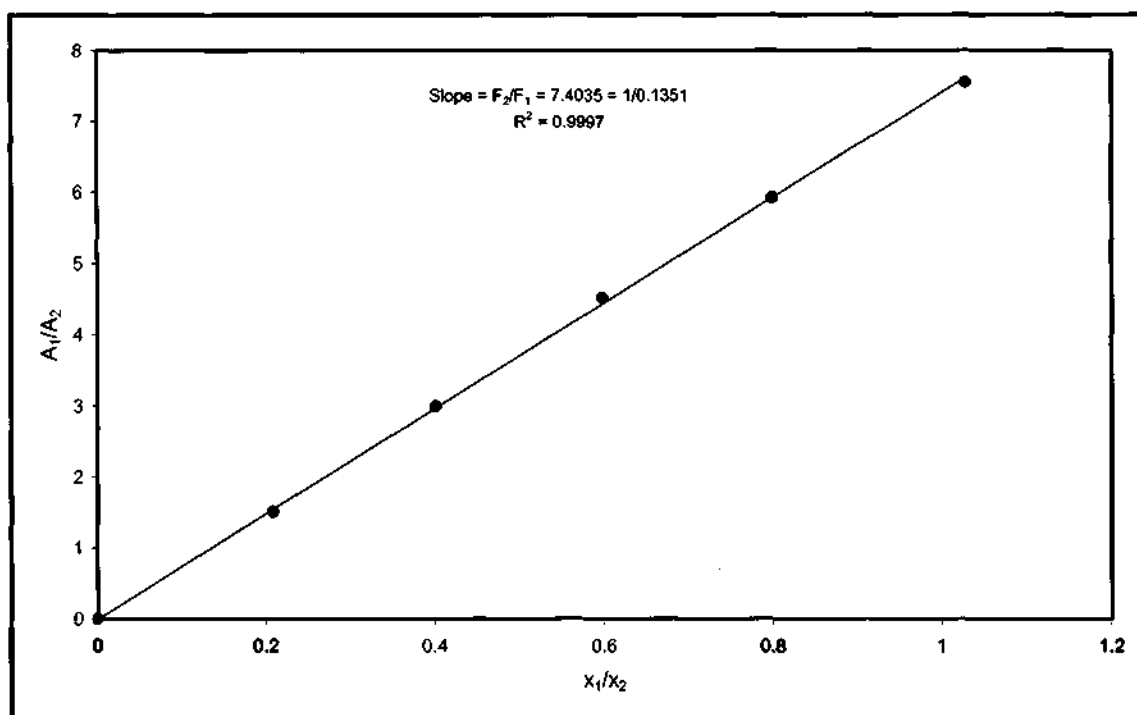
Figure 6-21: GC calibration graph for the 1-nonanol (1) + water (2) system (1-nonanol dilute region).
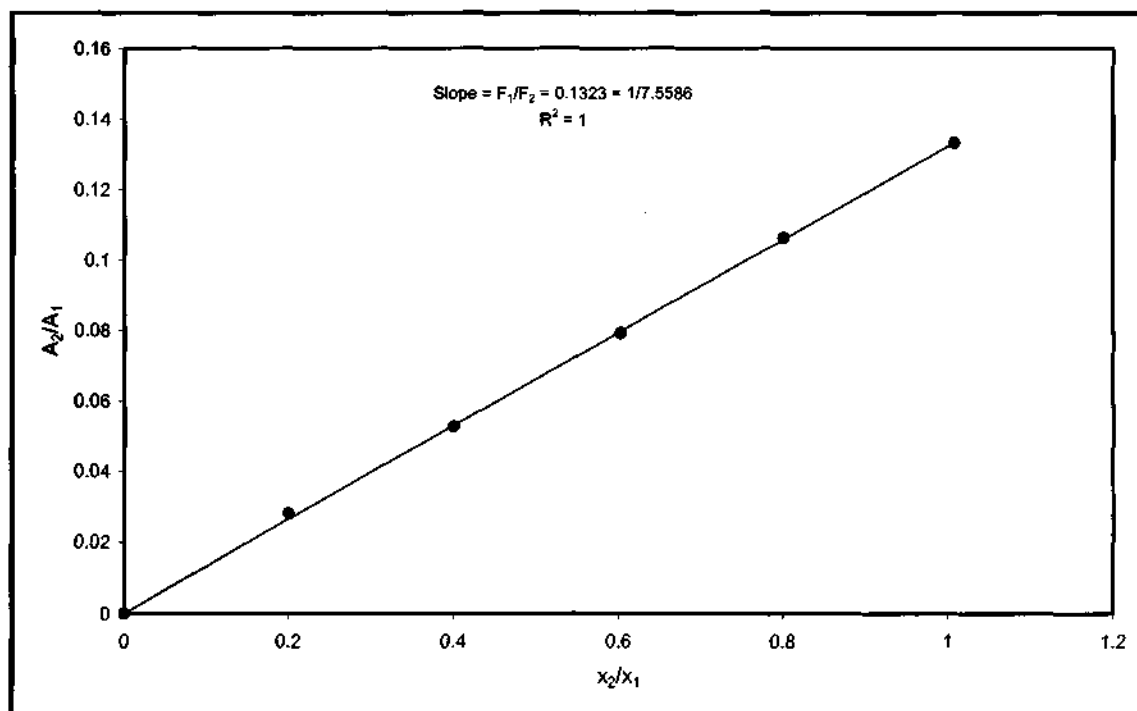
Figure 6-22: GC calibration graph for the 1-nonanol (1) + water (2) system (water dilute region).

Table 6-12: Liquid-liquid equilibrium data for 1-nonanol (1) + water (2) at 1 atm.

Temp	Phase I		Phase II	
[°C]	x_1	x_2	x_1	x_2
50.16	0.7443	0.2557	0.0035	0.9965
60.09	0.7272	0.2728	0.0066	0.9934
70.01	0.7148	0.2852	0.0074	0.9926
80.04	0.6990	0.3010	0.0086	0.9914
89.06	0.6857	0.3143	0.0095	0.9905
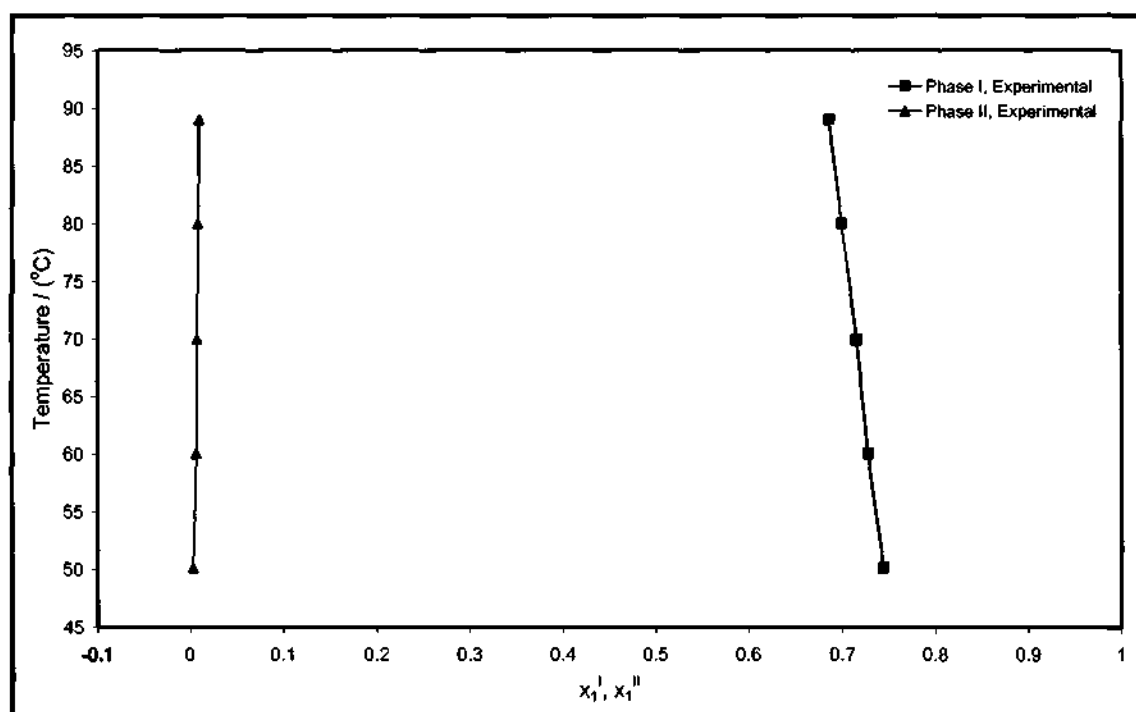
Figure 6-23: T-x plot for the 1-nonanol (1) + water (2) system at 1 atm.

6.4.2 Ternary Systems

The equilibrium liquid phase compositions were determined using the Chrompack 9000 gas chromatograph (TCD) under the operating conditions of Table 5-2. For ternary systems, the area ratio method of Raal and Mühlbauer (1998) was also employed. This method requires the calibration of two binary pairs of the ternary system, thus eliminating the need to calibrate all three binary pairs. For all ternary LLE systems measured, the estimated precision of the mole fraction composition was within 1×10^{-4}.

6.4.2.1 Heptane (1) + Toluene (2) + Methanol (3)

This system, measured at 298.15 K and 1 atm was used to test the operation of the LLE apparatus for ternary LLE measurements. The data measured by Nagatani et al. (1987) was used for comparison. This system exhibits a narrow LLE region and is thus difficult to measure. This therefore ensured the capability of the LLE apparatus to obtain ternary LLE data that is difficult to measure. The gas chromatographic calibration graphs, the experimental data and the triangle diagram are presented below.
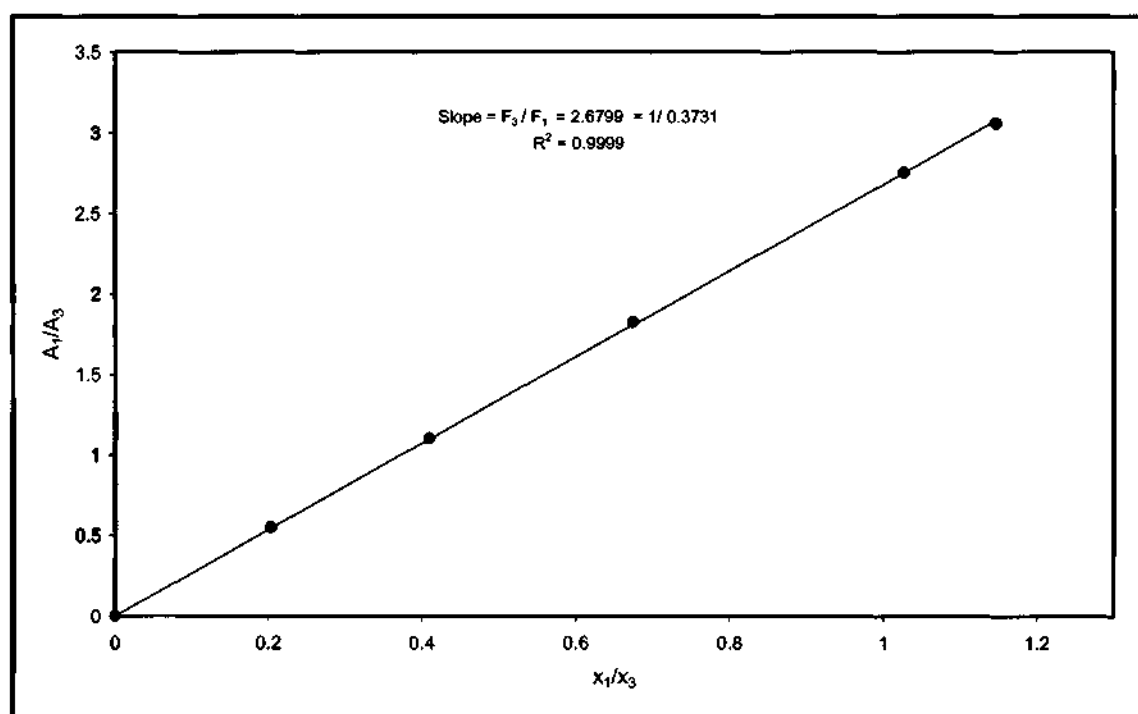
Figure 6-24: GC calibration graph for the heptane (1) + methanol (3) binary pair (heptane dilute region).
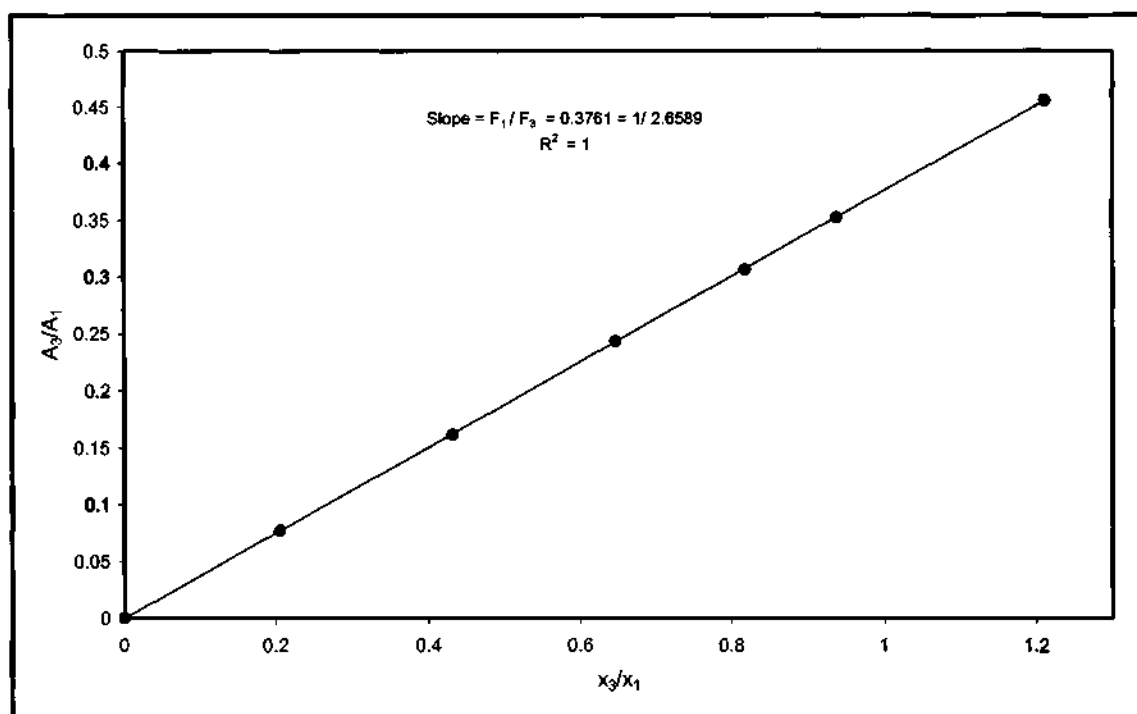
Figure 6-25: GC calibration graph for the heptane (1) + methanol (3) binary pair (methanol dilute region).
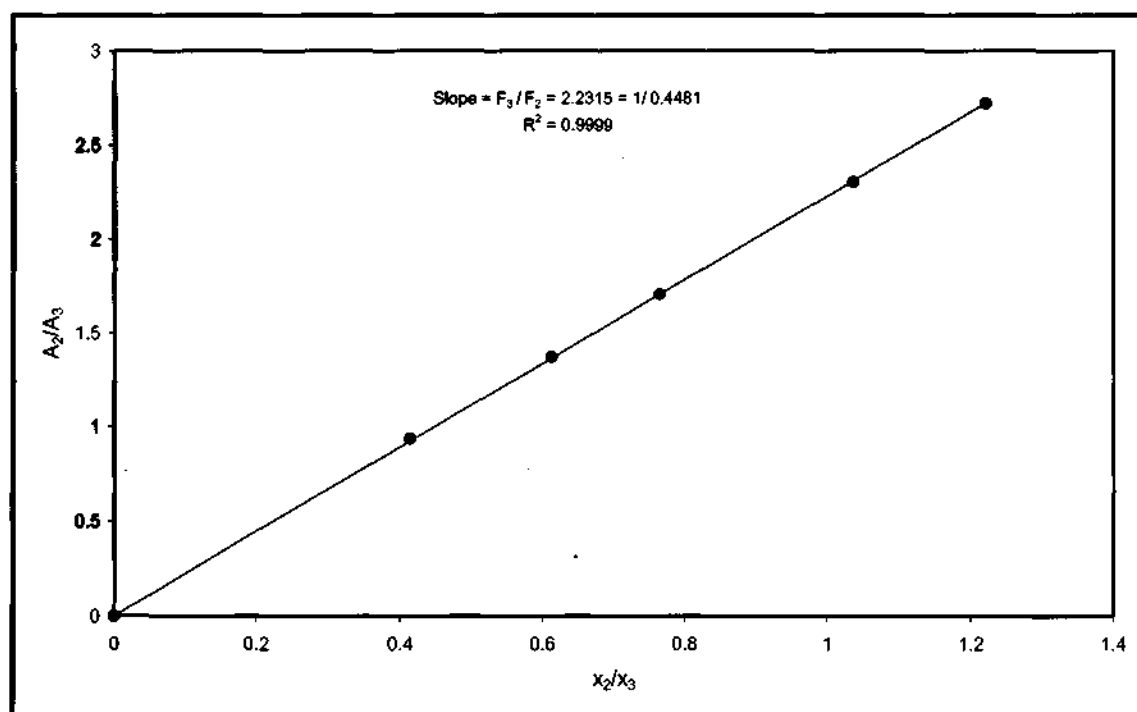
Figure 6-26: GC calibration graph for the toluene (2) + methanol (3) binary pair (toluene dilute region).
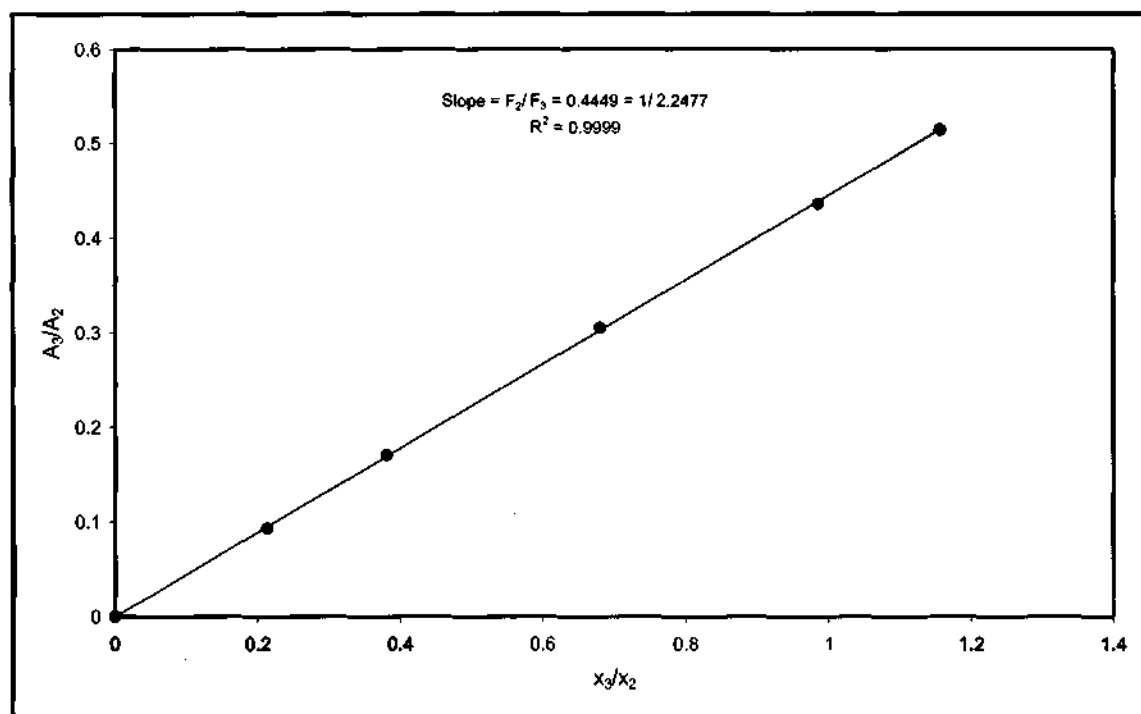
Figure 6-27: GC calibration graph for the toluene (2) + methanol (3) binary pair (methanol dilute region).

Table 6-13: Liquid-liquid equilibrium data for the heptane (1) + toluene (2) + methanol (3) system at 298.15 K and 1 atm.

Phase I			Phase II		
x_1	x_2	x_3	x_1	x_2	x_3
0.8456	0.0000	0.1544	0.0998	0.0000	0.9002
0.7682	0.0415	0.1903	0.1262	0.0142	0.8596
0.7054	0.0804	0.2142	0.1437	0.0316	0.8247
0.6210	0.1053	0.2738	0.1581	0.0495	0.7925
0.5993	0.1131	0.2876	0.1573	0.0513	0.7914
0.5660	0.1158	0.3182	0.1703	0.0587	0.7710
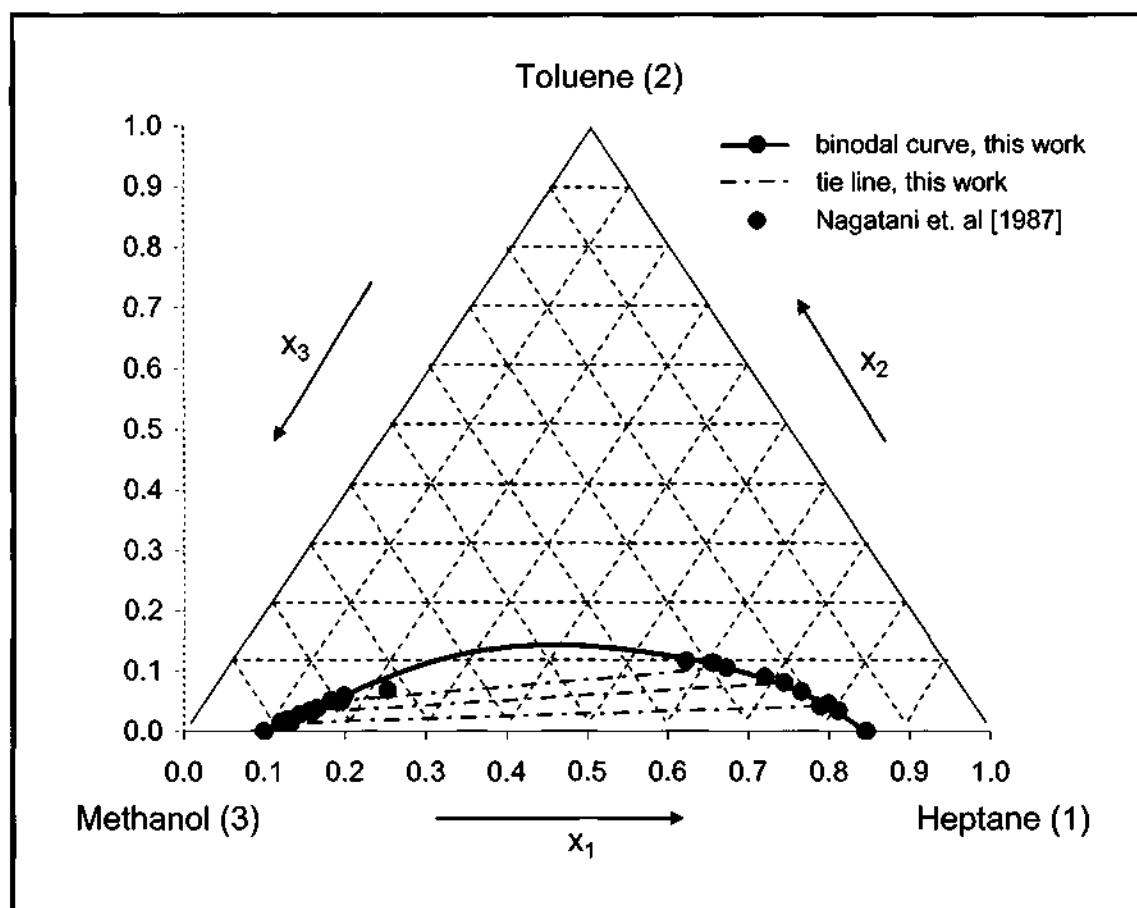
Figure 6-28: Ternary diagram for the heptane (1) + toluene (2) + methanol (3) system at 298.15 K and 1 atm.

6.4.2.2 Water (1) + Acetonitrile (2) + Heptanoic Acid (3)

This system has not been previously measured at 323.15 K and 1 atm and is thus presented as new LLE data. The gas chromatographic calibration graphs, the experimental data and the triangle diagram are presented below.
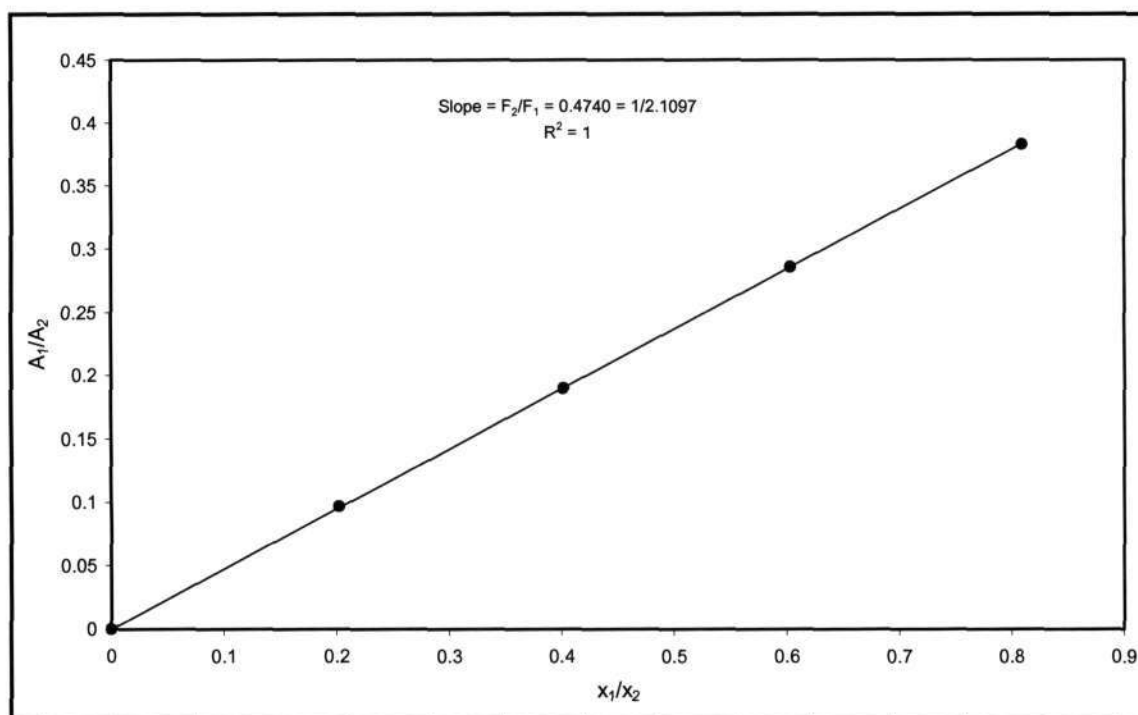
Figure 6-29: GC calibration graph for the water (1) + acetonitrile (2) binary pair (water dilute region).
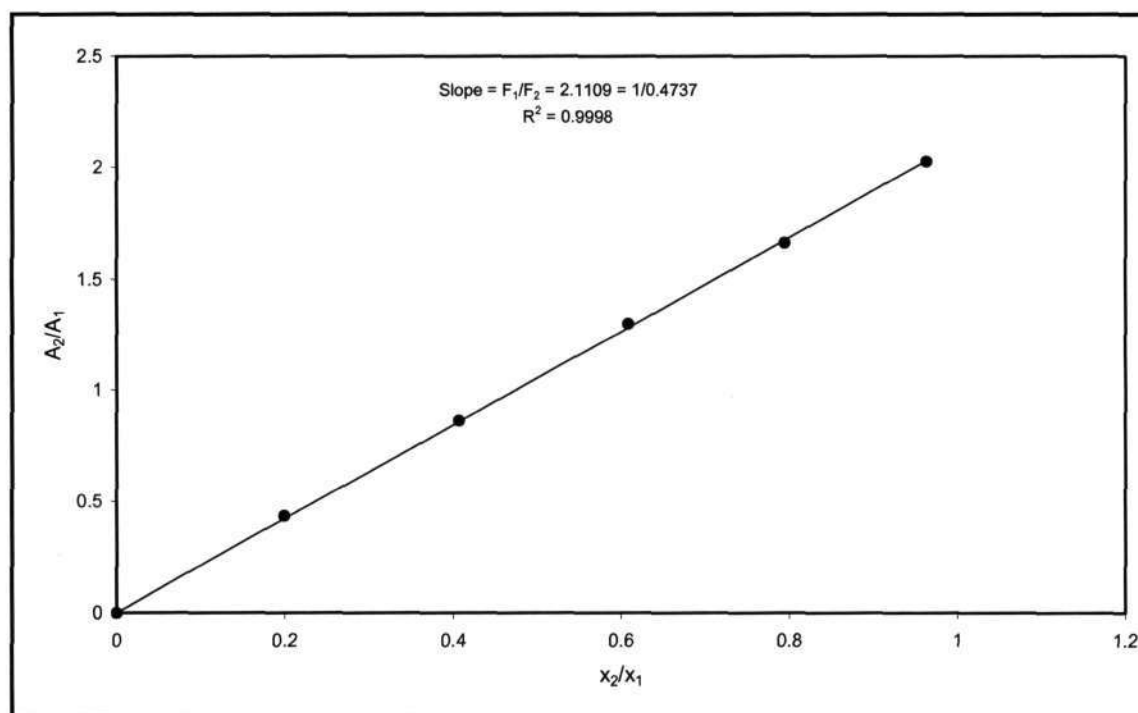
Figure 6-30: GC calibration graph for the water (1) + acetonitrile (2) binary pair (acetonitrile dilute region).
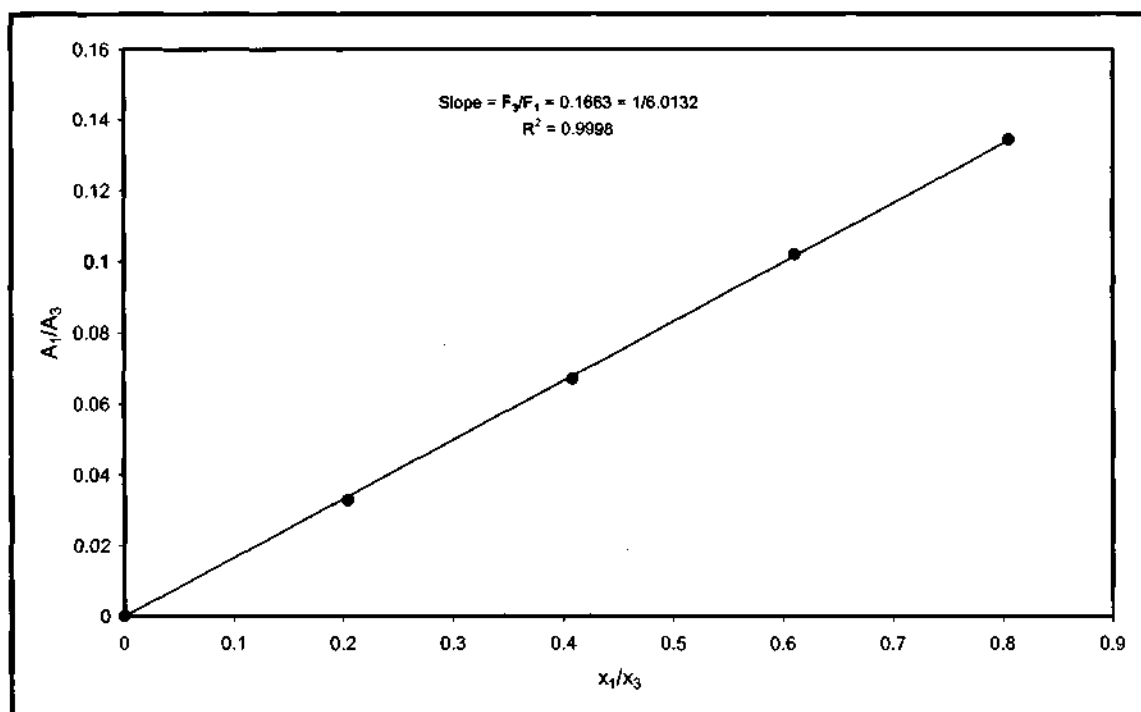
Figure 6-31: GC calibration graph for the water (1) + heptanoic acid (3) binary pair (water dilute region).
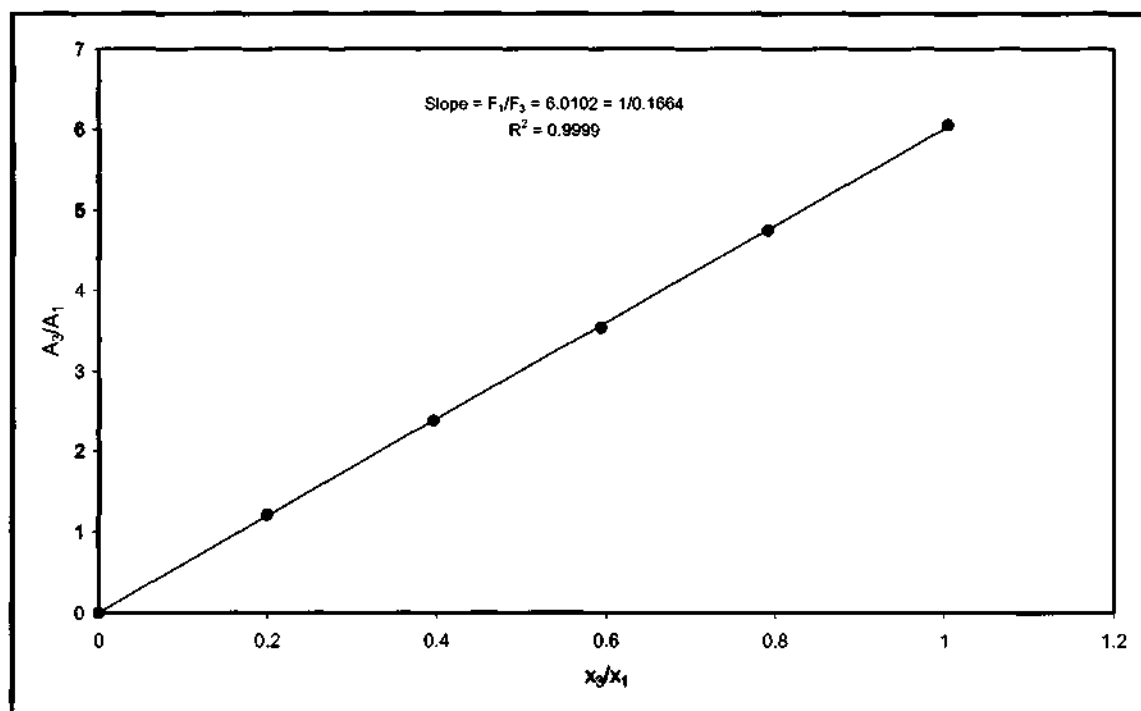
Figure 6-32: GC calibration graph for the water (1) + heptanoic acid (3) binary pair (heptanoic acid dilute region).

116

Table 6-14: Liquid-liquid equilibrium data for the water (1) + acetonitrile (2) +
heptanoic acid (3) system at 323.15 K and 1 atm.

	Phase I			Phase II	
X_1	X_2	X_3	X_1	X_2	X_3
0.2953	0.0000	0.7047	0.9984	0.0000	0.0016
0.3309	0.0325	0.6366	0.9891	0.0092	0.0017
0.3839	0.0775	0.5386	0.9787	0.0194	0.0019
0.4109	0.1152	0.4739	0.9693	0.0286	0.0021
0.4486	0.1675	0.3839	0.9579	0.0397	0.0024
0.4826	0.2351	0.2823	0.9407	0.0557	0.0036
0.5385	0.3126	0.1489	0.9086	0.0874	0.0040
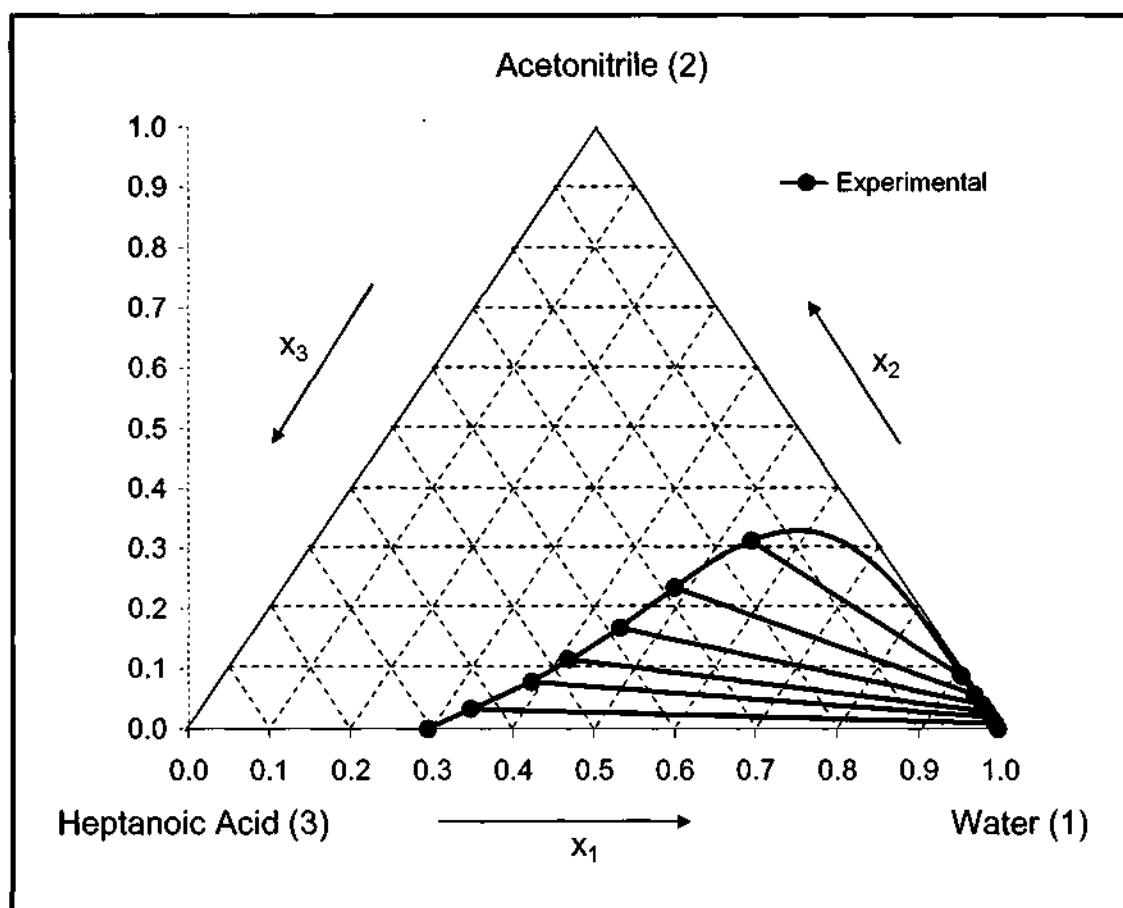
Figure 6-33: Ternary diagram for the water (1) + acetonitrile (2) + heptanoic acid (3)
system at 323.15 K and 1 atm.

6.4.2.3 Water (1) + Acetonitrile (2) + 1-Nonanol (3)

This system has also not been previously measured at 323.15 K and 1 atm and is thus presented as new LLE data. The gas chromatographic calibration graphs for the water (1) + acetonitrile (2) binary pair is the same as for the water (1) + acetonitrile (2) + 1-nonanol (3) system (Figures 6-29 and 6-30) and will thus not be repeated for this system. The other binary pair for the gas chromatographic calibration graphs, the experimental data and the triangle diagram are presented below.
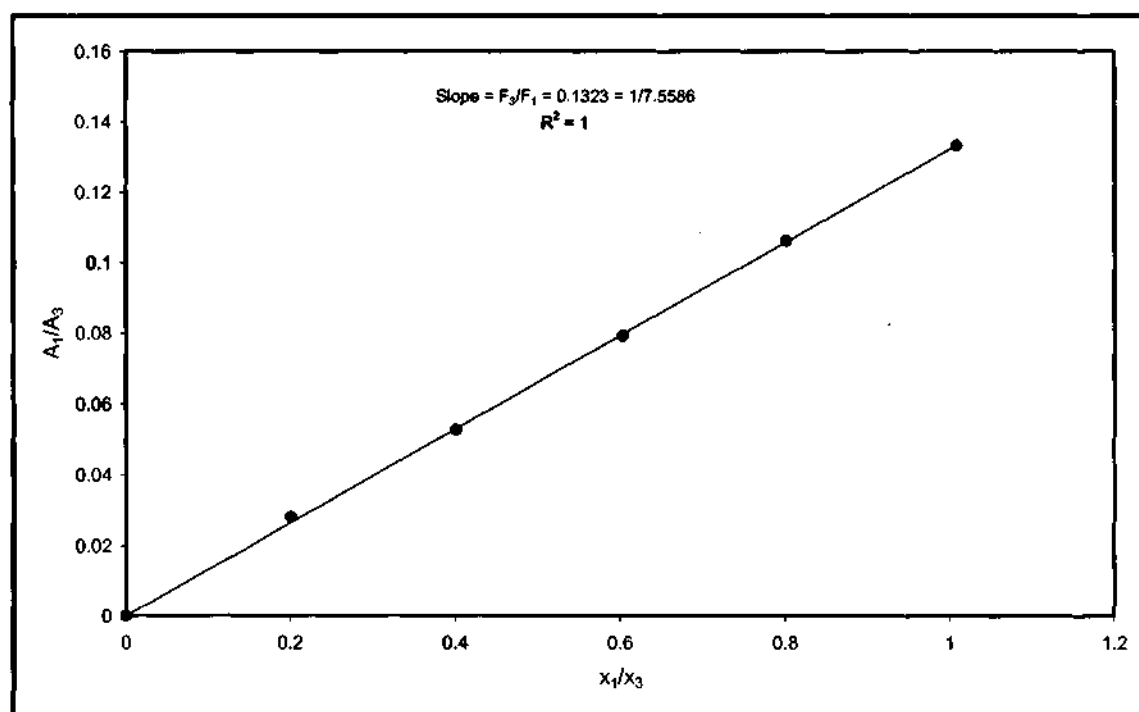
Figure 6-34: GC calibration graph for the water (1) + 1-nonanol (3) binary pair (water dilute region).
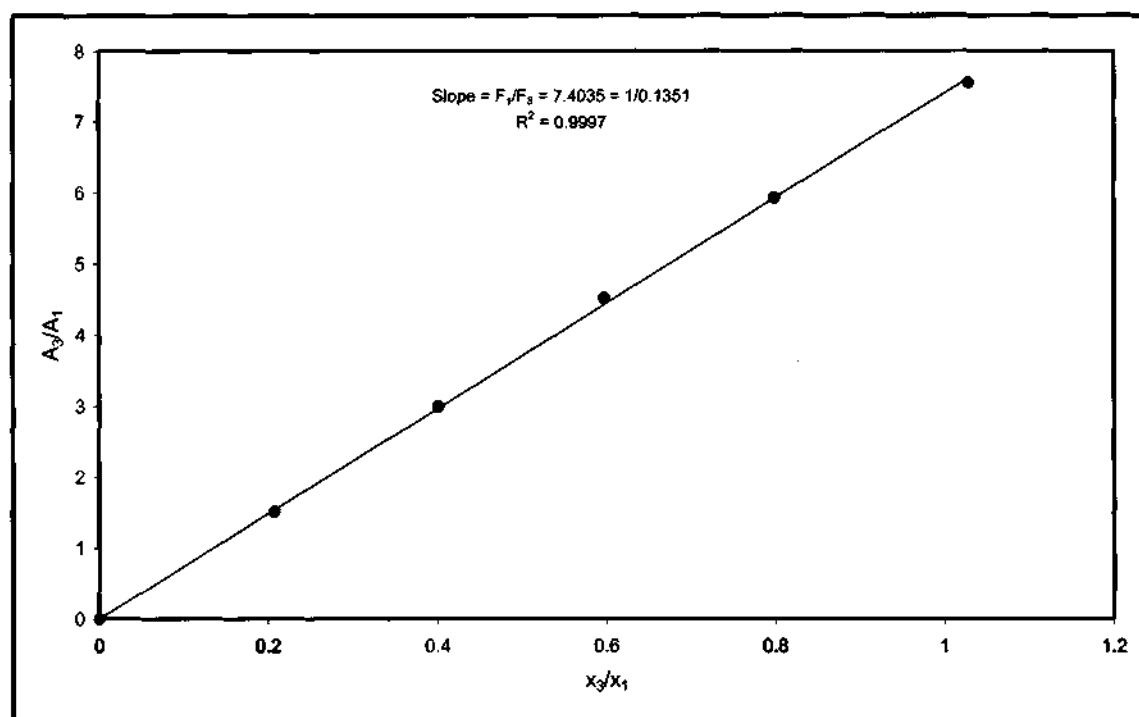
Figure 6-35: GC calibration graph for the water (1) + 1-nonanol (3) binary pair (1-nonanol dilute region).

Table 6-15: Liquid-liquid equilibrium data for the water (1) + acetonitrile (2) + 1-nonanol (3) system at 323.15 K and 1 atm.

Phase I			Phase II		
x_1	x_2	x_3	x_1	x_2	x_3
0.2604	0.0000	0.7396	0.9965	0.0000	0.0035
0.2630	0.0207	0.7163	0.9901	0.0076	0.0023
0.2687	0.0853	0.6460	0.9683	0.0291	0.0026
0.2849	0.1760	0.5391	0.9381	0.0591	0.0028
0.2873	0.2255	0.4872	0.9223	0.0740	0.0037
0.2987	0.2922	0.4091	0.9026	0.0947	0.0027
0.3177	0.3494	0.3329	0.8768	0.1197	0.0035
0.3426	0.4017	0.2557	0.8568	0.1398	0.0034
0.3726	0.4492	0.1782	0.8325	0.1655	0.0020
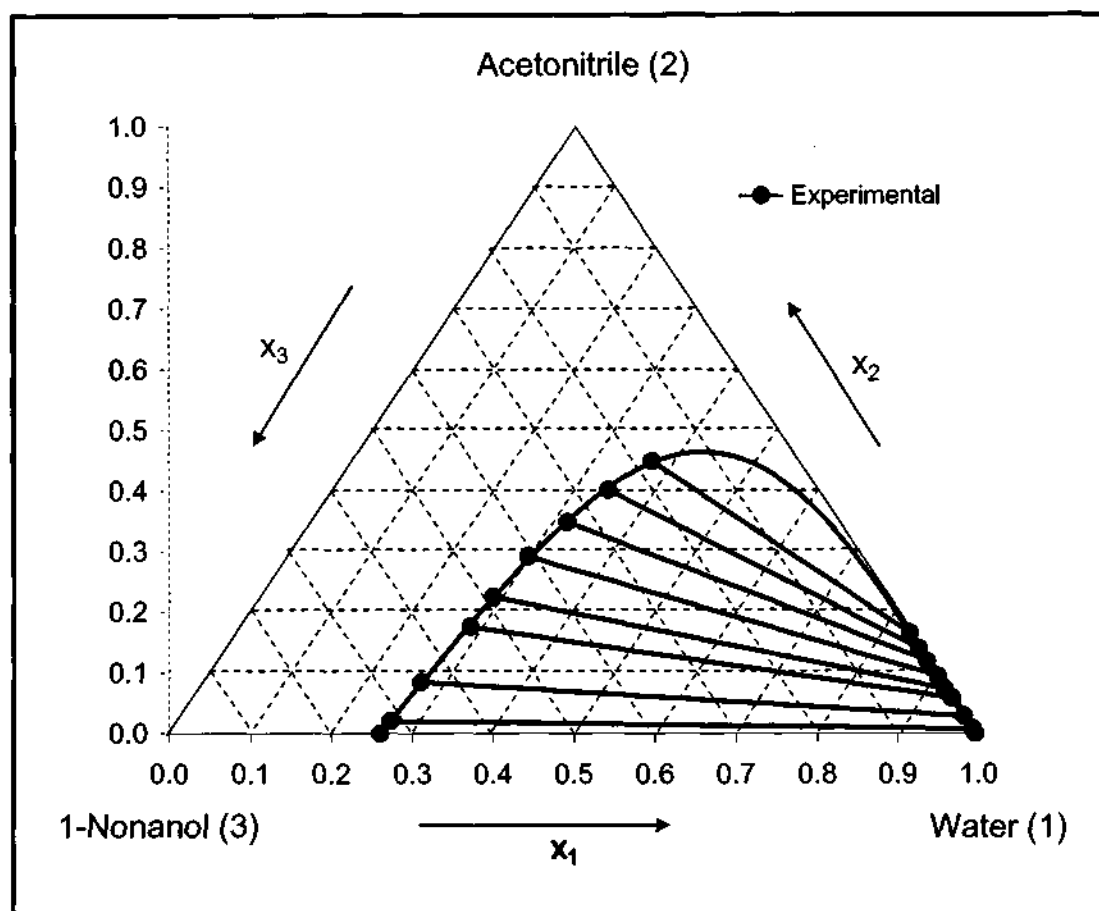
Figure 6-36: Ternary diagram for the water (1) + acetonitrile (2) + 1-nonanol (3) system at 323.15 K and 1 atm.

6.4.2.4 Water (1) + Acetonitrile (2) + Dodecane (3)

This system has also not been previously measured at 323.15 K and 1 atm and is thus presented as new LLE data. The gas chromatographic calibration graphs for the water (1) + acetonitrile (2) binary pair is the same as for the water (1) + acetonitrile (2) + 1-nonanol (3) system (Figures 6-29 and 6-30) and will thus not be repeated for this system. The other binary pair for the gas chromatographic calibration graphs, the experimental data and the triangle diagram are presented below.
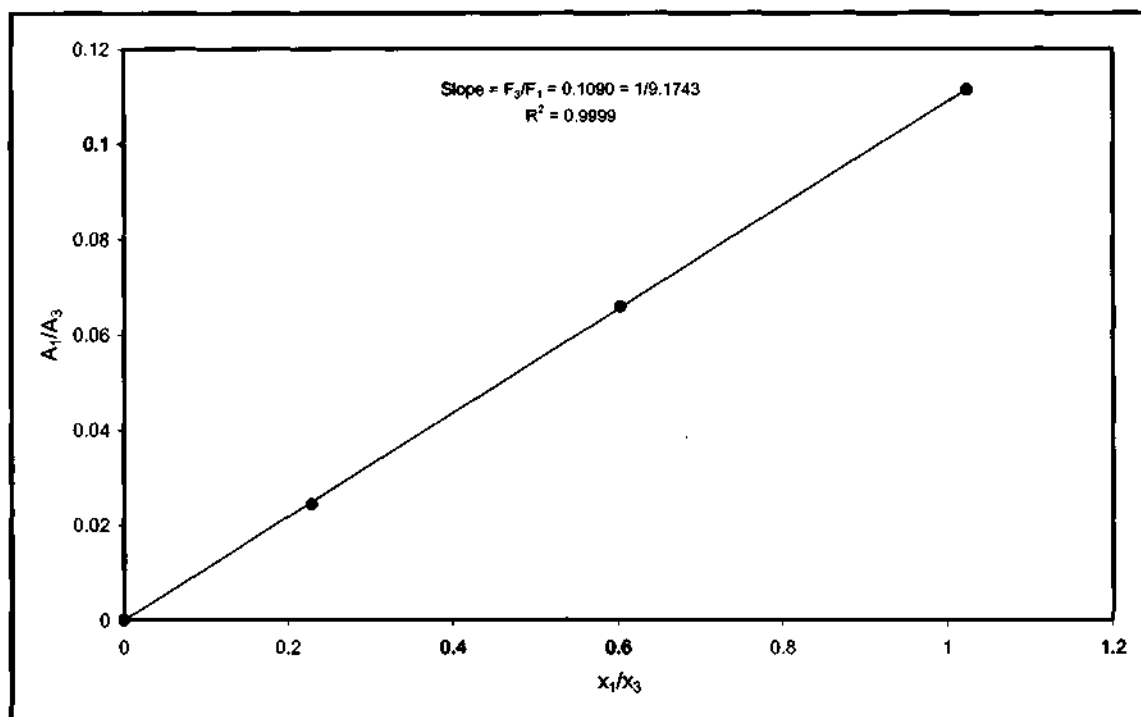
Figure 6-37: GC calibration graph for the water (1) + dodecane (3) binary pair (water dilute region).
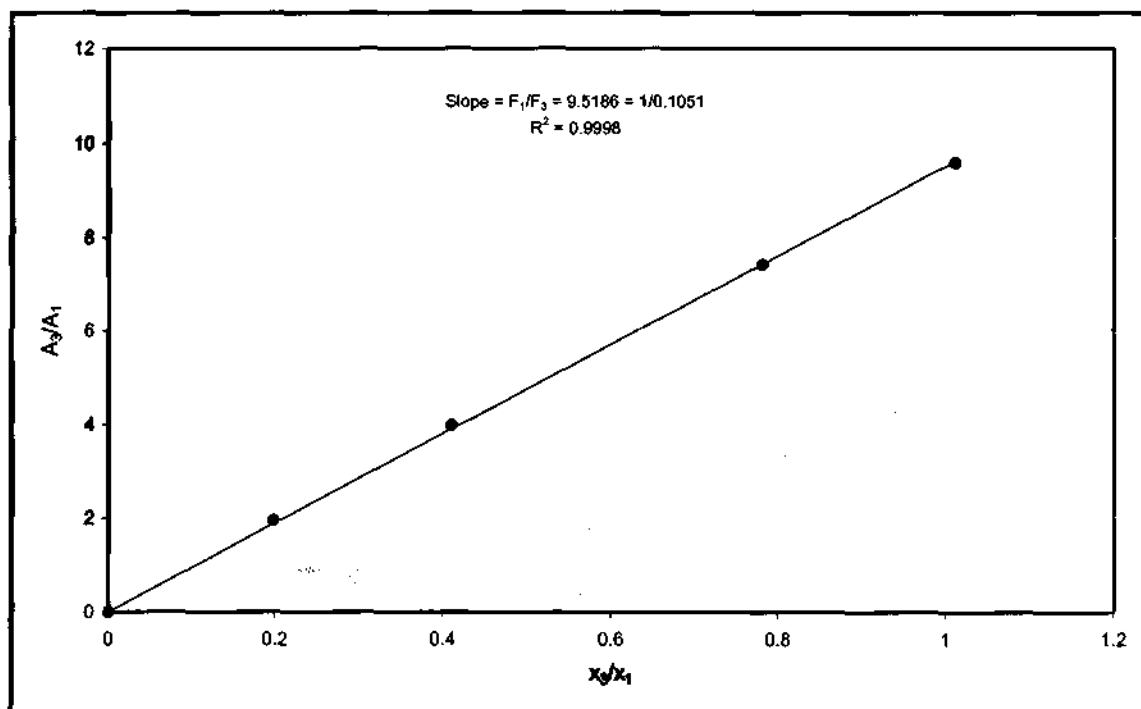
Figure 6-38: GC calibration graph for the water (1) + dodecane (3) binary pair (dodecane dilute region.

Table 6-16: Liquid-liquid equilibrium data for the water (1) + acetonitrile (2) + dodecane (3) system at 323.15 K and 1 atm.

Phase I			Phase II		
x_1	x_2	x_3	x_1	x_2	x_3
0.0045	0.0000	0.9955	0.9994	0.0000	0.0006
0.0047	0.0196	0.9757	0.9785	0.0208	0.0008
0.0051	0.0370	0.9579	0.9438	0.0553	0.0009
0.0051	0.0544	0.9405	0.8939	0.1053	0.0007
0.0048	0.0688	0.9264	0.8339	0.1653	0.0008
0.0046	0.0768	0.9186	0.6985	0.3004	0.0011
0.0053	0.0796	0.9151	0.5102	0.4883	0.0016
0.0052	0.0856	0.9092	0.3575	0.6406	0.0018
0.0038	0.0902	0.9060	0.2004	0.7943	0.0053
0.0029	0.0933	0.9038	0.1219	0.8687	0.0095
0.0000	0.1169	0.8831	0.0000	0.9839	0.0161
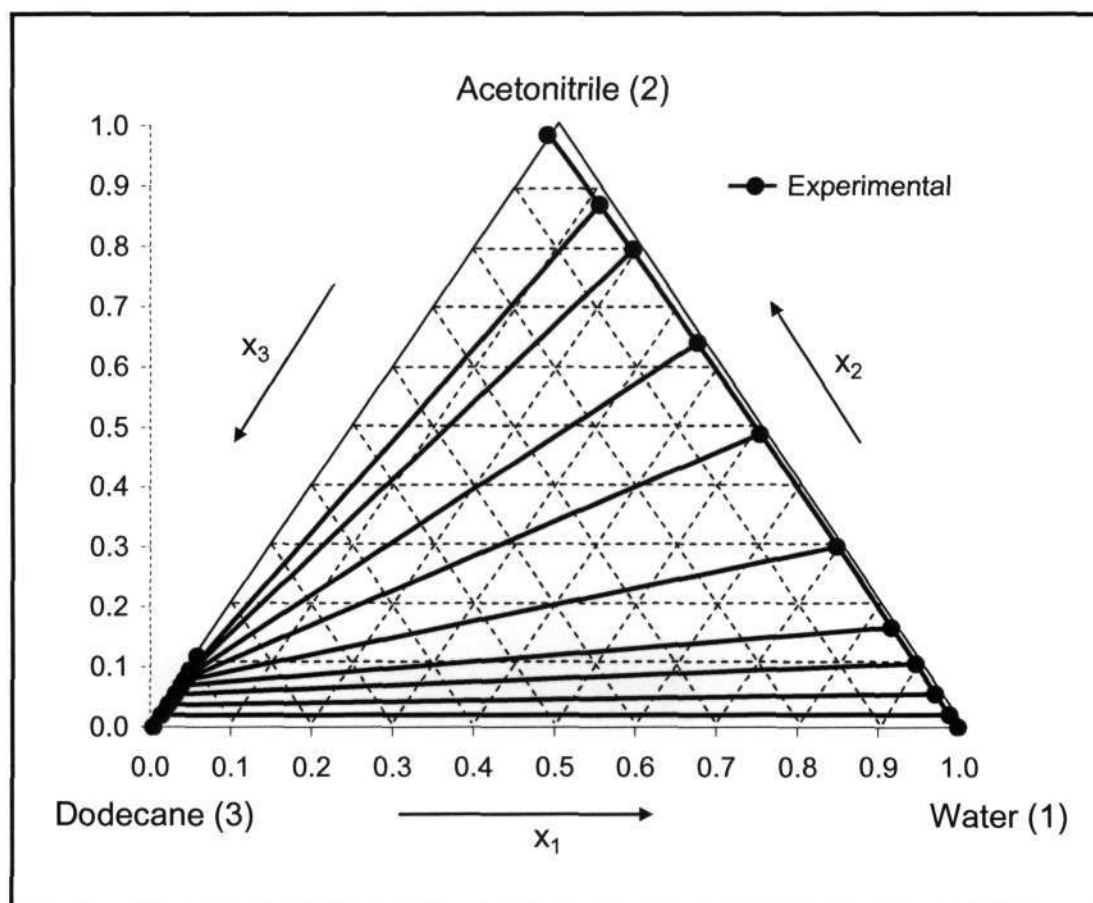
Figure 6-39: Ternary diagram for the water (1) + acetonitrile (2) + dodecane (3) system at 323.15 K and 1 atm.

6.4.2.5 Water (1) + Acetonitrile (2) + 1-Dodecene (3)

This system has also not been previously measured at 323.15 K and 1 atm and is thus presented as new LLE data. The gas chromatographic calibration graphs for the water (1) + acetonitrile (2) binary pair is the same as for the water (1) + acetonitrile (2) + 1-nonanol (3) system (Figures 6-29 and 6-30) and will thus not be repeated for this system. The other binary pair for the gas chromatographic calibration curves, the experimental data and the triangle diagram are presented below.
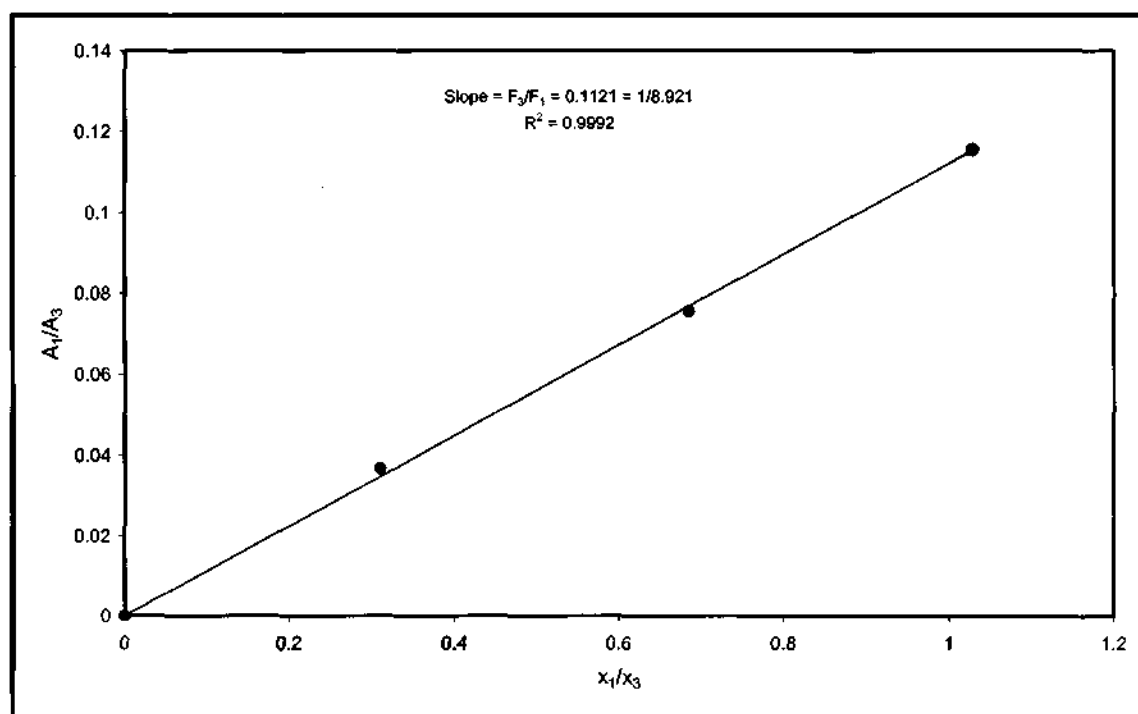
Figure 6-40: GC calibration graph for the water (1) + 1-dodecene (3) binary pair (water dilute region).
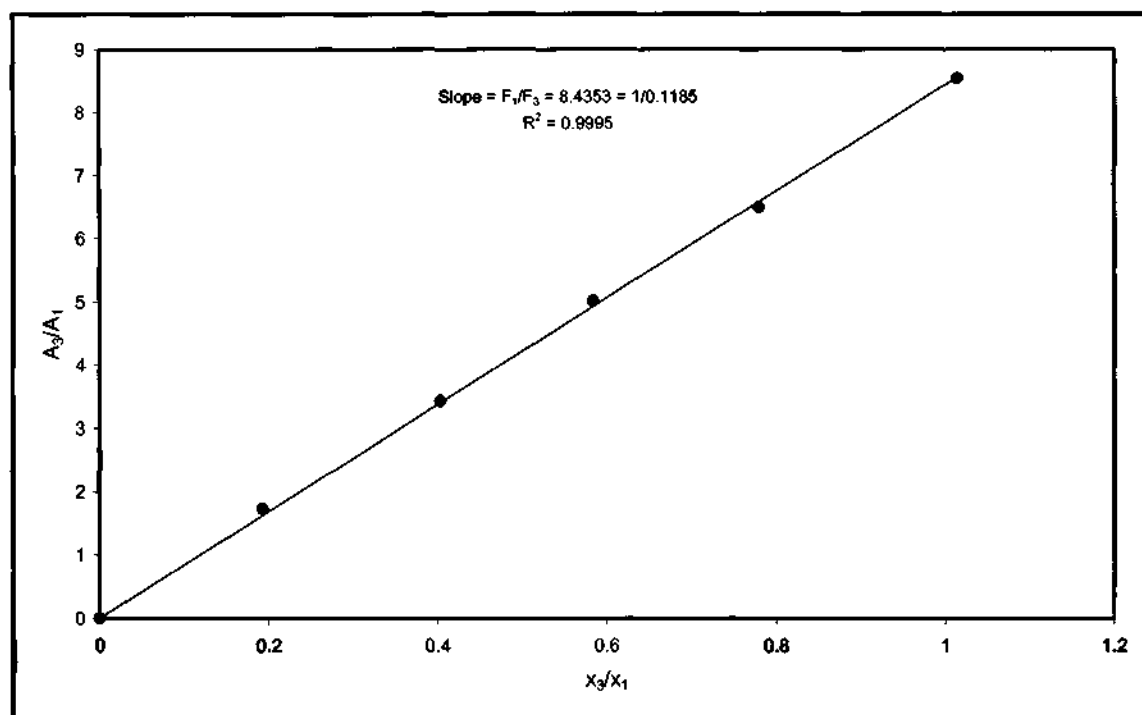
Figure 6-41: GC calibration graph for the water (1) + 1-dodecene (3) binary pair (1-dodecene dilute region).

Table 6-17: Liquid-liquid equilibrium data for the water (1) + acetonitrile (2) + 1-dodecene (3) system at 323.15 K and 1 atm.

Phase I			Phase II		
x_1	x_2	x_3	x_1	x_2	x_3
0.0067	0.0000	0.9933	0.9995	0.0000	0.0005
0.0080	0.0297	0.9623	0.9730	0.0265	0.0005
0.0088	0.0798	0.9114	0.9164	0.0791	0.0044
0.0102	0.1139	0.8759	0.7096	0.2791	0.0112
0.0092	0.1199	0.8709	0.6505	0.3347	0.0148
0.0087	0.1307	0.8606	0.4744	0.5019	0.0237
0.0085	0.1358	0.8557	0.3509	0.6240	0.0250
0.0058	0.1659	0.8283	0.1555	0.8127	0.0318
0.0000	0.2304	0.7696	0.0000	0.9521	0.0479
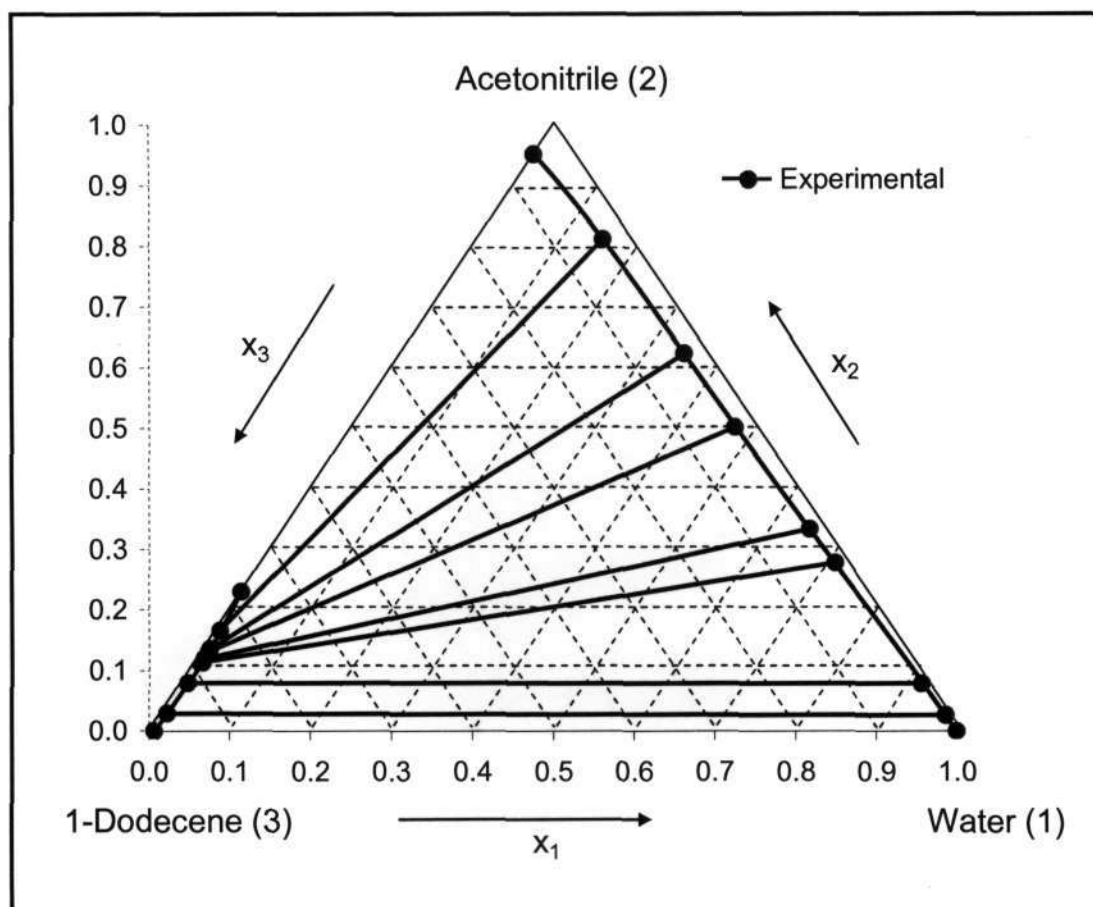
Figure 6-42: Ternary diagram for the water (1) + acetonitrile (2) + 1-dodecene (3) system at 323.15 K and 1 atm.

7

CHAPTER SEVEN

DATA ANALYSIS AND DISCUSSION

This chapter presents the analysis and discussion of the experimental results that were presented in Chapter 6. The chapter includes the vapour pressure data analysis with the Antoine and Wagner equations, determination of experimental activity coefficients, VLE data reduction employing the combined and direct methods, thermodynamic consistency testing for the measured VLE systems, LLE data reduction for the binary and ternary systems measured and concludes with a discussion on the VLLE systems studied in this work.

7.1 Pure Component Properties

The pure component properties of a substance depend directly on the nature of the molecules of the substance and play an important role in the analysis of thermodynamic data. Therefore accurate values of pure component properties are required for the correct theoretical treatment of phase equilibrium data. The pure component properties (critical temperature, critical pressure, critical volume and acentric factor) for all the chemicals (for VLE/VLLE systems) used in this work were obtained from the property data bank in Reid et al. (1988), except for the critical pressure and acentric factor of 1-nonanol which were unavailable. The critical pressure

for 1-nonanol was therefore estimated from the Ambrose method outlined in Reid et al. (1988) and the acentric factor of 1-nonanol was estimated from the Lee-Kesler method outlined in Reid et al. (1988). The second Virial coefficients were evaluated using the correlations of Pitzer and Curl (1957) and Tsonopoulos (1974), discussed in Sections 3.1.1.1 and 3.1.1.2 respectively. The liquid molar volumes were obtained using the equation of Rackett (1970), discussed in Section 3.1. The pure component properties for all the chemicals used in this work are presented in Appendix B.

7.2 Experimental Vapour Pressure Data

Vapour pressure data were measured for all chemicals used for VLE/VLLE systems studied in this work. These chemicals included: ethanol, cyclohexane, acetonitrile, water, 1-nonanol and 1-dodecene. According to Smith et al. (2001), the Antoine and Wagner equations are the most frequently used equations for the prediction of vapour pressure where the later equation offers greater complexity. Both these equations contain pure component constants that are valid for a specified temperature range.

Vapour pressures were measured using the VLE apparatus within the pressure and temperature range studied. The experimental data were regressed for other pure component constants such as the pure component constant of the Peng-Robinson-Stryjek-Vera equation of state (PRSV EOS) and the pure component constants of the Twu et al. (1991) alpha function. This provided a more accurate prediction when modelling VLE data.

7.2.1 Regression of Vapour Pressure Data

The vapour pressure data were regressed to determine the pure component parameters for the Antoine equation:

$$\ln(P) = A' - \frac{B'}{T + C'} \tag{7-1}$$

and the Wagner equation:

$$\ln\left(\frac{P}{P_c}\right) = \left(1 - x'\right)^{-1}\left[A''x' + B''\left(x'\right)^{1.5} + C''\left(x'\right)^3 + D''\left(x'\right)^6\right] \tag{7-2}$$

where

$$x' = 1 - \frac{T}{T_c}$$ (7-3)

For both the Antoine and the Wagner equations, the pressure is given in kPa and the temperature in Kelvin. The pure component parameters for these equations are given in Tables 7-1 and 7-2. The absolute differences between the experimentally measured vapour pressures and the predicted vapour pressures are given by:

$$\Delta P_i = \left| (P_i)_{measured} - (P_i)_{calculated} \right|$$ (7-4)

Table 7-1: Pure component parameters for the Antoine equation.

	Ethanol	Cyclohexane	Acetonitrile	Water	1-Nonanol	1-Dodecene
A'	17.3617	14.1725	14.5635	15.6066	15.6762	15.1312
B'	4073.4397	3021.8943	3148.4639	3389.0382	4168.9217	4353.3556
C'	-31.6926	-37.3809	-38.3499	-64.8210	-104.2469	-69.4845
S(ΔP^2)	0.1296	0.2500	0.0385	0.1755	0.0275	0.1129
Temp. Range [K]	309.96 to 351.06	308.05 to 352.78	303.92 to 354.71	342.71 to 371.00	374.20 to 423.18	362.30 to 423.18

Table 7-2: Pure component parameters for the Wagner equation.

	Ethanol	Cyclohexane	Acetonitrile	Water	1-Nonanol	1-Dodecene
A"	-12.6475	-1.0805	-16.2772	-9.6461	74.3397	18.4646
B"	10.8248	-12.2679	21.4010	5.3109	-190.7910	-61.4266
C"	-25.4293	16.4918	-31.7976	-6.3712	266.3823	84.4899
D"	72.7815	-37.8947	59.1974	-0.20199	-544.9020	-179.0757
S(ΔP^2)	0.0932	0.2273	0.0202	0.1749	0.0054	0.0900
Temp. Range [K]	309.96 to 351.06	308.05 to 352.78	303.92 to 354.71	342.71 to 371.00	374.20 to 423.18	362.30 to 423.18

It is evident from the S(ΔP^2) values in Tables 7-1 and 7-2 that for all components, the Wagner equation was found to provide a better correlation of the vapour pressure data than the Antoine equation. This result was anticipated as the Wagner equation has a greater degree of complexity and has four adjustable pure component constants as opposed to the three adjustable pure

component constants of the Antoine equation. However, it should be noted that both equations provide an excellent fit to the vapour pressure data. The pure component constants of the Antoine equation were used in the modelling of VLE systems as the lower degree of complexity allows for an ease of computation, especially for isobaric VLE reduction.

7.2.2 Pure Component Parameters for Equations of State

Stryjek and Vera (1986) found that the alpha function in the equation of state proposed by Peng and Robinson (1976) (Equation 3-48) provided inaccurate vapour pressures especially for polar and associating compounds. Therefore, Stryjek and Vera (1986) introduced a pure component parameter, κ_1 that allowed accurate reproduction of vapour pressure data for a variety of substances by modifying the expression for the alpha function (Equation 3-62). Stryjek and Vera (1986) mention that the value of κ_1 was obtained from the regression of vapour pressure data and was found to be sensitive to the critical properties of the pure component. Values of κ_1 can be found for a variety of compounds in the article published by Stryjek and Vera (1986). However, values for cyclohexane, 1-nonanol and 1-dodecene could not be found in their publication. Furthermore, the critical properties for the chemicals studied in this work were taken from a different source as compared to Stryjek and Vera (1986). Hence, the values of κ_1 for the components studied in this work were determined from the regression of the experimental vapour pressure data measured in this work. The recorded temperatures of the experimental vapour pressure data and critical properties were used as inputs to the regression programme. The value of κ_1 was then optimised by minimising the deviation of the calculated pressures from the experimental vapour pressures (Equation 7-4).

Twu et al (1991) also proposed an improvement to the accuracy of vapour pressure prediction by developing a new alpha function that catered for both low boiling and extremely high boiling components (Equation 3-64). This new alpha function contained three pure component parameters (L', M' and N') that were found from the regression of experimental vapour pressure data. According to Twu et al. (1991), this alpha function could be employed in any equation of state. Thus, the values of L', M' and N' would differ depending on the equation of state employed. For this work, the alpha function of Twu et al. (1991) was used in the Peng-Robinson equation of state (PR EOS). The values of L', M' and N' were determined from the regression of the experimental vapour pressure data measured in this work. The regression procedure that was employed to determine the κ_1 values for the PRSV EOS was also employed to determine the values of L', M' and N'.

According to Twu et al. (1991), the accurate prediction of the pure component vapour pressures greatly influences the accuracy of the vapour-liquid equilibrium calculations. It was therefore important to obtain accurate values for the pure component parameters of the PRSV EOS and the Twu et al. (1991) alpha function. The regressed values for κ_1 are presented in Table 7-3 and the regressed values for L', M' and N' are presented in Table 7.4.

Table 7-3: Regressed pure component parameter for the PRSV EOS.

	Ethanol	Cyclohexane	Acetonitrile	Water	1-Nonanol	1-Dodecene
κ_1	0.01374	-0.00898	-0.03634	-0.05831	0.40377	0.08025
$S(\Delta P^2)$	0.00904	0.01341	0.00875	0.00569	0.00025	0.00059

Table 7-4: Regressed pure component parameters for the Twu et al. alpha function.

	Ethanol	Cyclohexane	Acetonitrile	Water	1-Nonanol	1-Dodecene
L'	2.6463	1.9469	0.26586	0.13509	2.6527	2.9561
M'	4.5199	1.6978	0.88296	0.90602	0.33006	3.6857
N'	0.14906	0.24956	2.6929	4.8824	0.66498	0.13193
$S(\Delta P^2)$	0.00904	0.01344	0.00877	0.00569	0.00024	0.00059

The PRSV EOS and the Twu et al. (1991) alpha function show excellent prediction of pure component vapour pressures, as seen in the low values of $S(\Delta P^2)$ in Tables 7-3 and 7-4. It is however difficult to comment on which function provides the most accurate prediction of pure component vapour pressures as the $S(\Delta P^2)$ values are almost the same for all components.

7.3 Experimental Activity Coefficients for the VLE Systems

In order to determine the experimental activity coefficients, the vapour phase correction factor, Φ_i given by Equation (3-24), must first be evaluated using the second Virial coefficients. The values for the second Virial coefficients can be evaluated using one of the correlations discussed in Section 3.1.1. For this work, the correlation proposed by Tsonopoulos (1974) was used, as this correlation catered for both polar and non-polar compounds and required less pure component properties when compared to the correlation of Hayden and O'Connell (1975). Furthermore, the pure component properties for the correlation of Hayden and O'Connell (1975) were unavailable for the systems studied in this work. The experimental values of the vapour composition (y_i), liquid composition (x_i) and the calculated values of Φ_i were then

substituted into Equation (3-23), from which the activity coefficients were then calculated. These activity coefficients are known as the experimental activity coefficients as they are calculated directly from VLE data without the use of an activity coefficient model. The experimental activity coefficients are presented in Tables 7-5 and 7-6 for the systems measured in this work. Comparison of the experimental and calculated activity coefficients are presented in Section 7.4.

Table 7-5: Experimental liquid-phase activity coefficients for the cyclohexane (1) + ethanol (2) system at 20 kPa.

x_1	γ_1	γ_2
0.026	7.665	1.014
0.052	6.988	1.012
0.073	5.939	1.020
0.117	4.876	1.039
0.131	4.670	1.058
0.148	4.340	1.072
0.362	2.407	1.289
0.485	1.925	1.518
0.563	1.684	1.748
0.937	1.036	9.850
0.968	1.016	14.447
0.982	1.015	13.442

Table 7-6: Experimental liquid-phase activity coefficients for the 1-dodecene (1) + 1-nonanol (2) system at 403.15K.

x_1	γ_1	γ_2
0.097	2.058	0.981
0.170	1.884	0.986
0.311	1.772	0.932
0.367	1.632	0.956
0.444	1.461	1.028
0.586	1.227	1.254
0.643	1.147	1.394
0.685	1.108	1.488
0.718	1.081	1.575
0.834	0.984	2.134

7.4 Experimental VLE Data Reduction

The two most well-known techniques employed in the reduction of VLE data (the combined method and the direct method) were discussed extensively in Section 3.3.1. Both these techniques were applied in the reduction of the experimental VLE data measured in this work. For the combined method, the correlations of Pitzer and Curl (1957) and Tsonopoulos (1974) were used to determine the second Virial coefficients which were then used for the vapour phase correction. Three local-composition based liquid phase activity coefficient models (Wilson, NRTL and the modified UNIQUAC models) were used for the liquid phase correction. For the direct method, an equation of state (PRSV EOS) and a modified alpha function (Twu et al. (1991) alpha function in the PR EOS) were used for both the vapour and liquid phase corrections. In addition, the direct method required a mixing rule to accurately model the experimental VLE data. For this purpose, the mixing rules of Wong and Sandler (1992), and Twu and Coon (1996) were employed, discussed in Sections 3.1.3.1 and 3.1.3.2 respectively. These mixing rules both required an activity coefficient model to regress the VLE experimental data. For this purpose the NRTL activity coefficient model was employed. The regression combinations for the combined method are summarised in Table 7-7 and the regression combinations for the direct method are summarised in Table 7-8.

Table 7-7: Various regression combinations used for the combined method.

Second Virial Coefficient Correlation	Activity Coefficient Model	Abbreviation
Pitzer and Curl (1957)	Wilson	PC-WILSON
Tsonopoulos (1974)	Wilson	TS-WILSON
Pitzer and Curl (1957)	NRTL	PC-NRTL
Tsonopoulos (1974)	NRTL	TS-NRTL
Pitzer and Curl (1957)	Modified UNIQUAC	PC-UNIQUAC
Tsonopoulos (1974)	Modified UNIQUAC	TS-UNIQUAC

Table 7-8: Various regression combinations used for the direct method.

Equation of State	a Correlation	Mixing Rule	Activity Coefficient Model for Mixing Rule	Abbreviation
Peng and Robinson (1976)	Stryjek and Vera (1986)	Wong and Sandler (1992)	NRTL	PRSV-WS-NRTL
Peng and Robinson (1976)	Twu et al. (1991)	Wong and Sandler (1992)	NRTL	TWU-WS-NRTL
Peng and Robinson (1976)	Stryjek and Vera (1986)	Twu and Coon (1996)	NRTL	PRSV-TC-NRTL
Peng and Robinson (1976)	Twu et al. (1991)	Twu and Coon (1996)	NRTL	TWU-TC-NRTL

The Antoine equation was used to evaluate the saturated pressures/temperatures in the modelling of the VLE data. The Antoine equation was chosen as it offers a lower degree of complexity that allows for an ease of computation, especially for isobaric VLE modelling where the complexity is evident in the calculation of the saturated temperatures.

For both the combined and direct methods, the model parameters were optimised by minimising the temperature deviations for isobars or pressure deviations for isotherms between the experimentally measured temperatures or pressures and the calculated values given by the model. The difference between the experimental and model values is commonly termed a residual (d). According to Van Ness et al. (1978), minimising the temperature residuals for isobaric data provides a fit that is at least as good as any other and is the most simplest and direct objective function. The same result holds true for isothermal data, where the pressure residuals provides the best fit. Therefore these objective functions ($S = S(dT)^2$ for isobaric data and $S = S(dP)^2$ for isothermal data) were employed in this work. The regression programmes were written in Matlab, which offered a variety of built-in optimisation functions. For this work the *fminsearch* function was chosen, which finds the minimum of an unconstrained multi-variable function. The algorithm is based on the Nelder-Mead simplex method (Lagarias et al., 1998).

7.4.1 Cyclohexane (1) + Ethanol (2)

The GC was calibrated for the cyclohexane dilute region and the ethanol dilute region. Both dilute regions displayed a linear response as seen in Figures 6-7 and 6-8. The inverse of the response factor ratio of Figure 6-7 is almost equal to the slope or response factor ratio of Figure

6-8. Nevertheless, an average response factor was not calculated. Instead, care was taken to ensure the correct calibration graph was employed, depending on whether the samples were taken in the dilute cyclohexane region or dilute ethanol region.

The cyclohexane (1) + ethanol (2) system measured at 40 kPa was used as a test system to ensure that the VLE apparatus was operating correctly and to confirm that the experimental procedure was accurate. The measured data was then compared to reliable, accurate and consistent literature data. For this purpose, the data measured by Joseph et al. (2001) was employed. It was found that the experimental data compares well with the literature data, as seen in Figures 6-9 and 6-10.

This system also served to ascertain whether the techniques, equations and programmes that were developed to analyse experimental VLE data were functioning as desired. Generally, all the models (for both the combined and direct methods) provided a good fit to the experimental data. For the combined method, it was found that the second Virial coefficient correlation of Pitzer and Curl (1957) displayed a lower value for the objective function when used with all three liquid phase activity coefficient models. However, the NRTL model provided the best fit and the modified UNIQUAC model displayed the worst fit to the experimental VLE data and the experimental activity coefficients. For the direct method, the mixing rule of Twu and Coon (1996) with both the PRSV EOS and the modified alpha function of Twu et al. (1991), displayed a lower value for the objective function when compared to the mixing rule of Wong and Sandler (1992). Furthermore, the analysis revealed that the modified alpha function of Twu et al. (1991) provided a better fit to the experimental VLE data when compared to the PRSV EOS.

Overall, it was found that the modified alpha function of Twu et al. (1991) with the mixing rule of Twu and Coon (1996) provided the best fit to the experimental VLE data as it yielded the lowest value for the objective function and hence the average ΔT and Δy_i values. This result was not unexpected as the modified alpha function of Twu et al. (1991) is a more recently developed model in comparison to the PRSV EOS. The mixing rule of Twu and Coon (1996) was also anticipated to provide a better fit as this mixing rule contained an additional parameter that was varied during the optimisation process. On the other hand, the experimental activity coefficients were found to be best represented by the NRTL model. This could be due to the additional adjustable parameter (a) that represents the non-randomness of the mixture.

The parameters for the best fit models (PC-NRTL and TWU-TC-NRTL) and worst fit models (TS-UNIQUAC and PRSV-WS-NRTL) are presented in Table 7-9. All the other model

parameters are presented in Appendix C. The experimental data are presented together with the model that displayed the best fit and the model that displayed the worst fit for the x-y and T-x-y plots in Figures 7-1 and 7-2 for the combined method and Figures 7-3 and 7-4 for the direct method. The experimental activity coefficients and those calculated by the best fit model and the worst fit model are presented in Figure 7-5.

Table 7-9: Parameters for the best and worst fit models and their deviations from experimental values for the cyclohexane (1) + ethanol (2) system at 40 kPa.

Combined Method		Direct Method	
Best Models			
PC-NRTL		**TWU-TC-NRTL**	
$g_{12} - g_{11}$ / (J/mol)	6136.39	$g_{12} - g_{11}$ / (J/mol)	111723.62
$g_{21} - g_{22}$ / (J/mol)	3706.55	$g_{21} - g_{22}$ / (J/mol)	119319.45
a	0.4621	a	0.1726
Average ΔT / (K)	0.2034	k_{ij}	-0.1668
Average Δy_1	0.0080	l_{ij}	-0.0011
		Average ΔT / (K)	0.1456
		Average Δy_1	0.0073
Worst Models			
TS-UNIQUAC		**PRSV-WS-NRTL**	
$u_{12} - u_{11}$ / (J/mol)	10414.17	$g_{12} - g_{11}$ / (J/mol)	85066.53
$u_{21} - u_{22}$ / (J/mol)	-745.73	$g_{21} - g_{22}$ / (J/mol)	59676.36
Average ΔT / (K)	0.3322	a	0.3360
Average Δy_1	0.0135	k_{ij}	-0.0651
		Average ΔT / (K)	0.2512
		Average Δy_1	0.0112

Figure 7-1: Fit of the PC-NRTL and TS-UNIQUAC model combinations to the x-y plot of the cyclohexane (1) + ethanol (2) system at 40 kPa for the combined method.

Figure 7-2: Fit of the PC-NRTL and TS-UNIQUAC model combinations to the T-x-y plot of the cyclohexane (1) + ethanol (2) system at 40 kPa for the combined method.

Figure 7-3: Fit of the TWU-TC-NRTL and PRSV-WS-NRTL model combinations to the x-y plot of the cyclohexane (1) + ethanol (2) system at 40 kPa for the direct method.

Figure 7-4: Fit of the TWU-TC-NRTL and PRSV-WS-NRTL model combinations to the T-x-y plot of the cyclohexane (1) + ethanol (2) system at 40 kPa for the direct method.

Figure 7-5: Comparison of the experimental activity coefficients and those calculated from the PC-NRTL and the TS-UNIQUAC model combinations for the cyclohexane (1) + ethanol (2) system at 40 kPa.

7.4.2 1-Dodecene (1) + 1-Nonanol (2)

The GC calibrations for the 1-dodecene and 1-nonanol dilute regions revealed a linear response for both dilute regions, as shown in Figures 6-11 and 6-12, with the inverse of the response factor ratio of Figure 6-11 almost equal to the slope or response factor ratio of Figure 6-12. However to ensure accuracy, an average response factor was not utilised. Instead, care was taken to ensure the correct calibration curve was employed, depending on whether the samples were taken in the dilute 1-dodecene region or dilute 1-nonanol region.

For the combined method, the average ΔP and Δy_i values were found to be almost the same for each model when using the second Virial coefficient correlation of Pitzer and Curl (1957) or Tsonopoulos (1974), with the latter providing only a slight improvement. The NRTL liquid phase activity coefficient model was the only one which provided a satisfactory fit to the experimental VLE data and the modified UNIQUAC model displayed the worst fit. For the direct method, the analysis of the various combinations revealed that the modified alpha function of Twu et al. (1991) with the mixing rule of Wong and Sandler (1992) provided the best fit to the experimental VLE data as it displayed the lowest average Δy_i value. On the other

hand, the PRSV EOS with the mixing rule of Wong and Sandler (1992) provided the worst fit to the experimental VLE data as it displayed the highest average Δy_i value.

However, it was found that all models failed to provide an excellent fit to the experimental VLE data. The poor fit can be noted from the large deviations between the experimental vapour compositions and the model predictions for the experimental points between 8 kPa and 8.5 kPa (refer to Figures 7-6 to 7-9). This also affects the experimental activity coefficients (refer to Figure 7-10). According to Raal and Mühlbauer (1998), the vapour compositions are most likely subject to experimental errors therefore resulting in poor predictions for the models. However, these deviations are consistent for all models as a result of some experimental error. It should also be noted that the critical pressure and acentric factor of 1-nonanol were estimated from group contribution methods (as discussed in Section 7.1), which strongly influences the model prediction. Furthermore according Twu et al. (1995), heavy hydrocarbons have a higher value for the acentric factor and hence vapour pressure data at reduced temperatures for heavy hydrocarbons are inconsistent with the definition of the acentric factor.

The parameters for the best fit models (TS-NRTL and TWU-TC-NRTL) and worst fit models (PC-UNIQUAC and PRSV-WS-NRTL) are presented in Table 7-10. All the other model parameters are presented in Appendix C. The experimental data are presented together with the model that displayed the best fit and the model that displayed the worst fit for the x-y and T-x-y plots in Figures 7-6 and 7-7 for the combined method and Figures 7-8 and 7-9 for the direct method. Figure 7-10 shows the experimental activity coefficients and the different trends obtained from the TS-NRTL and PC-UNIQUAC model combinations for the liquid phase activity coefficients.

Unlike the Wilson and modified UNIQUAC models, the NRTL model contained three adjustable parameters, where the non-randomness parameter (a) is the third adjustable parameter that accounts for the non-randomness of the mixture. For the 1-dododene (1) + 1-nonanol (2) system at 403.15 K, a was found to provide a considerable improvement to the regression of experimental VLE data. The effect of a was most evident in the activity coefficient prediction. Usually, the infinite dilution activity coefficient is an extreme value. However, Figure 7-8 shows that the activity coefficient for 1-nonanol (2) exhibits a maximum at approximately $x_1 = 0.9$. This phenomenon is however not uncommon. Smith et al. (2001) also found this phenomenon for the ethanol + chloroform system at 323.15 K. It is believed that this phenomenon occurs for systems that do not contain adequate data in the very dilute regions, which according to Raal and Mühlbauer (1998) are quite difficult to measure. Interestingly though, when a was fixed during the regression technique (for a variety of values), the other two

adjustable NRTL parameters varied significantly, as shown in Table 7-11. Furthermore, the plot of ln γ_i versus x_i displayed a variety of trends as shown in Figure 7-11.

Table 7-10: Parameters for the best and worst fit models and their deviations from experimental values for the 1-dodecene (1) + 1-nonanol (2) system at 403.15 K.

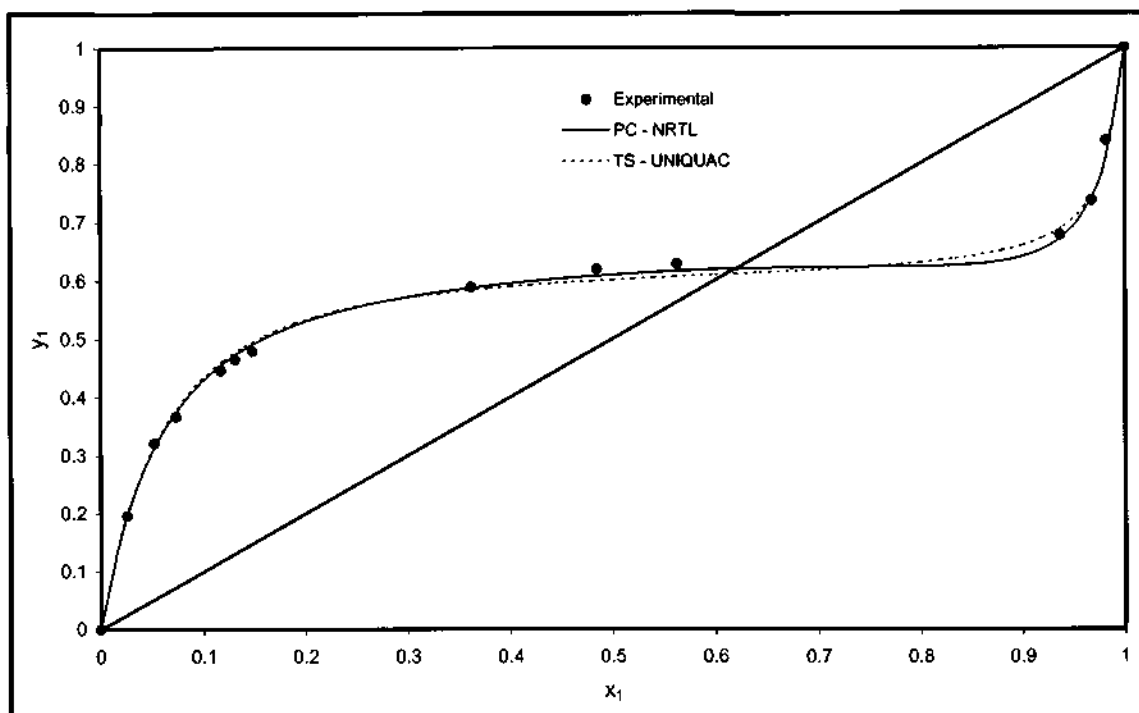| Combined Method		Direct Method	
Best Models			
TS-NRTL		**TWU-WS-NRTL**	
$g_{12} - g_{11}$ / (J/mol)	-7957.51	$g_{12} - g_{11}$ / (J/mol)	8380.01
$g_{21} - g_{22}$ / (J/mol)	4243.11	$g_{21} - g_{22}$ / (J/mol)	73763.54
a	-0.6342	a	0.0115
Average ΔP / (K)	0.0183	k_{ij}	-0.5657
Average Δy_1	0.0234	Average ΔP/ (K)	0.0273
		Average Δy_1	0.0103
Worst Models			
PC-UNIQUAC		**PRSV-WS-NRTL**	
$u_{12} - u_{11}$ / (J/mol)	1508.87	$g_{12} - g_{11}$ / (J/mol)	3811.82
$u_{21} - u_{22}$ / (J/mol)	-851.30	$g_{21} - g_{22}$ / (J/mol)	71551.93
Average ΔP / (K)	0.0311	a	0.0016
Average Δy_1	0.0283	k_{ij}	-0.4541
		Average ΔP / (K)	0.0208
		Average Δy_1	0.0249
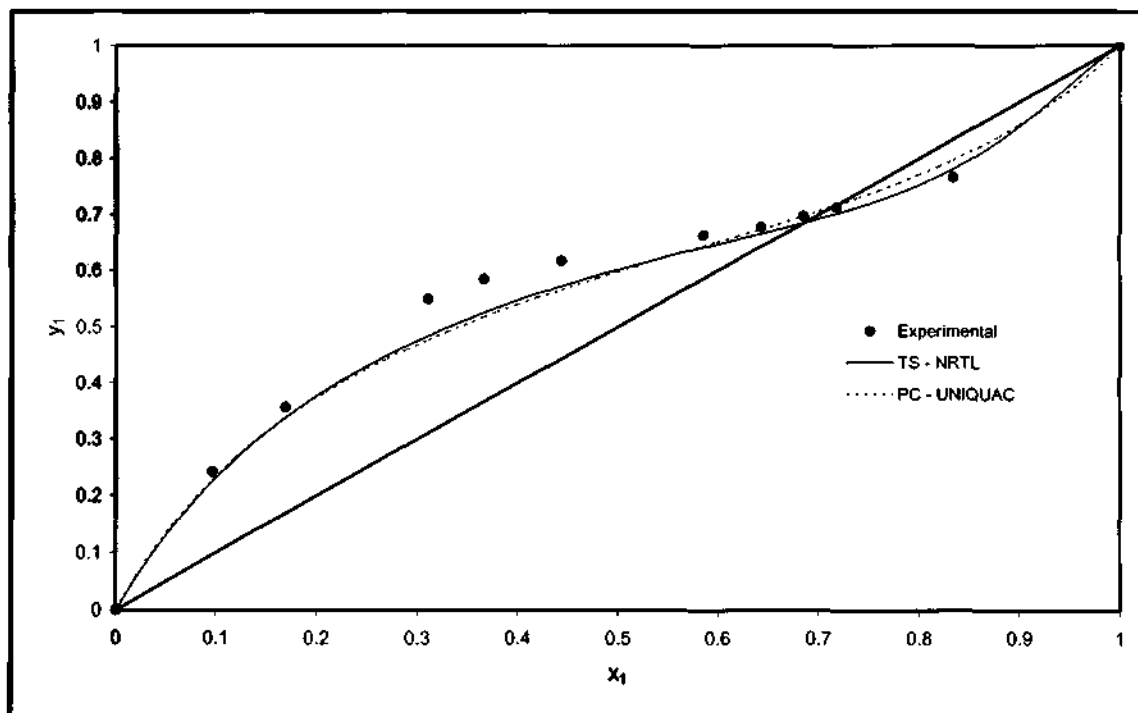
Figure 7-6: Fit of the TS-NRTL and PC-UNIQUAC model combinations to the x-y plot of the 1-dodecene (1) + 1-nonanol (2) system at 403.15 K for the combined method.
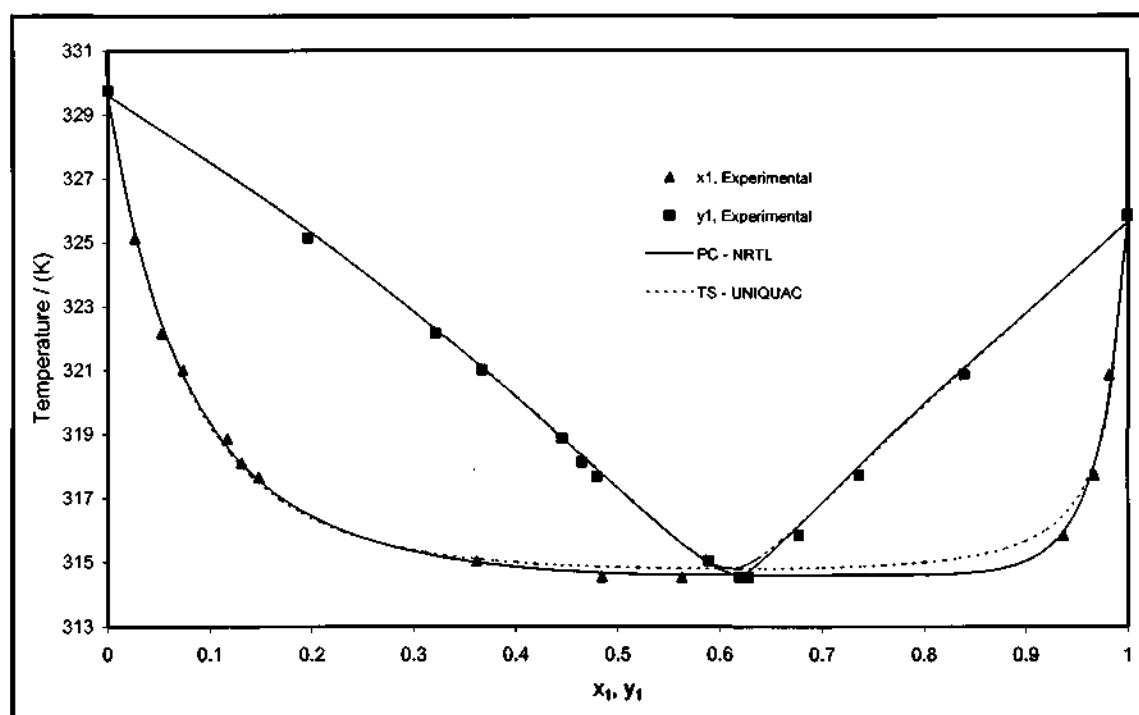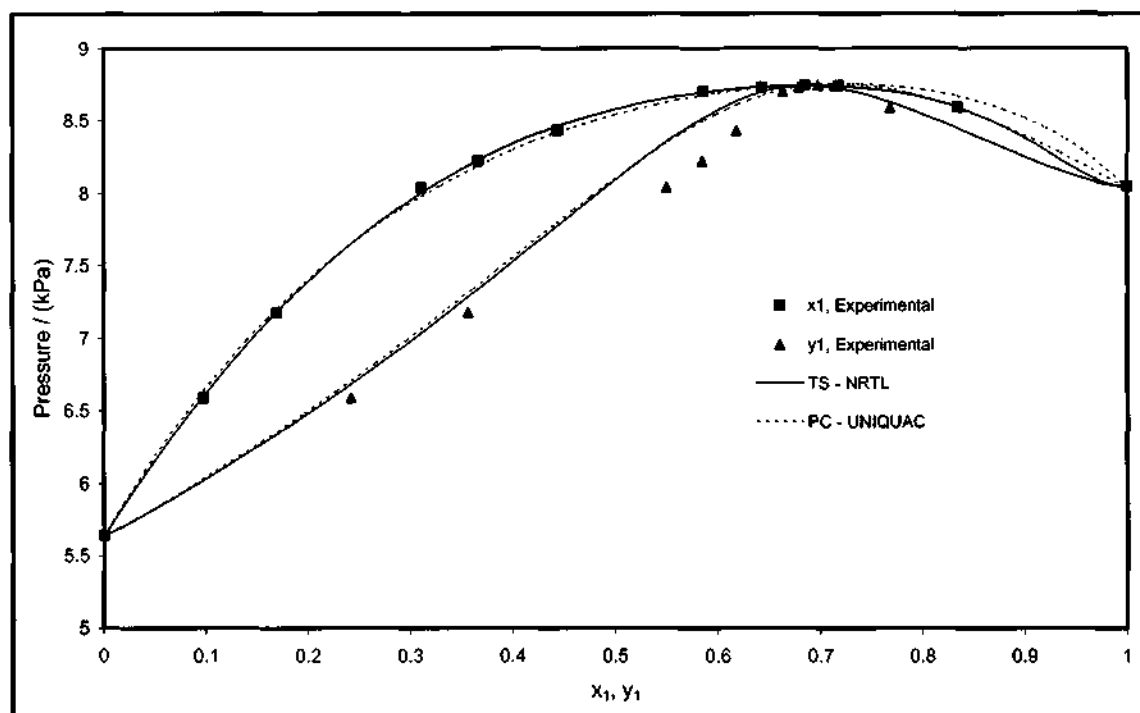
Figure 7-7: Fit of the TS-NRTL and PC-UNIQUAC models to the P-x-y plot of the   1-dodecene (1) + 1-nonanol (2) system at 403.15 K for the combined method.
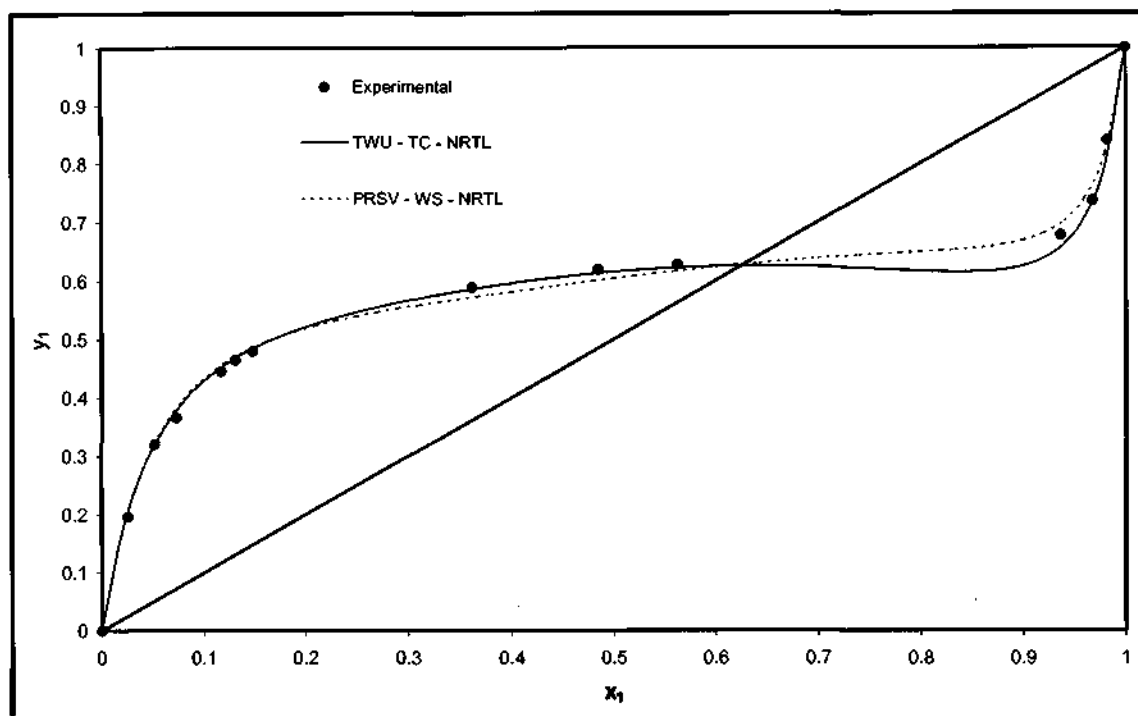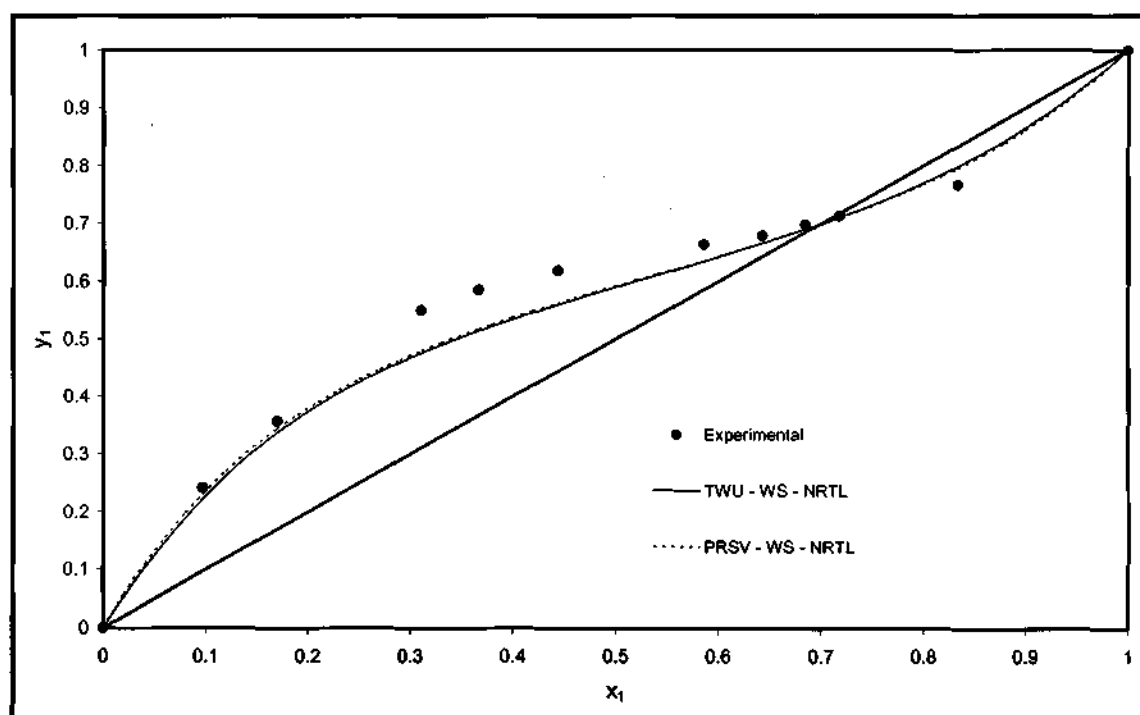

Figure 7-8: Fit of the TWU-WS-NRTL and PRSV-WS-NRTL model combinations to the x-y plot of the 1-dodecene (1) + 1-nonanol (2) system at 403.15 K for the direct method.
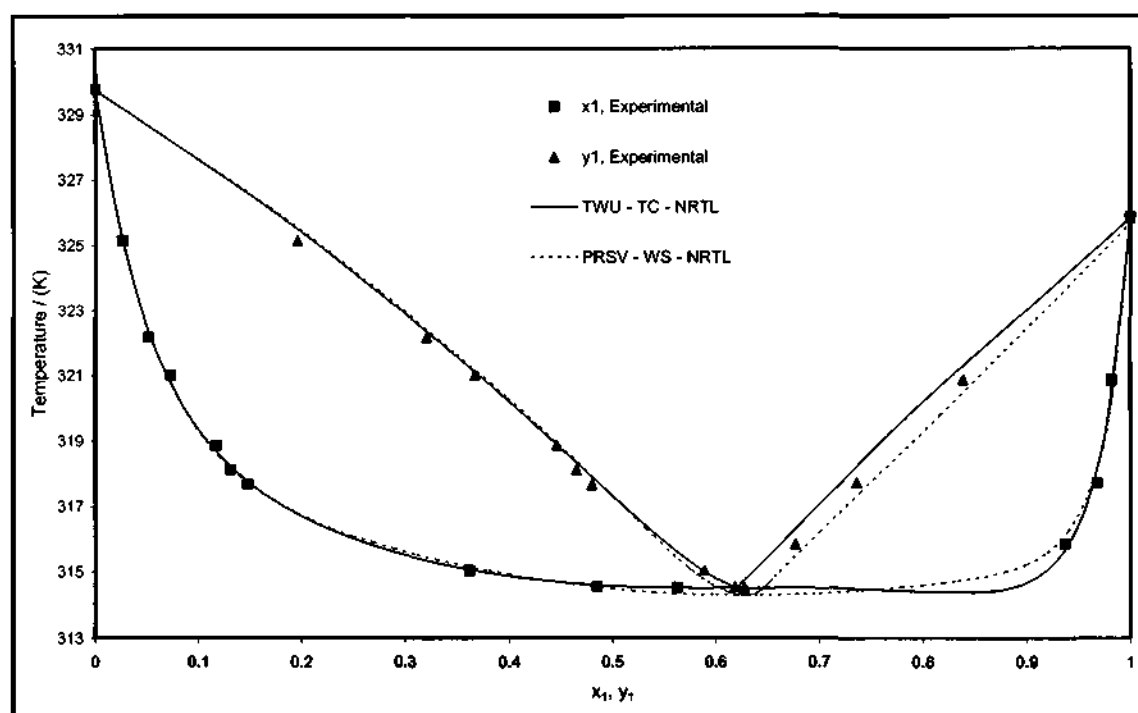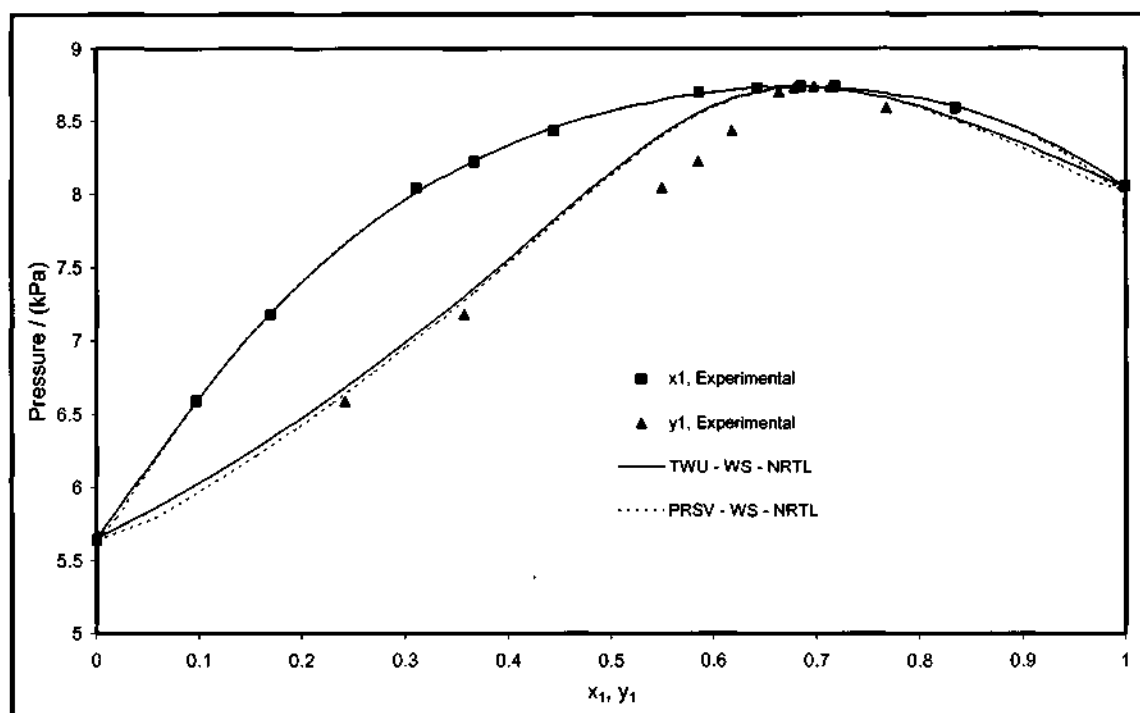
Figure 7-9: Fit of the TWU-WS-NRTL and PRSV-WS-NRTL model combinations to the P-x-y plot of the 1-dodecene (1) + 1-nonanol (2) system at 403.15 K for the direct method.
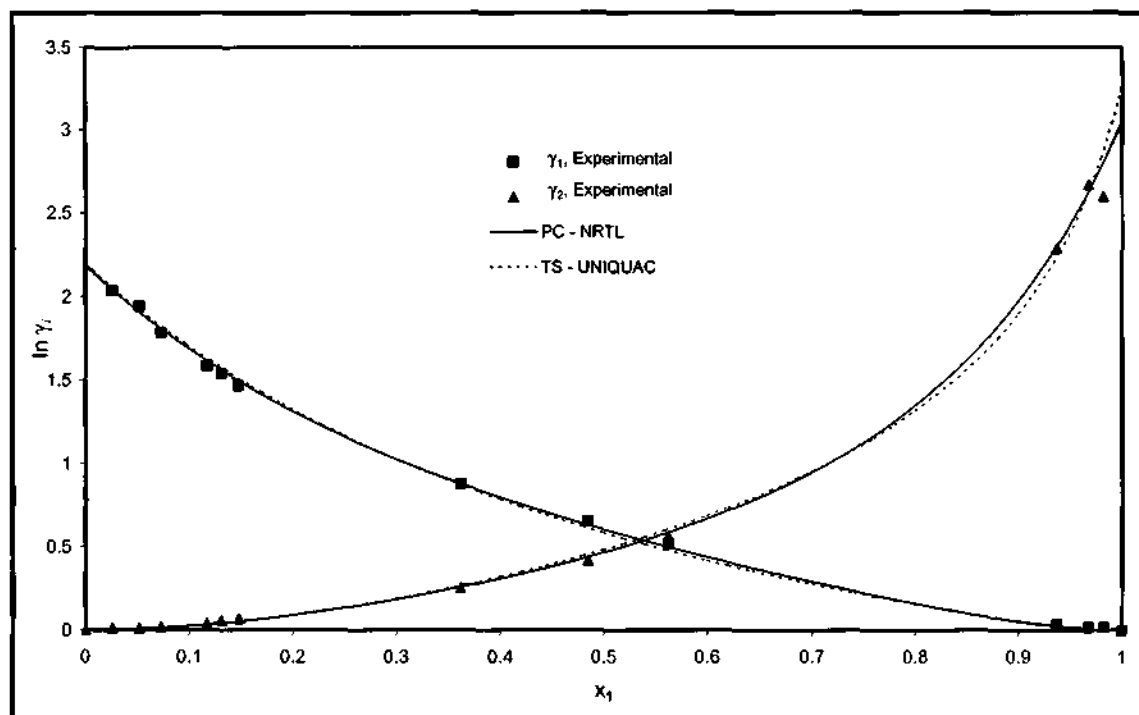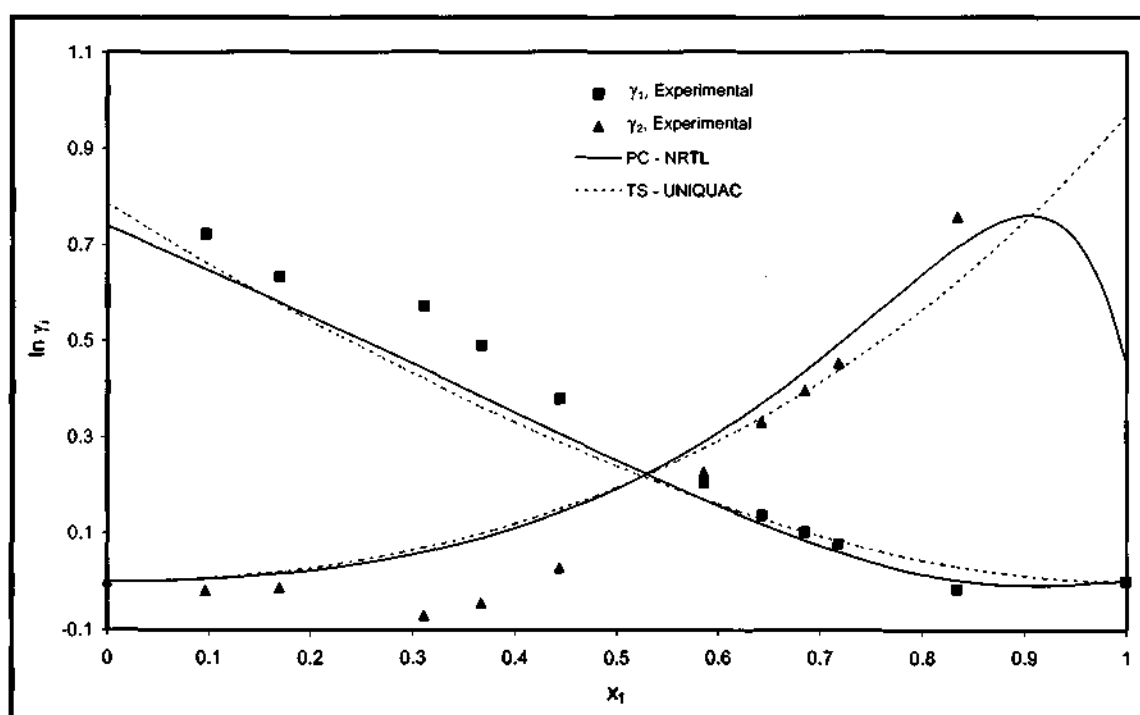

Figure 7-10: Comparison of the experimental activity coefficients and those calculated from the TS-NRTL and the PC-UNIQUAC model combinations for the 1-dodecene (1) + 1-nonanol (2) system at 403.15 K.

142

Table 7-11: NRTL model parameters for the combined method when a is fixed and their deviations from experimental values for the 1-dodecene (1) + 1-nonanol (2) system at 403.15 K.

a	t_{12}	t_{21}	Avg (ΔP)	Avg (Δy_1)
-1	-2.7533	0.8571	0.0382	0.0200
-0.5	-2.4154	1.4751	0.0128	0.0234
-0.25	-0.0371	0.8257	0.0273	0.0233
0.1	1.5287	-0.5244	0.0270	0.0233
0.2	1.0228	-0.0446	0.0273	0.0233
0.3	0.8576	0.1280	0.0279	0.0234
0.4	0.7821	0.2221	0.0286	0.0235
0.47	0.7531	0.2683	0.0294	0.0235
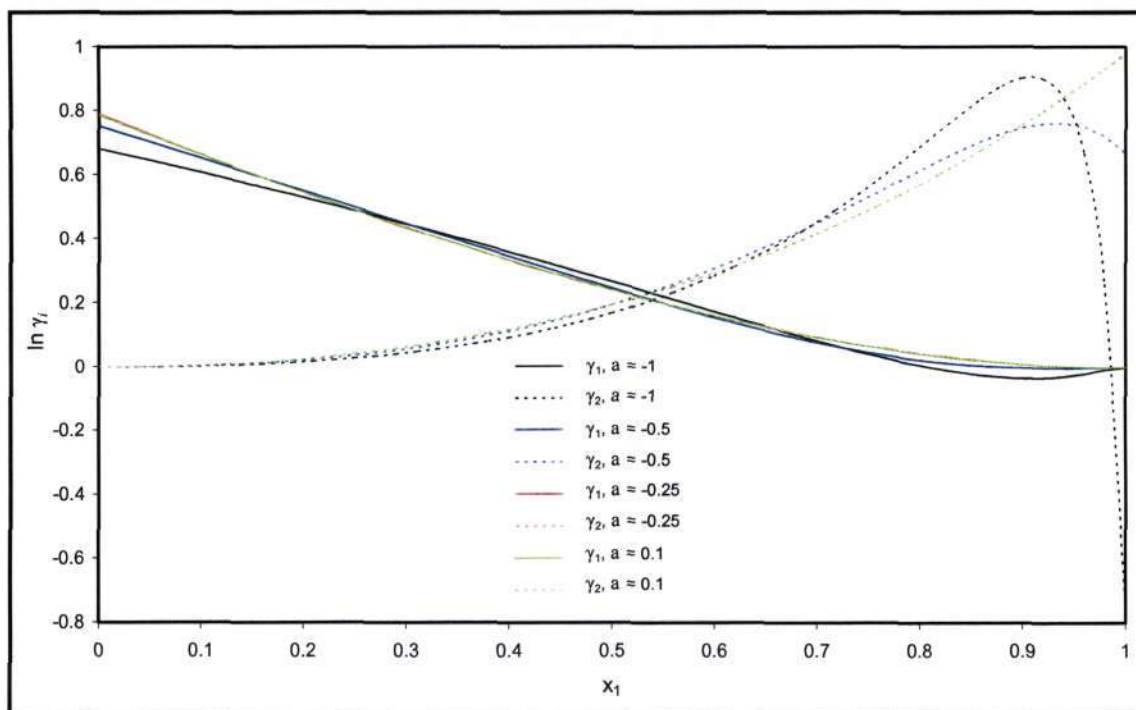
Figure 7-11: Comparison of the activity coefficients calculated from the NRTL model for fixed values of a for the 1-dodecene (1) + 1-nonanol (2) system at 403.15 K.

7.5 Thermodynamic Consistency Testing for VLE Systems

The *point test* of Van Ness et al. (1973) and the *direct test* of Van Ness (1995) were employed to test the thermodynamic consistency of the experimental data measured in this work. These tests were discussed in detail in Section 3.6. In this section the results obtained from each test for the experimental data will be presented and discussed.

7.5.1. Cyclohexane (1) + Ethanol (2)

The equation of state models can only be used to carry out the *point test*. As discussed in Section 3.6.1, the *point test* requires that the vapour compositions display an average absolute deviation less than 0.01 for data to be thermodynamically consistent. We will only consider the case of the best mixing rule for this system; the mixing rule of Twu and Coon (1996). It was found that the PRSV EOS and the Twu et al. (1991) alpha function pass this test. A summary of the results are presented in Table 7-12.

All the liquid phase activity coefficient models were used to carry out both the *point test* and the *direct test*. Only the NRTL model complies with this requirement and thus passes the *point test*. The Wilson model yields an average absolute deviation of 0.0101 for the vapour composition and thus does not strictly pass the *point test*. On the other hand, the modified UNIQUAC model yields an average absolute deviation of 0.0132 for the vapour composition and therefore does not pass the *point test*. Table 7-13 summarises the results obtained for the *point test* when using a liquid phase activity coefficient model. The modified UNIQUAC model was found to provide the worst fit for the cyclohexane (1) + ethanol system at 40 kPa for the VLE regression. Hence, it was concluded that the modified UNIQUAC model does not suit this system well and thus was likely to produce results that fail the tests for thermodynamic consistency. Overall, the analysis showed that the deviations obtained from the TWU-TC-NRTL model combination yielded the lowest average absolute Δy_i value and is presented in Figure 7-12. The Δy_i deviations obtained from the PRSV-TC-NRTL, PC-NRTL, PC-WILSON and PC-UNIQUAC model combinations can be viewed in Appendix D.

For the *direct test*, the NRTL model yielded the lowest value for the root mean square deviation (RSMD) of the residual $\{\delta\ln(\gamma_1/\gamma_2)\}$, as shown in Table 7-13. However both the NRTL and Wilson models yield an index value of 2 when compared with consistency index table of Van Ness (1995), as given in Table 3-1. According to Van Ness (1995), an index of 2 signifies that the thermodynamic consistency of the experimental data is very good. Figure 7-13 shows the degree of scatter about zero for the $\delta\ln(\gamma_1/\gamma_2)$ deviations for the PC-NRTL model combination.

144

The $\delta\ln(\gamma_1/\gamma_2)$ deviations obtained from the PC-WILSON and PC-UNIQUAC model combinations can be viewed in Appendix D.

Table 7-12: Results obtained for the point test when using an equation of state model for the cyclohexane (1) + ethanol (2) system at 40 kPa.

Model Combination	Average $|\Delta y_1|$
PRSV-WS-NRTL	0.0112
TWU-TC-NRTL	0.0073

Table 7-13: Results obtained for the point test and the direct test when using a liquid phase activity coefficient model for the cyclohexane (1) + ethanol (2) system at 40 kPa.

Model Combination	RMSD $\delta\ln(\gamma_1/\gamma_2)$	Average $|\Delta y_1|$
PC-WILSON	0.0458	0.0101
PC-NRTL	0.0355	0.0080
PC-UNIQUAC	0.0551	0.0132
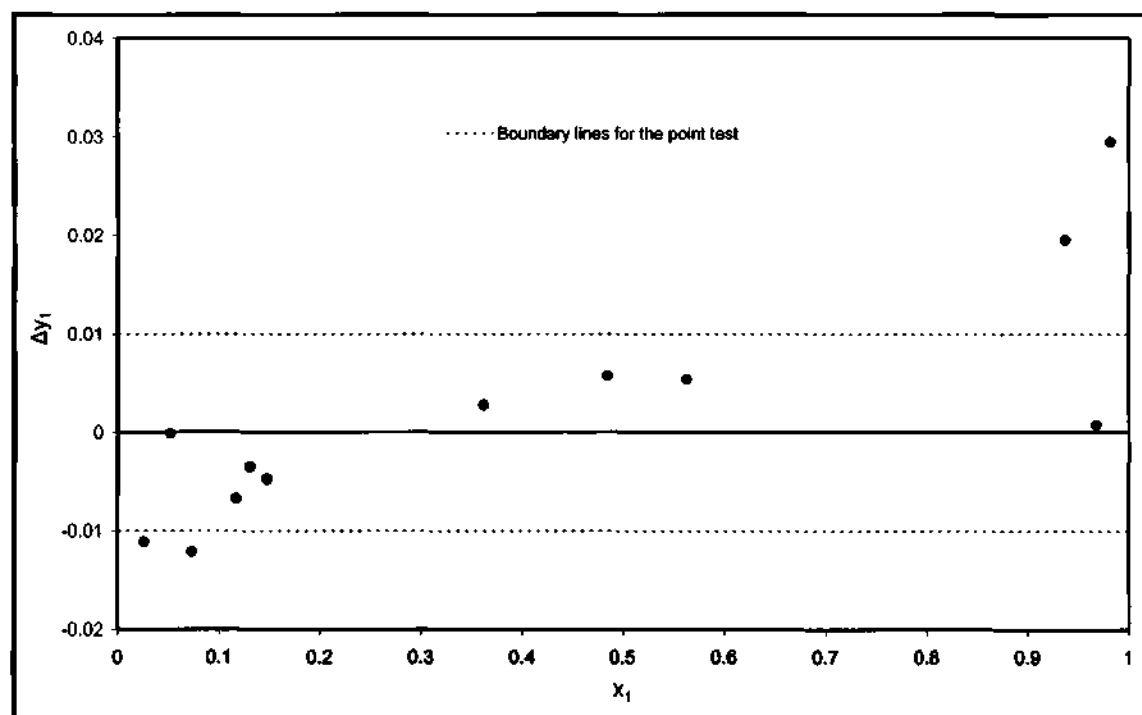
Figure 7-12: Plot used for the point test with the TWU-TC-NRTL model combination for the cyclohexane (1) + ethanol (2) system at 40 kPa.
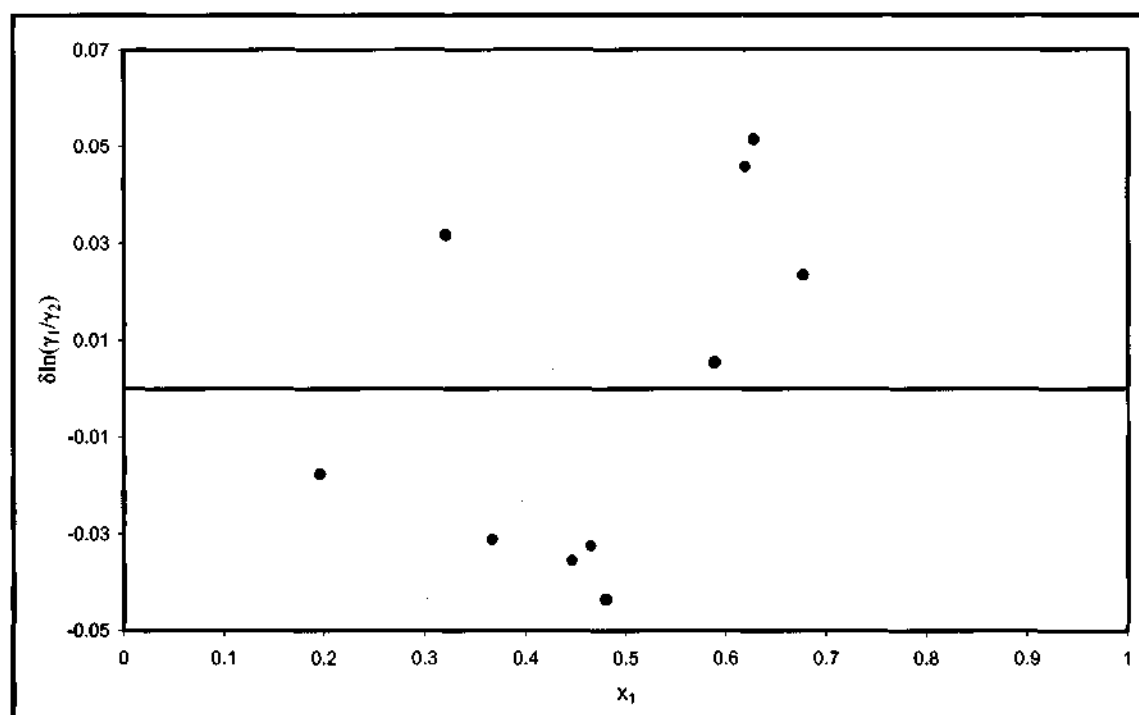
Figure 7-13: Plot used for the direct test with the PC-NRTL model combination for the cyclohexane (1) + ethanol (2) system at 40 kPa.

7.5.2. 1-Dodecene (1) + 1-Nonanol (2)

Application of the *point test* for the equation of state models showed that only the TWU-WS-NRTL model combination yielded the lowest absolute average vapour composition. This value however lies on the boundary of the point test and thus shows how a model affects the results for thermodynamic consistency tests. Hence the *point test* for the equations of state models is inconclusive. A summary of the results for the mixing rule that provided the lowest absolute average vapour compositions are presented in Table 7-14.

When using the liquid phase activity coefficient models for the *point test*, none of the liquid phase activity coefficient models complied with the requirement for this test. The NRTL model yielded the lowest average absolute deviation of 0.0234 for the vapour composition. The consistency tests rely on an appropriate model being employed, therefore it would be anticipated that the consistency tests would fail if the model failed to provide an excellent fit. Table 7-15 summarises the results obtained for the *point test* with a liquid phase activity coefficient model. Overall, the analysis showed that the deviations obtained from the TWU-WS-NRTL model combination yielded the lowest average absolute Δy_i value and is presented in Figure 7-14. The Δy_i deviations obtained from the PRSV-TC-NRTL, TS-NRTL, TS-WILSON and TS-UNIQUAC model combinations can be viewed in Appendix D.

146

For the *direct test*, the NRTL model yielded the lowest value for the RMSD of the residual $\{\delta\ln(\gamma_1/\gamma_2)\}$, as shown in Table 7-15. The NRTL model yielded an index value of 6 when compared with consistency index table of Van Ness (1995), as given in Table 3-1. The Wilson and modified UNIQUAC models both yielded an index value of 7. This therefore indicates that the 1-dodecene (1) + 1-nonanol (2) system at 403.15 K is not thermodynamically consistent. As explained earlier, according to Raal and Mühlbauer (1998), the vapour compositions are most likely subject to experimental errors. Furthermore, lack of experimental data in the dilute regions also contributes to thermodynamic inconsistency. Hence, all three models did not provide an excellent fit to the experimental data. Therefore, it should be expected that this system would most likely fail the *direct test*. Figure 7-15 shows the degree of scatter about zero for the $\delta\ln(\gamma_1/\gamma_2)$ deviations for the NRTL model. The $\delta\ln(\gamma_1/\gamma_2)$ deviations obtained from the PC-WILSON and PC-UNIQUAC model combinations can be viewed in Appendix D.

Table 7-14: Results obtained for the point test when using an equation of state model for the 1-dodecene (1) + 1-nonanol (2) system at 403.15 K.

Model Combination	Average $|\Delta y_1|$
PRSV-WS-NRTL	0.0215
TWU-WS-NRTL	0.0103

Table 7-15: Results obtained for the point test and the direct test when using a liquid phase activity coefficient model for the 1-dodecene (1) + 1-nonanol (2) system at 403.15 K.

Model Combination	RMSD $\delta\ln(\gamma_1/\gamma_2)$	Average $|\Delta y_1|$
Wilson	0.1609	0.0237
NRTL	0.1426	0.0232
Modified UNIQUAC	0.1610	0.0280
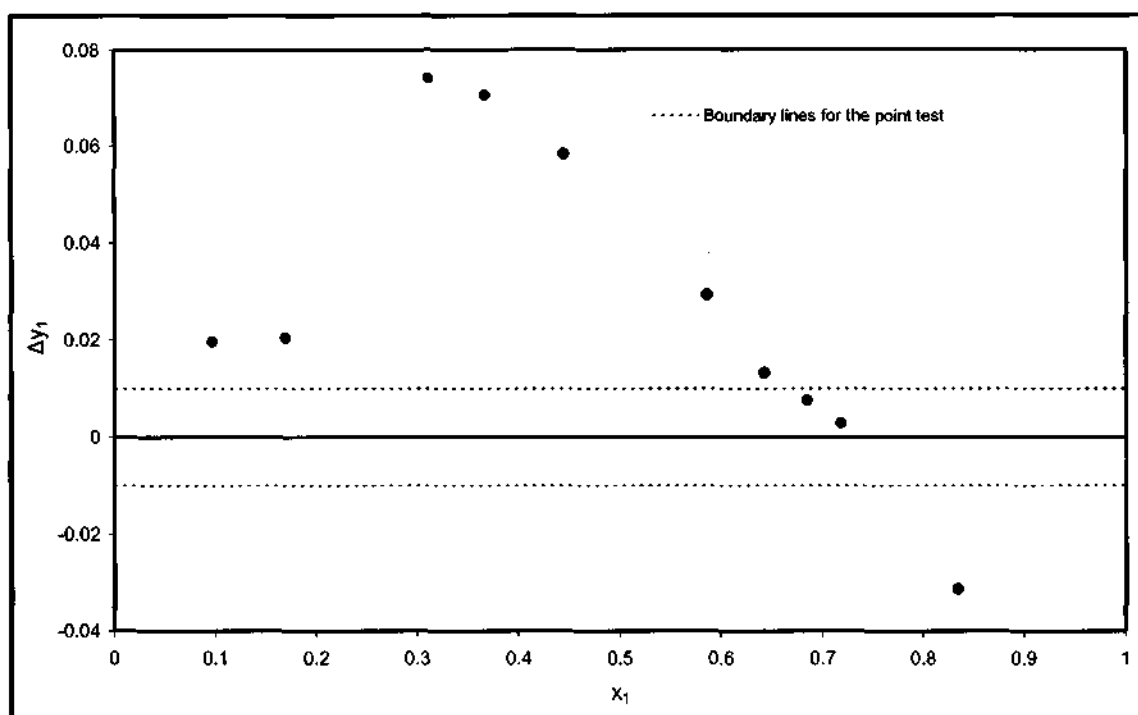
Figure 7-14: Plot used for the direct test with the TWU-WS-NRTL model combination for the 1-dodecene (1) + 1-nonanol (2) system at 403.15 K.
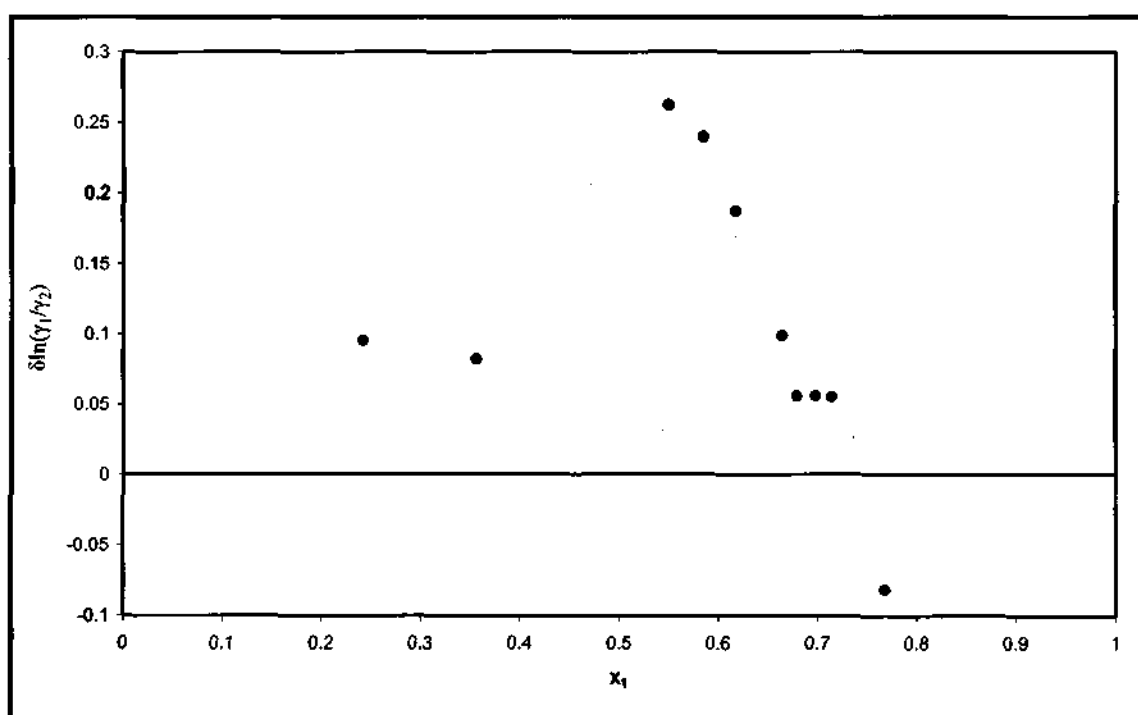
Figure 7-15: Plot used for the direct test with the TS-NRTL model combination for the 1-dodecene (1) + 1-nonanol (2) system at 403.15 K.

7.6 Experimental LLE Data Reduction

7.6.1 Binary Systems

Binary LLE data are also known as mutual solubility data, discussed in Section 3.4.4.1. There is no direct means for finding the activity coefficients from mutual solubility data but only the ratio of the activity coefficients (Raal and Mühlbauer, 1998). Therefore, mutual solubility data can only be used to obtain the parameters of a liquid phase activity coefficient model as a function of temperature. All the mutual solubility data measured in this work were regressed using the three-suffix Margules, Van Laar and the NRTL models. In the NRTL model, the non-randomness parameter (a) was fixed. In an attempt to establish values or limits of a for certain groups of compounds, Walas (1985) examined a values for a large range of systems given in the DECHEMA VLE data collection (Gmehling and Onken, 1977-1982). However, the results were rather inconclusive. On the other hand, all data in the DECHEMA LLE collection were correlated with a value of 0.2 for a (Sørensen et al., 1979-1987). Therefore, it was decided that a value of 0.20 would be used for a in the NRTL model for the correlation of all mutual solubility data in this work.

All the GC calibrations graphs presented in Figures 6-15, 6-16, 6-18, 6-19, 6-21 and 6-22 displayed a linear response. The inverse of the response factor ratio one dilute region was almost equal to the slope or response factor ratio of the other dilute region. Nevertheless, an average response factor was not calculated. Instead, care was taken to ensure the correct calibration graph was employed, depending on which dilute region the samples were taken from.

7.6.1.1 Heptane (1) + Methanol (2)

Similar to the VLE test system, the LLE test system was also used to ascertain whether the techniques, equations and programmes that were developed to analyse experimental binary LLE data were functioning as desired. The model parameters are presented in Table 7-16 and the temperature dependence of the parameters are presented in Figures 7-16 to 7-18. A second degree polynomial was found to fit all model parameters with a least squares deviation (R^2) sufficiently well, whereas the Van Laar model displayed the worst fit.

Table 7-16: Model parameters from mutual solubility data for the heptane (1) + methanol (2) system at 1 atm.

Temperature (K)	Models					
	Margules		Van Laar		NRTL with a = 0.2	
	A_{12}	A_{21}	A_{12}	A_{21}	$g_{12}\text{-}g_{22}$ (J/mol)	$g_{21}\text{-}g_{11}$ (J/mol)
298.19	2.7767	2.3889	10.9067	9.4063	1014.1264	10717.551
303.15	2.7008	2.1903	11.2763	9.2117	410.6530	11196.303
308.11	2.6350	2.0535	11.5492	9.1187	6.9276	11392.314
312.87	2.5292	1.9363	11.3844	8.8693	-596.0595	11679.117
318.14	2.4624	1.7187	13.8704	10.1001	-1418.625	12476.725
323.00	2.3669	1.4805	28.6029	19.5550	-2251.921	13028.849
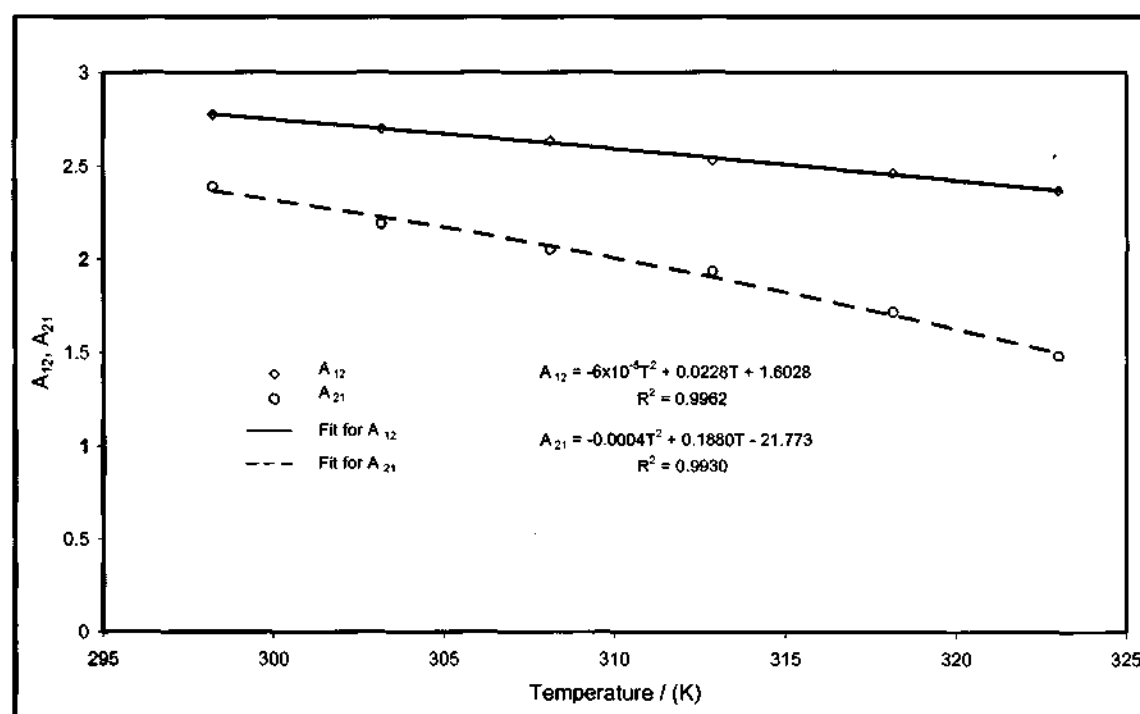
Figure 7-16: Temperature dependence of the three-suffix Margules model parameters for the heptane (1) + methanol (2) system at 1 atm.

150

Figure 7-17: Temperature dependence of the Van Laar model parameters for the heptane (1) + methanol (2) system at 1 atm.
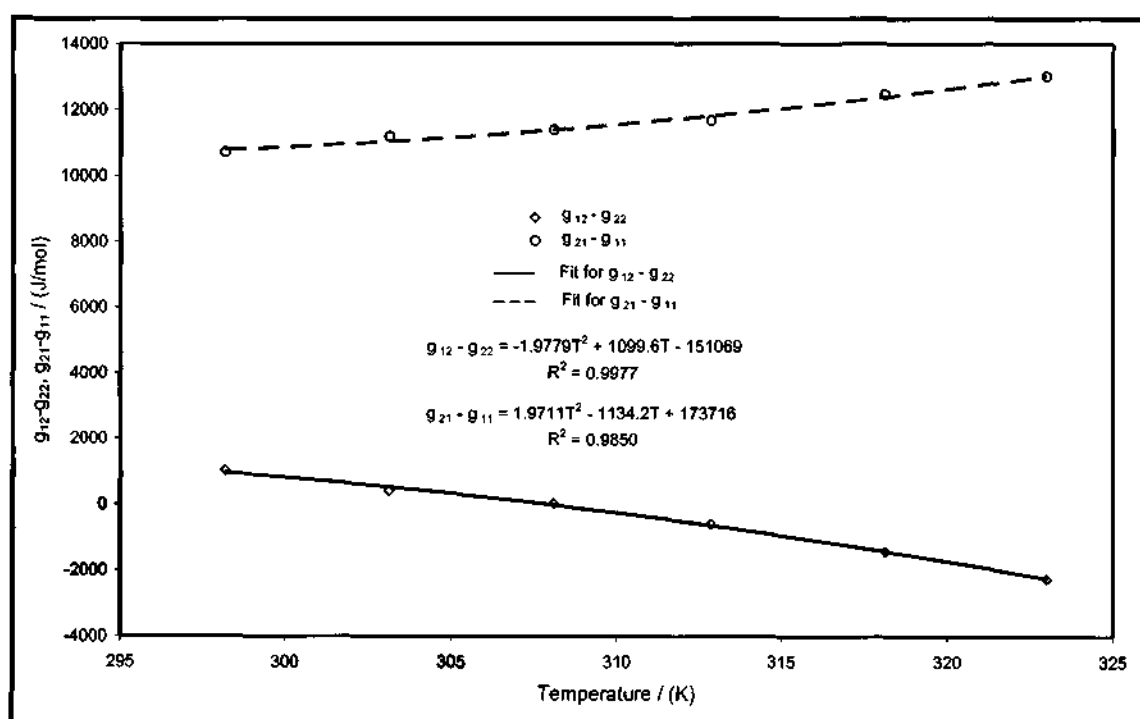
Figure 7-18: Temperature dependence of the NRTL model parameters with a = 0.2 for the heptane (1) + methanol (2) system at 1 atm.

151

7.6.1.2 1-Dodecene (1) + Acetonitrile (2)

For this system, it was found that the parameters of the Van Laar model failed to provide a temperature dependency. The Van Laar model was based on the Van der Waals equation of state. According to Walas (1985), the Van Laar model is regarded as purely empirical as the fit of activity coefficient data with the Van der Waals parameters is poor. Therefore, the Van Laar model may not always be able to correlate experimental data well, depending on the components of the system. On the other hand, the Margules and NRTL models were able to correlate the experimental data well for this system, where a second degree polynomial was found to fit both model parameters with a least squared deviation (R^2) sufficiently well. The model parameters are presented in Table 7-17 and the temperature dependence of the parameters are presented in Figures 7-19 and 7-20.

Table 7-17: Model parameters from mutual solubility data for the 1-dodecene (1) + acetonitrile (2) system at 1 atm.

| Temperature (K) | Models | | | |
| | Margules | | NRTL with a = 0.2 | |
	A_{12}	A_{21}	g_{12}-g_{22} (J/mol)	g_{21}-g_{11} (J/mol)
323.31	3.2518	1.6957	8225.2195	967.6729
328.17	3.0902	1.5592	8103.3664	954.9422
333.24	2.9934	1.4358	8062.2034	858.8602
338.20	2.8374	1.4112	7676.1726	646.7105
343.16	2.7088	1.3909	7589.1210	627.6717
348.23	2.5845	1.2730	7498.4733	434.2745
353.19	2.3242	1.2843	6841.8857	381.7361
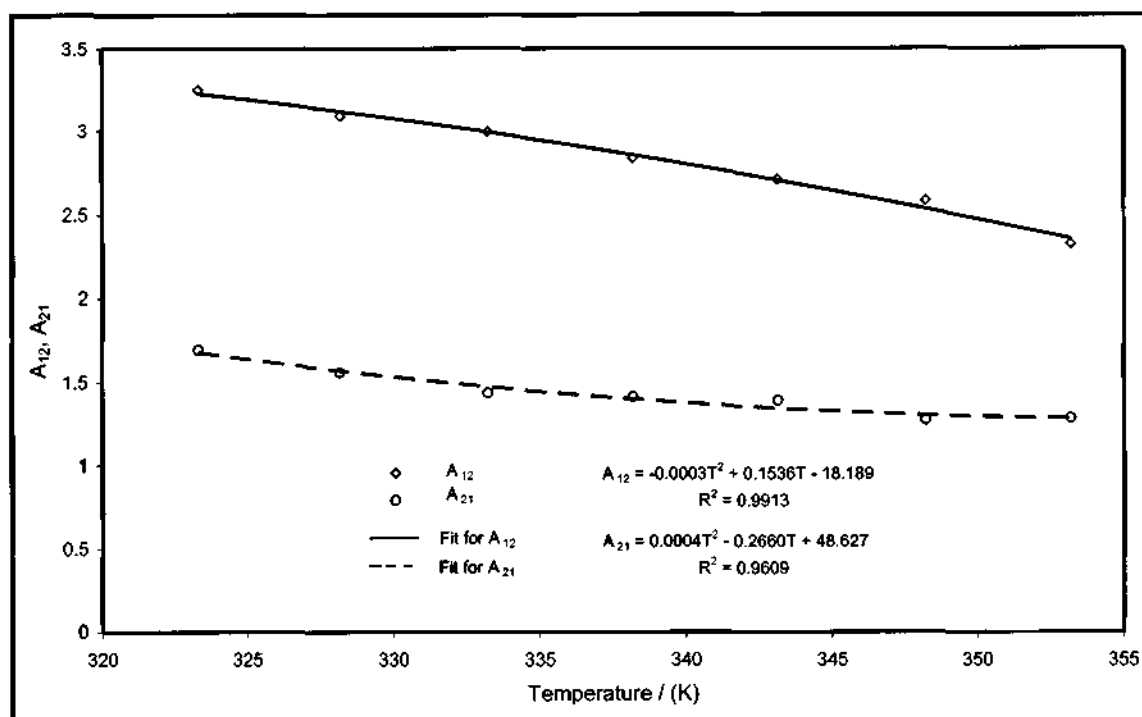
Figure 7-19: Temperature dependence of the Margules model parameters for the 1-dodecene (1) + acetonitrile (2) system at 1 atm.
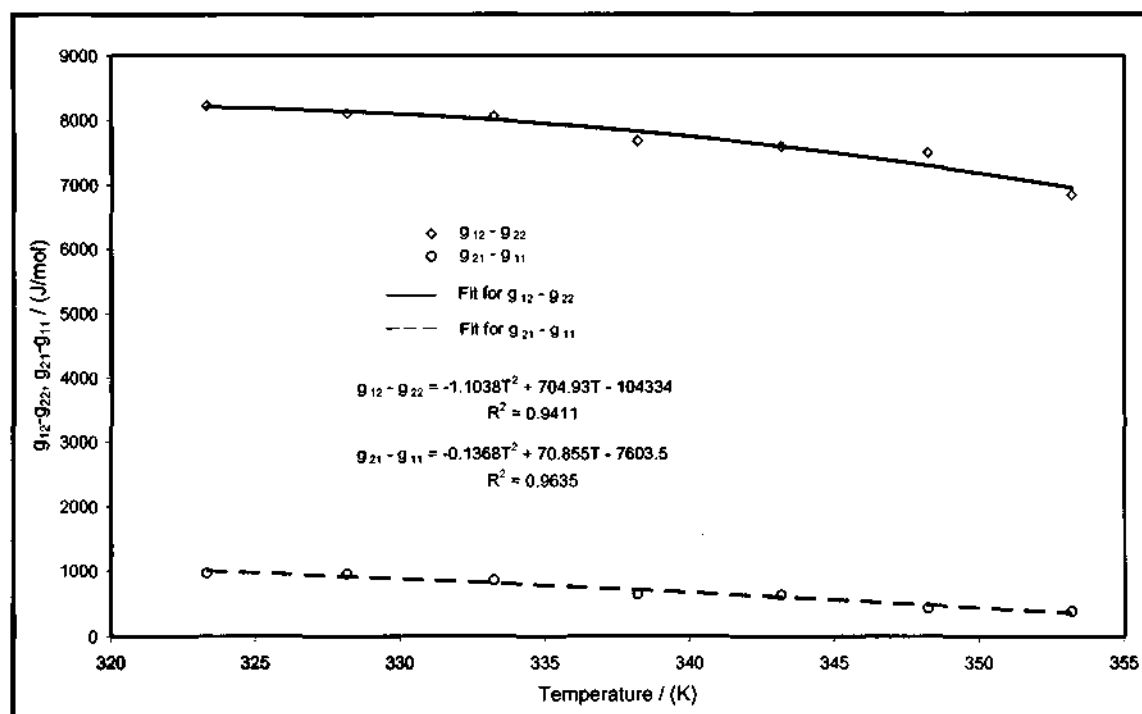
Figure 7-20: Temperature dependence of the NRTL model parameters with a = 0.2 for the 1-dodecene (1) + acetonitrile (2) system at 1 atm.

7.6.1.3 1-Nonanol (1) + Water (2)

All three model parameters were once again found to fit a second degree polynomial sufficiently well. The Van Laar model was the model that displayed the worst fit. For the NRTL model, no values of the parameters could be found for the solubility data at 323.31 K as the correlation chart did not cater for mole fractions less than 0.0050 (Renon and Prausnitz, 1968). However, the other four data points were sufficient to obtain the temperature dependence of the parameters. All the model parameters are presented in Table 7-18 and the temperature dependence of the parameters are presented in Figures 7-21 to 7-23.

Table 7-18: Model parameters from mutual solubility data for the 1-nonanol (1) + water (2) system at 1 atm.

Temperature (K)	Models					
	Margules		Van Laar		NRTL with a = 0.2	
	A_{12}	A_{21}	A_{12}	A_{21}	$g_{12}\text{-}g_{22}$ (J/mol)	$g_{21}\text{-}g_{11}$ (J/mol)
323.31	5.2255	-0.4435	121.0821	36.1818	-	-
333.24	4.6476	-0.2003	95.4011	31.4199	14655.799	-710.4217
343.16	4.5137	-0.3091	95.3556	31.4236	14793.825	-822.1510
353.19	4.3415	-0.4336	95.1670	31.4672	14929.961	-1025.220
362.21	4.2173	-0.5600	96.6240	31.8784	15119.930	-1172.578
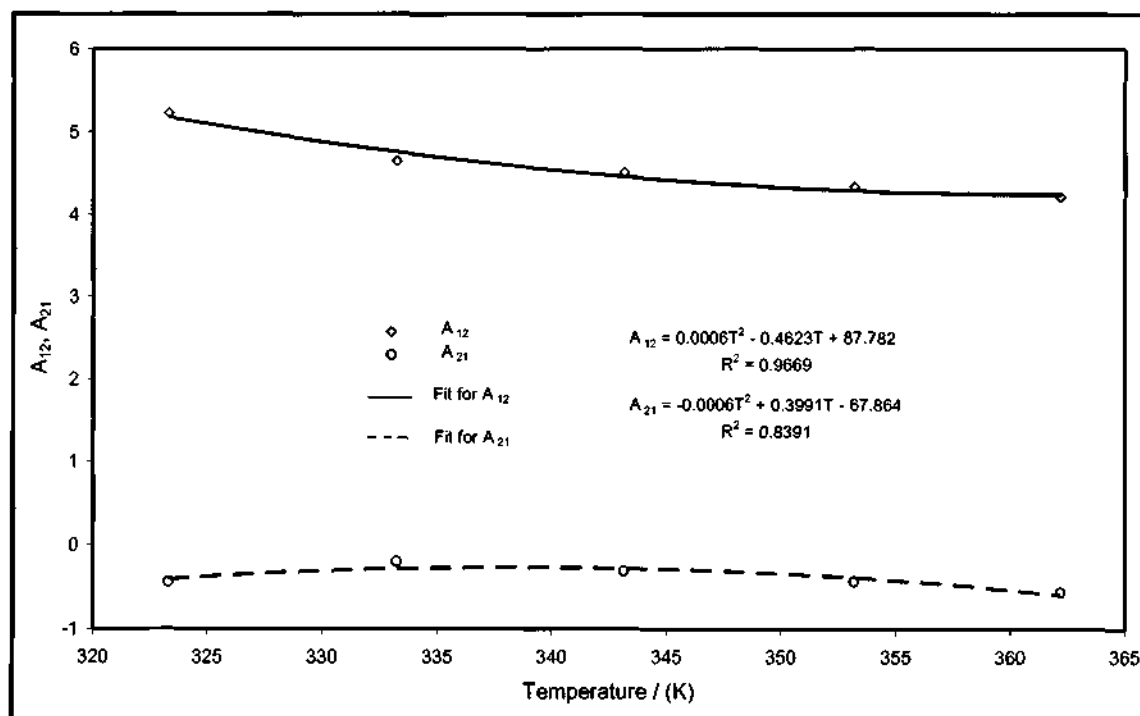
Figure 7-21: Temperature dependence of the Margules model parameters for the 1-nonanol (1) + water (2) system at 1 atm.
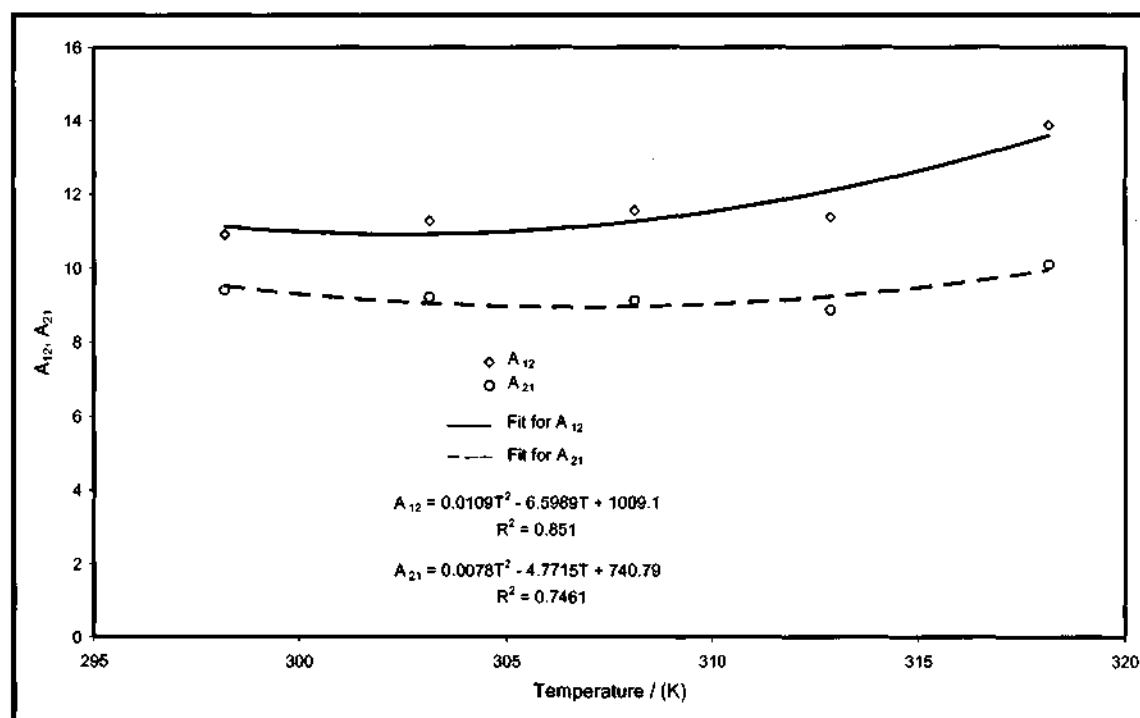
154
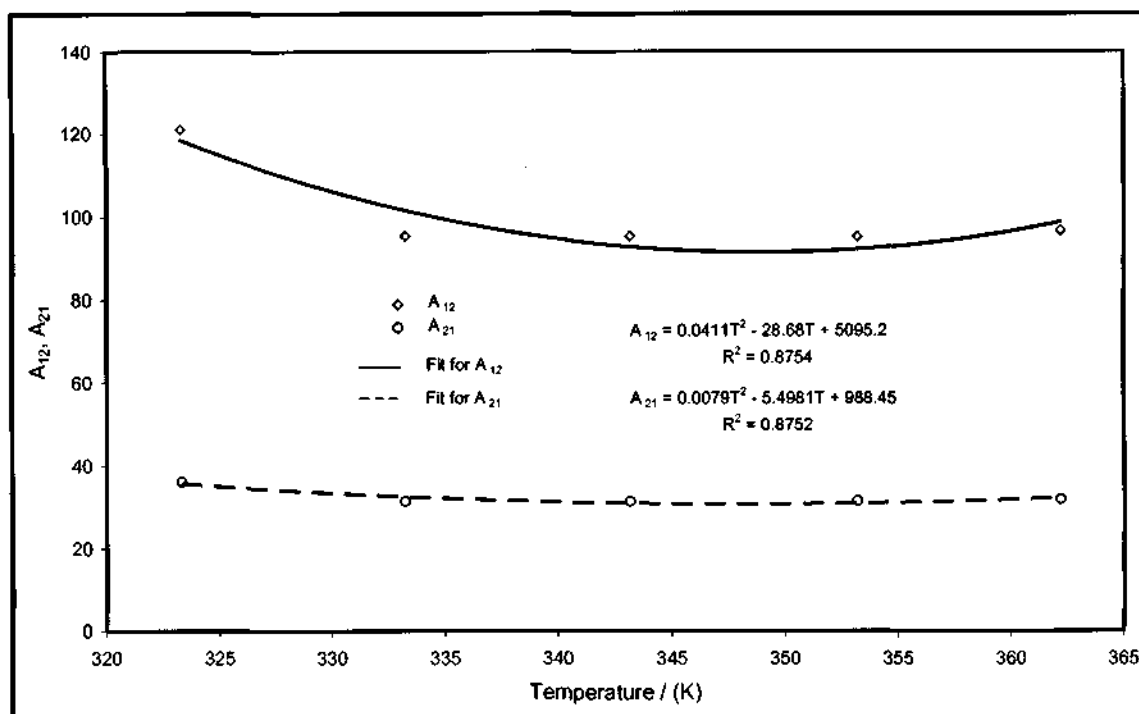
Figure 7-22: Temperature dependence of the Van Laar model parameters for the 1-dodecene (1) + water (2) system at 1 atm.
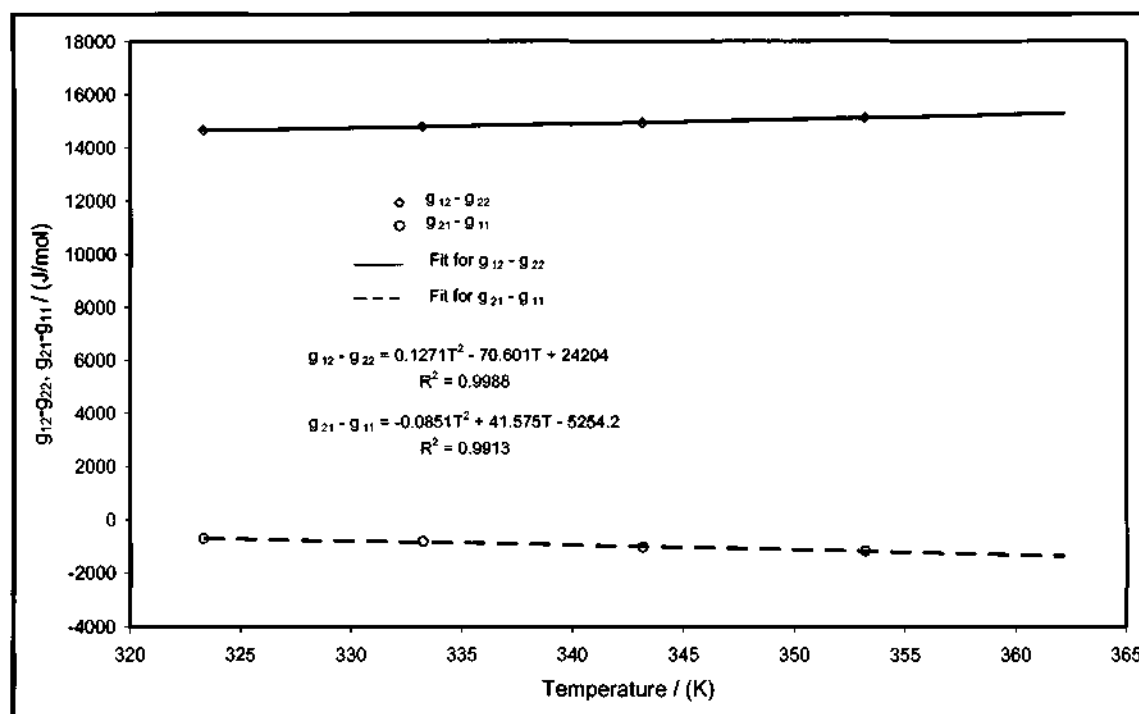
Figure 7-23: Temperature dependence of the NRTL model parameters with a = 0.2 for the 1-nonanol (1) + water (2) system at 1 atm.

155

7.6.2 Ternary Systems

The ternary systems measured in this work were subjected to a two part correlation: the tie-line correlation and the binodal curve correlation, as discussed in Sections 3.4.4.2 and 3.4.4.3 respectively. It should be noted that the tie-line correlation parameters are independent of the binodal curve correlation parameters. For this work, the tie-lines were correlated with the NRTL and the modified UNIQUAC liquid phase activity coefficient models. The non-randomness parameter (a_{ij}) in the NRTL model was made equal for all three binary pairs and fixed at either 0.20, 0.25, 0.30, 0.35 or 0.40. The binodal curves were correlated with the Hlavatý equation, ß-density function equation and the log γ equation.

The tie-lines were correlated following the method suggested by Walas (1985) with the least square objective function optimisation minimisation technique suggested by Novak et al. (1987). The regression programme was written in Matlab, which offered a variety of built-in optimisation functions. For this work the *fminsearch* function was chosen, which finds the minimum of an unconstrained multi-variable function. The algorithm is based on the Nelder-Mead simplex method (Lagarias et al., 1998). The best model was determined by the lowest value for the root mean square deviation (RMSD) as given by Equation (3-149). The binodal curves were correlated by minimising the sum of the squared difference between the experimental and calculated mole fractions. The regression technique was carried out using the Microsoft Excel programme which used the Newton-Raphson method. The best correlation was based on the lowest value for the standard deviation (s) of Sen and Srivastava (1990) as given by Equation (3-155).

The GC was calibrated for the dilute regions of two pairs of components. All the GC calibrations graphs presented in Figures 6-24 to 6-27, 6-29 to 6-32, 6-34, 6-35, 6-37, 6-38, 6-40 and 6-41 displayed a linear response. The inverse of the response factor ratio for one dilute region was almost equal to the slope or response factor ratio of the other dilute region for a particular pair of components. Nevertheless, an average response factor was not calculated. Instead, care was taken to ensure the correct calibration graph was employed, depending on which dilute region the samples were taken from.

7.6.2.1 Heptane (1) + Toluene (2) + Methanol (3)

Once more this test system also served to ascertain whether the techniques, equations and programmes that were developed to analyse experimental ternary LLE data were functioning as desired. The analysis revealed that the NRTL model with a = 0.35 provided a better correlation for the tie-lines compared to the modified UNIQUAC model. It was also found that the log γ equation provided the best fit for the binodal curve. The parameters for the NRTL model with a = 0.35 and the modified UNIQUAC model are presented in Table 7-19. The NRTL model parameters for the other a values are presented in Appendix E. The parameters for the binodal curve correlations are presented in Table 7-20. The best tie-line model and best binodal curve correlation are presented together with the experimental values in Figure 7-24.

Table 7-19: Model parameters for the tie-lines of the heptane (1) + toluene (2) + methanol (3) system at 298.15 K and 1 atm.

Models			
NRTL with a = 0.35		**Modified UNIQUAC**	
$g_{12} - g_{22}$ / (J/mol)	1298.5853	$u_{12} - u_{22}$ / (J/mol)	-4589.3425
$g_{21} - g_{11}$ / (J/mol)	-2302.5261	$u_{21} - u_{11}$ / (J/mol)	1557.1352
$g_{13} - g_{33}$ / (J/mol)	4461.3955	$u_{13} - u_{33}$ / (J/mol)	3660.9865
$g_{31} - g_{11}$ / (J/mol)	4842.9263	$u_{31} - u_{11}$ / (J/mol)	2365.3833
$g_{23} - g_{33}$ / (J/mol)	1534.8951	$u_{23} - u_{33}$ / (J/mol)	-1279.0238
$g_{32} - g_{22}$ / (J/mol)	1298.5853	$u_{32} - u_{22}$ / (J/mol)	-3388.2526
RMSD	0.0051	**RMSD**	0.0105

Table 7-20: Correlation parameters for the binodal curve of the heptane (1) + toluene (2) + methanol (3) system at 298.15 K and 1 atm.

Correlations					
Hlavatý		**ß Function**		**Log γ**	
A_1	0.0334	B_1	0.5196	C_1	0.4891
A_2	-0.0777	B_2	0.9021	C_2	0.8793
A_3	0.4838	B_3	1.0377	C_3	1.3711
s	0.0043	s	0.0044	s	0.0042
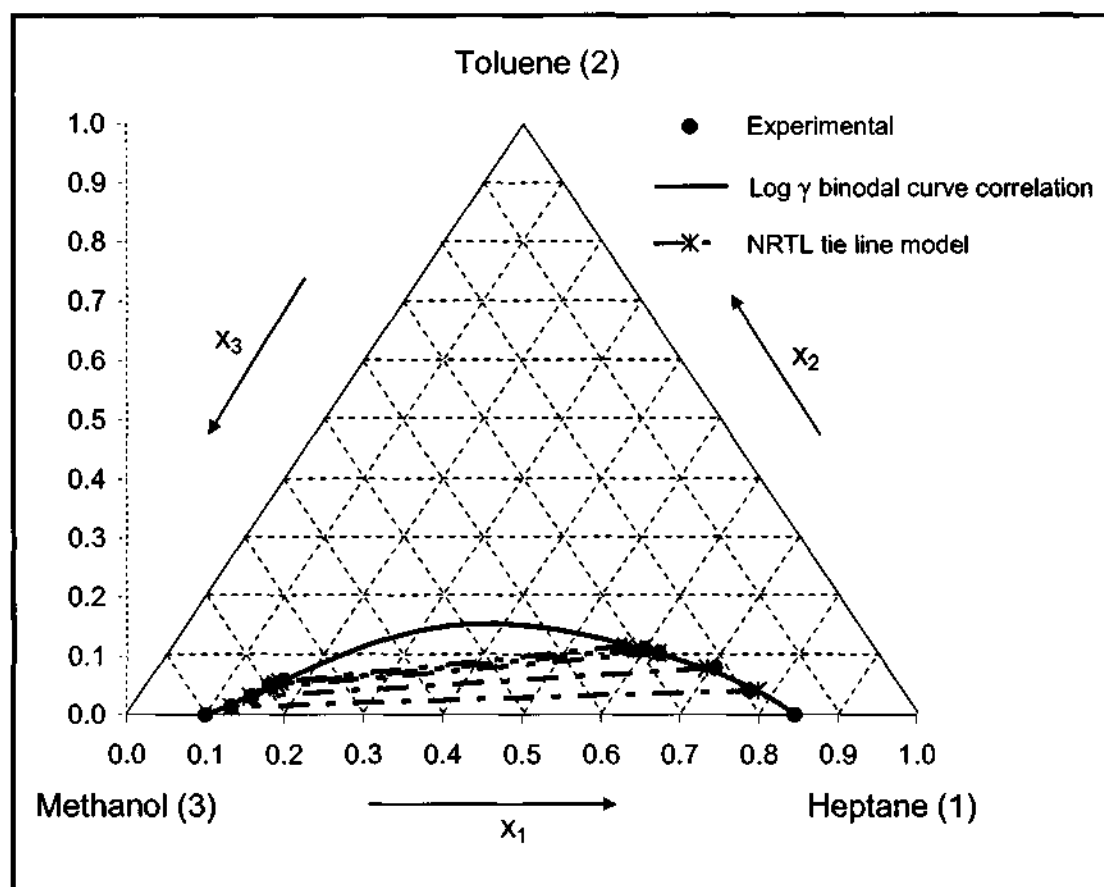
Figure 7-24: Fit of the NRTL model with a = 0.35 for the tie-lines and the log γ equation for the binodal curve for the ternary plot of the heptane (1) + toluene (2) + methanol (3) system at 298.15 K and 1 atm.

7.6.2.2 Water (1) + Acetonitrile (2) + Heptanoic Acid (3)

The experimental data revealed that acetonitrile is completely soluble in water or heptanoic acid at 323.15 K and thus this system can be classified as a type I system (Treybal, 1963). Figure 6-33 shows that the shape of the binodal curve for this system curves sharply towards the water rich region for small amounts of acetonitrile but decreases in sharpness for larger amounts of acetonitrile. This phenomenon was also observed by García et al. (1988), who investigated the effect of using heptanoic acid to separate water from ethanol.

To use water and acetonitrile as a feed mixture, the minimum composition of this mixture is found by drawing a tangent to the binodal curve from the apex that represents heptanoic acid on a ternary plot. Thus, to ensure a two phase region for this system, a minimum composition of x_1 = 0.63 is required as shown by point A in Figure 7-25.

The tie-line regression showed that the modified UNIQUAC model provided the best fit to the experimental data. It was also found that the ß function provided the best fit for the binodal curve. The parameters for the NRTL model for the a value that produced the lowest RMSD and the modified UNIQUAC model are presented in Table 7-21. The NRTL model parameters for the other a values are presented in Appendix E. The parameters for the binodal curve correlations are presented in Table 7-22. The best tie-line model and best binodal curve correlation are presented together with the experimental values in Figure 7-26.
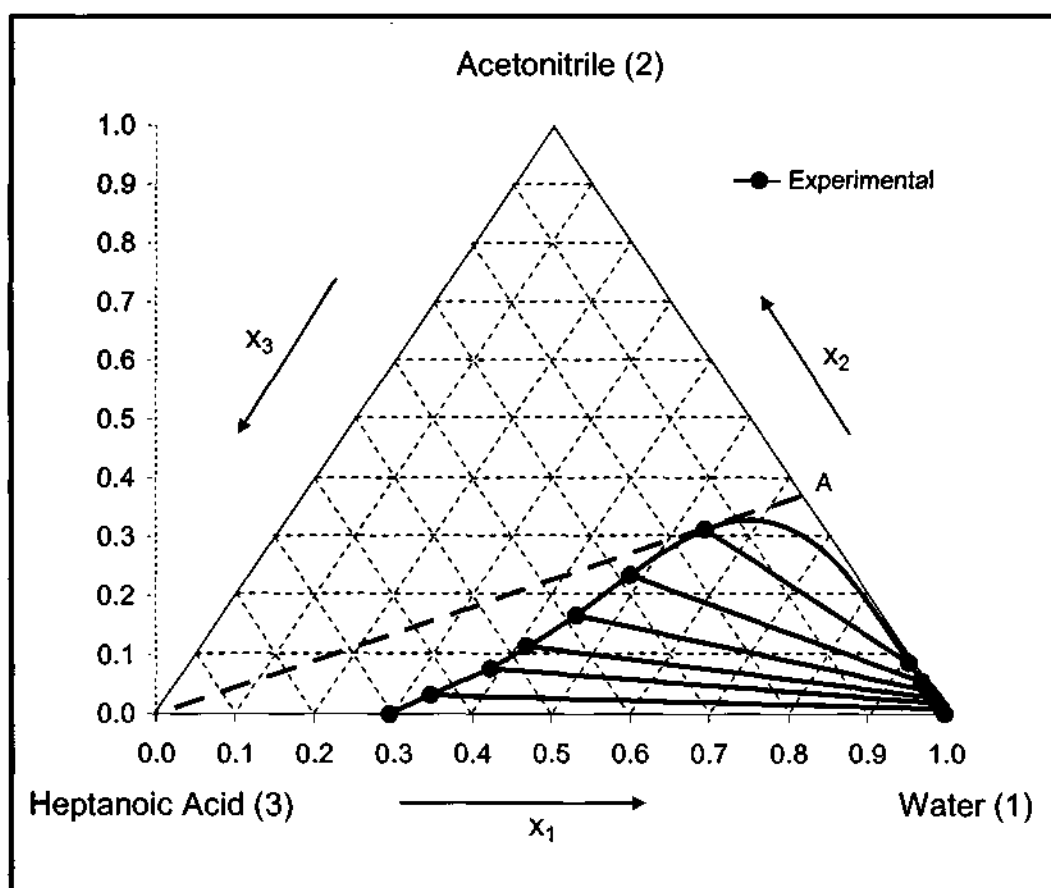
Figure 7-25: Ternary plot for the water (1) + acetonitrile (2) + heptanoic acid (3) system at 323.15 K and 1 atm showing the effect of solubility on the range of water and acetonitrile as feed mixture.

Table 7-21: Model parameters for the tie-lines of the water (1) + acetonitrile (2) + heptanoic acid (3) system at 323.15 K and 1 atm.

Models			
NRTL with a = 0.25		**Modified UNIQUAC**	
$g_{12} - g_{22}$ / (J/mol)	7870.0117	$u_{12} - u_{22}$ / (J/mol)	333.7437
$g_{21} - g_{11}$ / (J/mol)	-224.3438	$u_{21} - u_{11}$ / (J/mol)	2105.3709
$g_{13} - g_{33}$ / (J/mol)	10192.7962	$u_{13} - u_{33}$ / (J/mol)	161.6036
$g_{31} - g_{11}$ / (J/mol)	1513.5018	$u_{31} - u_{11}$ / (J/mol)	5478.0077
$g_{23} - g_{33}$ / (J/mol)	-879.2804	$u_{23} - u_{33}$ / (J/mol)	-2135.1499
$g_{32} - g_{22}$ / (J/mol)	2079.0865	$u_{32} - u_{22}$ / (J/mol)	6710.4027
RMSD	0.0134	**RMSD**	0.0030

Table 7-22: Correlation parameters for the binodal curve of the water (1) + acetonitrile (2) + heptanoic acid (3) system at 323.15 K and 1 atm.

Correlations					
Hlavatý		**ß Function**		**Log γ**	
A_1	0.7212	B_1	2.3492	C_1	2.2095
A_2	-0.1128	B_2	1.1435	C_2	1.1244
A_3	1.9061	B_3	1.9348	C_3	2.3945
s	0.0175	s	0.0085	s	0.0091
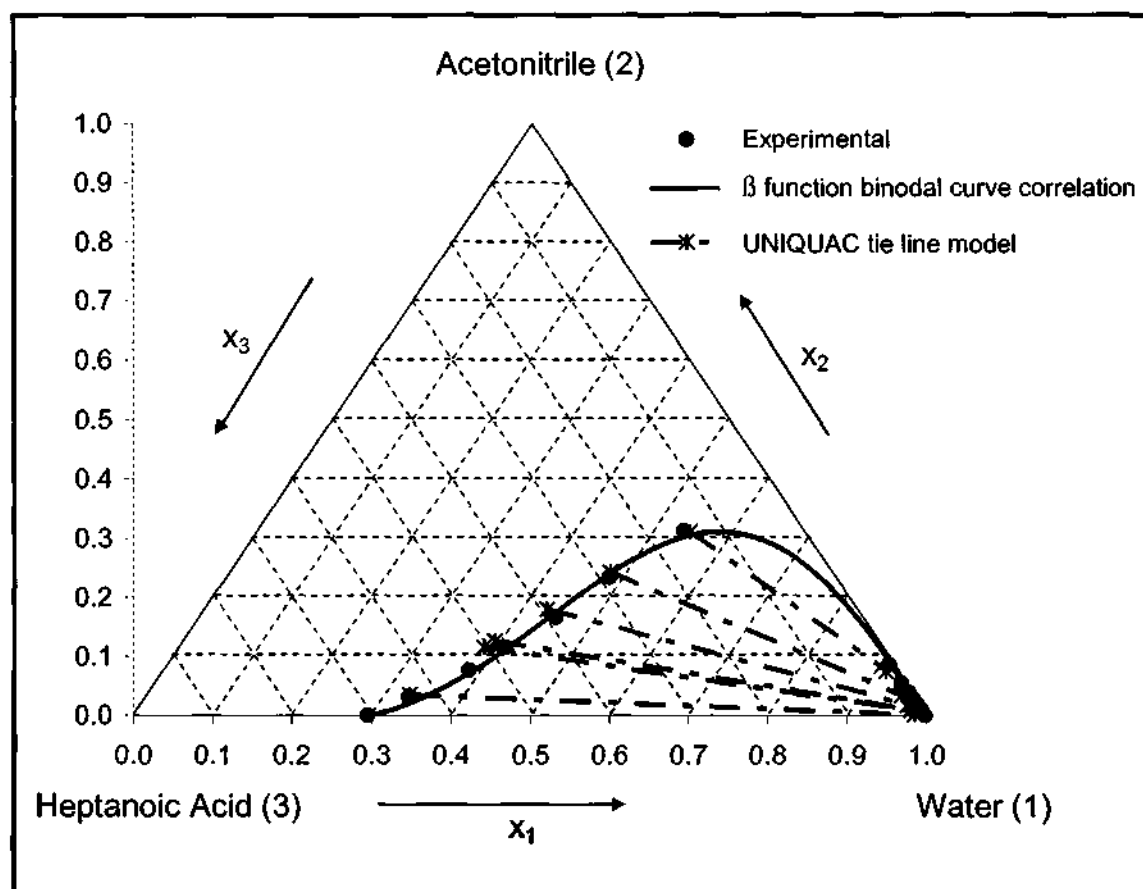
Figure 7-26: Fit of the UNIQUAC model for the tie-lines and the ß function for the binodal curve for the ternary plot of the water (1) + acetonitrile (2) + heptanoic acid (3) system at 323.15 K and 1 atm.

7.6.2.3 Water (1) + Acetonitrile (2) + 1-Nonanol (3)

The experimental data for this system exhibits a smooth binodal curve, typical of a type I system (Treybal, 1963). To use water and acetonitrile as a feed mixture, a minimum composition of $x_1 = 0.45$ is required to ensure a two phase region for this system, as shown by point A in Figure 7-27. The tie-line regression showed that the modified UNIQUAC model provided the best fit to the experimental data. It was also found that the ß function provided the best fit for the binodal curve. The parameters for the NRTL model for the a value that produced the lowest RMSD and the modified UNIQUAC model are presented in Table 7-23. The NRTL model parameters for the other a values are presented in Appendix E. The parameters for the binodal curve correlations are presented in Table 7-24. The best tie-line model and best binodal curve correlation are presented together with the experimental values in Figure 7-28.

161
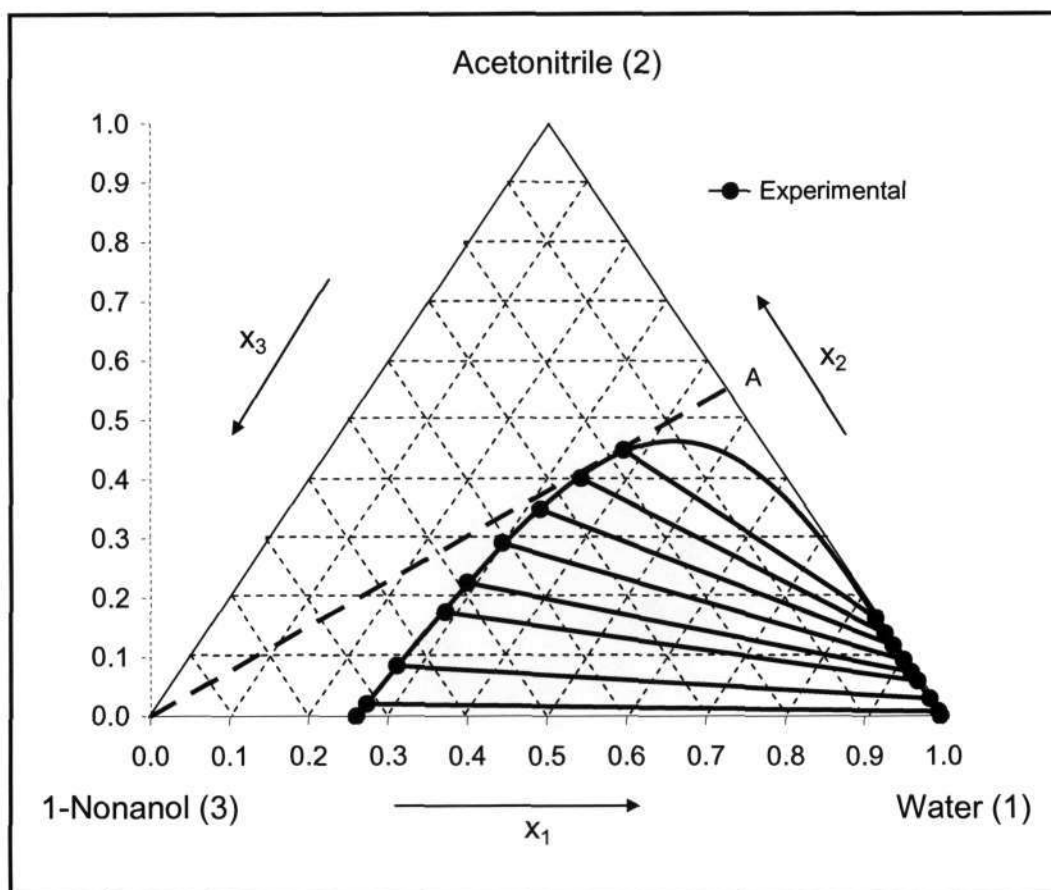
. Figure 7-27: Ternary plot for the water (1) + acetonitrile (2) + 1-nonanol (3) system at 323.15 K and 1 atm showing the effect of solubility on the range of water and acetonitrile as feed mixture.

Table 7-23: Model parameters for the tie-lines of the water (1) + acetonitrile (2) + 1-nonanol (3) system at 323.15 K and 1 atm.

Models			
NRTL with a = 0.25		**Modified UNIQUAC**	
$g_{12} - g_{22}$ / (J/mol)	2854.9913	$u_{12} - u_{22}$ / (J/mol)	-289.8089
$g_{21} - g_{11}$ / (J/mol)	5442.5669	$u_{21} - u_{11}$ / (J/mol)	3107.4440
$g_{13} - g_{33}$ / (J/mol)	16481.8933	$u_{13} - u_{33}$ / (J/mol)	939.4103
$g_{31} - g_{11}$ / (J/mol)	2091.1879	$u_{31} - u_{11}$ / (J/mol)	4283.6570
$g_{23} - g_{33}$ / (J/mol)	6615.1932	$u_{23} - u_{33}$ / (J/mol)	-950.7286
$g_{32} - g_{22}$ / (J/mol)	406.4684	$u_{32} - u_{22}$ / (J/mol)	3667.6123
RMSD	0.0065	**RMSD**	0.0023

Table 7-24: Correlation parameters for the binodal curve of the water (1) + acetonitrile (2) + 1-nonanol (3) system at 323.15 K and 1 atm.

Correlations					
Hlavatý		**ß Function**		**Log γ**	
A_1	0.4875	B_1	2.3783	C_1	2.1411
A_2	0.2100	B_2	1.1394	C_2	1.1016
A_3	2.7271	B_3	1.2723	C_3	1.6885
s	0.0074	s	0.0055	s	0.0066
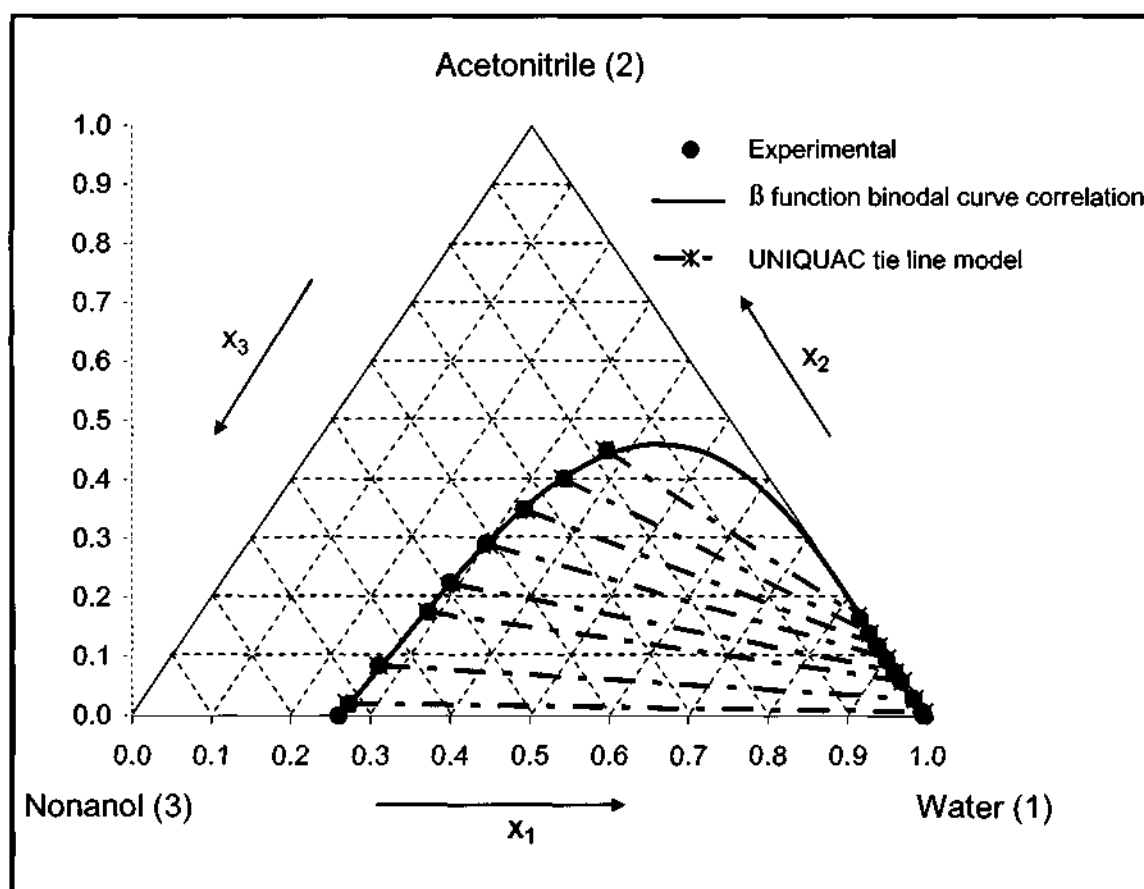
Figure 7-28: Fit of the UNIQUAC model for the tie-lines and the ß function for the binodal curve for the ternary plot of the water (1) + acetonitrile (2) + 1-nonanol (3) system at 323.15 K and 1 atm.

7.6.2.4 Water (1) + Acetonitrile (2) + Dodecane (3)

The experimental data revealed that dodecane is only partially soluble in water or acetonitrile at 323.15 K and thus this system can be classified as a type II system (Treybal, 1963). The experimental triangle plot for this system, as shown in Figure 6-39, reveals a very large immiscibility region that almost covers the entire triangle plot. Thus, dodecane is almost insoluble in water or acetonitrile. The tie-line regression showed that the NRTL model with a = 0.20 provided the best fit to the experimental data. It was also found that none of the binodal curve correlations could successfully fit the experimental data; however the log γ equation displayed the lowest standard deviation. This could be due to the inability of the binodal curve correlations to fit type II systems with a very large immiscibility region. The parameters for the NRTL model with a = 0.20 and the modified UNIQUAC model are presented in Table 7-25. The NRTL model parameters for the other a values are presented in Appendix E. The parameters for the binodal curve correlations are presented in Table 7-26. The best tie-line model is presented together with the experimental values in Figure 7-29.

Table 7-25: Model parameters for the tie-lines of the water (1) + acetonitrile (2) + dodecane (3) system at 323.15 K and 1 atm.

Models			
NRTL with a = 0.20		**Modified UNIQUAC**	
$g_{12} - g_{22}$ / (J/mol)	5243.6429	$u_{12} - u_{22}$ / (J/mol)	2471.5518
$g_{21} - g_{11}$ / (J/mol)	1129.5279	$u_{21} - u_{11}$ / (J/mol)	2952.5781
$g_{13} - g_{33}$ / (J/mol)	21172.4976	$u_{13} - u_{33}$ / (J/mol)	3558.7187
$g_{31} - g_{11}$ / (J/mol)	11348.2101	$u_{31} - u_{11}$ / (J/mol)	8883.6348
$g_{23} - g_{33}$ / (J/mol)	11153.5320	$u_{23} - u_{33}$ / (J/mol)	2661.6296
$g_{32} - g_{22}$ / (J/mol)	2225.2495	$u_{32} - u_{22}$ / (J/mol)	2471.5518
RMSD	0.0019	RMSD	0.0142

Table 7-26: Correlation parameters for the binodal curve of the water (1) + acetonitrile (2) + dodecane (3) system at 323.15 K and 1 atm.

Correlations					
Hlavatý		**ß Function**		**Log γ**	
A_1	0.9216	B_1	7.0350	C_1	5.8100
A_2	1.5718	B_2	1.5959	C_2	1.5079
A_3	6.9647	B_3	1.3493	C_3	1.8622
s	0.0386	s	0.0276	s	0.0247
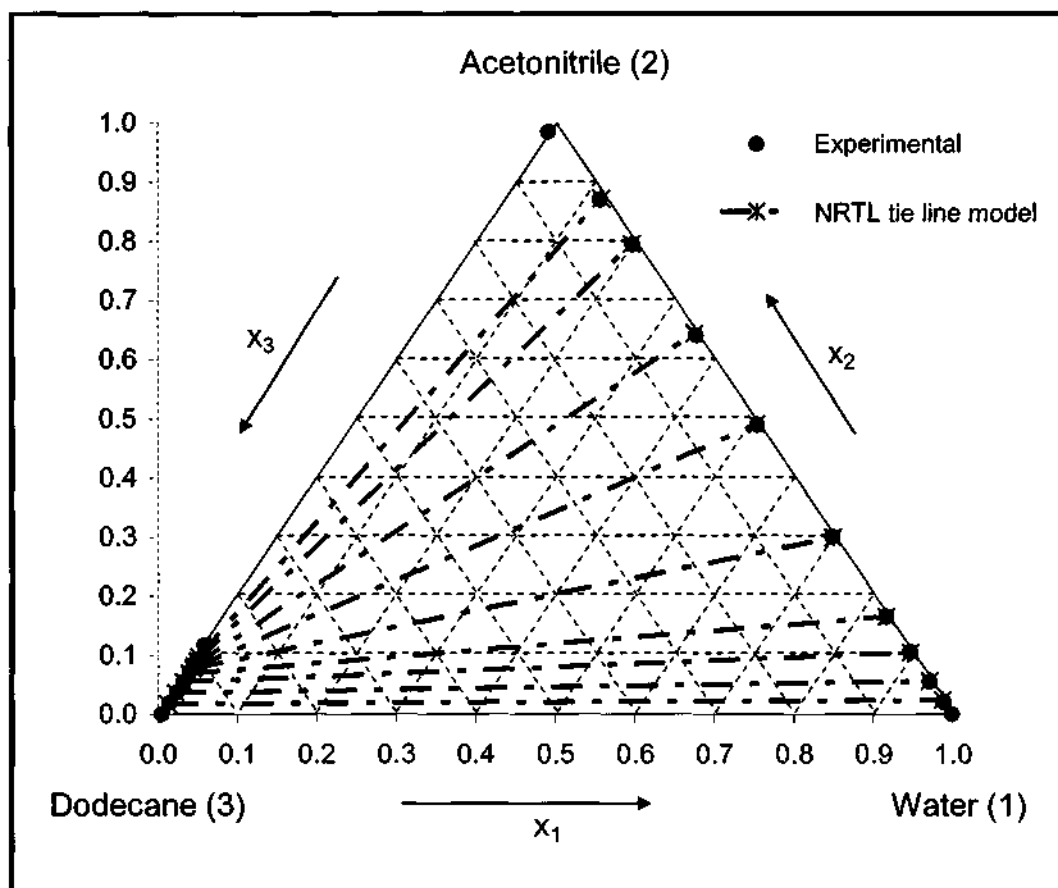
Figure 7-29: Fit of the NRTL model with a = 0.20 for the tie-lines for the ternary plot of the water (1) + acetonitrile (2) + dodecane (3) system at 323.15 K and 1 atm.

7.6.2.5 Water (1) + Acetonitrile (2) + 1-Dodecene (3)

Similar to the water (1) + acetonitrile (2) + dodecane (3) system at 323.15 K and 1 atm, this system is also classified as a type II system (Treybal, 1963). Furthermore, the experimental triangle plot for this system, as shown in Figure 6-42, is similar to the water (1) + acetonitrile (2) + dodecane (3) system at 323.15 K and 1 atm. Thus, the large immiscibility region implies that 1-dodecene is also almost insoluble in water or acetonitrile. However in this case, acetonitrile is more soluble in 1-dodecene than in dodecane. The tie-line regression showed that the NRTL model with a = 0.20 provided the best fit to the experimental data. It was also found that none of the binodal curve correlations could successfully fit the experimental data; however the log γ equation displayed the lowest standard deviation. This could be due to the inability of the binodal curve correlations to fit type II systems with a very large immiscibility region. The parameters for the NRTL model with a = 0.20 and the modified UNIQUAC model are presented in Table 7-27. The NRTL model parameters for the other a values are presented in Appendix E. The parameters for the binodal curve correlations are presented in Table 7-28. The best tie-line model is presented together with the experimental values in Figure 7-30.

Table 7-27: Model parameters for the tie-lines of the water (1) + acetonitrile (2) +
1-dodecene (3) system at 323.15 K and 1 atm.

Models			
NRTL with a = 0.20		Modified UNIQUAC	
$g_{12} - g_{22}$ / (J/mol)	6489.7682	$u_{12} - u_{22}$ / (J/mol)	1946.0007
$g_{21} - g_{11}$ / (J/mol)	7.6365	$u_{21} - u_{11}$ / (J/mol)	423.4470
$g_{13} - g_{33}$ / (J/mol)	10839.8280	$u_{13} - u_{33}$ / (J/mol)	789.5244
$g_{31} - g_{11}$ / (J/mol)	10590.7689	$u_{31} - u_{11}$ / (J/mol)	10094.9743
$g_{23} - g_{33}$ / (J/mol)	7758.8029	$u_{23} - u_{33}$ / (J/mol)	1397.0364
$g_{32} - g_{22}$ / (J/mol)	1625.3905	$u_{32} - u_{22}$ / (J/mol)	3876.6951
RMSD	0.0040	RMSD	0.01595

Table 7-28: Correlation parameters for the binodal curve of the water (1) + acetonitrile (2)
+ 1-dodecene (3) system at 323.15 K and 1 atm.

Correlations					
Hlavatý		ß Function		Log γ	
A_1	0.9216	B_1	7.0350	C_1	5.8100
A_2	1.5718	B_2	1.5959	C_2	1.5079
A_3	6.9647	B_3	1.3493	C_3	1.8622
s	0.0386	s	0.0276	s	0.0247

Figure 7-30: Fit of the NRTL model with a = 0.20 for the tie-lines for the ternary plot of the water (1) + acetonitrile (2) + 1-dodecene (3) system at 323.15 K and 1 atm.

7.7 VLLE Systems

7.7.1 Acetonitrile (1) + 1-Dodecene (2)

This VLLE system was investigated at an isotherm of 343.15 K. Mutual solubility data for this system revealed that both homogeneous regions were small but feasible to carry out VLE measurements. However during trial measurements, it was observed that the equilibrium temperature did not remain constant regardless of how long the system was left to attain equilibrium. This was mainly due to an extremely large difference in the vapour pressures (approximately 70 kPa) at 343.15 K. This gives rise to a very large relative volatility for this system. Furthermore, the large immiscibility region also contributes to the difficulty of attaining thermodynamic equilibrium. Hence, the temperature fluctuations can then be explained in terms of "flashing" of the more volatile component (acetonitrile). "Flashing" originates from the fact that a liquid at a pressure equal to or greater than its bubble point pressure "flashes" or partially evaporates when the pressure is reduced. When the vapour

condensate is returned to the boiling chamber, its temperature is higher than the boiling point of acetonitrile, therefore causing the acetonitrile to "flash". This problem of "flashing" was observed for both homogenous regions.

It was therefore decided to predict VLE for the homogenous regions of this system at 343.15 K from the LLE data already measured. This was achieved by employing the parameters of a liquid phase activity coefficient model in the combined method of the VLE regression technique. Therefore, the three-suffix Margules, Van Laar and NRTL models were used as these parameters were already found from the regression of mutual solubility data for this system. However, it was found that all three models failed to provide a reasonable prediction. The liquid phase activity coefficients model parameters can also be found from the infinite dilution activity coefficients (Walas, 1985). Unfortunately, it was not within the scope of this project to measure the infinite dilution activity coefficients. However in the recent years, the ebulliometer has received much attention on the measurement of infinite dilution activity coefficients and the reader is suggested to consult Raal et al. (2006).

To further explain the difficulty experienced with the measurement of VLE for the homogeneous regions of this system, a temperature-pressure sensitivity analysis was done. Raal et al. (2006) explains that the greatest difficulty in measurement is almost always in the very dilute regions. Raal et al. (2006) therefore developed an expression to estimate how precisely temperature or pressure needs to be controlled for VLE measurements in the very dilute regions. Their development extends from the triple product relationship:

$$\left(\frac{\partial T}{\partial P}\right)_{x_1} = -\frac{(\partial T / \partial x_1)_P}{(\partial P / \partial x_1)_T} \tag{7-5}$$

For dilute solutions and an ideal vapour phase, Raal et al. (2006) estimated the right hand side of Equation (7-5) for isothermal data as:

$$\left(\frac{\partial T}{\partial P}\right)_{x_1} = \frac{B^{**}\gamma_1\left\{x_1(d\ln\gamma_1/dx_1)+1\right\}}{\left\{1+B^{**}x_1\gamma_1\left(d\ln P_1^{sat}/dT\right)\right\}\left\{P_1^{sat}\gamma_1-P_2^{sat}\gamma_2\right\}\left\{1-x_2(d\ln\gamma_2/dx_1)\right\}} \tag{7-6}$$

where

$$B^{**} = \frac{(K_1-1)P_1^{sat}RT^2}{x_2\Delta H_{VAP,2}PK_1x_2} \tag{7-7}$$

$\Delta H_{VAP,2}$ is the enthalpy of vaporisation of component 2 and $K_i = y_i / x_i$. The enthalpy of vaporisation was estimated from the method suggested by Pitzer et al. (1955). The pressure is estimated as $P = \sum x_i \gamma_i P_i^{sat}$ and the vapour composition as $y_1 = x_1 \gamma_1 P_1^{sat} / P$. The liquid phase activity coefficients are found from a liquid phase activity coefficient model and the NRTL model (with the parameters from the regression of the mutual solubility data already measured) was employed for this work. The Antoine equation with the parameters regressed from experimental vapour pressure data was employed for the saturated pressures. In the limit as $x_1 \rightarrow 0$, Equation (7-6) reduces to:

$$\left(\frac{\partial T}{\partial P}\right)^{\infty} = \left(\frac{dP_2^{sat}}{dT}\right)^{-1} \tag{7-8}$$

The application of Equation (7-6) results in Figure 7-31. To interpret these results, consider a temperature-pressure sensitivity value from Figure 7-31, say 0.010 K/Pa. For isothermal operation, a variation of 0.05 K in the temperature caused by "flashing" for example, will produce a pressure response of 5 Pa at approximately $x_1 = 0.005$. However at a higher composition, say $x_1 = 0.015$, the temperature-pressure sensitivity becomes 0.0045 K/Pa. This means that for the same variation of 0.05 K in the temperature, the system will produce a pressure response of 11.1 Pa. Now according to Figure 7-31, as the composition increases the pressure response increases for a constant variation in the system temperature. This result is rather unexpected as one would expect the pressure response to decrease (for a constant variation in the temperature) with an increase in composition. Hence, such a system is very difficult to measure with a recirculating still. It is therefore recommended that such systems be investigated with a static apparatus.
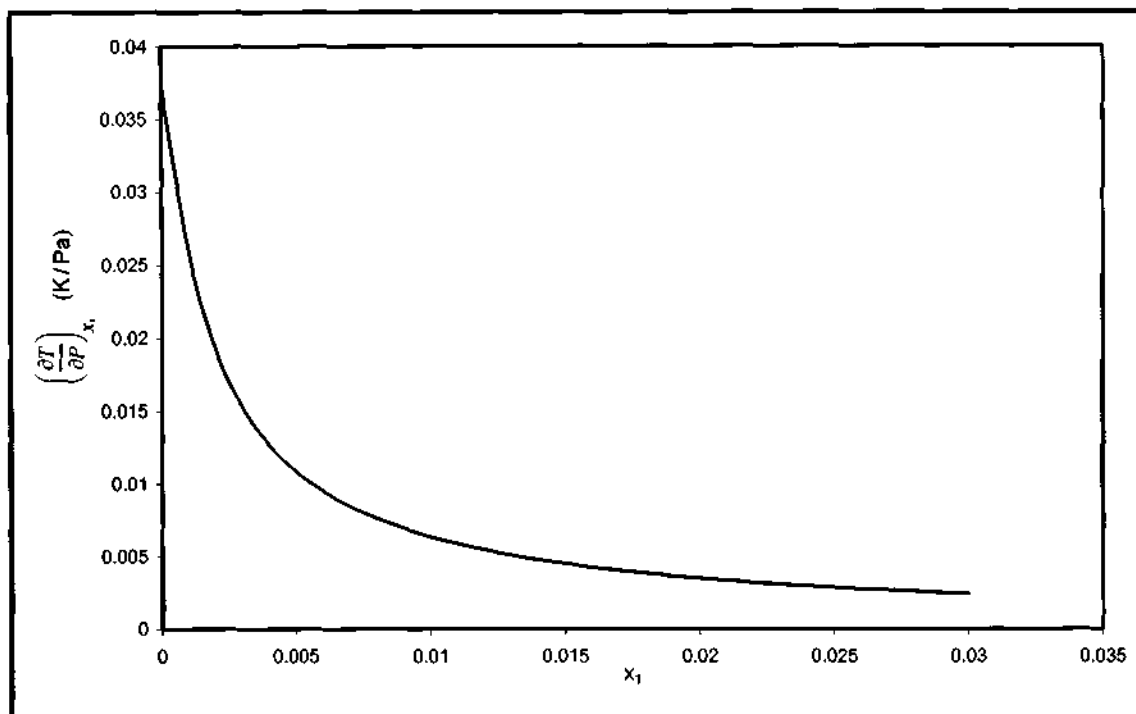
Figure 7-31: Temperature-pressure sensitivity for the acetonitrile (1) + 1-dodecene (2) system at 343.15 K calculated from Equation (7-6).

7.7.2 Water (1) + 1-Nonanol (2)

This VLLE system was investigated at an isotherm of 353.15 K. Mutual solubility data for this system revealed that only one homogeneous region was feasible to carry out VLE measurements. Similar to the acetonitrile (1) + 1-dodecene (2) system at 343.15 K, trial measurements for this homogeneous region showed that the equilibrium temperature did not remain constant regardless of how long the system was left to attain equilibrium. This was also mainly due to an extremely large difference in the vapour pressures (approximately 50 kPa) at 353.15 K. Again, this can be attributed to "flashing" of the more volatile component (water).

The prediction of VLE from LLE data was also attempted for this system, where the liquid phase activity coefficient model parameters were regressed from mutual solubility data. Once more, it was found that the three-suffix Margules, Van Laar and the NRTL models failed to provide a reasonable prediction.
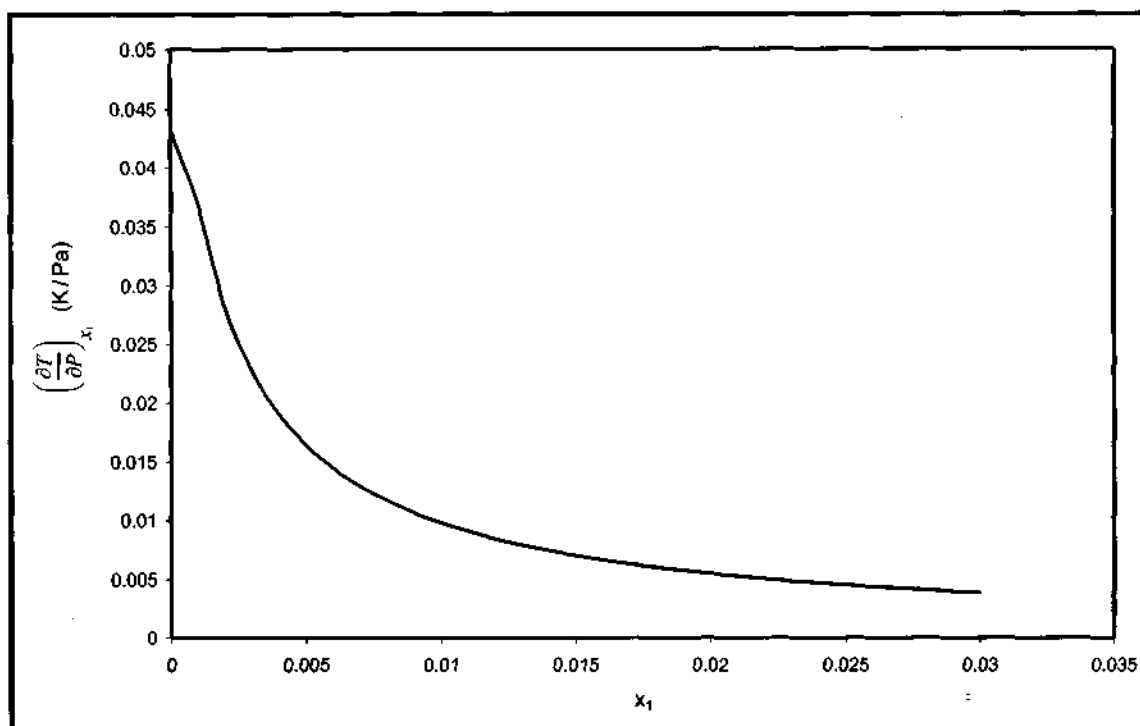
Figure 7-32: Temperature-pressure sensitivity for the water (1) + 1-nonanol (2) system at 353.15 K calculated from Equation (7-6).

In an effort to explain the difficulty experienced with the measurement of VLE for the homogeneous region of this system, a temperature-pressure sensitivity analysis was done. The result for the temperature-pressure sensitivity analysis is presented in Figure 7-32. The same conclusion drawn for the acetonitrile (1) + 1-dodecene (2) at 343.15 K can also be drawn for this system. As the composition of the more volatile component increases, the pressure response increases for a constant variation in the system temperature. However, the pressure response for this system increases less rapidly when compared to the acetonitrile (1) + 1-dodecene (2) system at 343.15 K. Again, it is recommended that such systems be investigated with a static apparatus.

8

CHAPTER EIGHT

CONCLUSION

This work was concerned with the phase equilibrium studies of the acetonitrile and water solvent on heavy hydrocarbons which included: heptanoic acid, 1-nonanol, dodecane and 1-dodecene. Binary vapour-liquid equilibrium (VLE), binary and ternary liquid-liquid equilibrium (LLE) and binary vapour-liquid-liquid equilibrium (VLLE) systems containing the above components were investigated.

The VLE/VLLE data were measured with the modified apparatus of Raal (Raal and Mühlbauer, 1998). The modification, introduced by Ndlovu (2005), catered for the measurement of VLLE data by allowing a vapour sample to be sent directly to a gas chromatograph for composition analysis. The cyclohexane + ethanol system at 40 kPa served as a test system to ensure the correct functioning of the apparatus and procedures employed. The data for this test system was found to be in excellent agreement with the data of Joseph et al. (2001). New VLE data for the 1-dodecene + 1-nonanol system at an isotherm of 403.15 K displayed an azeotrope at a mole fraction of 0.71 for 1-dodecene. It can be concluded that common distillation would not be able to separate these components at an isotherm of 403.15 K.

The LLE data were measured with the modified apparatus of Raal and Brouckaert (1992). The modification, introduced by Ndlovu (2005), improved thermal insulation and the sampling procedures. The binary heptane + methanol system at 1 atm and the ternary heptane + toluene + methanol system at 298.15 K and 1 atm were used as test systems to ensure the correct functioning of the apparatus and procedures employed. The data for these systems were found to be in excellent agreement with the data of Nagatani et al. (1987). The new binary and ternary LLE data revealed that acetonitrile and water can be used as a binary solvent to separate heptanoic acid and 1-nonanol from 1-dodecene or dodecane. However, the binary solvent needs to contain a minimum of 55% (mole percentage) of acetonitrile.

The experimental VLE data were regressed using two different methods: the combined method and the direct method. For the 1-dodecene + 1-nonanol system at 403.15 K, the regression analysis revealed that the direct method employing the alpha function of Twu et al. (1991) with the mixing rule of Wong and Sandler (1992) provided the lowest deviations between the calculated and experimental vapour mole fractions and pressures. The thermodynamic consistency tests revealed that the data for the 1-dodecene + 1-nonanol system at 403.15 K was thermodynamically inconsistent. The thermodynamic inconsistency was most likely due to some inaccuracy in the vapour compositions measured.

The regression of the experimental binary LLE data revealed that a second degree polynomial fitted all the model parameters with a least squares deviation sufficiently well. However, the Van Laar model displayed the worst fit for all the experimental binary LLE data. The experimental ternary LLE data were subjected to a two part correlation: the tie-line correlation and the binodal curve correlation. It was found that the water + acetonitrile + heptanoic acid and water + acetonitrile + 1-nonanol systems exhibited a type I system (Treybal, 1963). On the other hand, the water + acetonitrile + dodecane and water + acetonitrile + 1-dodecene systems exhibited a type II system (Treybal, 1963). The modified UNIQUAC model was found to provide the best fit to the tie-lines of the type I systems, while the NRTL model was found to provide the best fit to the tie-lines of the type II systems. The ß function was found to provide the best fit to the binodal curve of the type I systems, while the log γ equation was found to provide the best fit to the binodal curve of the type II systems.

The VLLE systems could not be measured with the modified VLE apparatus due to "flashing" of the more volatile component. The prediction of VLLE from mutual solubility data also failed to provide a reasonable phase diagram. The temperature-pressure sensitivity analysis revealed that such systems were very difficult to measure using a VLE recirculating still.

173

9

CHAPTER NINE

RECOMMENDATIONS

In order to improve the versatility and operation of the VLE apparatus for the measurement of VLLE data for systems that exhibit very high volatility, the VLE apparatus needs to be modified to further enhance the studies of these systems. These modifications are highlighted below:

1. The apparatus should be computer controlled to improve accuracy and a more precise control of the measured pressures and temperatures.

2. The inclusion of a small pre-mixing chamber with a magnetic stirrer before the boiling chamber. This chamber should also be heated to reach approximately the same temperature of the mixture in the boiling chamber. This arrangement would allow for efficient mixing and assist in the prevention of "flashing" for systems of very high volatility.

3. In addition to recommendations above, the influence of packing size, type and depth in the equilibrium chamber of the VLE apparatus could also be investigated. These variables may assist in the prevention of "flashing" of the more volatile component.

4. The VLE data for the 1-dodecene + 1-nonanol system at 403.15 K should be re-measured as the thermodynamic consistency tests were inconclusive. Furthermore, all

of the liquid phase activity coefficient models studied in this work could not model this system.   Therefore, other liquid phase activity coefficient models should be investigated, such as the liquid phase activity coefficient model of Tsuboka and Katayama (1975).

5. The VLE/VLLE measurement for systems that exhibit very high volatility could be investigated using a static apparatus. Such an apparatus eliminates the recirculation of the vapour phase, thus assisting in the prevention of "flashing".

REFERENCES

Abrams, D S and Prausnitz, J M, (1975), "Statistical Thermodynamics of Liquid Mixtures: A New Expression for the Excess Gibbs Energy of Partly or Completely Miscible Systems", *American Institute of Chemical Engineers Journal*, Vol. 21, pp. 116-128.

Alders, L, (1959), "Liquid-Liquid Extraction", 2nd edition, Elsevier, Amsterdam.

Anderko, A, (1990), "Equation-of-State Methods for the Modelling of Phase Equilibria", *Fluid Phase Equilibria*, Vol. 61, pp. 145-225.

Anderson, T F and Prausnitz, J M, (1978), "Application of the UNIQUAC Equation to Calculation of Multicomponent Phase Equilibria. 1: Vapour-Liquid Equilibria; 2: Liquid-Liquid Equilibria", *Industrial and Engineering Chemistry. Process Design and Development*, Vol. 17, pp. 552-567.

Baker, E M, Hubbard, R O H, Huguet, J H and Michalowski, S S, (1939), "Equilibria in the Systems Ethanol - Water, Ethanol - Cellosolve, and Cellosolve - Water", *Industrial and Engineering Chemistry*, Vol. 31, pp. 1260-1262.

Barker, J A, (1953), "Determination of Activity Coefficients from Total Pressure Measurements", *Australian Journal of Chemistry*, Vol. 6, pp. 207-210.

Benjamin, C Y, Ochi, K, Momose, M and Kojima, K, (1993), "Determination of Mutual Solubilities in Aniline + n-Hexane and Furfural + Cyclohexane Systems by a Laser Light Scattering Technique", *Canadian Journal of Chemical Engineering*, Vol. 71, pp. 982-985.

Black, C, (1958), "Vapour Phase Imperfections in Vapour-Liquid Equilibria", *Industrial and Engineering Chemistry*, Vol. 50, pp. 391-402.

Briggs, S W and Comings, E W, (1943), "Effect of Temperature on Liquid-Liquid Equilibrium: Benzene - Acetone - Water and Docosane - 1,6-Diphenylhexane - Furfural System", *Industrial and Engineering Chemistry*, Vol. 35, pp. 411- 417.

176

Cholinski, J, Szafranski, A and Wyrzykowska-Stankiewicz, D, (1986), "Computer Aided Second Virial Coefficient Data for Organic Individual Compounds and Binary Systems", PWN-Polish Scientific Publishers, Warsaw.

Clifford, S L, (2004), "Low-Pressure Vapour-Liquid Equilibrium and Molecular Simulation of Carboxylic Acids", Master of Science in Engineering (Chemical Engineering) Thesis, University of KwaZulu-Natal, South Africa.

Cottrell, F G, (1919), "On the Determination of Boiling Points of Solutions", *Journal of the American Chemical Society*, Vol. 41, pp. 721-728.

Coulson, E A, Hales, J L and Herington, E F G, (1948), "Fractional Distillation. II. The Use of Dilute Solutions of Thiophene in Benzene as Test Mixtures and a Comparison with Mixtures of Benzene and Ethylene Dichloride", *Transactions of Faraday Society*, Vol. 44, pp. 636-644.

Danner, R P and Gess, M A, (1990), "A Data Base Standard for the Evaluation of Vapour-Liquid Equilibrium Models", *Fluid Phase Equilibria*, Vol. 56, pp. 285-301.

Dymond, J H and Smith, E B, (1980), "The Virial Coefficients of Gases and Gaseous Mixtures", Clarendon Press, Oxford.

Ellis, S R M and Garbett, R D, (1960), "A New Equilibrium Still for the Study of Partially Miscible Systems", *Industrial and Engineering Chemistry*, Vol. 52, pp. 385-388.

Fredunslund, A, Gmehling, J and Rasmussen, P, (1977), "Vapour-Liquid Equilibrium using UNIFAC", Elsevier, Amsterdam.

García, I G, Pérez, A C and Calero, F C, (1988), "Liquid-Liquid Equilibrium Data for the Ternary Systems Water-Ethyl Alcohol-Organic Acid (Hexanoic, Heptanoic, Octanoic and Nonanoic Acid) and Water-Ethyl Alcohol-Phthalic Acid Dialkyl Ester (Diethyl, Dibutyl and Dioctyl Ester)", *Journal of Chemical and Engineering Data*, Vol. 33, pp. 468-472.

Gess, M A, Danner, R P and Nagvekar, M, (1991), "Thermodynamics Analysis of Vapour-Liquid Equilibria: Recommended Models and a Standard Data Base", Design Institute for Physical Property Data, American Institute of Chemical Engineers.

Gillespie, D T C, (1946), "Vapour-Liquid Equilibrium Still for Miscible Liquids", *Industrial and Engineering Chemistry, Analytical*, Vol. 18, pp. 575-577.

Gmehling, J and Onken, U, (1977-1982), "Vapour-Liquid Equilibrium Data Collection", DECHEMA Chemistry Data Series, Frankurt/Main.

Gomis, V, Ruiz, F and Asensi, J C, (2000), "The Application of Ultrasound in the Determination of Isobaric Vapour-Liquid-Liquid Equilibrium Data", *Fluid Phase Equilibria*, Vol. 172, pp. 245-259.

Gupta, S K and Rawat, B S, (1991), "Isothermal Vapor-Liquid Equilibria of Tetralin and 1-Methylnaphthalene with Triethylene Gylcol and N-Methylpyrrolidone at 160 °C", *Fluid Phase Equilibria*, Vol. 63, pp. 211-217.

Hála, E, Pick, J, Fried, V and Villim, O, (1967), "Vapour-Liquid Equilibrium", 2nd edition, Pergamon Press, Oxford.

Harlacher, E A and Braun, W G, (1970), "A Four-Parameter Extension of the Theorem of Corresponding", *Industrial and Engineering Chemistry. Process Design and Development*, Vol. 9, pp. 479-483.

Hayden, J D and O'Connell, J P, (1975), "Generalized Method for Predicting Second Virial Coefficients", *Industrial and Engineering Chemistry. Process Design and Development*, Vol. 14, pp. 209-216.

Heertjies, P M, (1960), "Determination of Vapour-Liquid Equilibrium of Binary Mixtures", *Chemical and Process Engineering*, Vol. 41, pp.385-386.

Herington, E F G, (1947), "A Thermodynamic Consistency Test for the Internal Consistency of Experimental Data of Volatility Ratios", *Nature*, Vol. 160, pp. 610-611.

Hernández-Garduza, O, García-Sánchez, F and Neau, E, (2001), "Generalization of Composition-Dependent Mixing Rules for Multicomponent Systems: Prediction of Vapour-Liquid and Liquid-Liquid Equilibria", *Chemical Engineering Journal*, Vol. 84, pp. 283-294.

Hlavatý, K, (1972), "Correlation of the Binodal Curve in a Ternary Liquid Mixture with One Pair of Immiscible Liquids", *Collection of Czechoslovak Chemical Communications*, Vol. 37, pp. 4005-4007.

Humphrey, J L, Rocha, J A and Fair, J R, (1984), "Essentials of Extraction", *Chemical Engineering (New York)*, Vol. 91, pp. 76-95.

Iwakabe, K and Kosuge, H, (2001), "Isobaric Vapour-Liquid-Liquid Equilibrium with a Newly Developed Still", *Fluid Phase Equilibria*, Vol. 192, pp. 171-186.

Joseph, M A, Raal, J D and Ramjugernath, D, (2001), "Phase Equilibrium Properties of Binary Systems with Diacetyl from a Computer Controlled Vapour-Liquid Equilibrium Still", *Fluid Phase Equilibria*, Vol. 182, pp. 157-176.

Kneisl, P, Zondlo, J W and Wallace, B W, (1989), "The Effect of Fluid Properties on Ebulliometer Operation", *Fluid Phase Equilibria*, Vol. 46, pp. 85-94.

Kollar, G Y, (1952), *Magyar Kem Foly*, Vol. 58, pp. 324, as given by Hála et al. (1967).

Lagarias, J C, Reeds, J A, Wright, M H and Wright, P E, (1998), "Convergence Properties of the Nelder-Mead Simplex Method in Low Dimensions", *SIAM Journal of Optimization*, Vol. 9, pp. 112-147.

Lee, S C, (1931), "Partial Pressure Isotherms", *Journal of Physical Chemistry*, Vol. 35, pp. 3558-3582.

Letcher, T M, Heyward, C and Wooten, S, (1986), "Phase Separation in Petrol - Alcohol Blends", *South African Journal of Chemistry*, Vol. 39, pp. 19-22.

Letcher, T M, Siswana, P M, van der Watt, P and Radloff, S, (1989), "Phase Equilibria for (an Alcohol + p-Xylene + Water) at 298.2 K", *Journal of Chemical Thermodynamics*, Vol. 21, pp. 1053-1060.

Liu, H, Hu, Y and Peng, C, (2002), "Liquid-Liquid Equilibria of Copolymer Mixtures Bases on an Equation of State", *Fluid Phase Equilibria*, Vol. 201, pp. 19-35.

Malanowski, S, (1982), "Experimental Methods for Vapour-Liquid Equilibria. Part I. Circulation Methods", *Fluid Phase Equilibria*, Vol. 8, pp. 197-219.

Marquardt, D W, (1963), "An Algorithm for Least-Squares Estimation of Non-Linear Parameters", *Journal. Society of Industrial and Applied Mathematics*, Vol. 11, pp. 431-441.

McClellan, A L, (1963-1974), "Tables of Experimental Dipole Moments", W. H. Freeman, San Franciso.

Michelsen, M L and Kistenmacher, H, (1990), "On Composition-Dependent Interaction Coefficients", *Fluid Phase Equilibria*, Vol. 58, pp. 229-230.

Moriyoshi, T, Uosaki, Y, Sakamoto, T and Hayashi, Y, (1989), "(Liquid + Liquid) Equilibria of (Water + Ethanol + 2,6-Dimethyl-4-heptanone) from 0.1 to 200 MPa at 298.15 and 323.15 K", *Journal of Chemical Thermodynamics*, Vol. 21, pp. 219-224.

Nagatani, M, Iwa, Y, Arai, Y, Higashiuchi and Sakuragi, Y, (1987), "Measurement and Correlation of Liquid-Liquid Equilibria of Binary and Ternary Systems Containing Methanol and Hydrocarbons", *Fluid Phase Equilibria*, Vol. 36, pp. 35-47.

Ndlovu, M, (2005), "Development of a Dynamic Still for Measuring Low Pressure Vapour-Liquid-Liquid Equilibria (Systems of Partial Liquid Miscibility)", Master of Science in Engineering (Chemical Engineering) Thesis, University of KwaZulu-Natal, South Africa.

Nothnagel, K H, Abrams, D S and Prausnitz, J M, (1973), "Generalized Correlation for Fugacity Coefficients in Mixtures at Moderate Pressures", *Industrial and Engineering Chemistry. Process Design and Development*, Vol. 12, pp. 25-35.

Novak, J P, Matous, J and Pick, J, (1987), "Liquid-Liquid Equilibria", Elsevier, Amsterdam.

Null, H R, (1980), "Phase Equilibrium in Process Design", Robert E Krieger, New York.

O'Connell, J P and Prausnitz, J M, (1967), "Emperical Correlation of Second Virial Coefficients for Vapour-Liquid Equilibrium Calculations", *Industrial and Engineering Chemistry. Process Design and Development*, Vol. 6, pp. 245-250.

Ohta, T, Todoriki, H and Yamada, T, (2004), "Representation of Liquid-Liquid Equilibria at Low and High Pressures using EOS-GE Mixing Rules", *Fluid Phase Equilibria*, Vol. 225, pp. 23-27.

Othmer, D F, (1928), "Composition of Vapours from Boiling Binary Solutions. Improved Equilibrium Still", *Industrial and Engineering Chemistry*, Vol. 20, pp. 743-766.

Peng, D Y and Robinson, D B, (1976), "A New Two Constant Equation of State", *Industrial and Engineering Chemistry Fundamentals*, Vol. 15, pp. 59-64.

Perry, R H and Green, D W, (1998), "Perry's Chemical Engineers' Handbook", 7th edition, McGraw-Hill, New York.

Pitzer, K S and Curl, R F, (1957), "Emperical Equation for the Second Virial Coefficient", *Journal of the American Chemical Society*, Vol. 79, pp. 2369-2370.

Pitzer, K S, Lippmann, D Z, Curl, R F, Huggins, C M and Petersen, D E, (1955), "The Volumetric and Thermodynamic Properties of Fluids. II. Compressibility Factor, Vapour Pressure and Entropy of Vapourization", *Journal of the American Chemical Society*, Vol. 77, pp. 3433-3440.

Prausnitz, J M, Anderson, T F, Grens, E A, Eckert, C A, Hseih, R and O'Connell, J P, (1980), "Computer Calculations for Multicomponent Vapour-Liquid and Liquid-Liquid Equilibria", Prentice-Hall, Englewood Cliffs, NJ.

Prausnitz, J M, Lichtenthaler, R N and de Azevedo, E G, (1999), "Molecular Thermodynamics of Fluid-Phase Equilibria", 3rd edition, Prentice-Hall, Upper Saddle River, New Jersey.

Raal, J D and Brouckaert, C J, (1992), "Vapour-Liquid and Liquid-Liquid Equilibria in the System Methyl Butenol-Water", *Fluid Phase Equilibria*, Vol. 74, pp. 253-270.

Raal, J D and Mühlbauer, A L, (1998), "Phase Equilibria: Measurement and Computation", Taylor and Francis, Bristol, PA.

Raal, J D, Gadodia, V, Ramjugernath D and Jalari, R, (2006), "New Developments in Differential Ebulliometry: Experimental and Theoretical", *Journal of Molecular Liquids*, Vol. 125, pp. 45-57.

Rackett, H G, (1970), "Equation of State for Saturated Liquids", *Journal of Chemical and Engineering Data*, Vol. 15, pp. 514-517.

Ramjugernath, D, (2000), "High Pressure Phase Equilibrium Studies", Doctor of Philosophy in Engineering (Chemical Engineering) Thesis, University of Natal, South Africa.

Redlich, O and Kister, A T, (1948), "Algebraic Representation of Thermodynamic Properties and the Classification of Solutions", *Industrial and Engineering Chemistry*, Vol. 40, pp. 345-348.

Redlich, O and Kwong, J N S, (1949), "On the Thermodynamics of Solutions. V. An Equation of State. Fugacities of Gaseous Solutions", *Chemical Reviews*, Vol. 44, pp. 233-244.

Reid, R C, Prausnitz, J M and Polling, B E, (1988), "The Properties of Gases and Liquids", McGraw-Hill, New York.

Renon, H and Prausnitz, J M, (1968), "Local Compositions in Thermodynamic Excess Functions for Liquid Mixtures", *American Institute of Chemical Engineers Journal*, Vol. 14, pp. 135-144.

Rifai, I and Durandet, J, (1962), *Rev. Inst. France di Petrol*, Vol. 17, pp. 1232, as given by Novak et al. (1987).

Rose, A and Williams, E T, (1955), "Vapour-Liquid Equilibrium Self-Lagging Stills. Design and Evaluation", *Industrial Engineering Chemistry*, Vol. 47, pp. 1528-1533.

Sameshima, J, (1918), "On the System Acetone-Ethyl Ether", *Journal of the American Chemical Society*, Vol. 40, pp. 1482-1508.

Scathard, G, Raymond, C L and Gilmann, H H, (1938), "Vapour-Liquid Equilibrium. I. Apparatus for the Study of Systems with Volatile Components", *Journal of the American Chemical Society*, Vol. 60, pp. 1275-1287.

Schultz, D M and Crouse, C F, (1973), "Random Splittings: A Model for a Mass-Size Distribution", *South African Statistic Journal*, Vol. 7, pp. 143-152.

Scott, R L, (1956), "Corresponding States Treatment of Nonelectrolyte Solutions", *The Journal of Chemical Physics*, Vol. 25, pp. 193-205.

Sen, A and Srivastava, M, (1990), "Regression Analysis Theory, Method and Application", Springer-Verlag, New York.

Sewnarain, R, Raal J D and Ramjugernath, D, (2002), "Isobaric Vapour-Liquid Equilibria for the Systems Propionic Acid + Butyric Acid, Isobutyric Acid + Butyric Acid, Butyric Acid + Isovaleric Acid and Butyric Acid + Hexanoic Acid at 14 kPa", *Journal of Chemical and Engineering Data*, Vol. 47, pp. 603-607.

Skoog, D A, West, D M and Holler, F J, (1991), "Fundamentals of Analytical Chemistry", 6th edition, Saunders College Publishing, Florida.

Smith, J M, Van Ness, H C and Abbott, M M, (2001), "Introduction to Chemical Engineering Thermodynamics", 6th edition, McGraw-Hill International Editions, New York.

Smith, T E and Bonner, R F, (1949), "Vapour-Liquid Equilibrium Still for Partially Miscible Liquids", *Industrial Engineering Chemistry*, Vol. 41, pp. 2867-2871.

Smyth, C P, (1955), "Dipole Moment and Molecular Structure", McGraw-Hill, New York.

Soave, G, (1972), "Equilibrium Constants from a Modified Redlich-Kwong Equation of State", *Chemical Engineering Science*, Vol. 27, pp. 1197-1203.

Sørensen, J M, Arlt, W, Macedo, M E A and Rasmussen, P, (1979-1987), "Liquid-Liquid Equilibrium Data Collection", DECHEMA Chemistry Data Series, Frankurt/Main.

Sørensen, J M, Magnussen, T, Rasmussen, P and Fredenslund, A, (1979), "Liquid-Liquid Equilibrium Data: Their Retrieval, Correlation and Prediction, Part I: Retrieval", *Fluid Phase Equilibria*, Vol. 2, pp. 297-309.

Sørensen, J M, Magnussen, T, Rasmussen, P and Fredenslund, A, (1979), "Liquid-Liquid Equilibrium Data: Their Retrieval, Correlation and Prediction, Part II: Correlation", *Fluid Phase Equilibria*, Vol. 3, pp. 47-82.

Sørensen, J M, Magnussen, T, Rasmussen, P and Fredenslund, A, (1980), "Liquid-Liquid Equilibrium Data: Their Retrieval, Correlation and Prediction, Part III: Prediction", *Fluid Phase Equilibria*, Vol. 4, pp. 151-163.

Stockhardt, J S and Hull, C M, (1931), "Vapour-Liquid Equilibria and Boiling-Point Composition Relations for Systems n-Butanol-Water and Isobutanol-Water", *Industrial Engineering Chemistry*, Vol. 23, pp. 1438-1440.

Stryjek, R and Vera, J H, (1986), "PRSV: An Improved Peng-Robinson Equation of State for Pure Compounds and Mixtures", *The Canadian Journal of Chemical Engineering*, Vol. 64, pp. 323-333.

Swietoslawski, W, (1945), "Ebulliometric Measurements", Reinhold, New York.

Tarakad, R R and Danner, R P, (1977), "An Improved Corresponding States Method for Polar Fluids: Correlations of Second Virial Coefficients", *American Institute of Chemical Engineers Journal*, Vol. 23, pp. 685-695.

Thornton, J D, (1952), "An Improved Type of Vapour-Liquid Equilibrium Still", *Journal of Applied Chemistry*, Vol. 1, pp. 237-239.

Treybal, R E, (1963), "Liquid Extraction", 2nd edition, McGraw-Hill, USA.

Trimble, H M and Potts, W, (1935), "Glycol-Water Mixtures, Vapour Pressure-Boiling Point-Composition Relations", *Industrial and Engineering Chemistry*, Vol. 27, pp. 66-68.

Tsonopoulos, C, (1974), "An Emperical Correlation of Second Virial Coefficients", *American Institute of Chemical Engineers Journal*, Vol. 20, pp. 263-272.

Tsuboka, T and Katayama, T, (1975), "Modified Wilson Equation for Vapour-Liquid and Liquid-Liquid Equilibria", *Journal of Chemical Engineering of Japan*, Vol. 8, pp. 181-187.

Twu, C H and Coon, J E, (1996), "CEOS/AE Mixing Rules Constrained by vdW Mixing Rule and Second Virial Coefficient", *American Institute of Chemical Engineers Journal*, Vol. 42, pp. 3212-3222.

Twu, C H, Bluck, D, Cunningham, J R and Coon, J E, (1991), "A Cubic Equation of State with a New Alpha Function and a New Mixing Rule", *Fluid Phase Equilibria*, Vol. 69, pp. 33-50.

Twu, C H, Coon, J E and Cunningham, J R, (1995), "An Approach for the Extension of a 3-Parameter Cubic Equation of State to Heavy Hydrocarbons", *Fluid Phase Equilibria*, Vol. 104, pp. 83-96.

Vakili-Nezhaad, G R, Mohsen-Nia, M, Taghikhni, V, Behpoor, M and Aghahosseini, M, (2004), "Salting-Out Effect of NaCl and KCl on the Ternary LLE Data for the Systems of (Water + Propionic Acid + Isopropyl Methyl Ketone) and of (Water + Propionic Acid + Isobutyl Methyl Ketone)", *Journal of Chemical Thermodynamics*, Vol. 36, pp. 314-348.

Valderrama, J O, (2003), "The State of the Cubic Equations of State", *Industrial and Engineering Chemistry Research*, Vol. 42, pp. 1603-1618.

Van der Waals, J D, (1873), "Over de Continuitet van den Gas - en Vloeistoftoestand", Doctoral Dissertation, Leiden, as given by Anderko (1990).

Van Laar, J J, (1910), "The Vapour Pressure of Binary Mixture", *Zeitschrift feur Physik Chemie*, Vol. 72, pp. 723-751, as given by Walas (1985).

Van Ness, H C, (1959), "Exact Forms of the Unrestricted Gibbs-Duhem Equation", *Chemical Engineering Science*, Vol. 10, pp. 225-228.

Van Ness, H C, (1995), "Thermodynamics in the Treatment of Vapour/Liquid Equilibrium (VLE) Data", *Pure and Applied Chemistry*, Vol. 67, pp. 859-872.

Van Ness, H C, Byer, S M and Gibbs, R E, (1973), "Vapour-Liquid Equilibrium: Part I. An Appraisal of Data Reduction Methods", *American Institute of Chemical Engineers Journal*, Vol. 19, pp. 238-244.

Van Ness, H C, Pedersen, F and Ramussen, P, (1978), "Part V. Data Reduction by Maximum Likelihood", *American Institute of Chemical Engineers Journal*, Vol. 24, pp. 1055-1063.

Van Ness, HC and Abbott, M M, (1982), "Classical Thermodynamics of Nonelectrolyte Solutions: With Applications to Phase Equilibria", McGraw-Hill, New York.

Van Zandijcke, F and Verhoeye, L, (1974), "The Vapour-Liquid Equilibrium of Ternary Systems with Limited Miscibility at Atmospheric Pressure", *Journal of Applied Chemistry and Biotechnology*, Vol. 24, pp. 709-729.

Walas, S M, (1985), "Phase Equilibrium in Chemical Engineering", Butterworth, Boston.

Weast, R C, Astle, M J and Beyer, W H, (1982-1984), "Handbook of Chemistry and Physics", 64th edition, CRC Press: Boca Raton, FL.

Wilson, G M, (1964), "Vapour-Liquid Equilibrium. XI: A New Expression for the Excess Free Energy of Mixing", *Journal of the American Chemical Society*, Vol. 86, pp. 127-130.

Wong, D S and Sandler, S I, (1992), "A Theoretically Correct Mixing Rule for Cubic Equations of State", *American Institute of Chemical Engineers Journal*, Vol. 38, pp. 671-680.

Yerazunis, S, Plowright, J D and Smola, F M, (1964), "Vapour-Liquid Equilibrium Determination by a New Apparatus", *American Institute of Chemical Engineers Journal*, Vol. 10, pp. 660-665.

Appendix A

Criterion For Phase Equilibrium

In any closed system, the temperature and pressure are related to the Gibbs energy, from the primary thermodynamic properties and the definition of Gibbs energy, by the following expression:

$$d(nG) = (nV)dP - (nS)dT \qquad \text{(A-1)}$$

If Equation (A-1) is applied to a single-phase fluid, in which there is no chemical reaction, the composition of such a system is constant and the following expressions can be deduced:

$$\left[\frac{\partial(nG)}{\partial P} \right]_{T,n} = nV \qquad \text{(A-2)}$$

and

$$\left[\frac{\partial(nG)}{\partial T} \right]_{P,n} = -nS \qquad \text{(A-3)}$$

where n is the number of moles of all chemical species in the system. The subscript n, indicates that all the chemical species in the system are held constant.

In an open system, the surrounding can interchange matter with the system; however, the Gibbs energy is still a function of temperature and pressure. Consequently, the Gibbs energy also becomes a function of n_i, the number of moles of a specific chemical species in the system. Therefore:

$$nG = g(P,T,n_i) \qquad \text{(A-4)}$$

Taking the total differential of Equation (A-4) results in the following expression:

$$d(nG) = (nV)dP - (nS)dT + \sum_i \mu_i dn_i \qquad \text{(A-5)}$$

with

$$\mu_i = \left[\frac{\partial(nG)}{\partial n_i}\right]_{P,T,n_j}$$

(A-6)

where μ_i, has special significance and is referred to as the chemical potential of species i in the mixture. Equation (A-6) is known as the fundamental property relation.

When two phases are in equilibrium in an overall closed system, each individual phase becomes an open system that is free to transfer mass to the other phase. If one assumes the equilibrium temperature and pressure to be uniform throughout the closed system, Equation (A-5) can then be written for each phase:

$$d(nG)^\alpha = (nV)^\alpha dP - (nS)^\alpha dT + \sum_i \mu_i^\alpha dn_i^\alpha$$

(A-7)

$$d(nG)^\beta = (nV)^\beta dP - (nS)^\beta dT + \sum_i \mu_i^\beta dn_i^\beta$$

(A-8)

where the superscripts α and β refer to each phase.

The change in the total Gibbs energy for this system is obtained by summing Equations (A-7) and (A-8). Each total system property can be expressed by the following relation:

$$nM = \left(nM\right)^\alpha + \left(nM\right)^\beta$$

(A-9)

Applying this relation to Equations (A-7) and (A-8) leads to:

$$d(nG) = (nV)dP - (nS)dT + \sum_i \mu_i^\alpha dn_i^\alpha + \sum_i \mu_i^\beta dn_i^\beta$$

(A-10)

Given that this is a closed system, Equation (A-1) is also applicable. An evaluation of Equations (A-1) and (A-10) at equilibrium shows that:

$$\sum_i \mu_i^\alpha dn_i^\alpha + \sum_i \mu_i^\beta dn_i^\beta = 0$$

(A-11)

The changes $dn_i{}^\alpha$ and $dn_i{}^\beta$ are only as a result from mass transfer between the two phases. Bearing in mind that this system is non-reactive, mass conservation necessitates that $dn_i{}^\alpha = -dn_i{}^\beta$. Therefore Equation (A-11) becomes:

$$\sum_i \left(\mu_i^\alpha - \mu_i^\beta \right) dn_i^\alpha = 0 \qquad (A\text{-}12)$$

The changes $dn_i{}^\alpha$ are independent and arbitrary and hence the only solution to Equation (A-12) is obtained when each term in parenthesis is separately equated to zero. This therefore results in:

$$\mu_i^\alpha = \mu_i^\beta \qquad (A\text{-}13)$$

This result can be generalised to include more than two phases by successively considering pairs of phases. For a closed system consisting of N chemical species and p phases at the same temperature and pressure, the general result is:

$$\mu_i^\alpha = \mu_i^\beta = \dots = \mu_i^\pi \qquad (A\text{-}14)$$

where $i = 1, 2, \dots, N$.

Therefore, the criterion for phase equilibrium of a system consisting of multiple phases at the same temperature and pressure is achieved when the chemical potential of each species is the same in all phases. A more detailed proof can be found in Smith et al. (2001).

Appendix B

Physical Properties of Chemicals

The critical properties of all chemicals (for VLE/VLLE systems) were obtained from the property data bank in Reid et al. (1988), except for the critical pressure and acentric factor of 1-nonanol that were unavailable. The critical pressure for 1-nonanol was therefore estimated from the Ambrose method outlined in Reid et al. (1988) and the acentric factor of 1-nonanol was estimated from the Lee-Kesler method outlined in Reid et al. (1988). The UNIQUAC pure component constants were obtained from group contributions as a sum over all the groups contained in a particular molecule as tabulated in Raal and Mühlbauer (1998).

Table B-1: Physical properties of chemicals used.

Component	T_c [K]	P_c [kPa]	V_c [cm^3/mol]	ω
Acetonitrile	545.5	4830	173	0.327
1-Dodecene	657	1850	700.5	0.558
Nonanol	671	2575	546	0.602
Water	647.3	22120	57.1	0.344
Ethanol	513.9	6140	167.1	0.644
Cyclohexane	553.5	4070	308	0.212

Table B-2: Pure component constants for the modified UNIQUAC model.

Component	r	q	q'
Acetonitrile	1.87	1.72	1.72
Methanol	1.43	1.43	1.43
Heptane	5.17	4.40	4.40
Toluene	3.92	2.97	2.97
Heptanoic Acid	6.71	6.31	6.31
Dodecane	8.55	7.10	7.10
1-Dodecene	8.32	6.88	6.88
Nonanol	6.62	5.83	5.83
Water	0.92	1.40	1.00
Ethanol	2.11	1.97	0.92
Cyclohexane	4.05	3.24	3.24

Appendix C

Model Parameters for the Combined and Direct Methods

C.1 Cyclohexane (1) + Ethanol (2)

Table C-1: Model parameters for the combined method and their deviations from experimental values for the cyclohexane (1) + ethanol (2) system at 40 kPa.

	Wilson			NRTL		UNIQUAC	
	$\lambda_{12}-\lambda_{11}$ [J/mol]	$\lambda_{21}-\lambda_{22}$ [J/mol]	a	$g_{12}-g_{22}$ [J/mol]	$g_{21}-g_{11}$ [J/mol]	$u_{12}-u_{22}$ [J/mol]	$u_{21}-u_{11}$ [J/mol]
Pitzer-Curl	1655.25	8370.27	0.4621	6136.39	3706.55	10375.02	-756.59
Avg (ΔT) / [K]	0.2669		0.2034			0.3226	
Avg (Δy)	0.0101		0.0080			0.0132	
Tsonopolous	1694.22	8410.14	0.4586	6153.16	3713.23	10414.17	-745.73
Avg (ΔT) / [K]	0.2743		0.2065			0.3322	
Avg (Δy)	0.0103		0.0083			0.0135	

Table C-2: Model parameters for the direct method and their deviations from experimental values for the cyclohexane (1) + ethanol (2) system at 40 kPa.

	PRSV EOS	Twu et al. (1991) a function
Wong and Sandler (1992)		
k_{ij}	-0.0651	-0.1073
$g_{12}-g_{22}$ / [J/mol]	85066.53	87557.81
$g_{21}-g_{11}$ / [J/mol]	59676.36	57706.91
a	0.336	0.3005
Avg (ΔT) / [K]	0.2512	0.2322
Avg (Δy)	0.0112	0.0088
Twu and Coon (1996)		
k_{ij}	-0.1455	-0.1669
l_{ij}	-0.0034	-0.0011
$g_{12}-g_{22}$ / [J/mol]	106588.49	111723.62
$g_{21}-g_{11}$ / [J/mol]	110749.37	119319.45
a	0.1961	0.1726
Avg (ΔT) / [K]	0.2108	0.1456
Avg (Δy)	0.0112	0.0073

C.2 1-Dodecene (1) + 1-Nonanol (2)

Table C-3: Model parameters for the combined method and their deviations from experimental values for the 1-dodecene (1) + 1-nonanol (2) system at 403.15 K.

	Wilson			NRTL		UNIQUAC	
	$\lambda_{12}-\lambda_{11}$ [J/mol]	$\lambda_{21}-\lambda_{22}$ [J/mol]	a	$g_{12}-g_{22}$ [J/mol]	$g_{21}-g_{11}$ [J/mol]	$u_{12}-u_{22}$ [J/mol]	$u_{21}-u_{11}$ [J/mol]
Pitzer-Curl	183.77	3239.92	-0.6929	-20177.77	2781.66	1508.87	-851.30
Avg (ΔP) / [kPa]	0.0306		0.0103			0.0310	
Avg (Δy)	0.0240		0.0234			0.0283	
Tsonopolous	187.05	3273.37	-0.6342	-7957.51	4243.11	1522.29	-857.25
Avg (ΔP) / [kPa]	0.0308		0.0099			0.0311	
Avg (Δy)	0.0237		0.0232			0.0280	

Table C-4: Model parameters for the direct method and their deviations from experimental values for the 1-dodecene (1) + 1-nonanol (2) system at 403.15 K.

	PRSV EOS	Twu et al. (1991) a function
Wong and Sandler (1992)		
k_{ij}	-0.4541	-0.5657
$g_{12}-g_{22}$ / [J/mol]	3811.82	8380.01
$g_{21}-g_{11}$ / [J/mol]	71551.93	73763.54
a	0.0016	0.0115
Avg (ΔP) / [kPa]	0.0208	0.0273
Avg (Δy)	0.0249	0.0103
Twu and Coon (1996)		
k_{ij}	-0.1077	-0.0972
l_{ij}	0.0011	-0.0003
$g_{12}-g_{22}$ / [J/mol]	16579.70	1463.92
$g_{21}-g_{11}$ / [J/mol]	94545.95	99427.79
a	0.0407	0.0305
Avg (ΔP) / [kPa]	0.0215	0.0235
Avg (Δy)	0.0215	0.0204

Appendix D

Thermodynamic Consistency

The graphs used in the determination of thermodynamic consistency for the measured VLE data are presented in this appendix. The *point test* of Van Ness et al. (1973) and the *direct test* of Van Ness (1995) were employed to test the experimental data measured in this work. An equation of state model and a liquid phase activity coefficient model can be used for the *point test*. On the other hand, only a liquid phase activity coefficient model can be used for the *direct test*. For the equation of state models, only the graphs for the mixing rule that displayed the lowest absolute deviation will be presented here. For the liquid phase activity coefficient models, only the graphs for the second Virial coefficient correlation that displayed the lowest absolute deviation will be presented here.
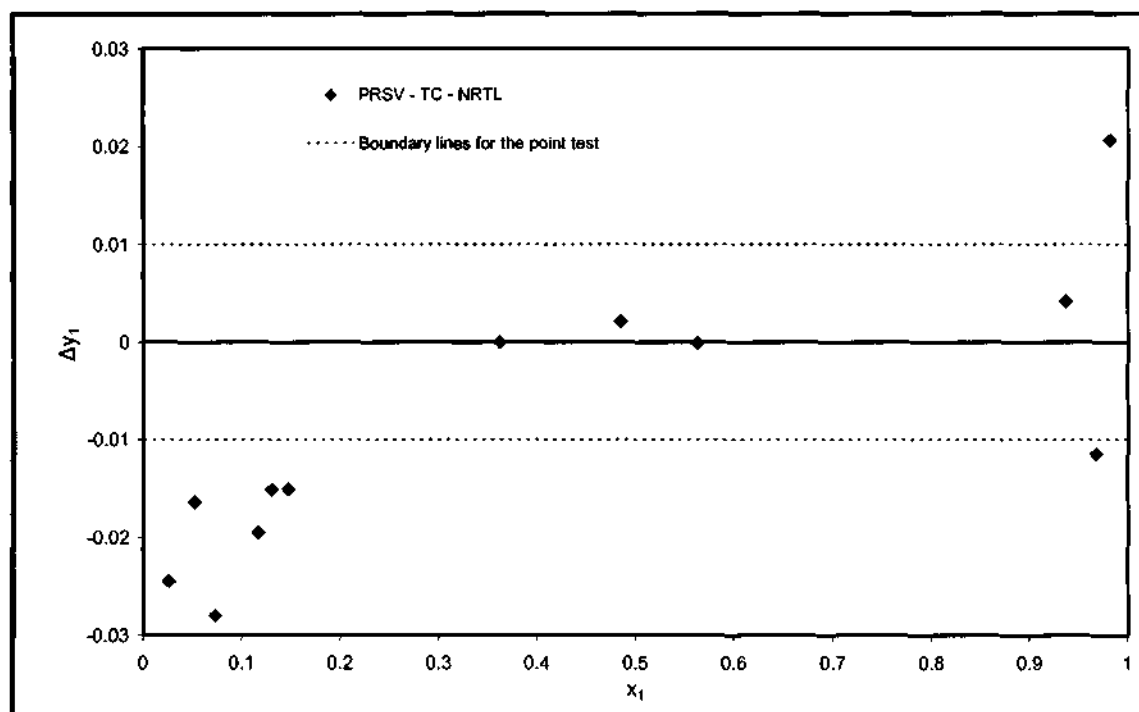
D.1 Cyclohexane (1) + Ethanol (2)

Figure D-1: Plot used for the point test with the PRSV-TC-NRTL model combination for the cyclohexane (1) + ethanol (2) system at 40 kPa.
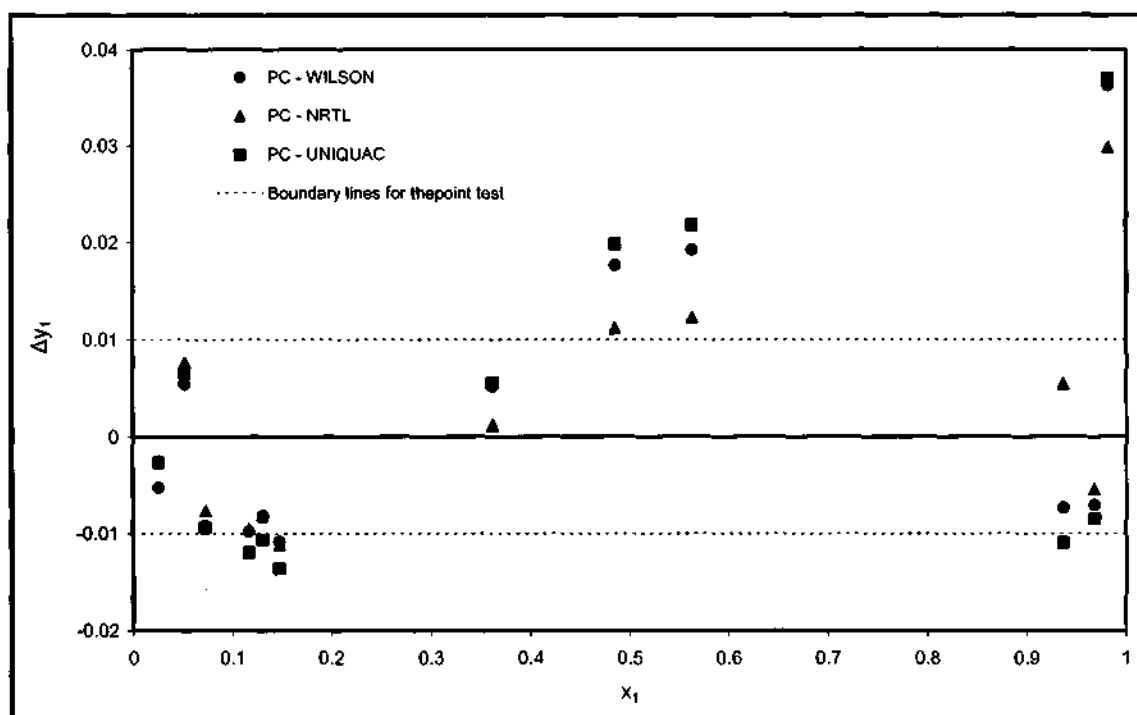
Figure D-2: Plot used for the point test with the PC-WILSON, PC-NRTL and the PC-UNIQUAC model combinations for the cyclohexane (1) + ethanol (2) system at 40 kPa.
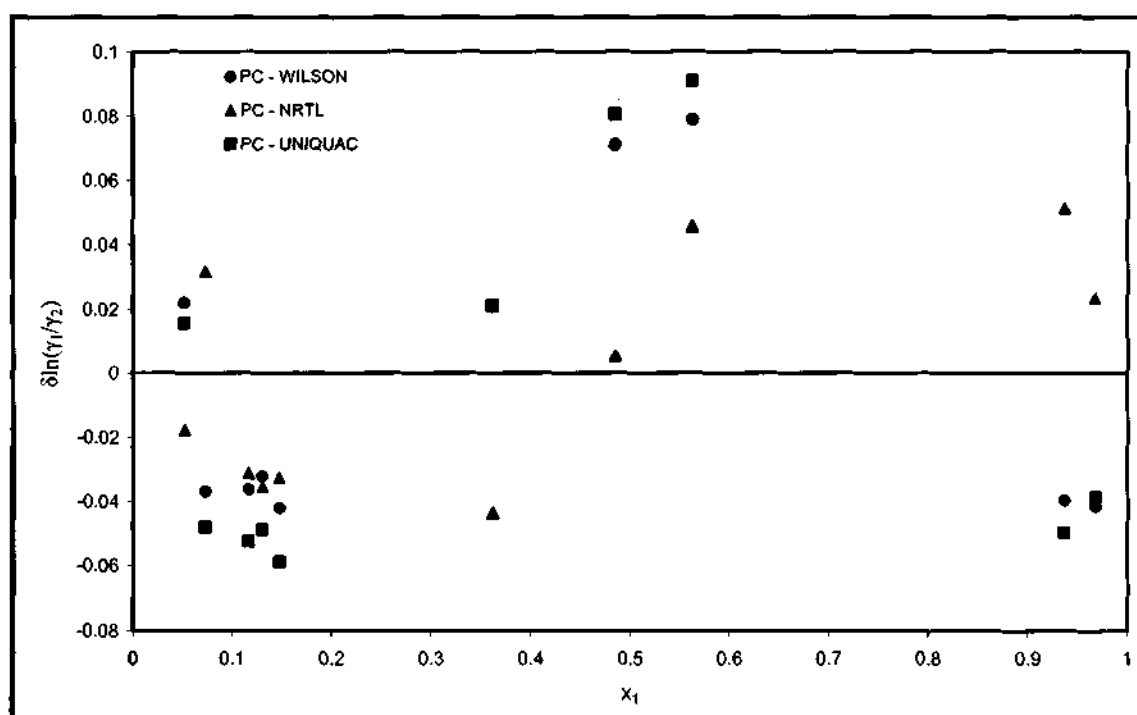

Figure D-3: Plot used for the direct test with the PC-WILSON, PC-NRTL and the PC-UNIQUAC model combinations for the cyclohexane (1) + ethanol (2) system at 40 kPa.

D.2 1-Dodecene (1) + 1-Nonanol (2)

Figure D-4: Plot used for the point test with the PRSV-WS-NRTL model combination for the 1-dodecene (1) + 1-nonanol (2) system at 403.15 K.

Figure D-5: Plot used for the point test with the TS-WILSON, TS-NRTL and the TS-UNIQUAC model combinations for the 1-dodecene (1) + 1-nonanol (2) system at 403.15 K.

Figure D-6: Plot used for the direct test with the TS-WILSON, TS-NRTL and the TS-UNIQUAC model combinations for the 1-dodecene (1) + 1-nonanol (2) system at 403.15 K.
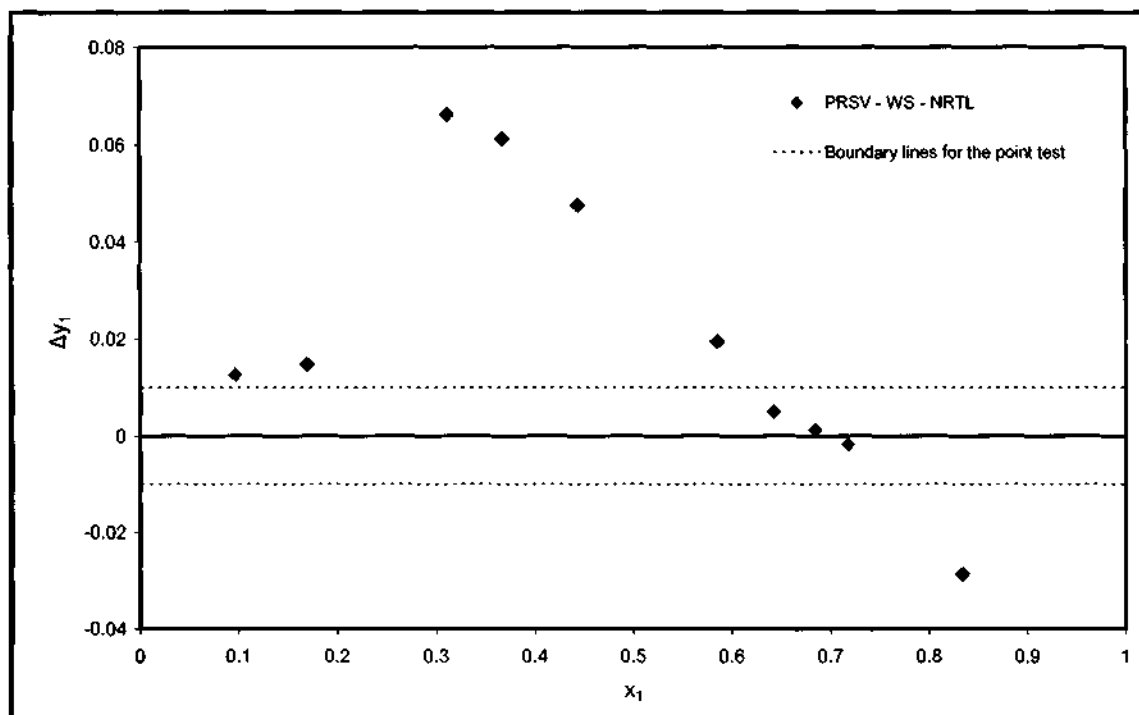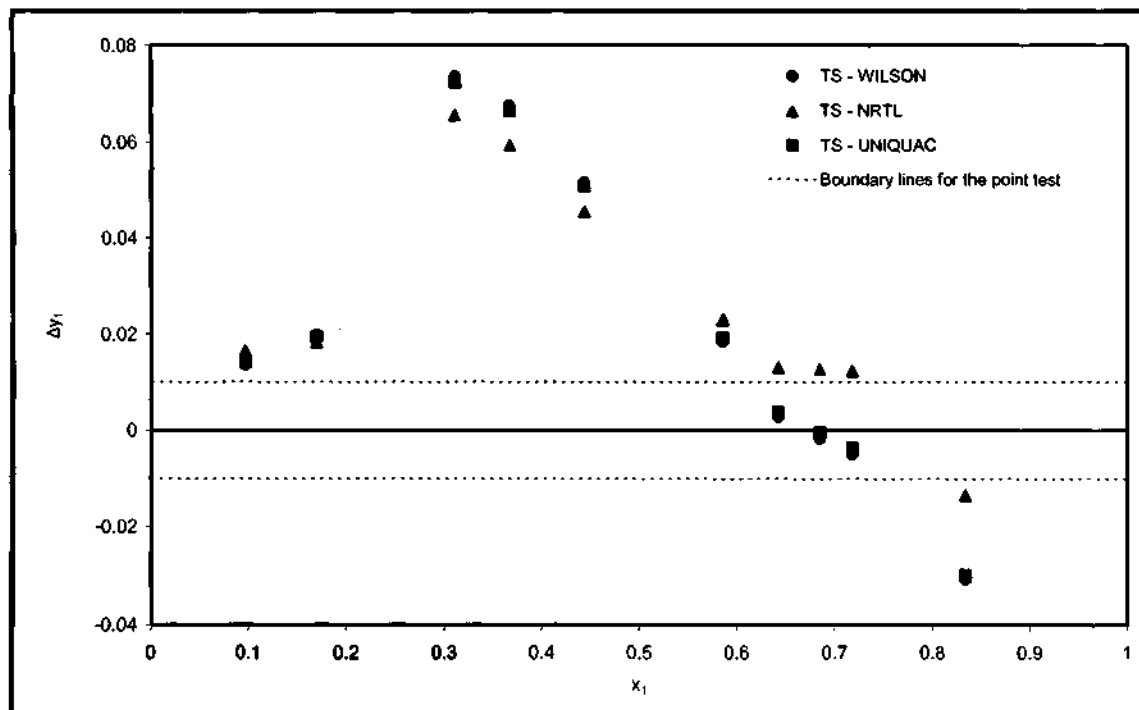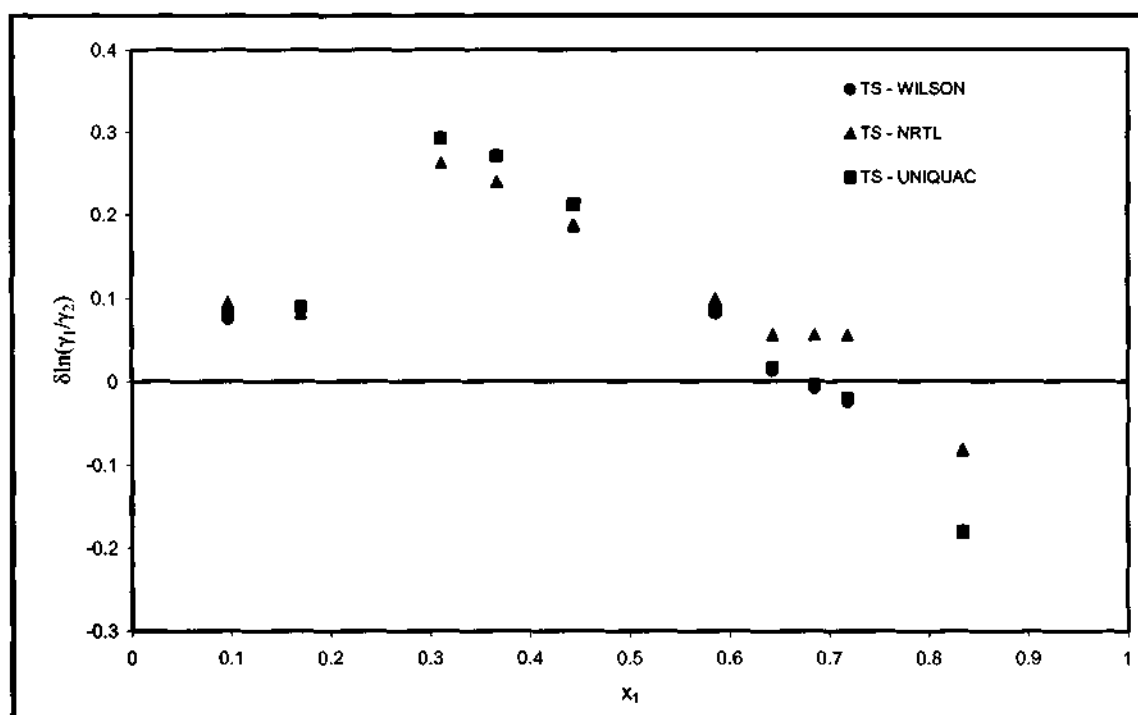
Appendix E

NRTL Parameters for Ternary LLE Systems

E.1 Heptane (1) + Toluene (2) + Methanol (3)

Table E-1: NRTL model parameters for the tie-lines of the heptane (1) + toluene (2) + methanol (3) system at 298.15 K and 1 atm.

a	0.20	0.25	0.30	0.35	0.40
$g_{12} - g_{22}$ / (J/mol)	561.5140	-256.9095	1860.5364	1298.5853	-322.5582
$g_{21} - g_{11}$ / (J/mol)	-6660.3250	-5328.6887	-3986.2829	-2302.5261	-222.8235
$g_{13} - g_{33}$ / (J/mol)	3456.6000	3494.1996	3944.0626	4461.3955	5128.7373
$g_{31} - g_{11}$ / (J/mol)	3959.5132	4316.8731	4553.6640	4842.9263	5667.0779
$g_{23} - g_{33}$ / (J/mol)	-785.9929	1059.3046	1860.5364	1534.8951	2283.0924
$g_{32} - g_{22}$ / (J/mol)	-2340.8507	-2777.3216	-53.7793	1298.5853	1934.8797
RMSD	0.0068	0.0097	0.0069	0.0051	0.0274

E.2 Water (1) + Acetonitrile (2) + Heptanoic Acid (3)

Table E-2: NRTL model parameters for the tie-lines of the water (1) + acetonitrile (2) + heptanoic acid (3) system at 323.15 K and 1 atm.

a	0.20	0.25	0.30	0.35	0.40
$g_{12} - g_{22}$ / (J/mol)	11598.5794	7870.0117	7461.0629	11967.4047	10144.9273
$g_{21} - g_{11}$ / (J/mol)	-2734.6081	-224.3438	366.2498	355.1186	563.0925
$g_{13} - g_{33}$ / (J/mol)	10169.6018	10192.7962	9214.4908	9750.4479	9619.0724
$g_{31} - g_{11}$ / (J/mol)	709.1667	1513.5018	2446.1568	3587.3216	6097.7514
$g_{23} - g_{33}$ / (J/mol)	-2410.2665	-879.2804	-603.4335	23370.2877	6551.9759
$g_{32} - g_{22}$ / (J/mol)	4707.7606	2079.0865	1238.4486	6682.9914	7579.2957
RMSD	0.0169	0.0134	0.0137	0.0228	0.0192

E.3 Water (1) + Acetonitrile (2) + 1-Nonanol (3)

Table E-3: NRTL model parameters for the tie-lines of the water (1) + acetonitrile (2) + 1-nonanol (3) system at 323.15 K and 1 atm.

a	0.20	0.25	0.30	0.35	0.40
$g_{12} - g_{22}$ / (J/mol)	538.1280	2854.9913	3655.1784	3699.5481	5313.2282
$g_{21} - g_{11}$ / (J/mol)	8428.9641	5442.5669	5617.8069	5387.5786	3888.6298
$g_{13} - g_{33}$ / (J/mol)	15815.4387	16481.8933	13652.7353	11521.1428	9369.9272
$g_{31} - g_{11}$ / (J/mol)	727.5127	2091.1879	3047.2708	4205.7163	5814.2381
$g_{23} - g_{33}$ / (J/mol)	1556.5794	6615.1932	8408.2490	1873.0290	1846.6496
$g_{32} - g_{22}$ / (J/mol)	473.7423	406.4684	492.5724	2007.6155	3098.8820
RMSD	0.0066	0.0065	0.0087	0.0075	0.0193

E.4 Water (1) + Acetonitrile (2) + Dodecane (3)

Table E-4: NRTL model parameters for the tie-lines of the water (1) + acetonitrile (2) + dodecane (3) system at 323.15 K and 1 atm.

a	0.20	0.25	0.30	0.35	0.40
$g_{12} - g_{22}$ / (J/mol)	5243.6429	5062.0472	4901.9264	5093.5296	6618.4190
$g_{21} - g_{11}$ / (J/mol)	1129.5279	1576.7357	2179.0859	2909.7054	10416.4047
$g_{13} - g_{33}$ / (J/mol)	21172.4976	19263.2873	16634.8740	15027.0356	21517.8650
$g_{31} - g_{11}$ / (J/mol)	11348.2101	13374.6142	15357.1685	17555.7454	15198.3137
$g_{23} - g_{33}$ / (J/mol)	11153.5320	10755.5774	11233.9423	11165.5148	9364.0123
$g_{32} - g_{22}$ / (J/mol)	2225.2495	3278.7242	4355.9388	5671.2797	7483.3464
RMSD	0.0019	0.0020	0.0023	0.0037	0.0274

E.5 Water (1) + Acetonitrile (2) + 1-Dodecene (3)

Table E-5: NRTL model parameters for the tie-lines of the water (1) + acetonitrile (2) + 1-dodecene (3) system at 323.15 K and 1 atm.

a	0.20	0.25	0.30	0.35	0.40
$g_{12} - g_{22}$ / (J/mol)	6489.7682	6205.4353	5849.8701	4941.6891	11036.0199
$g_{21} - g_{11}$ / (J/mol)	7.6365	598.0259	1295.6451	2639.3229	7083.0911
$g_{13} - g_{33}$ / (J/mol)	10839.8280	11249.2708	12540.0778	12274.9679	10306.4838
$g_{31} - g_{11}$ / (J/mol)	10590.7689	12421.0286	15538.9478	15063.7233	13545.0941
$g_{23} - g_{33}$ / (J/mol)	7758.8029	7599.1306	7542.4325	7879.9448	9761.9119
$g_{32} - g_{22}$ / (J/mol)	1625.3905	2358.4498	3194.6267	4320.9125	6074.5506
RMSD	0.0040	0.0041	0.0048	0.0096	0.0175